CONTRIBUTION OF TROPONIN-I TO THE REGULATION OF CARDIAC MUSCLE

by

WAYNE WILLIAM ALFRED MITCHELL

A thesis submitted to
The University of Birmingham
for the degree of
DOCTOR OF PHILOSOPHY

College of Medical and Dental Sciences
The University of Birmingham
September 2010

Abstract

Troponin-I (TnI) is one of the three components that makes up the troponin complex, which along with tropomyosin regulates striated muscle contraction. The cardiac isoform of TnI (cTnI) has a ~30 residue N-terminal extension, which contains two serines (Ser22/23) that become phosphorylated by protein kinase A upon β-adrenergic stimulation. However, the function of the N-terminus of cTnI remains unclear. Questions also remain about the function of the C-terminal region of cTnI, although its importance has been demonstrated by mutagenesis and deletion studies. With the use of ^{1}H nuclear magnetic resonance (NMR) spectroscopy it has been possible to investigate the F-actin binding capability of the N-terminal and C-terminal regions of cTnI. The extreme C-terminal region of (human) hcTnI was demonstrated to interact with F-actin and assist in the localisation of hcTnI to the thin filament. This thesis also demonstrates that a region of the N-terminus of hcTnI, close to the site of phosphorylation, interacts with F-actin and that this interaction was maintained upon monophosphorylation. The interaction between F-actin and the N-terminus of hcTnI was also detected when in a complex with hcTnC. The conclusions suggest a mechanism for regulating contractile activity in a manner specific to cardiac TnI.

Acknowledgements

In memory of Professor Samuel Victor Perry.

I would like to thank my PhD supervisors, Val Patchell and Barry Levine for their help and support throughout the PhD. Their knowledge of this subject has been a real inspiration to me. Thank you to the Director of the BMedSc course during my undergraduate studies. Many thanks to Dr. Doug Ward whose help with Mass spectrometry and general advice has been very much appreciated. Thank you to Dr. Clare Gallon for her advice and support at the beginning of the PhD. Thank you to Dr. Eva Hyde and the other members of the Protein Structure Function Club, Biosciences, for giving me the opportunity to present my work. Thank you to Professor Jim Evans for talking through certain aspects of the thesis with me. Thank you to everyone in the East Wing for being so friendly, with special thanks to Rumel for helping me towards the end of the thesis. Thank you to my friends during my undergraduate studies, Saif Khan, Amjad Iqbal and Amit Chavda, who helped make my undergraduate experience what it was. Thank you to my peers at Birmingham Medical School for their friendship during the PhD, Dr William Cheung and Andy Holmes. Many thanks to my family especially my parents, Patricia and Lawrence Mitchell who have always been there for me and whose support I have always relied on. Many thanks also to the many staff, colleagues and undergraduate students I have met and had the pleasure of working with at Birmingham Medical School and at various conferences over the past few years. I have enjoyed my experience at the University of Birmingham and very much appreciate the opportunities I have been given. This studentship was funded by the British Heart Foundation, to whom I am extremely grateful.

List of abbreviations

ADP	adenosine diphosphate
ATP	adenosine triphosphate
ATPase	adenosine triphosphatase
DMSO	dimethylsulfoxide
DTT	dithiothreitol
EDC	1-Ethyl-3-(3-dimethylaminopropyl)-carbodiimide
ERK	extracellular signal-regulated kinase
FHCM	familial hypertrophic cardiomyopathy
hcTnI	human cardiac troponin I
hcTnC	human cardiac troponin C
HMM	heavy meromyosin
HPLC	high performance liquid chromatography
HSQC	heteronuclear single-quantum correlation
IAEDANS	((((2iodoacetyl)amino)ethyl)amino)napthalene-1-sulfonic acid
ka	association constant
K_d	dissociation constant
k_{on}	On rate
k_{off}	Off rate
MAPK	mitogen-activated protein kinase
MLCK	myosin light chain kinase
MS	mass spectrometry
NHS	N-Hydroxysuccinimide
NMR	nuclear magnetic resonance
NOESY	nuclear Overhauser effect spectroscopy
PCR	polymerase chain reaction
pyrene	(N-(1-Pyrenyl)iodoacetamide)
rcTnI	rabbit cardiac troponin I
RF	radiofrequency
rsTnI	rabbit skeletal troponin I
S1	myosin subfragment 1
S2	myosin subfragment 2
hc-	human cardiac-
hcßM	human cardiac β-myosin heavy chain
fs-	fast skeletal-
ss-	slow skeletal-
Tm	tropomyosin
Tn	troponin
TnC	troponin C
TnI	troponin I
TnT	troponin T
TOCSY	total correlation spectroscopy

List of contents

List of Figures

Appendix I

1 Introduction

1.1 Summative overview

Several thin-filament protein components are involved in the molecular mechanism by which Ca^{2+} sensitivity of striated muscle contraction is regulated [Perry, 1996]. The heterotrimeric troponin complex (Tn) located on the thin (actin) filament is at the heart of the transduction of the Ca^{2+} signal that initiates the actomyosin MgATPase activity associated with contractile activation [Tobacman, 1996; Gordon et al, 2000, 2001; Kobayashi and Solaro, 2005; Bers, 2008].

The means by which calcium regulation of the thin filament is coupled to actin-myosin crossbridge interaction is believed to involve the relief of steric hindrance by tropomyosin (Tm) (Fig 1.1) [Huxley, 1990].

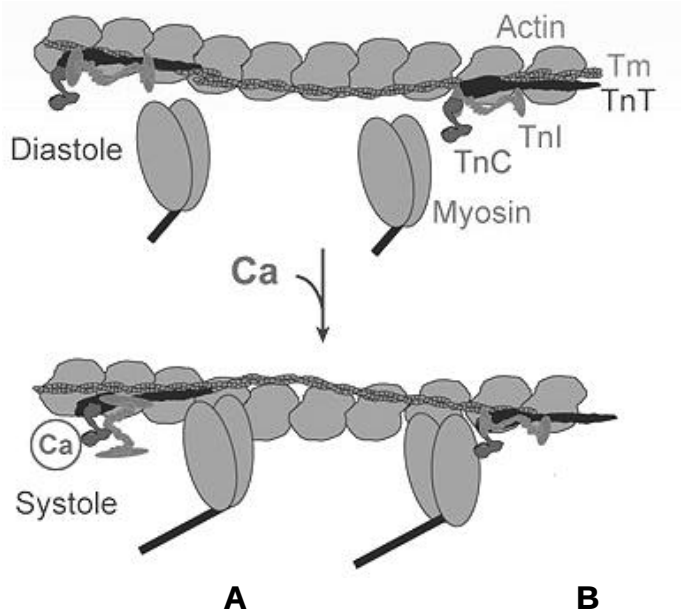

Figure 1.1 The thin-filament protein assembly of cardiac (striated) muscle Diagrammatic representation of the thin-filament protein assembly of cardiac (striated) muscle switching from diastole to systole upon calcium entry into the sarcoplasmic space showing the movement of tropomyosin (Tm) to expose binding sites for myosin heads on actin upon calcium binding to troponin-C (TnC). The transition from the myosin 'blocked' to myosin accessible ('active') state of the thin filament involves conformational changes propagated via the troponin complex described in the text below. (Diagram adapted from Bers 2008)

The diastole to systole transition is associated with calcium binding to the TnC troponin subunit causing the inhibitory region of troponin-I (TnI) to swap partners from actin to TnC [Perry, 1996]. The movement of the TnI inhibitory region away from actin, along with conformational changes in troponin-T (TnT) and tropomyosin (Tm), are believed to promote actomyosin crossbridge formation and, hence, actin-activation of the MgATPase of the myosin head and, the development of tension [Perry, 1996]. Interaction of myosin heads with actin is believed to shift Tm deeper into the actin groove, to enhance calcium affinity through stabilisation of troponin subunit interactions (Fig 1.1A) and, to increase crossbridge formation at neighbouring locations on the thin filament (Fig 1.1B) thereby resulting in cooperativity [e.g. Bers, 2008].

The nature and sequence of the molecular transitions involved in the inactivation of crossbridges and the return of cardiac muscle to the diastolic state are however not as well characterised. The relaxation process is generally perceived to entail the sequential reversal of the activating steps - release of Ca^{2+} from TnC in concert with a reduction in the sarcoplasmic calcium level and, an associated decline in actomyosin cross-bridge interaction [Kobayashi and Solaro, 2005; Bers, 2008].

Since modulation of the Ca^{2+} affinity of the TnC subunit via alteration of its partner interactions is crucial to the regulation of Ca^{2+} mediated contractility by troponin, the response of the thin-filament assembly to calcium may involve regulatory inputs at different components/nodes of the relaxation process. The contribution of cardiac isoform-specific characteristics to the return to the diastolic state is indeed indicated by, for example, developmental changes in the TnI isoform, with adult hearts showing

reduced Ca^{2+} sensitivity associated with the expression of the cardiac TnI isoform (cTnI) in place of the slow skeletal TnI (ssTnI) isoform found in neonatal hearts [Perry 1999; Westfall and Metzger, 2001]. Furthermore, altered Ca^{2+} sensitivity of cTnC has been associated with phosphorylation of the isoform-specific N-terminal region of cTnI resulting from β-adrenergic stimulation [Solaro, Moir and Perry, 1976; Perry 1999; Solaro et al, 2008].

The study described in this thesis focuses on characterisation of the contribution of the N- and C-terminal segments of human cTnI to the contraction-relaxation mechanism in cardiac muscle.

In this context the evidence for how Ca^{2+} binding/release by cTnC influences actomyosin crossbridge formation/inhibition via cTnI will be reviewed. The following sections therefore consider

A. the actin-myosin interaction so as to illustrate the nature of the complex that leads to muscle contraction upon the relief of inhibition,

B. the segments of cTnI whose actin-associated function(s) have been studied,

C. the overlap (changeover) of function for the cTnI inhibitory region and the interactions between cTnI and cTnC so as to identify the ‘on’ vs ‘off’ state and the switching between them and,

D. the calcium binding properties of cTnC and how these are influenced by the swapping of cTnI between cTnC and actin and the associated modulation of the calcium affinity of cTnC.

1.2 The actin-myosin crossbridge in the activation of cardiac contractility

The thick (myosin) filaments overlapping with the thin filaments made up of actin, tropomyosin and the Tn complex together comprise the contractile unit of striated muscle, the sarcomere [Perry, 1996]. The interaction between myosin heads and actin causes relative motion of the filaments thereby reducing sarcomeric length (Fig 1.2).

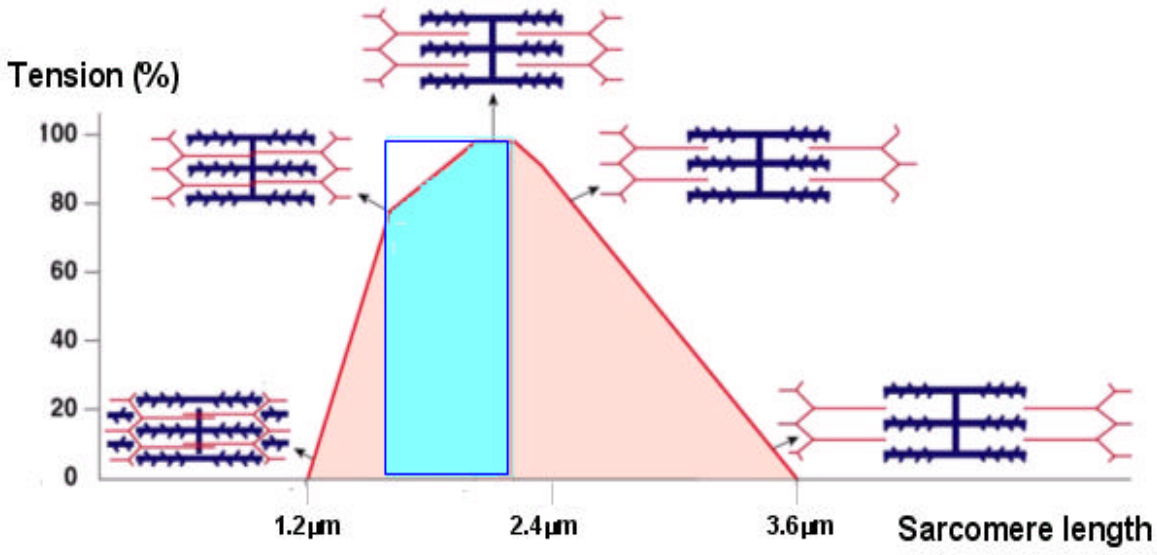

Figure 1.2 Length-tension relationship in striated muscle
The variation of tension and sarcomere length associated with the sliding of the myosin filaments relative to the actin-containing thin filaments. Myofilament overlap governs the number of potentially available force-generating cross-bridges. The sarcomere length range during a normal cardiac cycle, ~ 1.6-2.1µm, is indicated by the rectangle. (Diagram adapted from Gordon et al, 1966, Bers 2002 and Martini and Nath, 2008).

The extent of overlap between the myosin and actin filaments influences the population of potential actomyosin crossbridges and thus tension [Perry, 1996; Gordon et al, 1966]. However, tension in cardiac striated muscle increases over a sarcomere length range associated with a relatively constant degree of myofilament overlap (Fig 1.2) [Bers, 2002; Shiels and White, 2008]. Thus, alteration of myofilament sensitivity for Ca^{2+} and cooperativity within the thin filament (Fig 1B) are considered to be processes that regulate the number of force-generating crossbridges and thereby cardiac muscle tension and the pressure in the ventricle [reviewed in Bers, 2008; Kobayashi and Solaro

2005]. Furthermore, since during each beat in the resting heart just some 25% of the available crossbridges are thought to be involved in force generation [Hincken and Solaro 2007], it is likely to be the turnover rate of the actin-activated myosin MgATPase cycle that defines the rate of sliding of the filaments.

1.3 The nucleotide-bound myosin head and actin binding

Striated muscle myosin, myosin-II, is composed of two identical heavy chains with ventricular human cardiac myosin filaments primarily comprised of the β-myosin II isoform [Perry, 1996]. Each heavy chain has a structure made up of a head region (S1) that has two bound light chains and is connected to a long α-helical tail domain that forms a coiled coil dimer with the other heavy chain. The enzymatically-competent domain of myosin and its actin-binding region are located on the S1 head of each heavy chain as indicated, for example, by *in vitro* motility assays showing that individual S1 were able to move actin filaments [Toyoshima et al, 1987]. The regions on the surface of S1 involved in actin binding were subsequently modelled by docking the actin and S1 crystallographic structures guided by electron density maps of skeletal muscle S1-decorated F-actin [Rayment et al, 1993; Geeves and Holmes, 1999].

The crystal structures of several isoforms of myosin S1 revealed a common domain structure with a nucleotide binding pocket some 4–5 nm away from the actin binding region [Geeves and Holmes, 1999; Holmes et al, 2004] (Fig 1.3). It is thought that changes in the nucleotide binding region during the cycle from ATP to ADP+phosphate (Pi) and then ADP alone, are relayed via connecting segments of the S1 structure to change the way that the myosin head interacts with actin. The intramolecular relay between the actin- and nucleotide-binding sites is believed to involve an open ? closed

transition of a cleft between two regions of a domain of the myosin head (Fig 1.3) and it has been demonstrated that this cleft movement is coupled to actin binding and dissociation [Conibear et al, 2003].

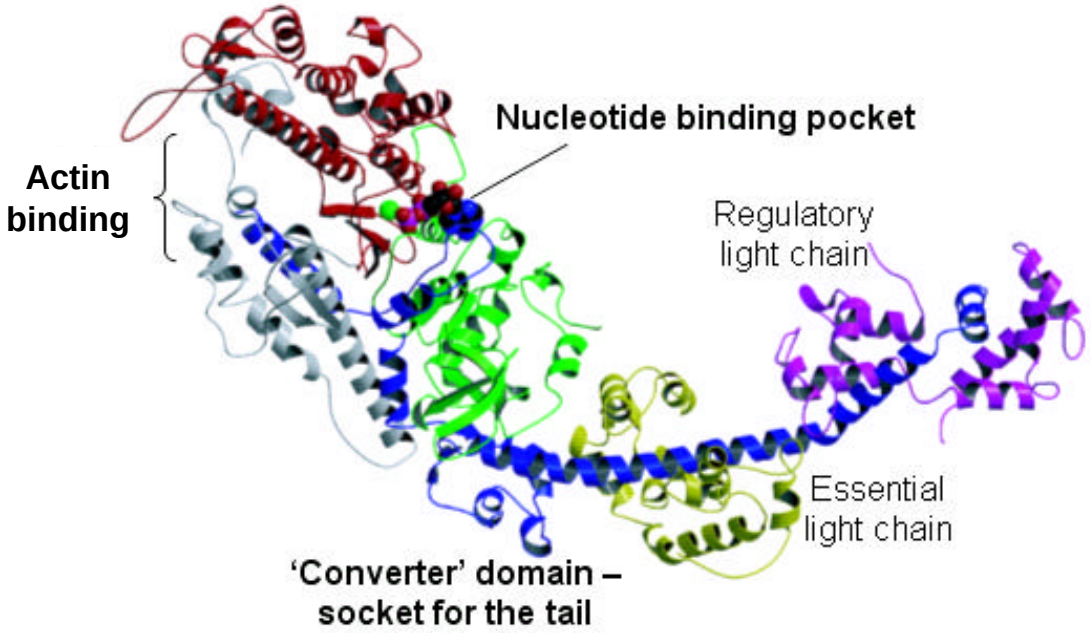

Figure 1.3 Location of functional regions in the structure of the myosin head
The structure of myosin II S1 [PDB ID 2MYS] shown in ribbon format to highlight the relaying helical 'rods' and the cleft region that extends from the nucleotide-binding site to the actin-binding region. The 'converter' domain acts to orient the C-terminal a-helical tail to which are bound the two light chains of myosin [Holmes et al, 2004].

The molecular mechanism put forward to account for force generation by actomyosin entails the movement of the helical C-terminal of S1 (fig 1.4) that acts as a swinging 'lever arm' to amplify structural changes relayed via the 'converter' domain during ATP hydrolysis [Geeves and Holmes, 1999; Hopkins et al, 2002]. The modelled 'pre-power stroke' to 'post-power stroke' transition (Fig 1.4 A to B) [Holmes et al, 2004; Geeves and Holmes, 1999; Steffen et al, 2003] shows the resulting reorientation of the end of the lever arm. The movement of the lever arm relative to the globular S1 head provides the mechanical basis for the 'rowing-like' gliding of myosin along the actin filament (Fig 1.4C).

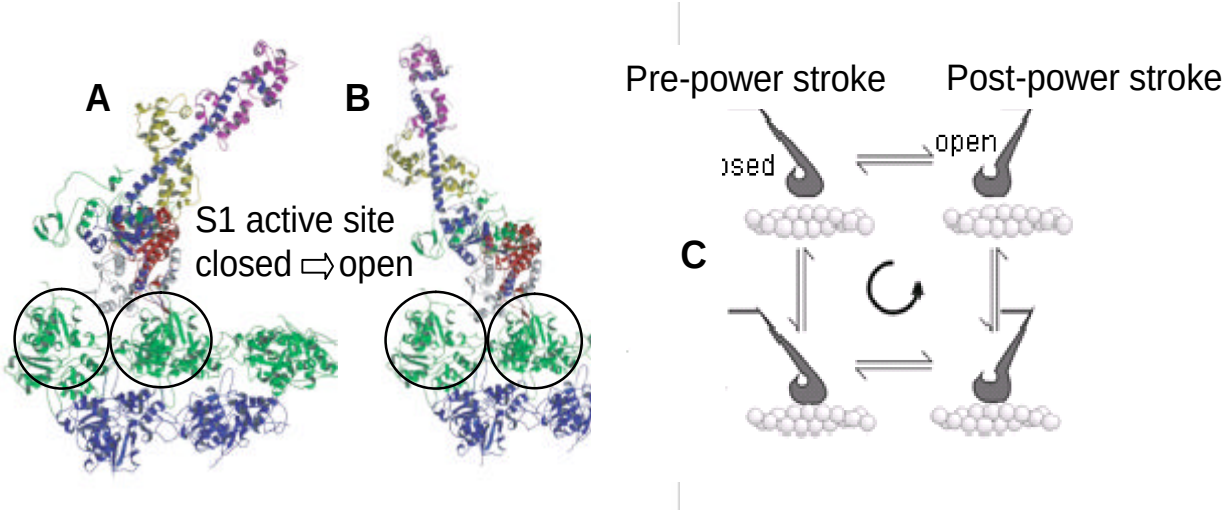

Figure 1.4 The working stroke transition
The modelled actin-bound S1 head shown in the 'pre-power stroke' (A) and 'post-power stroke' (B) states [Geeves and Holmes, 1999; Steffen et al, 2003].
(C) Myosin in the closed state binds to actin before changing to the open state with an associated rowing-like movement in the lever arm.
The actin-myosin crossbridge is shown as involving contact with two actin monomers along the F-actin filament as identified by the circles (see text below).

1.4 The crossbridge cycle

In the absence of ATP, myosin is bound with high affinity to the actin filament (the strong binding 'rigor complex', Fig 1.5). Binding of ATP to the myosin head leads to its release from actin and subsequent reformation of the actin-myosin crossbridge in the pre-power-stroke state with the myosin head bound to the products of hydrolysis (ADP and Pi) [Perry, 1996]. In its ADP.P_i state myosin reattaches weakly to actin and is believed to undergo conformational changes that enable a weak-to-strong (mM/μM to nM) binding transition [Holmes et al, 2004; Sweeney and Houdusse 2004]. This strongly bound actomyosin crossbridge results in force generation (the "power stroke") and phosphate release [Geeves and Holmes, 1999; Sweeney and Houdusse, 2004; Takagi et al, 2004].

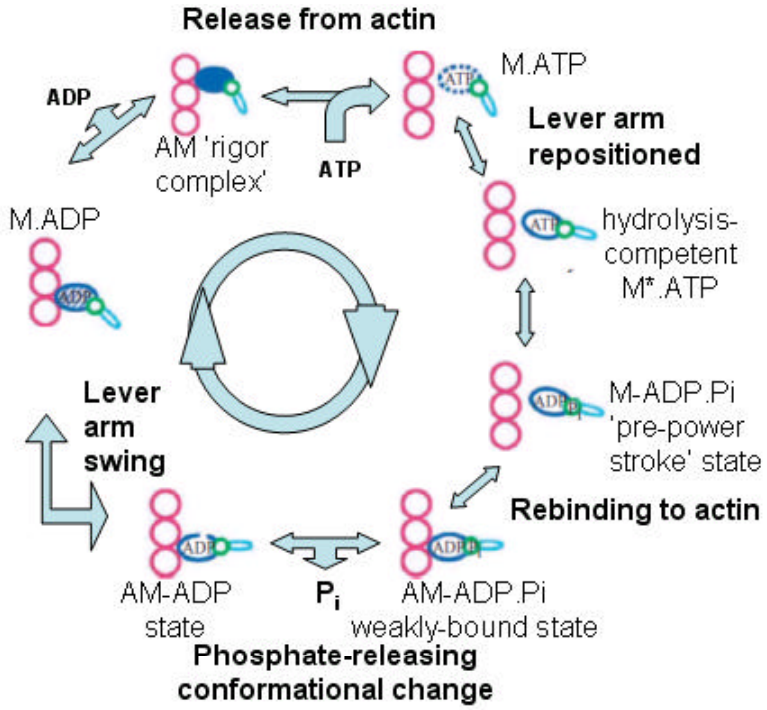

Figure 1.5 The actomyosin MgATPase cycle
Summary of different states of the crossbridge cycle correlating the hydrolysis of ATP with the structural changes that generate force. A, actin; M, myosin; P_i, inorganic phosphate. Cycle begins at the top left with the dissociation of a strongly bound actomyosin crossbridge upon binding of ATP. M-ADP.Pi initially binds actin weakly and then strongly to generate force and dissociation of Pi (Diagram adapted from Sweeney and Houdusse, 2004).

The energy transduction step of the cyclic interaction of myosin with actin, the weak to strong actomyosin crossbridge transition, is dependent upon the accessibility of actin binding sites on the thin filament that is modulated by calcium. The crossbridge transition has been minimally characterized in terms of an initial weak interaction that is converted to a strong interaction when the power stroke occurs to generate the force necessary for contraction [e.g. Sweeney and Houdusse, 2004]. The two states of the crossbridge have been modelled based upon the fit of structures of a variety of S1 isoforms in the absence and presence of different nucleotides/analogues to EM electron density reconstructions of rabbit skeletal actin decorated with chicken skeletal S1 [Rayment et al, 1993; Holmes et al, 2004]. The weakly bound actomyosin crossbridge

is believed to involve primarily electrostatic interactions that are then complemented by hydrophobic contacts enabled by a conformational change in the cleft that separates the actin-binding surface from the nucleotide-binding site of S1 [Conibear et al, 2003; Holmes et al, 2004].

1.5 How myosin anchors to actin

The actin-binding surface of myosin has been modelled as being made up of three main regions common to all isoforms of the myosin family [Rayment et al, 1993]. One is a positively charged surface loop (loop 2, typified by residues 626-647 of chicken skeletal myosin) implicated in the weak binding of S1 to actin but unresolved in the currently available crystal structures of the myosin head. The loop 2 region that has been found to crosslink to actin [Sutoh, 1982], contains a proteolytic cleavage site protected in the presence of actin [Mornet et al, 1981] and is reported to contribute to actin interactions that affect both the Pi and the ADP product release steps of the actomyosin cycle [Yengo and Sweeney, 2004].

Modelled as making contact with actin in the strong-binding state are a helix-turn-helix motif (residues 526-559 of chicken skeletal myosin, Fig 1.6) and a well-defined surface loop protrusion (chicken skeletal myosin residues 403-416, Fig 1.6), the 'cardiomyopathy' loop, so called since an Arg→Gln mutation in this segment of the ß chain of human cardiac myosin is associated with familial hypertrophic cardiomyopathy [Epstein et al, 1992; Watkins et al, 1992]. Residue deletion in this loop region resulted in the loss of the strong binding of actin to myosin [Sasaki et al, 1999].

In the light of the observation that a peptide comprising the cardiomyopathy (CM) loop of human β-cardiac myosin, Gly398-Gly414, inhibited the steady-state actin-activated MgATPase of S-1[Bartegi et al, 1997] and since both loop regions were devoid of intramolecular contacts with the S1 myosin head (Figure 1.6), the use of peptides comprising these two human β-cardiac myosin loop sequences was considered to be a viable means of probing F-actin interaction in competition assays with other potential ligands.

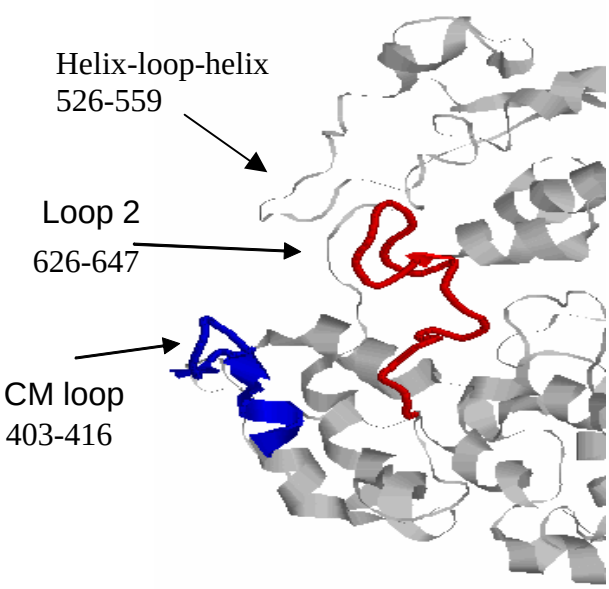

Figure 1.6 Two of the protruding loop regions on chicken skeletal myosin S1 (PDB identifier 1ALM) that face actin (see left hand side of figure 1.3)

1.6 The thin-filament and contractile activation

The F-actin array, a double-helical structure with 13 G-actin monomers per helical turn, is the backbone of the structure of the thin filament [Gordon et al, 2000, 2001; Moss et al, 2004]. Associated with the actin filament is tropomyosin (Tm) that is wound as a coiled coil stabilised by head to tail association of individual Tm molecules. Each tropomyosin spans 7 actin monomers that is a repeat also associated with the localisation of the troponin complex (Figure 1.7A) [Perry, 1996].

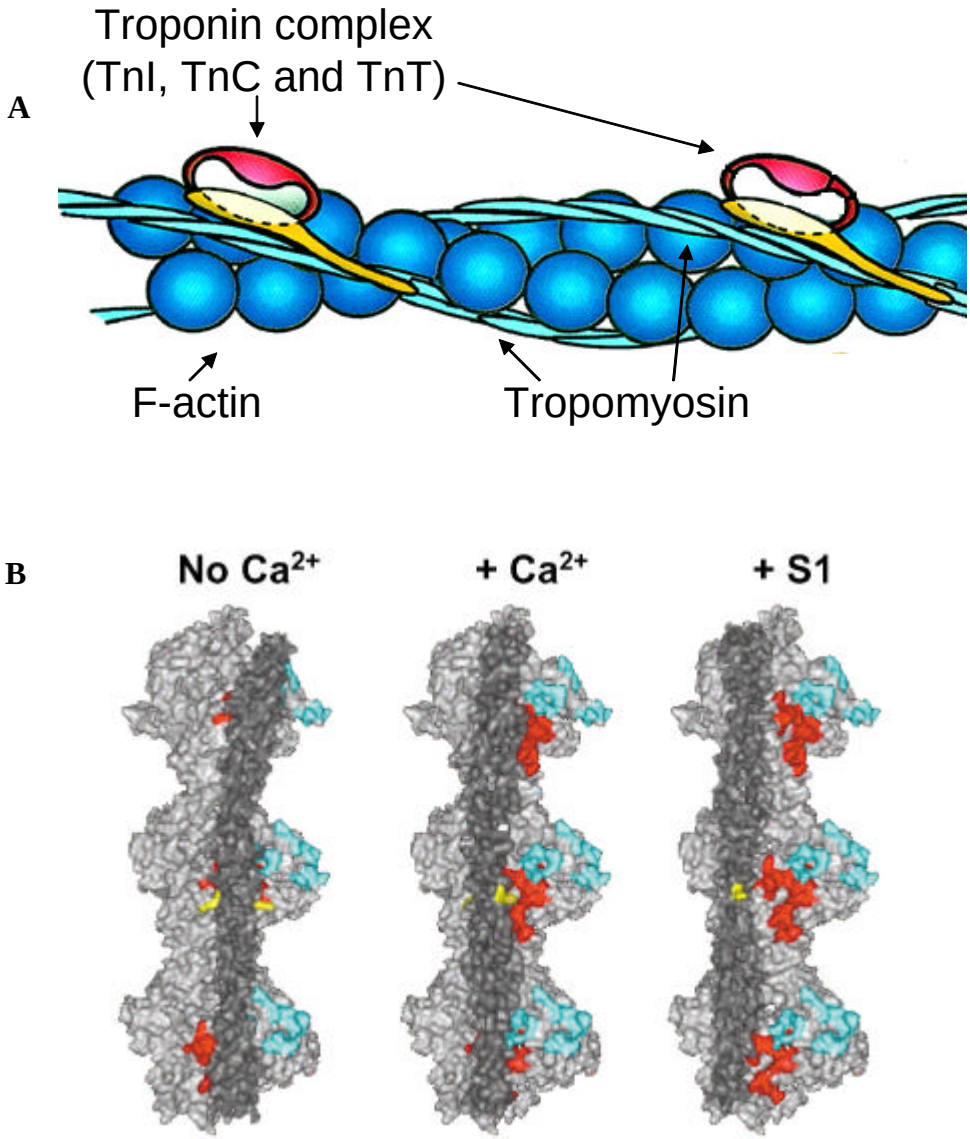

Figure 1.7A The thin filament array showing the association of the tropomyosin strands that stretch along F-actin (shown as linked globular monomers) and the localisation of the troponin trimer complex (Figure adapted from Moss et al, 2004).
Figure 1.7B Average position of tropomyosin on the surface of the actin filament in the absence and presence of Ca^{2+} (blocked and closed states) and its position in the open state (in the presence of the myosin head). Figure reproduced from Gordon et al, 2001.

The head to tail link of the tropomyosin strands is thought to underlie the movement of tropmyosin (Figure 1.7B) inferred originally from changes in the X-ray diffraction pattern of frog muscle during contraction, observations that led to the steric blocking hypothesis [Haselgrove 1972; Huxley 1972]. This view suggests that relaxation occurs

when, in the absence of Ca^{2+}, tropomyosin blocks the binding of the myosin cross-bridge to actin with tropomyosin movement from the blocked state upon resulting in activation by Ca^{2+}. This model has since been refined [e.g. McKillop and Geeves 1993; Gordon et al, 2001; Pirani et al, 2006] and points to three states/positions of tropomyosin on the F-actin filament, corresponding to the blocked, closed and open states of the thin-filament (Figure 1.7B). The association between F-actin and tropomyosin is considered to be shape-driven [Holmes and Lehman 2008] and that this dynamic/'fuzzy' association allows the 'rock/roll' movement of tropomyosin on the surface of F-actin [Gordon et al, 2001]. The position of tropomyosin represented in Figure 1.7B is therefore an average and it has been estimated that, in the presence of saturating Ca^{2+}, the position of tropomyosin is such that ~20% of the F-actin myosin-binding sites are in the open state and ~80% are in the closed state [McKillop and Geeves 1993].

The Ca^{2+}-dependent equilibrium between three thin-filament states suggests that at low concentrations of Ca^{2+} the troponin complex constrains the position of tropomyosin to the blocked state in which the F-actin binding sites for the myosin head are not exposed. The increase in concentration of Ca^{2+} upon neuromuscular stimulation causes a conformational change in the troponin complex with the subsequent movement of tropomyosin resulting in the exposure of some of the S1 binding sites on F-actin. The resulting initial interaction with the myosin heads is then thought to alter the equilibrium location of tropomyosin to allow exposure of the myosin interaction sites on the actin filament.

1.7 Troponin-I and inhibition of actomyosin activity

While the steric blocking overview of thin-filament regulation makes use of the calcium binding properties of the troponin-C troponin subunit, it does not relate specifically to the contribution made by the troponin I (TnI) subunit [Perry 1999]. TnI has been shown to be capable of inhibiting in vitro actomyosin ATPase activity in the absence of tropomyosin (Tm) [Perry, 1996]. The inhibition effected by TnI was enhanced in the presence of Tm, was found to be maximal at a molar ratio of 7:1 Tm:Tn and could be relieved by Ca^{2+}-bound TnC [reviewed by Perry 1999]. The actomyosin inhibitory capacity of TnI has also been indicated by *in vitro* motility measurements used to characterise the distinctive functional roles of the individual troponin subunits [Bing et al, 1997]. These confirmed that that the inhibitory activity of troponin I was regulated by Ca^{2+} binding to troponin C and that the inhibition effective at low Ca^{2+} was due to TnI.

The inhibitory property of TnI has been used in numerous studies as an experimental tool for localising functional properties to different regions of the sequence of TnI. The fast and slow skeletal isoforms of the protein each have a molecular mass ~ 21kDa with an approximately 30 residue long N-terminal extension (Figure 1.8) distinguishing the cardiac isoform of TnI (a feature of the sequence that has enabled the development of cardiac TnI as a biomarker for myocardial injury) [Cummins and Cummins, 1987].

```
hcTnI   ADGSSDAAREPRPAPAPIRRRSSNYRAYATEPHAKKKSKISASRKLQLKTLLLQIAKQELEREAEERRG
hfsTnI  -------------------------------GDEEKRNRAITARRQHLKSVMLQIAATELEKEESRREA
hssTnI  -------------------------------PEVERKPKITASRKLLLKSLMLAKAKECWEQEHEEREA
```

Figure 1.8 Sequence alignment of the N-terminal sequences of human cardiac, fast skeletal and slow skeletal TnI [EXPASY database]. Note the $(Xaa\text{-}Pro)_4$ motif that precedes the PKA phosphorylation site (S22/S23) of the hcTnI sequence and interestingly, is a repeat also found in the N-terminus of the LC1 myosin light chain.

Studies using a dissective (fragment-based) approach identified regions located in the sequence common to all TnI isoforms that were binding sites for the troponin-C (TnC, calcium binding) and troponin-T (TnT, tropomyosin binding) subunits [reviewed by Perry, 1999]. These interaction sites have now been resolved in X-ray structures of both the cardiac and skeletal troponin complexes [Takeda et al, 2003; Vinogradova et al, 2005].

Interaction of TnI with F-actin was first localised to a fast skeletal (fs) TnI cleavage fragment (residues 96-116 of rabbit fsTnI) that was found to be capable of inhibiting actin-Tm activated myosin-ATPase activity ~40-70% as effectively as the intact protein [Syska et al, 1976; Wilkinson et al, 1978]. Subsequent studies using synthetic peptides identified fsTnI residues 105-114 as the minimal inhibitory region [Tripet et al, 1997]. Together these studies suggested that the inhibitory region sequence, strongly-conserved across all TnI isoforms, was a site of TnI interaction with both F-actin and TnC. The deriving model for the regulation of inhibition by Ca^{2+} binding proposed that the inhibitory region oscillates between being bound to F-actin at low Ca and being bound to TnC upon Ca binding by TnC.

The study by Tripet et al [Tripet et al, 1997] showed that a peptide comprising fsTnI residues 96-148 inhibited actomyosin ATPase activity as effectively as intact TnI to a level similar to the intact protein. The enhanced potency compared to the shorter inhibitory region was shown to arise from an interaction with F-actin/Tm by fsTnI residues 140-148, a segment that was not itself capable of inhibition. The linking segment, fsTnI 116-131, the so-called ‘switch region’ of TnI, was also not inhibitory but was found to be important for the Ca^{2+}-dependent interaction with TnC that relieved inhibition by the inhibitory region of TnI [Tripet et al, 1997; Pearlstone et al, 1997].

A further region of interaction with TnC was localised to the N-terminus of TnI immediately preceding the sequence unique to the cardiac isoform. This interaction, not associated with occurring at activating levels of Ca^{2+}, is an anchoring interaction involving binding to the C-domain of TnC [Takeda et al, 2003]. The overall findings are summarised in Figure 1.9 that shows the primary structure locations of the characterised interactions of TnI along with the less well characterised C-terminal region common to all TnI isoforms. Shown in Figure 1.10 is the X-ray-based structural interpretation of the Ca^{2+}-switch that occurs in troponin [Vinogradova et al, 2005].

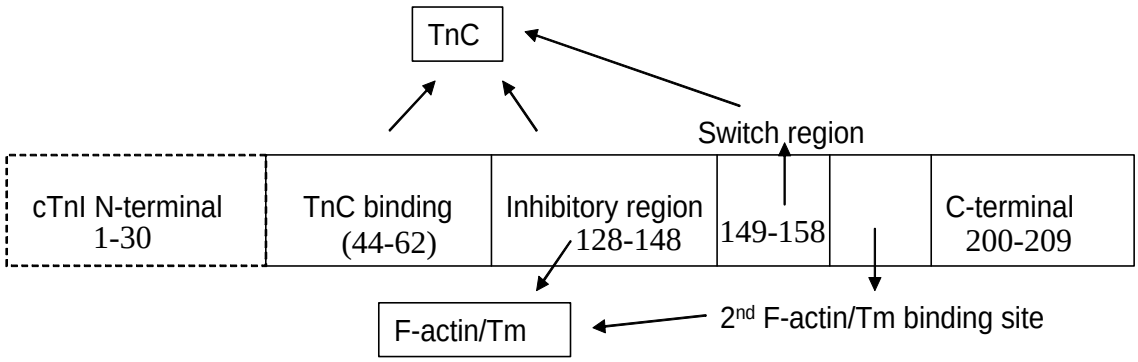

Figure 1.9 Primary structure representation of the characterised interaction sites in the TnI sequence. The N-terminal extension unique to cardiac TnI (cTnI) is also shown.

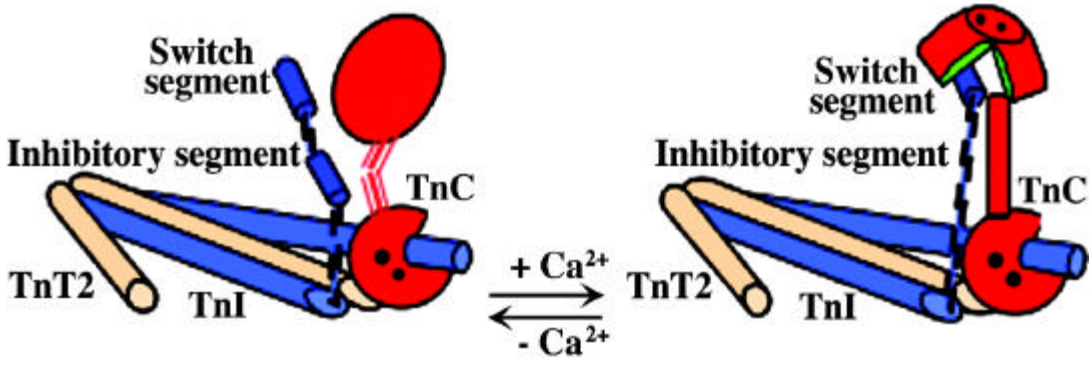

Figure 1.10 Illustration of the structural transition in (fast skeletal) troponin in response to binding by activating levels of calcium. Binding to the N-terminal domain of TnC exposes a hydrophobic cleft that engages the switch peptide region of TnI and stabilises the interaction between the TnI inhibitory region and TnC. TnI is shown anchored to the Ca^{2+}-bound TnC via its N- terminal that is connected to TnT that binds to tropomyosin and anchors the troponin complex on the thin filament.

The transition shown in Figure 1.10 illustrates the widely held view of the response of troponin to activating levels of Ca^{2+}. In relaxed muscle the inhibitory region of TnI is bound to F-actin and restrains cross-bridge cycling. In response to regulatory Ca^{2+}, the switch region of TnI binds to the N-terminal lobe of TnC thereby aiding the transition of the inhibitory region of TnI away from its binding sites on F-actin. The cardiac isoform of TnC possesses only a single functional Ca^{2+} binding site on its N-terminal domain but the transition illustrated in Figure 1.10 for fsTn is also indicated from the crystallographic studies of the partial cardiac Tn complex [Takeda et al, 2003]. Absent from both crystallized complexes were the C-terminal regions of TnI while the construct of cardiac TnI used to generate the cardiac Tn complex was missing the N-terminal extension characteristic of cardiac TnI. The inability to resolve these head and tail segments of cardiac TnI in the Tn complex meant that their locations within Tn remained undefined. This was particularly relevant since the Ca^{2+} affinity of cardiac TnC is believed to be modulated by PKA phosphorylation of sequential serine residues (Ser22 and Ser23 of hcTnI, Figure 1.8) first detected upon treatment of perfused heart with adrenaline [Ray and England, 1976, Solaro et al, 1976, Moir et al, 1980].

1.8 Calcium regulated contractility and the phosphorylation of cardiac TnI

Activation by calcium is initiated by a series of events initiated by an action potential and is illustrated by Booth (2004) below.

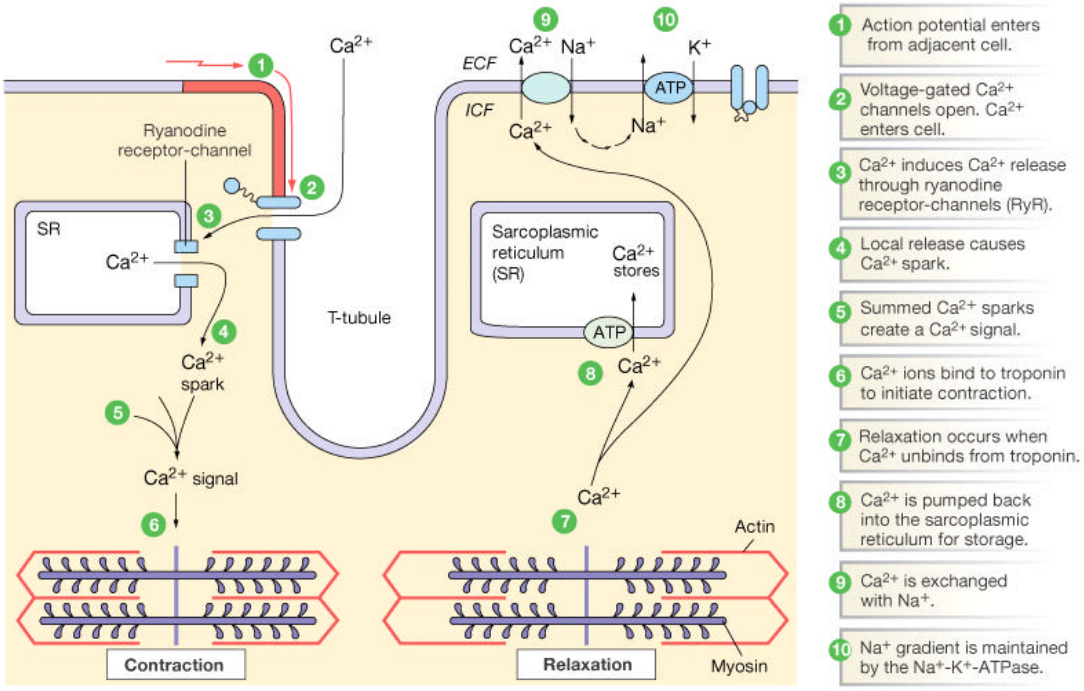

Figure 1.11 Excitation-contraction coupling and relaxation in cardiac muscle. Showing the sequence of events after the action potential (Booth, 2004).

The mechanism for calcium mediated regulation of contractility involving TnI identifies this component of the thin filament as the effector molecule of the regulatory protein assembly. Cardiac muscle contractility is also markedly enhanced upon ß-adrenergic stimulation with consequent phosphorylation of several targets by activated catalytic subunit of PKA leading to modulation of their activity [reviewed by Metzger and Westfall, 2004; Bers 2008]. These targets include phospholamban whose phosphorylation enhances Ca^{2+} pumping by the sarcoplasmic reticulum Ca-Mg ATPase, the sarcolemmal Ca^{2+} channel and TnI. The precise contribution(s) of these different targets in altering cardiac performance during ß-adrenergic stimulation is still a matter of debate [e.g. Metzger and Westfall 2004; Solaro and van der Velden, 2010] but only the consequences of cTnI phosphorylation are summarised here since this PKA target is at the heart of this thesis.

PKA phosphorylation of cTnI occurs at adjacent residues on the N-terminal region specific to the cardiac isoform of the protein with the interplay between kinase and phosphatase activity suggesting the potential occurrence of 4 forms of the human cardiac protein (hcTnI) - unphosphorylated, monophosphorylated at Ser 22, monophosphorylated at Ser 23 and bisphosphorylated. The physiological response to the phosphorylation of Ser 22 and Ser 23 has been characterised by perfused heart studies, pearmeabilised cardiac muscle preparations, biochemical solution studies and the use of transgenic mouse models [reviewed by Solaro et al, 1998 and Metzger and Westfall, 2004]. These observations point to a role for cTnI phosphorylation in modulation of the Ca^{2+} sensitivity of cardiac contractility and suggest that cTnI phosphorylation is the origin of the increase in relaxation and cross-bridge cycling. This correlation focuses attention on the N-terminal extension of cTnI as being the region responsible for modulating the Ca^{2+} affinity of cTnC, a role corroborated by solution studies [Robertson et al, 1982; Ward et al, 2002, 2004a]. The diagram below, reproduced from Ward et al 2002, illustrates the typical magnitude of the change in pCa^{2+} that is observed.

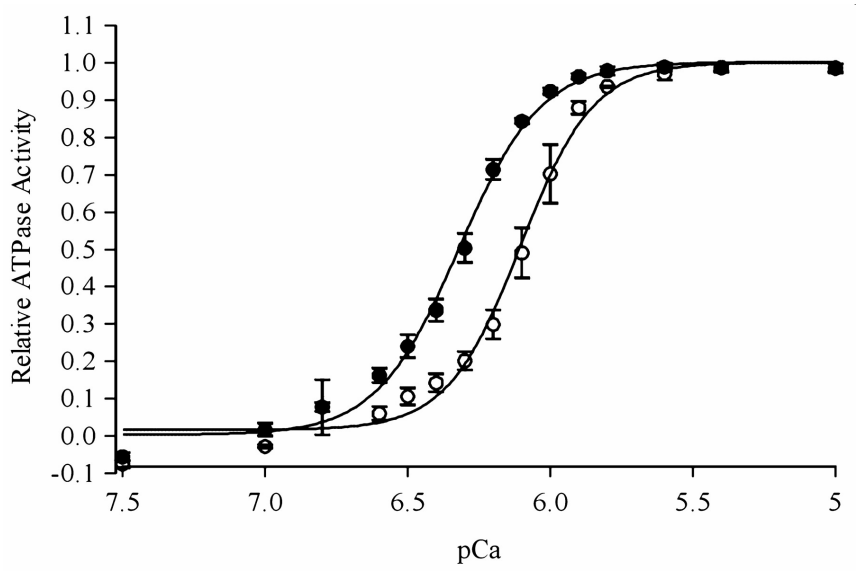

Figure 1.12 This graph shows the effect of phosphorylation of cTnI on the calcium dependence of actomyosin ATPase activity. The filled symbols are with unphosphorylated cTnI and the hollow symbols are PKA bisphosphorylated cTnI. Note the shift to the right with phosphorylated cTnI i.e. a decrease in Ca^{2+} sensitivity, (Ward et al, 2002).

The phosphorylation-dependent decrease in Ca^{2+} affinity is considered to be the result of an altered interaction between the N-terminus of cTnI and the regulatory N-domain of cTnC. The overall Ca^{2+} affinity of this regulatory site of cTnC was shown to be dependent upon interactions between cTnC and the other Tn components [Davis and Tikunova 2008] with a reported decrease in Ca^{2+} off rates from the N-domain of cTnC upon the sequential addition of TnI and TnT from more than 1000 s^{-1} to ~120 s^{-1} and then to ~35 s^{-1}. An increase in Ca^{2+} off rate back to 105 s^{-1} was observed upon the addition of F-actin/Tm.

1.9 Overview of project aims

As described by Perry [Perry 1999] and Solaro [Solaro et al, 2008] cardiac troponin-I is a critical component in the control of cardiac muscle contraction and relaxation. PKA phosphorylation of adjacent sites on the isoform-specific N-terminal region of cardiac troponin-I is correlated with reduced calcium sensitivity. This region of troponin-I was

unresolved in the structure of the reconstituted cardiac troponin complex [Takeda et al, 2003] and its molecular role in the regulatory function of cardiac troponin-I is believed to involve interaction with the N-terminal domain of cTnC. The details of this reportedly weak association are not well characterised [Sadayappan et al, 2008]. The question remained as to whether the N-terminal of cTnI impacted directly on the rate of Ca^{2+} dissociation from cTnC or whether the deletion influenced the rate of crossbridge detachment during relaxation via the separate modulation of other thin-filament protein interactions. The possibility that the N-terminus of cTnI may associate with F-actin or with F-actin/Tm was the first objective for the study described here.

The further aim of the work was to characterise any possible interaction with F-actin or with F-actin/Tm by the second 'loose end' of cTnI, the C-terminal tail sequence of the molecule. Unlike the N-terminal extension of cTnI, the C-terminal ~30-40 residues have a sequence that is highly homologous across TnI isoforms. The reference here to the C-terminal tail of hcTnI as a 'loose end' comes about firstly because of the observation that it is not constrained by interaction with the rest of the troponin complex and secondly because of the relatively ill-defined functional properties of this region that have only recently begun to be clarified [Galinska et al, 2010 and this thesis].

2 Materials and Methods

This chapter presents the underlying principles and experimental detail for the approaches used in this study to characterise the binding of the N- and C-terminal regions of hcTnI to F-actin. The reader is referred to standard texts for the background to NMR and fluorescence spectroscopy relevant to the study of complex formation. The level of the coverage described below reflects my background at the outset of the study and the specific methodological aspects essential to the analysis of the interactions observed.

Materials

2.1 hcTnI, hcβ–Myosin and β–thymosin peptides – synthesis, purification and composition

The sequences of the peptides and the hcTnI 1-64 construct used in this study are tabulated below.

Sequence from:	Residues	Sequence
hcTnI	1-30	ADGSSDAAREPRPAPAPIRRRSSNYR AYAT
hcTnI	1-18	ADGSSDAAREPRPAPAPI
hcTnI	16-37	APIRRRSSNYRAYATEPHAKKK
hcTnI	16-37 SSp	APIRRRSSp NYRAYATEPHAKKK
hcTnI	16-37 SpS	APIRRRSp SNYRAYATEPHAKKK
hcTnI	16-41	APIRRRSSNYRAYATEPHAKKKSKIS
hcTnI	16-29	APIRRRSSNYRAYA
hcTnI	36-52	KKSKISASRKLQLKTLL
hcTnI	1-64	ADGSSDAAREPRPAPAPIRRRSSNYR AYATEPHAKKKSKISASRKLQLKTLL LQIAKQELEREM
hcTnI	128-153	TQKIFDLRGKFKRPTLRRVRISADAM
hcTnI	147-180	RISADAMMQALLGARAKESLDLRAHL KQVKKEDT
hcTnI (S165T)	162-182	AKE*T*LDLRAHLKQVKKEDTEK
hcTnI	165-196	SLDLRAHLKQVKKEDTEKENREVGDW RKNIDA
hcTnI	170-191	AHLKQVKKEDTEKENREVGDWR
hcTnI	179-209	DTEKENREVGDWRKNIDALSGMEGRK KKFES
hcßMyosin	622-646	ANYAGADAPIEKGKGKAKKGSSFQT
hcßMyosin	398-414	GLCHPQVKVGNEYVTKG
Thymosin	3-26	KPDMAEIEKFDKSKLKKTETQEKN

Table 2.1 list of peptides used

The unblocked peptide comprising residues 398–414 of human cardiac β-myosin was synthesised by Syntem (Montpellier) and purified as previously described in a study of its interactions with F-actin [Bartegi et al, 1997]. All other peptides were synthesised by Alta Bioscience (University of Birmingham) by Fmoc polyamide chemistry and purified by reversed-phase HPLC on a Vydac C18 column (Waters), with a

water/acetonitrile gradient. Eluted peptides were freeze-dried twice to remove the solvent. Apart from hcTnI 1-30 and 1-18, the peptides were synthesised with blocked N- and C-terminal residues.

The homogeneity and composition of each peptide was confirmed by NMR and electrospray mass spectral analysis. This quality control step was crucial to ensuring the reliability of the study and on several occasions during the study peptide material obtained was discarded following mass spectral analysis.

Mass spectral analysis requires vaporised charged or ionised species that are subjected to electrical and magnetic fields so as to separate the components of the sample according to their mass-to-charge ratio (m/z). In electrospray ionisation, the sample solution is desolvated by spraying into the interface between cathode and anode across a high potential difference to produce multiply charged ions [Downard, 2004]. An example of such analysis is shown in the m/z spectrum of three hcTnI peptides; 1-30, 165-196 and 179-209 (Figure 2.1). The m/z spectrum (A) shows dominant ions of hcTnI 1-30 at m/z 3302 consistent with the expected peptide molecular mass of 3300Da including the N-Acetyl group, as calculated using EXPASY protparam. The ^{1}H NMR spectrum of the peptide is shown in Fig 3.1 (Chapter 3). The remaining peptides shown also correspond to their molecular weights of 3862Da including the N-acetyl group for hcTnI 165-196 and 3694Da including the N-acetyl group for hcTnI 179-209. Their ^{1}H spectra are shown in Chapter 6 (Figs 6.10, 6.11, 6.16 and 6.17).

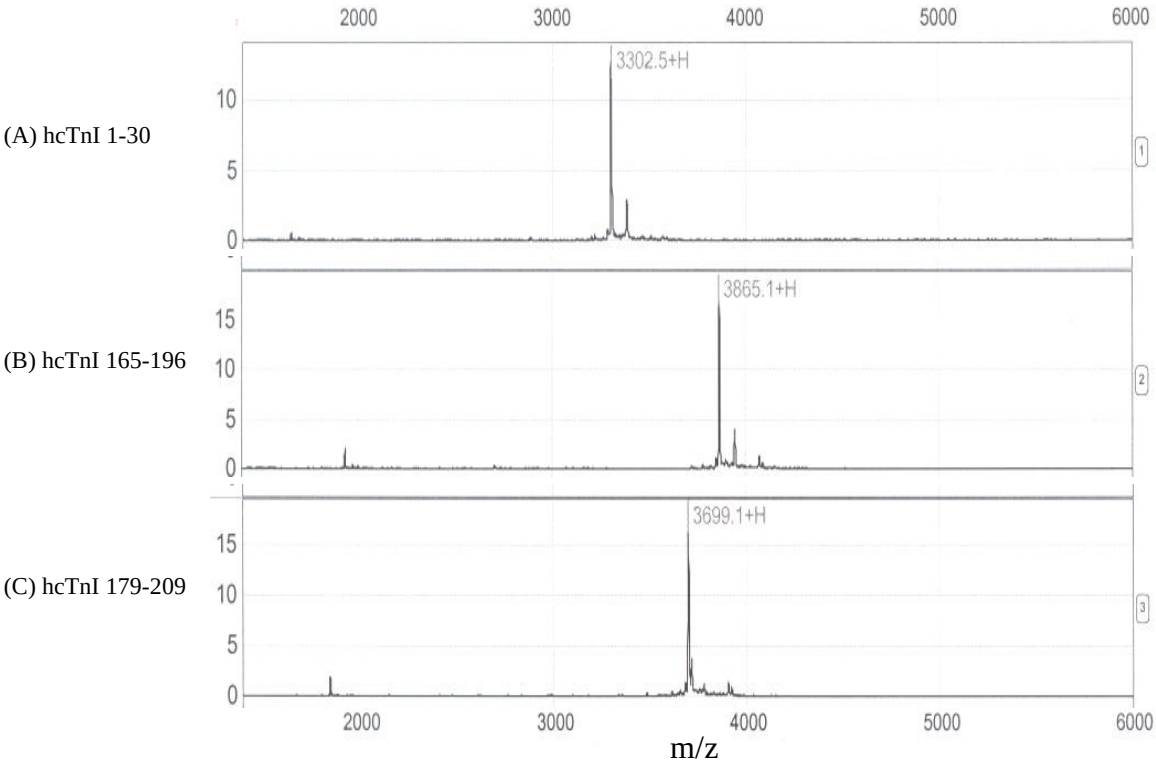

Figure 2.1 Mass spectra of three peptides of hcTnI. hcTnI 1-30 (A), hcTnI 165-196 (B) and hcTnI 179-209 (C). The y axis (arbitrary units) corresponds to the signal intensity of the ionised species.

Mass spectra were obtained by Dr D G Ward (Birmingham) on a Ciphergen PBS IIC spectrometer, typically using peptide samples that were made up at different dilutions to enable monitoring of the extent of any contaminants in the peptide preparations. The purity of each of the synthetic peptides used in this study was judged on the basis of the NMR and mass spectral analyses as being > 97%.

2.2 hcTnI 1-64, hcTnC and hcTnC domain constructs

hcTnI 1-64, obtained from Dr D G Ward, was purified from a CNBr digest of an expressed mutant hcTnI with a methionine residue introduced at position 64 as described by Ward et al (2003). The samples of recombinant hcTnC and its N- and C-domain constructs (hcTnC

residues 1-91 and 89-161 respectively) were provided by Dr D G Ward and prepared as described by Calvert et al (2000). The purity and identity of the proteins were checked by SDS-PAGE and by MALDI-TOF mass spectrometry.

2.3 F-actin, F-actin/tropomyosin and pyrene-labelled G-actin

Rabbit skeletal actin was used given the small quantities available from heart muscle preparations. Freeze dried actin, prepared by the method of Spudich and Watt (1971), was dissolved at 10mg/ml in 5mM triethanolamine-HCl, pH 8.0, 0.2mM $CaCl_2$, 0.2mM ATP, 0.2mM DTT, and dialysed for 3 hours against the same buffer until fully depolymerised. It was then centrifuged at 13,000g for 10 min and the concentration of the G-actin in the supernatant determined by measuring absorbance at 290 nm using an absorption coefficient of 0.63mg ml^{-1} cm^{-1}. The G-actin was polymerised by making the solution 2mM $MgCl_2$ and 50mM KCl. The F-actin was then dialysed overnight against several changes of of 10ml of 5mM sodium phosphate buffer, pH 7.0, in H_2O or ^2H_2O.

The F-actin/ tropomyosin complex was made by adding G-actin (prepared as described above) to a stock solution of 1 mg/ml rabbit skeletal tropomyosin in 50mM Tris-HCl, pH 7.6, 0.1M KCl, to give a final concentration of 2.5 mg/ml actin, 0.5 mg/ml tropomyosin, i.e. a molar ratio of actin:tropomyosin of approximately 7:1 and the actin was polymerised by adding 2mM $MgCl_2$ and 50mM KCl. The complex was dialysed into several changes of 5mM phosphate buffer, pH 7.0, in H_2O or ^2H_2O. Complex formation and the absence of free protein was confirmed by comparison of the electrophoretic patterns of the free proteins by electrophoresis on 10% non-denaturing polyacrylamide gels run in 10% (v/v) glycerol, 25 mM Tris-80 mM glycine, pH 8.3.

G-actin labelled at a 1:1 molar ratio on Cys-374 with *n*-(1-pyrenyl)iodoacetamide (pyrene, obtained from Molecular Probes) was prepared according to the method of Kouyama and Mihashi (1981). Actin (1mg/ml) was dialysed exhaustively against 5mM triethanolamine-HCl, pH 8, 0.2mM ATP, 0.2mM $CaCl_2$ and incubated with 10 fold molar excess of pyrene dissolved in DMSO overnight at room temperature in the dark. After incubation, the unreacted dye was removed by addition of 1% (wt/wt) Whatman CF-11 cellulose. The cellulose and the adsorbed unreacted dye were then removed by centrifugation in a microcentrifuge. After removal of dye, the labelled G-actin was polymerised by the addition of 2mM $MgCl_2$ and 50mM KCl and, after approximately 20 minutes, sedimented by centrifugation at 100,000 *g* for 1hr and resuspended in buffer A (2mM triethanolamine, pH 7.0, 0.2mM $CaCl_2$, 0.2mM ATP and 1mM DTT). The actin was then dialysed against buffer A at 4^oC, in the dark, for a minimum of 3 hours. To remove any non-depolymerised or denatured actin, the solution was then microcentrifuged at 13,000 rpm for 2 minutes. The concentration of labelled G-actin was determined using the molar absorbance of pyrene-labelled G-actin, 2.2×10^4 M^{-1} cm^{-1} at 344nm.

2.4 Fluorescence measurements

2.4.1 Background

The following outline description of the physical basis for fluorescence is intended as a brief introduction to the work described in this thesis. Details of the method and its uses can be found in the book by J. R. Lakowicz, "Principles of Fluorescence Spectroscopy". Fluorescent species absorb energy by excitation of delocalised electrons from their ground state. Relaxation occurs rapidly ($<10^{-12}$sec) and the energy may be lost as heat

to the environment due to atomic vibrations/rotations and, by collisions with other molecules. In situations when the loss of energy from the excited state is slow, the excited state loses energy by radiative emission of a photon, leading to fluorescence. During the lifetime of the excited state some non-radiative loss of energy frequently occurs to the environment before radiative emission of the bulk of energy. This results in the energy of the emitted photon being lower than that of the absorbed photon; therefore fluorescence is at a longer wavelength than the corresponding excitation wavelength.

Fluorescence spectroscopy was used to detect polymerisation of G-actin catalysed by increasing ionic strength or added ligand. The introduction of *N*-(1-pyrenyl)iodoacetamide (pyrene) as the chromophore covalently attached to actin meant that a single species contributing to the emission spectrum could be monitored. Pyrene (M_r = 385 Da) has been shown to preferentially bind to the thiol group of the Cys-374 residue of G-actin monomers [Korn, 1982] without altering the thermodynamic properties of actin [Cooper et al, 1983]. It was found that the intensity of pyrene emission (~ 386 nm) increased ~7–12 fold upon polymerization and this pyrene intensity assay has been validated by several studies [Kouyama and Mihashi 1981; Cooper et al, 1983].

2.4.2 Fluorescence spectra

All fluorescence emission spectra were obtained using a Perkin-Elmer LS50B fluorescence spectrometer interfaced to a computer. The excitation wavelength for pyrene was 347nm. Emission fluorescence intensity values were corrected for the

corresponding solvent emission fluorescence values and the dilution effects (<5%) resulting from the titration carried out. The fluorescence intensity changes quoted are values corresponding to 370-440nm.

The alteration in emission intensity of pyrene-labelled G-actin as a function of added salt or ligand reflected changes in the environment of the pyrene label associated with polymerisation (see Figure 2.2 below for an example).

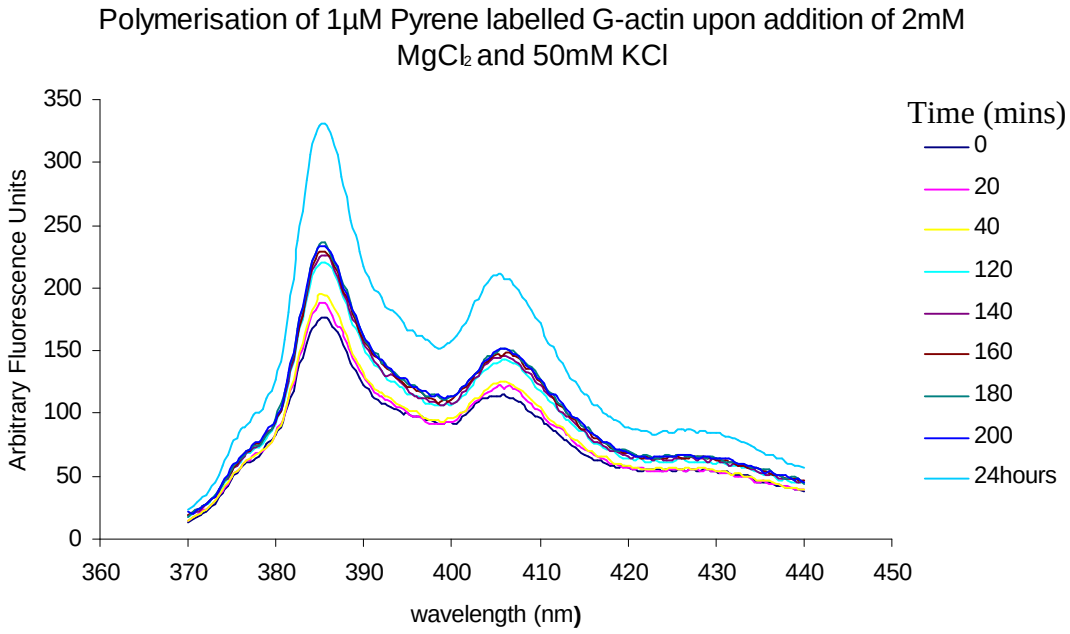

Figure 2.2 Fluorescence spectra of the polymerisation of pyrene G-actin upon addition of MgCl and KCl.

The purpose of the assay in this study was to report on the response of G-actin to the presence of different hcTnI peptides in order to gauge their relative abilities to catalyse polymerisation. Although the absence of a detectable enhancement in pyrene emission could not be used to infer the absence of binding to G-actin by the added ligand, the observation of differential responses in pyrene emission reflected differences in the nature of the interactions by the different peptides.

2.5 Nuclear magnetic resonance (NMR) measurements

2.5.1 Background

This section describes the basis for the experimental approach used in this thesis to obtain information through the use of proton (^{1}H) magnetic resonance about the interaction between F-actin and the different regions of hcTnI studied. Comprehensive coverage is not intended since NMR methods are described in a number of texts (e.g. "NMR of Macromolecules- A Practical Approach" edited by G. C. K. Roberts). The information presented here is therefore primarily qualitative so as to provide an empirical background for the deductions made from the observation of changes in resonance energy (chemical shift) or resonance broadening (relaxation) that reflect complex formation.

NMR detects the radiofrequency absorptions of atomic nuclei that possess a magnetic moment (spin) and that experience a net magnetic field. The presence of the magnetic field (both externally applied and that arising from the electronic environment of each nucleus) results in a population difference between different orientations with respect to the field and it is the associated transition that is excited in the NMR experiment. Studying a peptide molecule in solution by NMR spectroscopy enables one to record differences in the magnetic environments of the various nuclei present and, due to the dependence of the relaxation process upon the number and proximity of neighbouring nuclei that act as energy sinks, to deduce the intimacy of contact of these nuclei when interacting with F-actin or hcTnC as target.

The radiofrequency necessary for resonance depends upon both the strength of the external magnetic field and on the nuclear type being detected. The relationship between the NMR absorption frequency (ν) of a nucleus and the strength of the magnetic field it experiences (B_{exp}) is given by

$$\nu = \frac{\gamma B_{exp}}{2\pi}$$

where B = sum of the magnetic field that is externally applied and that experienced by the nucleus as a consequence of its local electronic environment and, γ is the gyromagnetic ratio unique to each nuclear type and equal to the ratio between the nuclear magnetic moment (μ) and the spin quantum number (I).

In the presence of a uniform external magnetic field (Bo) the electrons circulating any nucleus generate a much smaller, local magnetic field (B_{local}) that opposes Bo.
As a consequence, the total field strength experienced by the nuclei in the sample is reduced due to shielding from Bo by the electron cloud surrounding each nucleus.

$$B_{experienced} = B_{applied} - B_{local}$$

Since each chemical group in a molecule is in a slightly different electronic environment, each group's nucleus is shielded to a different extent. Changes in local electronic shielding, e.g. as a consequence of altered ionisation when changing pH or, as a consequence of a perturbation of the solution conformation upon phosphorylation, are therefore reflected as altered absorption frequencies.

2.5.2 Resonance positions as an indicator of conformational preference

The primary observables in a ^1H MR spectrum are the resonance energies (chemical shifts). Since these depend on the local magnetic field experienced by each proton, they

therefore reflect the local molecular environment [Wishart and Case, 2001]. In the absence of any restriction on the conformational averaging possible for a peptide/protein molecule in solution, the resonance energy of signals from any one residue type are expected to correspond to those of a 'random coil', coming about from fast interconversion between all possible conformations. So, the closer the prevailing structure (and flexibility) of a polypeptide matches the unfolded state, the more the chemical shifts of its protons tend to correspond to their corresponding random coil values. Any dispersion observed for chemical shifts for signals of a given group type is therefore a reliable indication of local structural preference. Upfield shifts result from an increase in electronic shielding and downfield shifts from deshielding. Thus, the observation of distinctive resonance energies for nuclei of the same groups present in the same residue type located at different positions along a protein/peptide sequence is an indication of local conformational preferences.

The experimentally observed shift can, however, arise from several factors contributing to the electronic shielding environment and this complicates any attempt to characterise in detail the prevailing conformation based upon shift alone. However, the deviation of chemical shifts from their random coil values has frequently been used to qualitatively approximate the extent of structural preference [Fiaux et al, 2002]. The 'random coil' shifts used in this study as reference values were obtained from studies of small model peptides [Wüthrich, 1986]. Significant deviation from these values and/or the observation of distinctive resonance energies for nuclei of the same groups present in the same residue type located at different positions along the peptide sequence was

taken as an indication of local conformational preferences. The shifts of the sidechain groups of different residues in small peptides are listed in Appendix II.

2.5.3 Sensitivity of detection by ^{1}H NMR

The capability to detect energy absorption relies upon the population difference between the upper (excited) and lower (ground) nuclear states. A relatively small population difference ($N^{upper}/N^{lower} = e^{-\Delta E/kT}$) results from the radiofrequency energy difference between the higher and lower energy states of a ^{1}H (spin ½) nucleus experiencing a magnetic field. NMR is therefore relatively insensitive compared to UV-frequency based fluorescence spectroscopy. The natural abundance of ^{1}H however enables its more ready detection compared to ^{15}N and ^{13}C that typically requires isotope enrichment. Increased sensitivity (signal to noise) derives from the use of high (applied) fields while absorption detection in this thesis study was enhanced by use of a cryoprobe (where the detector coil and the pre-amplifier are maintained at a low operating temperature to reduce inherent noise associated with resistance to the current generated by the altered magnetisation). The sample concentration requirements for ^{1}H signal detection were therefore in the range 10^{-4} to 10^{-5} M.

2.5.4 Nuclear relaxation as indicator of complex formation

The excited nuclei undergo energy loss (relaxation) in order to return to their ground state. The probability of spontaneous relaxation is negligible because the transition energy gap is small and so relaxation to re-establish an equilibrium distribution primarily occurs by stimulated emission, for example by the transfer of energy to nearby nuclei, the lattice. The relaxation process occurs via a magnetic interaction whose efficiency depends upon the proximity of the neighbouring nuclei and the correlation time characterising that proximity. Namely, relaxation relies upon fluctuating dipolar

interactions produced by fluctuating local magnetic fields generated by molecular motions. The efficiency of relaxation therefore depends on the extent of the overlap between the frequency spectrum of the molecular motions (characterized by an overall effective correlation time) and the relevant nuclear resonance radiofrequencies. Lower frequency molecular motions are therefore fluctuations that are particularly dominant in NMR relaxation processes in proteins and peptides.

The effective correlation time of a molecule (τ_c) is a measure of the extent of the motions of any molecule in solution. It is dependent on the nature of the rotational and translational motions and reflects the residence time for a molecule in any given conformation. The correlation time for any molecule is therefore determined by factors including sample temperature, molecular mass, overall shape and the viscosity of the solvent, while intramolecular motions for individual pairs of atoms in a molecule can result in distinctive correlation times.

In the simple case of a spherical molecule undergoing isotropic motion the magnitude of the correlation time, τ_c can be approximated by Stokes' Law :-

$$\tau_c = \frac{4\,\pi\eta r^3}{3kT}$$

where η = solvent viscosity
r = radius of molecule
k = Boltzmann's constant
T = absolute temperature

Since efficiency of relaxation depends on the overlap between the range of frequencies of the molecular motions and the prevailing nuclear resonance frequencies, it can be seen that increasing molecular mass and consequent alteration of internal motions lead

to faster relaxation characteristics. Hence, while the ^{1}H signals in the spectra of the hcTnI peptides are sharp (well resolved) and therefore are indicative of rapid rotational/translational motions and relatively inefficient (intramolecular) relaxation processes, the spectrum of F-actin is relatively broad as is characteristic of its larger mass and well-defined conformation that results in correspondingly slower molecular motions (longer effective correlation time, in the tens of nanosecond range [Prochniewicz and Thomas, 1999] with resonance linewidths ~ 200 Hz.

Complex formation with F-actin restricts the molecular motions available to an isolated peptide and leads to enhanced relaxation of the peptide resonances (shown schematically in Figure 2.3).

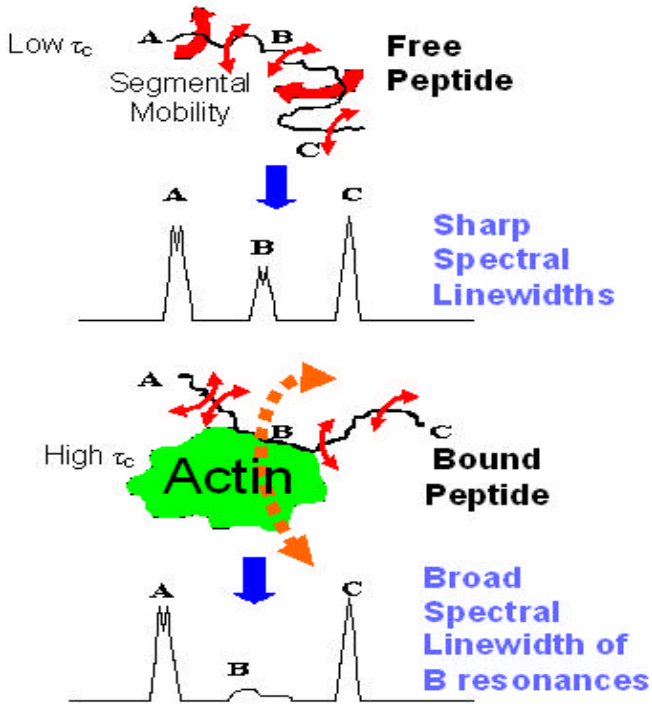

Figure 2.3 Cartoon illustrating the effect of F-actin interaction by a segment of a peptide ligand on the resonance linewidth of groups involved in contact with F-actin (B). Signals of regions of the peptide that retain mobility independent of the association with F-actin (A and C) do not show a comparably significant linewidth change.

It is the observation of more efficient relaxation of specific peptide groups in the presence of F-actin that was used in this thesis study to map the intimacy and extent of contact. Distinctively smaller/negligible relaxation perturbation was observed in the presence of hcTnC or its C-terminal domain reflecting their smaller molecular mass (and faster internal motions) compared to F-actin.

The extent of the relaxation resulting from association of any hcTnI peptide with a protein target (F-actin or hcTnC) can be inferred from the linewidth of each of the peptide resonances since that measurable parameter depends on the (transverse/spin-spin) relaxation time T_2, the lifetime of the nuclear magnetisation in the transverse plane (XY plane).

The relationship is : resonance width at half-height = linewidth = $(pT_2)^{-1}$

The linewidth (ν) of any signal can be obtained by inspection of the peptide spectrum while an increase in linewidth (signal broadening as a consequence of enhanced relaxation) correlates with an observed decrease in the signal height (intensity). This can be seen from the fact that the signal's area is dependent upon the number of contributing nuclei and that each signal can be approximated as being triangular with an area = base length x half height. Thus, the monitoring of the relative intensity of different peptide signals will report on their corresponding relaxation enhancement as a consequence of association with a protein surface acting as an effective relaxation sink (as in the case of F-actin).

An additional approach to the analysis of the relaxation enhancement resulting from complex formation with F-actin was to make use in this study of Carr Purcell two-pulse spin echo acquisitions [Carr & Purcell, 1954; Campbell et al, 1975]. This experiment type, described below, makes use of a delay introduced before the spectral acquisition pulse. Inclusion of the delay period means that rapidly relaxing nuclei do not contribute to the resulting spectrum. This spectral simplification has several benefits. First, no signal deriving from F-actin is observable provided the delay period is set to exceed the relaxation time of its nuclei (~ 2msec given the observed ~ 200 Hz linewidths, below, and consistent with its rotational correlation time [Prochniewicz et al, 1996]). Secondly, signals of groups relaxed by interaction with F-actin contribute to the spectrum but with their residual amplitude dictated by their relaxation time, thereby enabling the intimacy of contact to be extracted via inspection of the change in amplitude observed in the presence of F-actin. The third advantage of this acquisition method is that, for any given delay period, the sign of the resulting amplitude of the peptide resonances is dependent upon the fine structure of each signal that is determined by the electron-nucleus coupling constant dictated by the chemical bonding particular to each group.

The following brief description of the Carr Purcell two-pulse spin echo experiment (Figure 2.4) considers first the behaviour of a doublet resonance with components at d1 and d2 (i.e. a coupling constant equal to the magnitude of the difference between the chemical shifts, d1 and d2, that is typically some 7 Hz for the sidechains of most amino acid residues). The initial 90 degree ($\pi/2$) pulse, shown as a 90_x pulse, flips the nuclear magnetization in the xy plane to create magnetization along the -y axis. During the first

time delay, *t* , the magnetization precesses about the z axis at a rate determined by its resonance frequency (chemical shift).

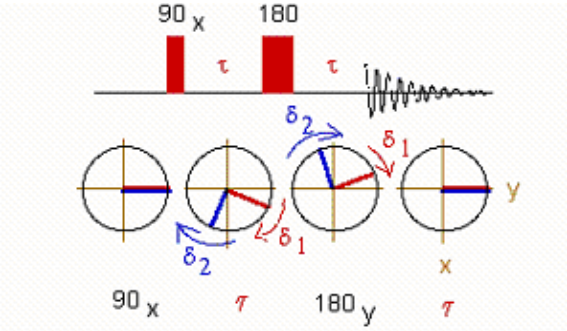

Figure 2.4 Representation of the Carr-Purcell two pulse sequence that generates the refocusing of nuclear spins (spin echo) after the second delay, t [Carr and Purcell, 1954; Campbell et al, 1975].

A 180 degree pulse is then applied (shown about the x axis in Figure 2.4) to result in the inversion of the magnetization. If the nucleus with resonance frequency d1 has precessed clockwise during the first t delay, it will have precessed by the same amount during the delay following the inversion pulse. So, by the end of the second, equal t delay, the magnetization has refocused to give rise to an echo (superposition of direction of magnetisation) after the 2 t delays. The amplitude of this echo is dependent upon the spin-spin relaxation processes and its sign (signal appearance up or down) is dependent upon the signal's coupling constant (the frequency difference between the components [Campbell et al, 1975]. These spectral properties aid the detection of the relative extent of relaxation of different groups on any hcTnI peptide that results from binding to F-actin.

2.5.5 ^{1}H-NMR spectral acquisition

1D ^{1}H-NMR spectra were obtained using a Bruker AMX500 spectrometer at 295K using a 5 kHz (10 ppm) sweep width with a delay of 3 s between acquisition pulses to allow full relaxation. Typically 128 scans were acquired using 50 μM peptide solutions

made up in 20mM Tris, pH 7.2 buffer in D_2O to a volume of 600µl. Peptides containing cysteine were reduced with DTT to decrease the probability of any disulphide bridge formation between the free peptides. Detection of linewidth perturbation was effected by both 'pulse and collect' and two-pulse spin-echo experiments, the latter using a (180-τ-90-τ) sequence with a delay time, τ = 60ms and an overall inter-acquisition delay of 4s to enable complete recovery o the magnetisation. Titration of the peptides with F-actin was carried out by addition of aliquots of F-actin (10mg/ml) or F-actin-tropomyosin (5mg/ml F-actin). Titration of the hcTnI peptides with F-actin or F-actin-tropomyosin was also on occasions carried out by the addition of small aliquots (1-5µl) of a stock solution of the peptide to 0.6 ml of solution containing F-actin at a concentration of 2.5-4.0 mg/ml.

2.6 NMR detection of dynamic equilibrium states

2.6.1 Background

The equilibrium binding of a peptide (P) to F-actin (A) is characterised by the dissociation constant, K_d, which for the simplest case of a single binding site is defined as =[P][A]/[PA]

where [P], [A] and [PA] are the equilibrium concentrations of peptide, F-actin and the complex, respectively. K_d has the units of concentration and a value of K_d ~ 100 µM implies a ratio of free to bound states ~ 1:10,000 in an equimolar mixture of 1M peptide and F-actin. Evaluation of the dissociation constant requires analysis of the equilibrium concentrations of free and bound states and the basis for this via a ligand-monitored NMR binding assay is described below.

2.6.2 Exchange between free and bound states

The rate at which the two participants in the F-actin peptide complex interconvert/exchange between their free and bound states is a critical aspect of the NMR approach to characterising their interaction. This can be readily seen from the relationship that, for 1:1 binding, K_d = the ratio k_{off}/k_{on} where k_{off} is the rate constant of the complex dissociation reaction, and k_{on} is the rate constant of the association reaction. If the association/dissociation is very rapid (diffusion-limited on rate and fast chemical exchange due to a relatively short lifetime of the bound state), then the observed response of a peptide's NMR signal is the mole-fraction weighted average of the NMR parameters of the free and bound states [Fischer & Jardetzky, 1965; Sarrazin et al, 1972] and is given by [Fielding, 2007]

$$M_{obs}=X_{L(free)}M_{L(free)}+X_{L(bound)}M_{L(bound)} \qquad \text{Equation 1}$$

where M_{obs} is the NMR observable, $X_{L(free)}$ and $X_{L(bound)}$ are the mole fractions of free and bound ligand, and $M_{L(free)}$ and $M_{L(bound)}$ are the NMR relaxation parameters of the peptide ligand in its free and bound states, respectively.

It is therefore the case that, under conditions of fast exchange, the presence of even only a few F-actin binding sites can affect the overall relaxation rates and, hence, the resonance linewidths of a relatively concentrated solution of a ligand (here the hcTnI peptide) given the marked relaxation enhancement resulting from the association with the F-actin filament. The fast exchange phenomenon is illustrated in Figure 2.5 below where extensive relaxation is observed for the signals of the entire peptide population even at a mole ratio of ~12:1 of hcTnI peptide to F-actin. Progressively greater effects

are seen in the presence of increasingly higher concentrations of F-actin, a feature of fast exchange of peptide molecules between free and bound states.

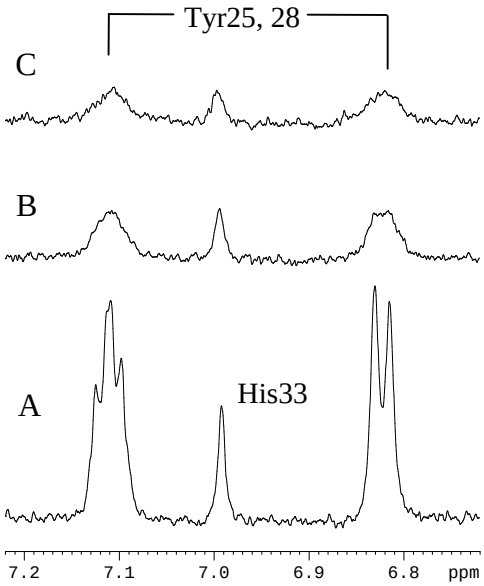

Figure 2.5 ^{1}H MR spectra of the aromatic region of 50µM hcTnI 16-37 S23P (A) in the presence of 4µM F-actin (B) and 7.5µM F-actin (C). Progressive changes in linewidth induced by increasing concentrations of F-actin here illustrated for S23P hcTnI 16-37 (SS_P) demonstrating the average signal reporting on the fast exchange equilibrium for the interaction with F-actin

The cross-relaxation that occurs when the peptide is bound to F-actin comes about as a result of nuclear-nuclear dipole interactions. When the peptide dissociates from its binding site it carries with it spin polarisation and so, binding to F-actin therefore leads to the affected nuclei in the dissociated peptide molecules being able to act as relaxation 'sinks' if they happen to interact with another target. This cross-relaxation or saturation-transfer [Roberts, 1993; Mayer and Meyer, 2001] can be used to monitor any equilibrium involving 'flitting' of the hcTnI peptide between F-actin and another partner such as hcTnC whose resonances can be separately resolved. The cross saturation process is both very efficient and very selective. Namely, in a solution containing F-actin, hcTnC and a peptide of hcTnI, the observation that a specific set of resonances of hcTnC experience saturation transfer therefore reports on the group(s) of

hcTnC affected by cross-relaxation from the hcTnI peptide that had also ‘visited’ the surface of F-actin. The difference spectrum obtained will show a response only as a consequence of interaction with hcTnC by hcTnI peptide molecules that were at some time associated with F-actin. This exchange of magnetisation between groups of hcTnC and groups of the hcTnI peptide aided the exploration of regions of hcTnI that were able to to bind in fast exchange with both hcTnC and F-actin.

The contrasting extreme of the exchange condition, slow exchange, when the affinity is very high and a long lifetime exists for the bound state, is illustrated below in the case of the interaction between hcTnI 1-64 and the C-terminal domain of hcTnC. Slow exchange conditions are apparent from the observation (Figure 2.6) of increasing contributions from signals of the bound ligand (hcTnI 1-64) with concomitant reduction in the intensity of the signals of the free ligand.

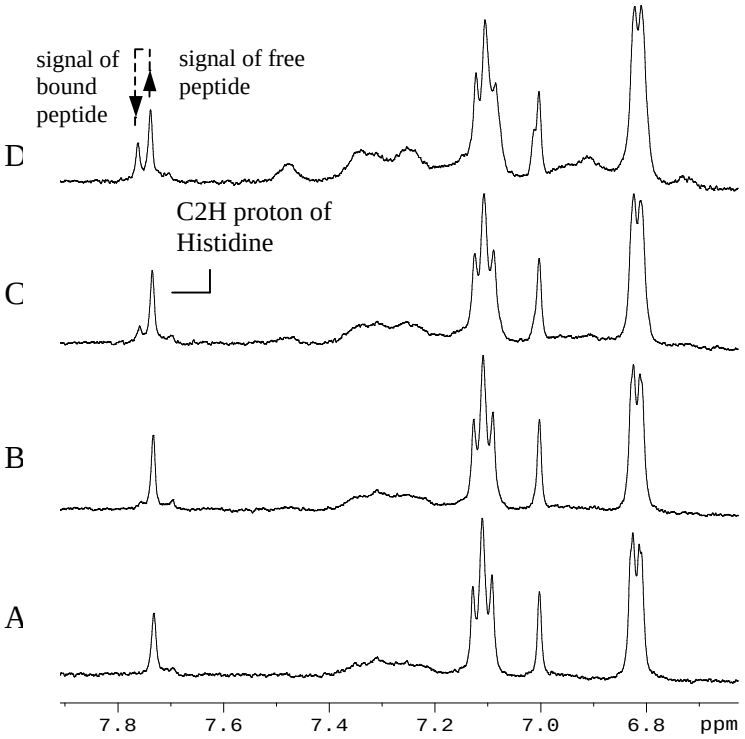

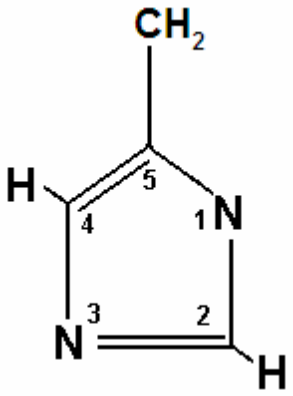

Histidine sidechain

Figure 2.6 ^{1}H MR spectra of the aromatic region of hcTnI 1-64 at different stages of titration with C-domain hcTnC·Ca^{2+}. 50μM hcTnI 1-64 (A), upon addition of 6μM C-domain hcTnC (B), addition of 12μM C-domain hcTnC (C) addition of 25μM C-domain hcTnC (D).

The observation of slow exchange conditions permits the extraction of an upper limit for the rate constant for the dissociation of the complex based upon the shift difference(s) observed between the signals of the bound and free forms [Roberts 1993, a practical approach, Chapter 6]. Under conditions of slow exchange, k_{off} << the chemical shift difference. For the example shown in Figure 2.6, using the small shifts observed for the C4H signals of His33 of hcTnI 1-64, an off rate of <<25 s^{-1} is obtained, consistent with an upper limit for K_d of 0.25 μM if a diffusion-limited on rate value of 10^8 $M^{-1}s^{-1}$ is used. Confirmation of tight complex formation was obtained by the use of non-dissociating native gel electrophoresis.

2.7 Approach to the evaluation from the NMR data of apparent K_d for hcTnI peptide interaction with F-actin

The principal advantages for the NMR assay as used in this study were that

(a) it allowed one to monitor the behaviour of signals of specific groups of defined segments of hcTnI in the absence or presence of the (potential) binding partner, F-actin, and

(b) amplification of the binding event occurred when the population of the bound species was quite low, coming about because of the existence of fast exchange conditions that enabled averaging of the peptide population.

The resulting approach taken in this work for the derivation of K_d values, detailed in Appendix III, is summarised here. When fast exchange conditions are indicated by progressive alterations in the single signal reporting on each peptide group during titration with F-actin, it can be concluded that the spectral response is proportional to the molar fraction weighted average of the bound (B) and free (F) states [Fielding, 2007]. Applying Equation 1 above, the observed (obs) resonance linewidth, υ_{obs} , is dependent upon the fraction of peptide bound , f_B and is given by $\upsilon_{obs} = \upsilon_F + f_B(\upsilon_B - \upsilon_F)$ where $f_B \sim [\text{F-actin}]/([\text{peptide}]+K_d)$ (Appendix III). Since the area under any resonance depends on the number of contributing nuclei, the resonance linewidth is correlated with the intensity (I) of each resonance.

The derivation of the following equation linking K_d to the ratio of the readily monitored signal intensity in the presence of F-actin (I_B) and that of the free peptide (I_F) is shown in Appendix III :

$$I_B/I_F = 1 \div \{1 + c[\text{F-actin}]_{total}/([P]_{total} + K_d)\} \quad \text{Equation 2}$$

where c is a constant = $\{(\upsilon_B/\upsilon_F)-1\}$.
Given the observed linewidths of the free peptides (υ_F ~ 7 Hz) and the linewidth associated with the resonances of F-actin (υ_B ~ 200 Hz) [Prochniewicz and Thomas, 1999], the value of c = 30 was used for the purpose of any calculation.

The signal intensity ratio I_B/I_F observed at any stage of the titration with F-actin at constant peptide thus reports on the mole ratio of bound:free peptide, $[P_B]/[P_F]$ and, hence, Kd.

This relationship between different values of I_B/I_F and the associated ratio of $[P_B]/[P_F]$ is illustrated in Figure 2.7A as obtained using Equation 2 for a concentration of 7.5μM F-actin and 50 μM peptide and c=30.

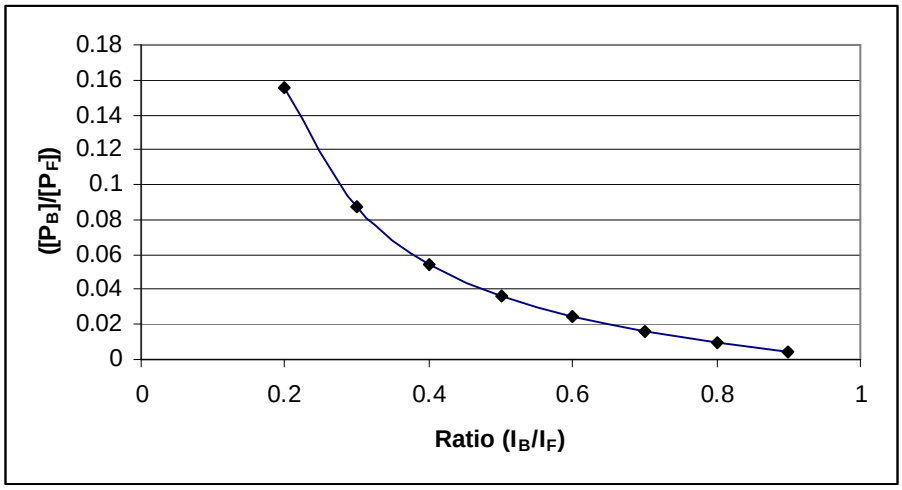

Figure 2.7A The variation of the ratio of $[P_B]/[P_F]$ reported by different values of I_B/I_F as calculated using c=30 for a solution containing 7.5μM F-actin and 50μM peptide.

The correspondence between different possible observable signal intensity ratios, I_B/I_F , and the K_d estimated from the associated proportion of bound:free peptide at concentration of 7.5μM F-actin and 50 μM peptide (Figure 2.7A) is illustrated in Figure

2.7B. The $\log_{10}$ scale used for K_d in Figure 2.7B displays the range of K_d values (mM range down to ~5μM) accessible by the NMR assay. Figure 2.7B also shows the imprecision inherent in K_d evaluation as a consequence of errors in the measurement of signal intensity changes. The estimated values of K_d quoted in this thesis were therefore based on the I_B/I_F ratios observed for different signals and at different stages of titration with F-actin (i.e. using an average over a set of observations for a given peptide). As also suggested by Figure 2.7B, the quantitation enabled by this approach could be most confidently used to compare the relative K_d of peptides that displayed I_B/I_F ratios differing by at least ~ 0.2.

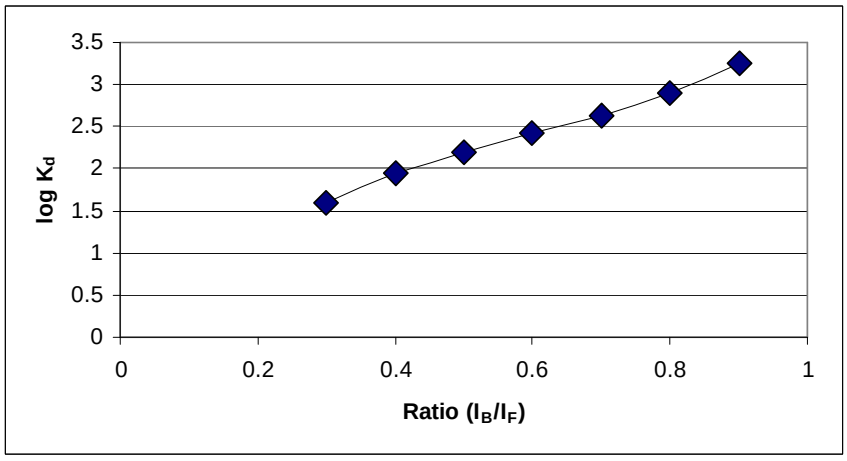

Figure 2.7B The values of $\log_{10} K_d$ reported by different I_B/I_F as calculated using c=30 for a solution containing 7.5μM F-actin and 50μM peptide.

It should also be emphasised that the approach taken to extract K_d from the data assumed the presence of 1:1 association between hcTnI peptide and F-actin and, the absence of any contribution to the spectral perturbation (and hence, I_B) resulting from other, non-specific, binding. Any collisional, non-specific binding was expected to result in generalised broadening that was equivalent for all resonances and so K_d data was only extracted from spectra showing that specific signals were affected more than

others. The possibility of multiple binding modes (i.e. more than a single 1:1 complex) contributing to the spectral perturbations was more challenging to gauge (see "Results" chapters for the tactic taken) and so apparent K_d values are quoted.

2.8 Detection of hcTnC interaction with hcTnI 1-64 by native gel electrophoresis

Native gel electrophoresis was used for monitoring the interaction of hcTnI 1-64 with hcTnC and, its isolated N- and C-domain constructs. hcTnI 1-64 was dissolved in 10mM glycine, 30mM Tris (pH 8.6), 1mM $CaCl_2$, 10% (v/v) glycerol and 1% (v/v) mercaptoethanol (final concentration of 100µM) and was mixed with hcTnC or its domain constructs (molar ratio protein/hcTnI 1-64 1:1). After incubation for 10–15 min at room temperature the 40µl samples were subjected to native gel electrophoresis on 10% gels in running buffer containing 25mM Tris, 80mM Glycine and 10% glycerol. Samples were run in the presence of 1mM $CaCl_2$. Gels were stained with Coomassie Blue R250 and scanned.

3 The N-terminus of hcTnI contains a specific F-actin binding region

In its unphosphorylated state, the isoform-specific N-terminal extension of hcTnI is believed to be able to interact with the N-terminal domain of cTnC; however the details of this reportedly weak association are not well characterised [Sadayappan et al, 2008]. Studies of transgenic mice overexpressing the deletion of mouse cTnI residues 2-11 identified a resulting reduction in cardiac myofibrillar maximal Mg^{2+}-ATPase activity and absolute force without alteration in Ca^{2+} affinity [Sadayappan et al, 2008]. Transgenic mice that expressed a longer deletion, mouse cTnI residues 2–28 showed a faster rate of myocardial relaxation [Barbato et al, 2005]. The observed increase in crossbridge cycling rate correlated with reduced Ca^{2+} affinity that would lead to faster relaxation by increasing the rate of thin filament deactivation. It was unclear, however, whether the deletion of residues 2-28 at the N-terminus of cTnI impacted directly on the rate of Ca^{2+} dissociation from cTnC or whether the deletion influenced the rate of crossbridge detachment during relaxation via the separate modulation of other thin-filament protein interactions. The possibility that the N-terminus of cTnI may associate with F-actin and with F-actin tropomyosin is therefore first examined here. Binding assays using a variety of peptides comprising different regions of the sequence of the N-terminal extension of hcTnI were carried out by ^{1}H NMR spectroscopy. The data identified an interaction with F-actin by a specific segment within the N-terminal region of hcTnI. These studies were subsequently extended using actin-binding regions of human cardiac myosin as peptide probes. These studies reported on the specificity and consequences of the observed association between F-actin and the N-terminal extension of hcTnI.

3.1 Characterisation of the interaction of F-actin with the N-terminus of hcTnI

Since F-actin is a large fibrous protein assembly it gives rise to a generally broad ^{1}H NMR spectrum that contrasts, for example, with the better resolved spectrum of monomeric G-actin [Slósarek et al, 1994]. The greater linewidths found for signals of F-actin are due to its slow rotational tumbling and the associated short nuclear relaxation times of the filamentous structure's ^{1}H nuclei (typical relaxation time of some 5 msec and resulting linewidth ~ 200 Hz), [Slósarek et al, 1994] compared to those of a much smaller, freely tumbling peptide molecule (linewidths ~ 5-10Hz). Two advantages derive from the poor resolution of the F-actin resonances. Namely, F-actin resonances hardly contribute to the spectrum of a mixture of F-actin and a potential peptide ligand. The peptide resonances can then be directly resolved. Secondly, since F-actin acts as a relaxation sink for molecules that it interacts with, association with a peptide ligand can be characterised by changes in the peptide resonances of groups at the peptide/F-actin interface. Binding to F-actin would therefore be expected to result in an increased linewidth of the ^{1}H signals from groups of the peptide whose mobility was constrained by the interaction, consistent with a longer correlation time (slower tumbling) of the bound peptide. Analysis of the nature and specificity of any observed interaction comes about from characterisation of the extent of the peptide sequence whose mobility is altered and, from the dependence of the interaction upon factors such as ionic strength and competing ligands.

3.2 A restricted segment of hcTnI residues 1-30 interacts with F-actin

The first investigation into whether the N-terminus of hcTnI contained an actin binding region made use of an unblocked peptide (N and C-terminal residues), hcTnI residues

1-30, that corresponded to almost the entire N-terminal extension of cTnI. The ability of this peptide to associate with F-actin was monitored by ^{1}H NMR during a titration with increasing concentrations of F-actin. Sidechain signals originating from different residues along the hcTnI 1-30 sequence were used as specific monitors of any relaxation effects resulting from the presence of F-actin. A prerequisite to characterisation of F-actin binding determinants was the identification of the signal(s) corresponding to each type of residue. This was in the first instance obtained by examination of the value of the absorption energy (chemical shift) that is known to be characteristic of different sidechain groups [Wüthrich, 1986]. Where relevant to the interpretation of the data, the correlations between particular signals and specific residues were subsequently confirmed by the use of overlapping sequences as described below.

Guided by the spectral data available from studies of the resonances of different residues in short (and hence expected to be flexible/unstructured) peptide sequences (Appendix II), it was possible to assign the sidechain signals of several residues of hcTnI 1-30 on the basis of the homology in their chemical shift positions (Figure 3.1, below). Readily identified were sidechain resonances of:- Ala1, Asp2 and 6, Ile18, Asn24, Tyr25, 28 and, Thr30. As seen from the primary structure of hcTnI 1-30

ADGSSDAAREPRPAPAPIRRRSSNYRAYAT

this meant that residues uniquely located in the N- and the C- termini of the peptide provided reporter signals for specific locations along the sequence and hence the means by which any interacting region(s) could be identified.

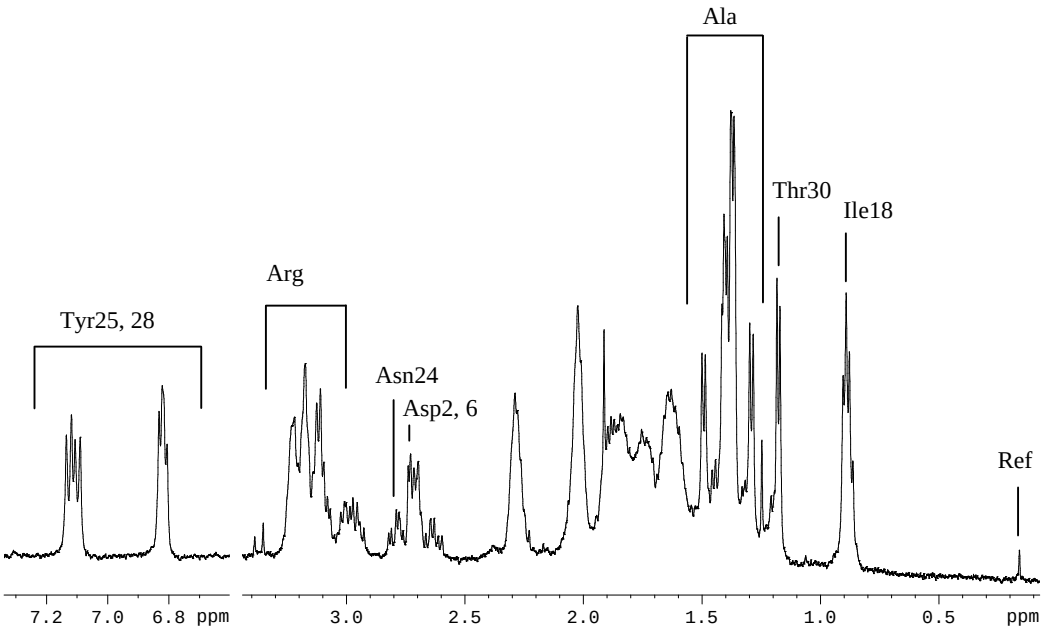

Figure 3.1 ^{1}H MR spectrum of 50µM hcTnI 1-30. This shows identifiable amino acid sidechain signals that can be monitored before and after F-actin titration. The spectral region in the vicinity of the signal from water (3.5-4.5ppm) has been omitted pH 7.2, T=298K.

Further, consistent with the sharp resonances and resolvable fine structure observed, the correlation found between signal position for the sidechains of the different residue types (Ala, Arg, Asn, Asp, Ile, Thr and Tyr, Fig 3.1) that were reported in studies of small flexible peptides suggesting that hcTnI 1-30 lacked any long-lived (correlated) regular secondary structure. The observation of some dispersion of the chemical shift positions for specific sidechain groups (e.g. from left to right in Fig 3.1, Tyr C2,6H at ~7.15ppm, Arginine δCH_2 at ~ 3.2ppm , Asp/Asn βCH_2 at ~2.7ppm and, Ala βCH_3 at ~ 1.4ppm) however indicated local variability in the shielding environment of the corresponding groups This meant that identical sidechain groups do not have identical electron environments. The dispersion in the resonance energies from groups of the same type suggested the existence of a conformational preference at their different sequence locations. The restriction on the conformational averaging that is possible in solution and that would result in such (or more substantial) shielding differences will be

taken up in a later chapter in this thesis. In the context here of the study of F-actin binding, the observed dispersion in chemical shifts in the spectrum of hcTnI 1-30 was used simply as a means for distinguishing sidechains deriving from the same residue type.

Figure 3.2 compares the spectrum of hcTnI 1-30 with that obtained during titration with F-actin. Progressive changes in resonance lineshape of specific signals were observed with increasing concentration of F-actin. Since each resonance reflects the entire population of the corresponding groups of hcTnI 1-30, these progressive effects indicated the existence of a dynamic equilibrium involving rapid interconversion between free and F-actin bound populations, i.e. taking place on the fast exchange timescale. The extent of the signal broadening effects increased during titration consistent with an increase in the population bound to F-actin. The titration enabled the resolution of the relative broadening effects for the different signals (difference spectrum shown in Figure 3.2C, below) and thereby identified the nature of the residues most constrained by the observed association of hcTnI 1-30 with the surface of F-actin.

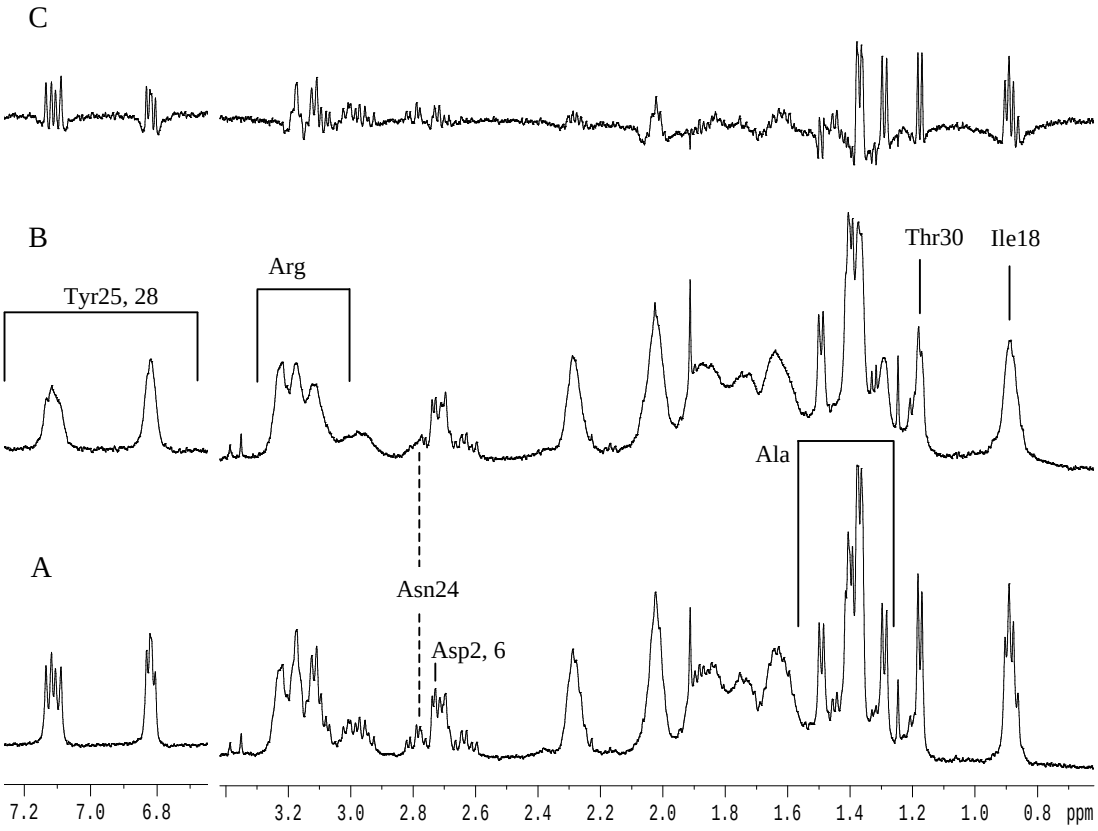

Figure 3.2 The C-terminus of hcTnI 1-30 interacts with F-actin. ^{1}H MR spectrum of 50µM hcTnI 1-30 (A) and in the presence of 7.5µM F-actin (B) and a difference spectrum (C). The peaks observed in the difference spectrum are those most affected in the presence of F-actin, e.g. Ile18, Tyr25, 28 and Thr30. Peaks that are not prominent in the difference spectrum are less affected by interaction with F-actin e.g. Asp2, 6 and an alanine signal at 1.5ppm, possibly originating from the N-terminal alanine (Ala1), pH 7.2, T=298K.

The difference spectrum shows the quite remarkable selectivity of the relaxation effects that resulted from the presence of F-actin. This observation served to illustrate that the association between hcTnI 1-30 and F-actin involved specific binding determinants. Non-specific binding (or viscosity changes potentially arising upon the addition of F-actin) would have been expected to lead to generalised broadening effects detectable on all the peptide signals in contrast to the selective resonance relaxation observed during titration. The contribution to the difference spectrum of the sidechain signals of Ile18 (0.9ppm), Tyr25, 28 (6.8 and 7.1ppm) and Thr30 (1.2ppm) signal, along with the lack

of detectable changes for sidechain signals of Asp2 and 6 (2.7ppm), identified the C-terminal region of hcTnI 1-30 as making intimate contact with F-actin.

Confirmation that the mobility of the region preceding Ile18 was comparatively unaffected by association of hcTnI 1-30 with F-actin was obtained by study of hcTnI residues 1-18. The spectra acquired during titration of hcTnI 1-18 with F-actin revealed no detectable linebroadening when monitored up to the 2:1 mole ratio of peptide to F-actin used in the experiment (Figure 3.3).

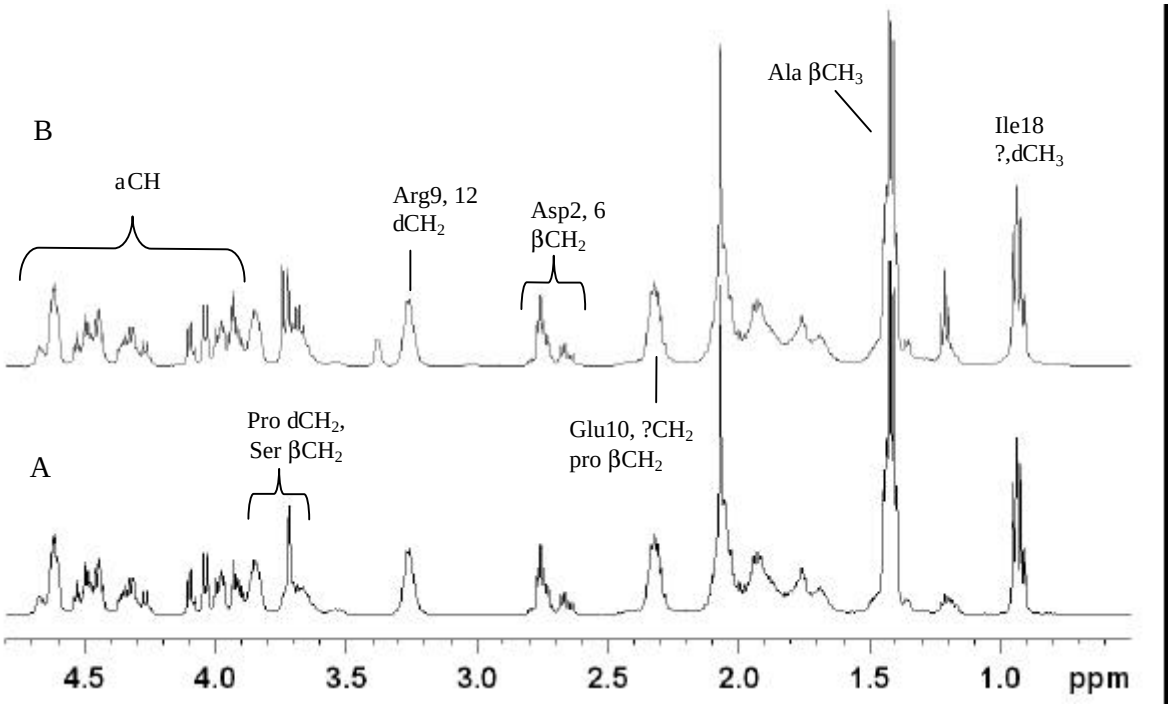

Figure 3.3 The lack of interaction between F-actin and hcTnI 1-18 is demonstrated by the absence of detectable broadening. ^{1}H MR spectrum of 100μM hcTnI 1-18 (A) and upon addition of 50μM F-actin (B). The assignment of the signals of hcTnI 1-18 was based upon their chemical shifts. The corresponding resonance positions were also observed in the spectrum of hcTnI 1-30 enabling the assignment of the signals of the residues at the N-terminus of the peptide – as labelled in Figure 3.2, pH 7.2, T=298K.

These observations showed that the actin binding properties of the N-terminal hcTnI residues 1-30 are not reliant upon residues 1-18 and, that the primary anchor residues

must be located in the C-terminal portion of hcTnI 1-30. This study further provided a separate control experiment showing that addition of the relatively viscous F-actin solution did not affect signal sharpness or intensity. It also enabled the identification to residues 1-18 of specific signals in the spectrum of hcTnI 1-30 on the basis of their observed chemical shifts. These signal assignments included the distinct resonance positions in the hcTnI 1-30 spectrum (Figure 3.2) for the βCH_2 sidechain groups of Asp 2 and 6, the δCH_2 sidechain groups of Arg 9 and 12, as well as the chemical shifts for the proline sidechain protons and the βCH_3 groups of the alanine residues that preceded proline in the sequence (i.e. A-P-A-P). A more expansive characterisation of the hcTnI 1-30 binding determinants was therefore possible and the analysis below begins with consideration of the sidechain signals of Tyr25 and 28, the only aromatic residues in the sequence.

Resolvable chemical shift differences were observed for each of the C2,6H (7.1ppm) and C3,5H (6.8ppm) sidechain signals of Tyr25 and 28 (Figure 3.4). The differing resonance position of Tyr25 and Tyr28 C2,6H protons (near the backbone) indicated that their ring protons experience distinct shielding environments that reflected sidechain orientations arising from a conformational preference for the corresponding segment of the peptide chain. Equivalent line broadening occurred for both sidechains in the presence of F-actin (Figure 3.4B) and indicated that the segment encompassing both Tyr25 and Tyr 28 came into contact with the actin surface.

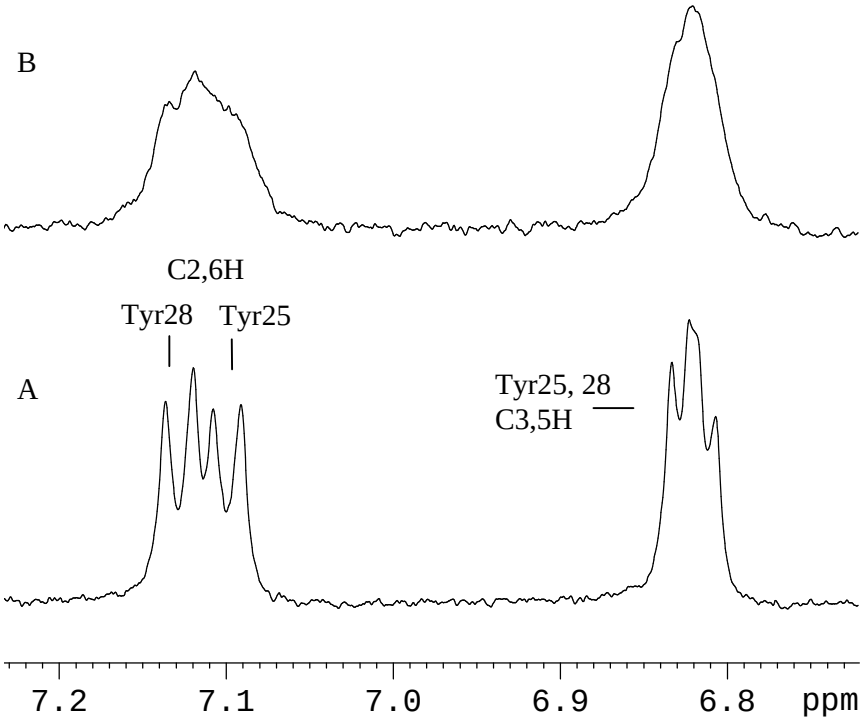

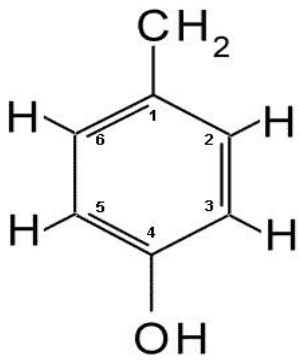

Tyrosine sidechain

Figure 3.4 The aromatic region of hcTnI 1-30 and upon F-actin titration**.** ^{1}H MR aromatic region of the spectrum of 50µM hcTnI 1-30 (A) and in the presence of 7.5µM F-actin (B). The assignment of the separate signals of Tyr25 and Tyr28 was obtained by Keane et al 1997. There is not currently a separate assignment for the C3,5H protons of Tyr25, 28 at 6.8ppm, pH 7.2, T=298K.

Consistent with the involvement of Tyr25, 28 in binding was the linebroadening of the signal of the Asn24 βCH_2 group that in the free peptide gave rise to distinct resonances for each of its two protons. This provided a further reflection of the conformational preference characteristic of this C-terminal segment of the molecule (Figure 3.5). The limited residue span contributing to the contact between hcTnI 1-30 and F-actin could be inferred from the comparatively small number of backbone CαH that experienced enhanced relaxation and from the observation that contribution to the difference spectrum arising from arginine sidechain groups derived only from those in the hcTnI residue range 19-26 (Figure 3.5C).

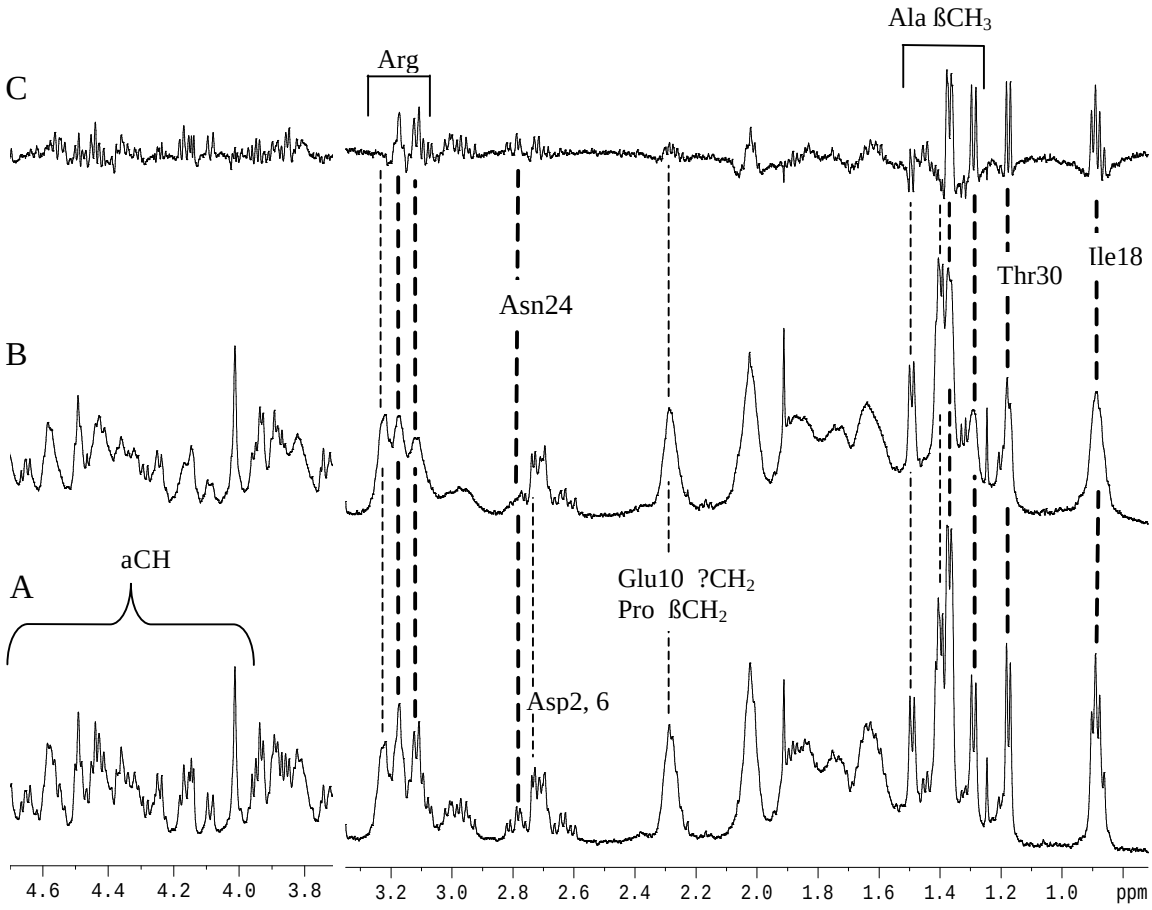

Figure 3.5 Expansion of ^{1}H MR 0.9-4.6ppm region of the spectrum of 50µM hcTnI 1-30 (A) and in the presence of 7.5µM F-actin (B) difference spectrum (C), pH 7.2, T=298K.

Inspection of the upfield region of the hcTnI 1-30 spectrum (range ~1.2-1.5ppm, Fig 3.5) identified the distinctive resonance positions of the βCH_3 from alanine residues in the sequence, with Ala1 at 1.5ppm and additional signals of Ala27 and Ala29, one within the signal at 1.4ppm and the other giving rise to an additional signal at 1.3ppm assignments. While the downfield shifted resonance of Ala1 (1.5ppm) could be ascribed to its positively charged amino terminal (NH_3^+) , the upfield shift of Ala27 or 29 (1.3ppm) reflected a conformational preference also suggested by the shifts of Asn24, Tyr25 and Tyr28. Evidence in support of the selective binding of this more structured C-terminal segment of hcTnI 1-30 to F-actin came from the marked

broadening of the sidechain resonances of Ala27 or 29 and Thr30 (Figure 3.5). Together with the observed linewidth increase for the sidechain of Ile18 and, the relative lack of perturbation reported by signals of Ala1, Asp2, Asp6 and the proline residues, these data demarcated the extent of the interaction between hcTnI 1-30 and F-actin. The data also indicated that the region N-terminal to Ile18 retained substantial mobility independent of F-actin, extending away from the bound C-terminal segment.

3.3 Characterisation of the interaction of the C-terminus of hcTnI 1-30 with F-actin

With a view to obtaining a more quantitative interpretation of the relaxation effects induced by interaction with F-actin and aiming to derive an estimate of the affinity of the peptide for F-actin, the Carr-Purcell (CP) two-pulse spin echo approach was also used to acquire spectra during the titration. As described in Chapter 2, this acquisition mode allows signals to be observed with an intensity that directly reflected the prevailing T_2 relaxation time of the corresponding nuclei while groups/nuclei that relax during the acquisition delay interval (2τ) do not contribute to the spectrum. Increased relaxation of resonances of hcTnI 1-30 as a consequence of binding to F-actin could therefore be monitored directly through the changes in signal amplitude, while the inherently broad signals of F-actin were absent from the CP spectrum obtained. As illustrated in Figure 3.6A, it was also possible using a suitable delay interval (τ=60 msec) to distinguish doublet signals that appear negative in the CP spectrum (eg the sidechain signals of Tyr, the βCH_3 groups of Ala, γCH_3 of Thr and γCH_3 of Ile) from singlet/triplet signals that appear positive (here, the dCH_3 triplet signals of Ile) and thereby compare the reduction in amplitude arising from enhanced relaxation as a function of added F-actin.

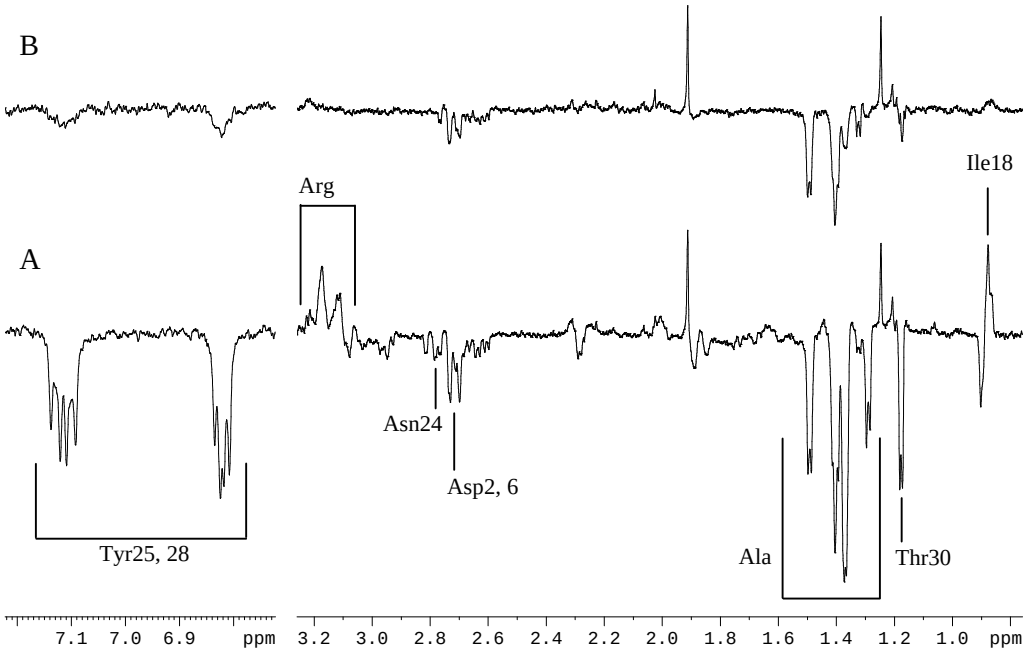

Figure 3.6 ^{1}H MR two pulse spin echo spectrum of 50µM hcTnI 1-30 (A) and in the presence of 7.5µM F-actin (B) pH 7.2, T=298K.

Figure 3.6B presents the CP spectrum obtained at a mole ratio of peptide:F-actin of ~3:1. The spectral change (Fig 3.6A vs 3.6B) illustrates that the magnitude of the reduction in relaxation time reported by the sidechains of Ile-18, Tyr-25 and 28, Ala 27/29 and Thr-30 as a consequence of their association with the surface of F-actin was some 4-fold greater than that experienced by the alanine residues located in the N-terminal segment that displayed a shorter correlation time and retained rotational mobility independent of F-actin.

Using the decrease in peak heights that resulted from the addition of F-actin into solution at an effectively constant peptide concentration (dilution effects = 5%), it was possible to evaluate the fraction of the peptide population that was bound (f_B) and hence, obtain an estimate for the dissociation constant for the F-actin – peptide complex (relationship derived in Appendix III). This estimate involved the measurement of the

ratio of the peptide peak height(s) in the presence and absence of F-actin (I_B/I_F) at any given concentration of F-actin and made use of the proportional change in peptide linewidth during titration that came about from the bound peptide resonance(s) adopting the linewidth of F-actin. Namely, under the observed conditions of fast exchange, the observed (obs) resonance linewidth (υ_{obs}) is given by:-

$\upsilon_{obs} = \upsilon_F + f_B(\upsilon_B - \upsilon_F)$ where f_B ~ [actin]/([peptide]+K_d) (see Chapter 2). Since the peptide linewidth when bound (B) to F-actin was significantly greater than that for the free (F) peptide, the ratio of the peptide linewidth(s) in the presence and absence of F-actin represented the prevailing concentration of free peptide (Chapter 2 and Appendix III).

The linewidth changes for the hcTnI 1-30 peptide as compiled from the spectra shown in Figures 3.2, 3.3, 3.4, and 3.6 yielded an estimate for K_d in the range 200-400 μM (calculation shown in Chapter 2). While this value for K_d is of the same order of magnitude as to that reported for the binding of the cTnI switch peptide to cTnC [Baryshnikova et al, 2008] or, for example, for the association of tyrosine phosphorylated peptides to some SH2 domains of [Zhou et al, 1995], it is two orders of magnitude higher than the reported K_d for actin binding by thymosin [Webber et al, 1992] or the hcTnI inhibitory region peptide [Patchell et al, 2002]. In view of the observed contribution of the C-terminus of hcTnI 1-30 to the interaction with F-actin, it was therefore relevant to study the binding properties of an equivalent peptide blocked at its N- and C-terminal residues.

The nature of the resonances perturbed by F-actin binding to the blocked hcTnI 1-30 peptide was unaltered but, as shown in Fig 3.7Aii, marked spectral changes were observed even at the lowest concentrations of added F-actin. While it was of note that amidation of the C-terminal Thr 30 had affected the chemical shift dispersion of the C2,6H resonances of Tyr25 and 28 (Fig 3.7Ai), indicative of an effect of the negative charge on the average conformation adopted by this segment, the spectral data for the blocked hcTnI 1-30 peptide also provided evidence that the charge on the C-terminal carboxylate impeded the binding to F-actin. Therefore it is suggested that the blocked form (similar to the chemical nature of this region in the intact protein) has an affinity for F-actin higher than the unblocked peptide. The derived K_d for the blocked hcTnI 1-30 peptide was in the range 30-50μM, indicating a 10-fold increase in affinity as a result of the neutralisation of the charge on Thr30.

Given the inference from these data of a previously unidentified actin binding site that exists in N-terminal extension of cTnI, the specificity of the interaction of hcTnI 1-30 with F-actin was explored by study of the consequence of the presence of the hcTnI inhibitory region, residues 128-153.

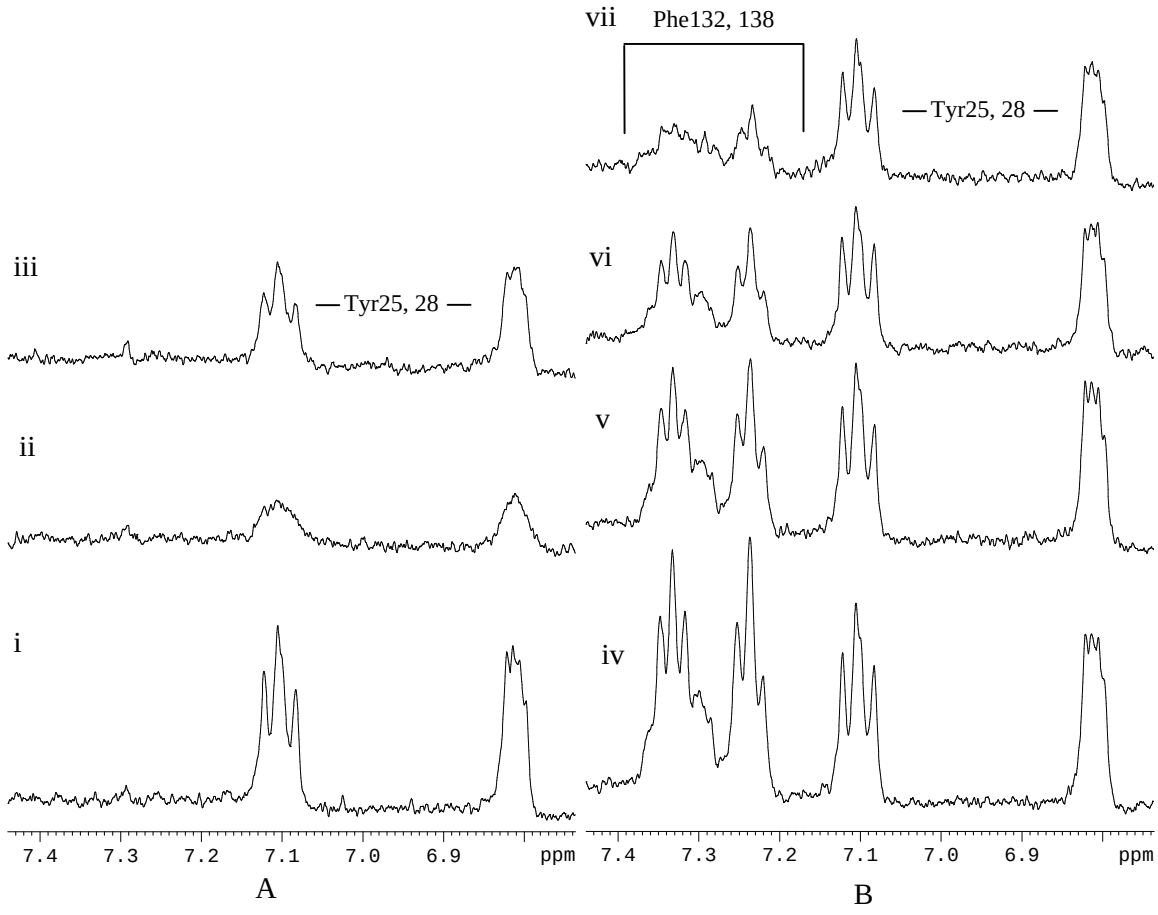

Figure 3.7 The ability of hcTnI 1-30 to interact with F-actin is reduced in the presence of hcTnI 128-153. ^{1}H MR of the aromatic region of the spectrum of 50μM hcTnI 1-30 (Ai) in the presence of 4μM F-actin (Aii) and then 6μM addition of hcTnI 128-153 (inhibitory peptide) (Aiii). This is compared to 50μM hcTnI 1-30 in the presence of 50μM hcTnI 128-153 (the inhibitory peptide) (Biv) upon addition of 4μM F-actin (Bv) 7.5μM F-actin (Bvi) and 15μM F-actin (Bvii). pH 7.2, T=298K.

As seen from Fig 3.7Aiii, the addition of the inhibitory peptide (mole ratio ~25:2:3 hcTnI 1-30:actin:inhibitory region) resulted in a reduced spectral perturbation of hcTnI 1-30 (compare Fig 3.7Aii and 3.7Aiii) reflecting a decrease in the population of hcTnI 1-30 bound to F-actin (derived apparent K_d ~ 200 μM in the presence of the inhibitory peptide). The data suggested a ~ 10-fold decrease in bound hcTnI 1-30 under these solution conditions but, from these observations alone, it was not possible to distinguish whether the two peptides competed for the same site or, whether the mechanism for the observed antagonism was non-competitive in nature. Titration of an equimolar mixture

of hcTnI 1-30 and hcTnI 128-153 was therefore carried out (Fig 3.7B). This approach was aimed at quantifying the relative binding affinity of the two peptides. At the initial F-actin concentration used in the titration (mole ratio ~12:1 of each peptide : F-actin) saturation of F-actin binding by hcTnI 128-153 was anticipated given its K_d (~ 3μM, [Patchell et al, 2002]). The data in Fig 3.7B indeed showed the more rapid decrease in signal intensity of the inhibitory peptide resonances of Phe 132 and 138 compared to the gradual change with added F-actin that was observed for the signals of Tyr 25 and 28. The concurrence of these spectral changes upon each addition of F-actin however suggested that both peptides were able to simultaneously interact with F-actin and, that their binding was 'non-competitive'.

The variation in signal intensity for each peptide was used to obtain the ratio of bound:free peptide at the different concentrations of F-actin. The relative slopes of the plots of these data (Fig 3.8) identified a 5-fold higher affinity of the inhibitory peptide for F-actin compared to hcTnI 1-30.

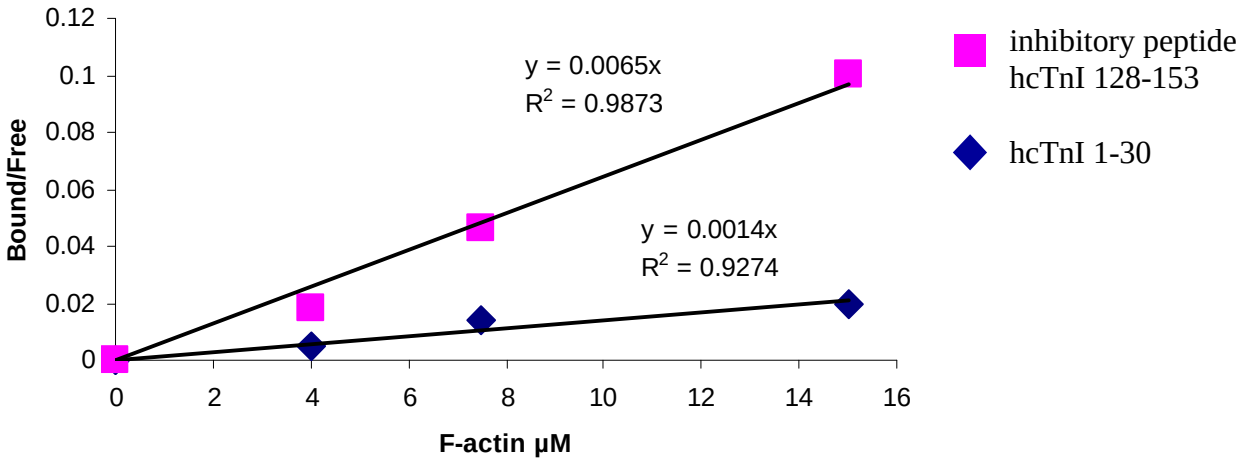

Figure 3.8 Estimation of the relative affinity of hcTnI 1-30 and hcTnI 128-153 for F-actin. The ratio of bound to free peptide (Y-axis) was obtained from the intensity of each peptide's signals at different concentrations of F-actin relative to the corresponding resonance intensity in the spectrum of the free peptide (Appendix III). The gradient of the plot ([P]B/[P]F)/[F-actin]Total provides an estimate of each peptide's affinity as derived using this approach (Appendix III). The ratio of the slopes ~5:1, is an indication of their relative affinities.

The apparent K_d , estimated from the titration data for each peptide in the mixture, and confirmed by separately fitting the bound and free concentrations shown in Fig 3.8 to a 1:1 binding curve, were 650±100 µM for hcTnI 1-30 and 110±30 µM for hcTnI 128-153. These apparent K_d values reflected the extent to which the binding of each peptide influenced the other's affinity for F-actin and this was modelled on the basis of a non-competitive binding scheme (below).

A + (1-30) ? A.(1-30)

? ?

+ (128-153) +(128-153)

? ?

A(128-153) +(1-30) ? A.(128-153).(1-30)

Based on this scheme it was possible to estimate the extent to which the binding of one peptide altered the affinity of F-actin for the other peptide via evaluation of the constant, α, in the expression:

$$Kapp = K_d (1 + [\text{'Inhibitor'}]/K_I) / (1 + [\text{'Inhibitor'}]/\alpha K_I)$$

A value of $\alpha \sim 2.5$ was thus derived for the inhibition of hcTnI 1-30 binding by hcTnI 128-153 while the reverse inhibition yielded a lower limit for α of greater than 10. Even qualitatively, these observations suggested that the two peptides influenced each others binding and showed the ability of the N-terminus of hcTnI to affect the binding equilibrium of the inhibitory region. This 'cross-talk' possibility represented a previously uncharacterized potential mechanism for regulating contractile activity in a manner specific to cardiac TnI.

The conclusion that the N-terminal extension of hcTnI and the inhibitory region are both able to interact with F-actin raised the question of what factors could be introduced to modulate either (or both) interactions. The strategy adopted here was to study the consequence of the addition of calcium saturated hcTnC into the mixture containing hcTnI 1-30, hcTnI 128-153 and F-actin as shown in Figure 3.9.

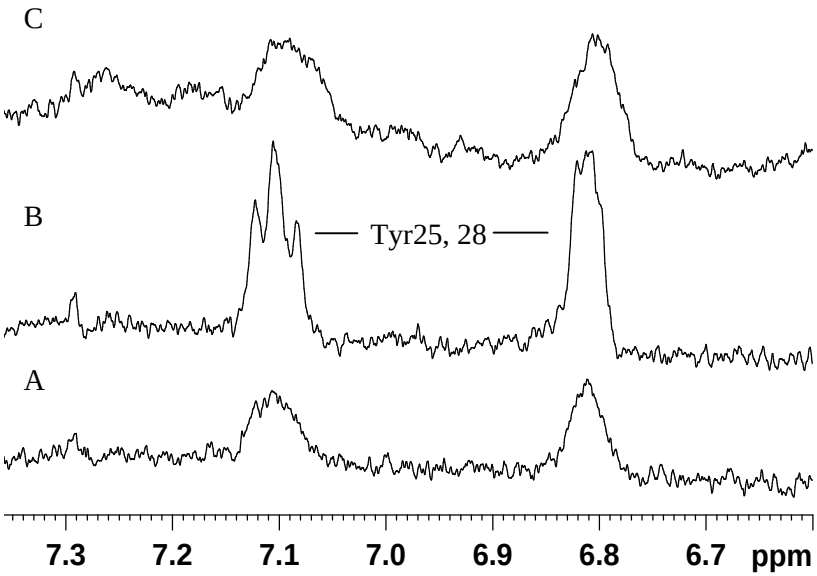

Figure 3.9 The binding of hcTnI 128-153 by calcium-saturated hcTnC allows hcTnI 1-30 to interact with F-actin. ^{1}H MR of the aromatic region of the spectrum of 50µM hcTnI 1-30 (N- and C-termini blocked) in the presence of 4µM F-actin (A) upon addition of 6µM hcTnI 128-153 (inhibitory peptide) (B) and upon addition of 8µM hcTnC·Ca^{2+} (C). F-actin induced broadening of Tyr25, 28 was observed upon addition of hcTnC·Ca^{2+} indicating that hcTnI 128-153 had been removed from F-actin, pH 7.2, T=298K.

It was anticipated that, in the presence of hcTnC, the hcTnI inhibitory region would swap from being bound to F-actin to being bound by hcTnC and that a similar switch in bound population may also occur for hcTnI 1-30 since the N-terminal extension of hcTnI was also expected to associate with hcTnC. Figure 3.9C demonstrates the change in intensity of the signals of Tyr25, 28 of hcTnI 1-30 upon addition of hcTnC. The linebroadening observed, consistent with an increase in the F-actin bound population of hcTnI 1-30, indicated the relocation of the inhibitory region to being primarily associated with hcTnC.

Interaction with the ~18kDa hcTnC was not expected to result in significant linebroadening given its relatively short rotational correlation time compared to that of F-actin (as is explored further in the next chapter). Thus, the observation reflected in

the linebroadening of Tyr25, 28 indicated that in the presence of hcTnC, the population of hcTnI 1-30 bound to F-actin had increased. This supported the notion that the N-terminal extension of hcTnI is more stably associated with F-actin than with calcium bound hcTnC.

3.4 Investigation of the extent of the binding determinants for the interaction between the N-terminus of hcTnI and F-actin

The observation that binding to F-actin involved the C-terminal 'half' of hcTnI 1-30 led to the study of a peptide starting at residue 16 and extending the C-terminus to residue 41 (hcTnI 16-41). This peptide sequence contained residues at its C-terminus that provided additional reporter groups (His33, Lys35-37 and 39).

16-APIRRRSSNYRAYATEPHAKKKSKIS-41

The interaction observed between hcTnI 16-41 and F-actin was again judged by spectral changes of different peptide signals upon titration (Fig 3.10).

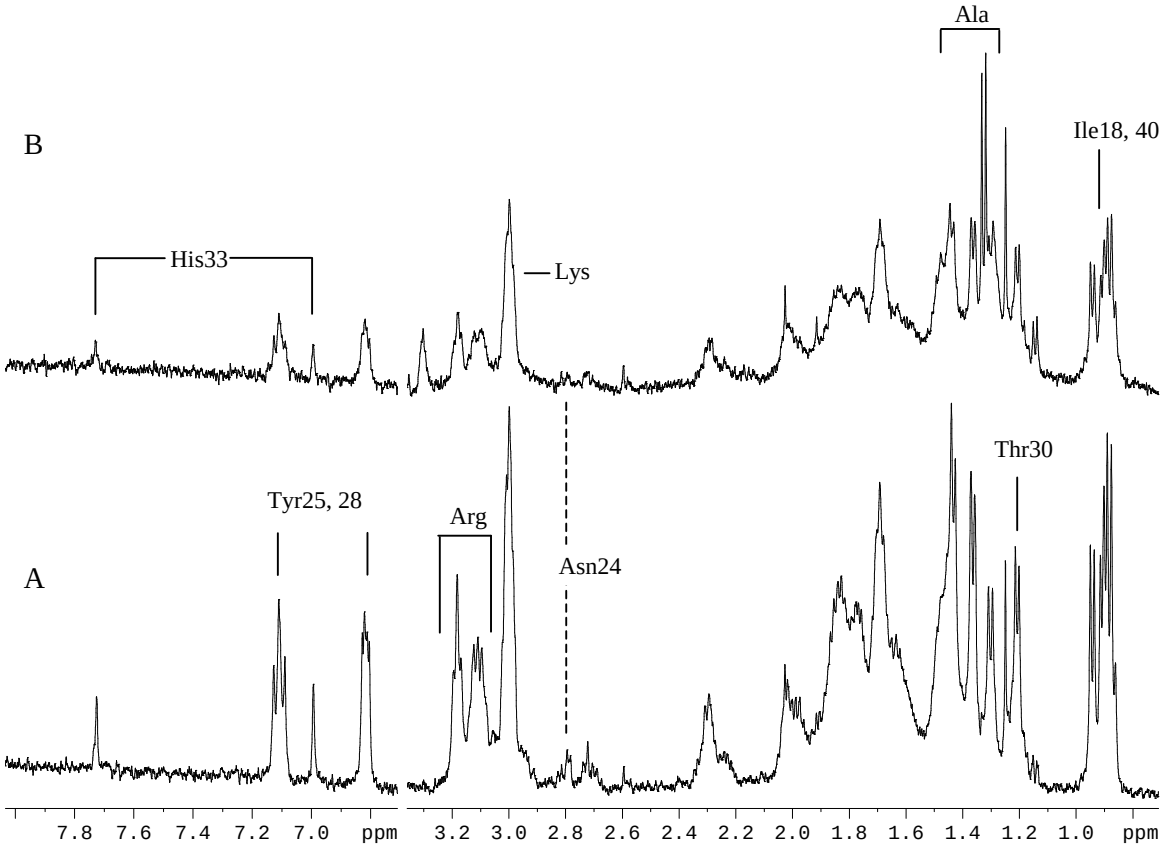

Figure 3.10 Interaction between F-actin and hcTnI 16-41 involves the entire peptide. ^{1}H MR of the spectrum of 50μM hcTnI 16-41 (A) in the presence of 12μM F-actin (B). Signals from the N-terminus of peptide are affected; Ile18, Asn24 and Tyr25, 28 as well as those from the C-terminus Ile40, Lys, His33, pH 7.2, T=298K.

Progressive alteration in signal intensity was observed for many of the peptide signals (Fig 3.10). The occurrence of broadening for signals of residues at different locations along the peptide sequence (Ile18, Arg, Asn24, Tyr25, 28, Thr30 and the Lys residues at the C-terminus) indicated that the entire length of the peptide was being relaxed by contact with F-actin. This observation supported the idea that the association of this N-terminal region of hcTnI with F-actin was aided by the possible contribution of determinants downstream of Thr30. The presence of a basic cluster at each end of the hcTnI 16-41 peptide (19-RRR-21 and 35-KKKSK-39) however raised the possibility that the C-terminal interaction observed may have resulted from the presence of the

lysine residues in the region hcTnI 35-39. It was also possible that the spectral changes observed came about because peptide binding was taking place with either the N-terminal arginine residues as a positive 'anchor' or, with the C-terminal lysine residues as 'anchor'.

To investigate the involvement of the C-terminal portion of hcTnI 16-41 in directing the interaction, a peptide spanning hcTnI 36-52 was synthesised for use in competition experiments. It was expected that hcTnI residues ~42 onward would not be involved in an interaction with F-actin since this region was observed to be bound to the C-terminal domain hcTnC in the partial cardiac troponin crystal structure. This expectation was affirmed by the spectral changes observed during a titration of F-actin into hcTnI 36-52. As shown in Figure 3.11 signals of residues in the C-terminus of this peptide [Thr50 (1.2ppm)] were relatively less affected than the composite signal of the lysine residues (3.0ppm) and Ala42 (1.4ppm) at its N-terminus.

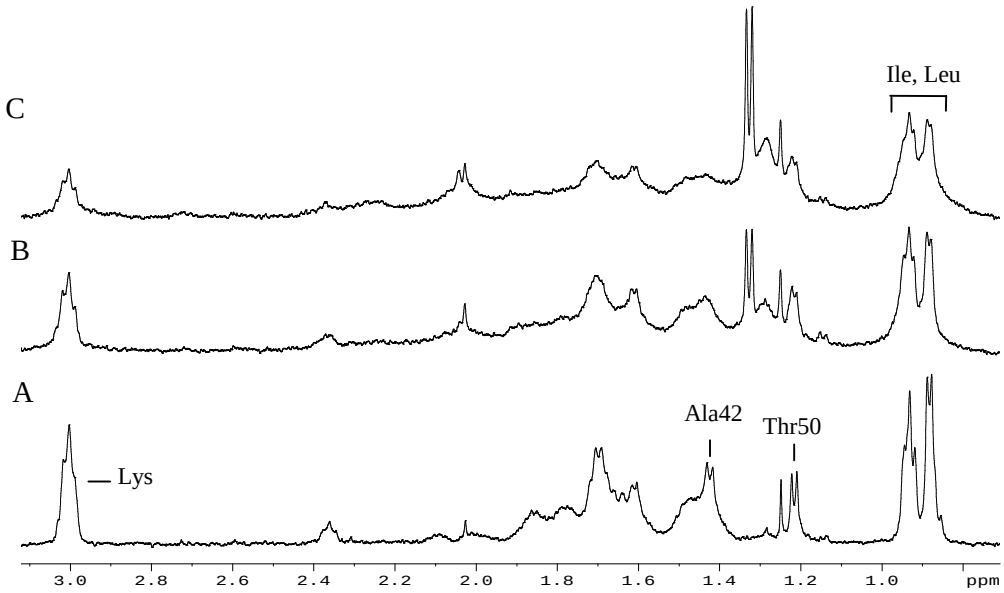

Figure 3.11 The N-terminus of hcTnI 36-52 is more involved in the interaction with F-actin than its C-terminus. ^{1}H MR of the 0.8-3.1ppm region of the spectrum of 50µM hcTnI 36-52 (A) in the presence of 24µM F-actin (B) and 48µM F-actin (C). Note the greater broadening of Ala42 compared to Thr50 (B), pH 7.2, T=298K.

A relatively high concentration of F-actin was required to induce marked broadening effects on hcTnI 36-52 (Fig 3.11B and C). This suggested that interaction with F-actin was relatively weak. A low binding affinity, consistent with a limited electrostatic interaction, was indeed indicated by the K_d estimated from the change in signal intensity during titration (K_d ~600-900µM). In keeping with this, a high concentration of hcTnI 36-52 was also required to detect competition with hcTnI 16-41 binding to F-actin as shown in Figure 3.12 below.

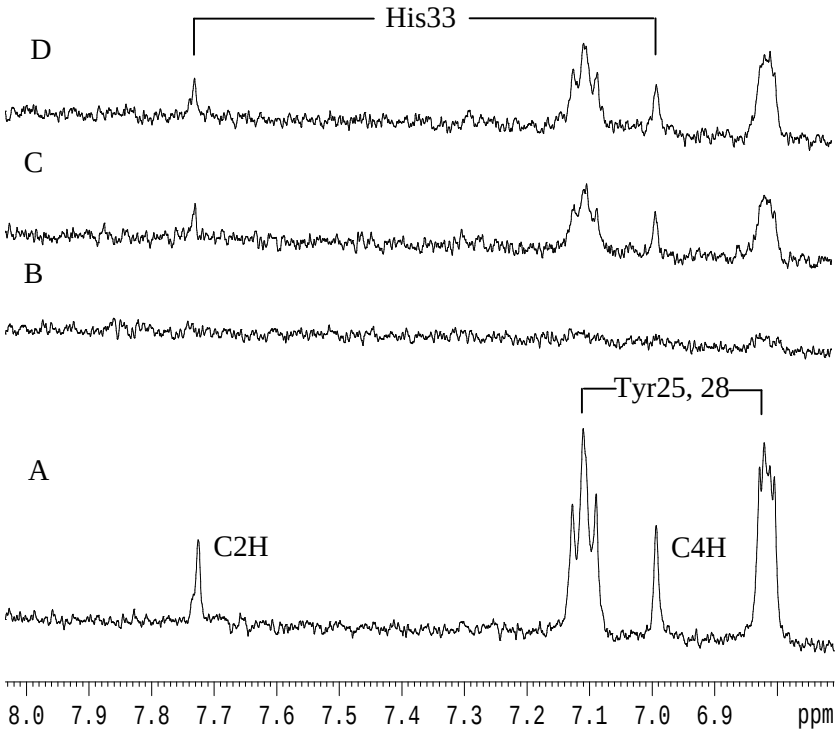

Figure 3.12 High concentrations of hcTnI 36-52 were able to reduce the population of hcTnI 16-41 bound to F-actin. ^{1}H MR of the aromatic region of the spectrum of 50µM hcTnI 16-41 (A) in the presence of 24µM F-actin (B), upon addition of 48µM hcTnI 36-52 (C) and upon addition of 96µM hcTnI 36-52 (D). The return of the signals of His33 and Ty25, 28 showed that hcTnI 16-41 was being displaced at high concentrations of hcTnI 36-52 (C and D). This suggested that the 36-41 region of hcTnI 16-41 was not the predominant region involved in binding of hcTnI 16-41 to F-actin, pH 7.2, T=298K.

This was monitored via the signals of Tyr25, 28 and His33 that are unique to 16-41 (Fig 3.12). The weak ability of hcTnI 36-52 to reduce the population of hcTnI 16-41 bound to F-actin led to the conclusion that the C-terminal lysine cluster of hcTnI 16-41

provided only a moderate contribution to F-actin interaction. The hcTnI 36-52 peptide was therefore used to also probe a shorter hcTnI N-terminal peptide, residues 16-37.

The F-actin titration data obtained using hcTnI 16-37 showed perturbation of the signals in the residue range 25-33 as illustrated in Figure 3.13. The spectra shown focus on the sidechain signals of Tyr25, 28 and His33. The K_d estimated from these spectral changes, assuming 1:1 complex formation, was of the order of 30 ± 10μM. The spectra highlighted that, as previously observed for peptides that included His33, the change in signal intensity for Tyr25, 28 as a function of added F-actin was matched by a corresponding proportional change in the intensity of the C2H and C4H resonances of His33. This reflected similar relaxation of these residues resulting from the association of hcTnI 16-37 with F-actin and confirmed that the interaction apparently involved residues 25-33.

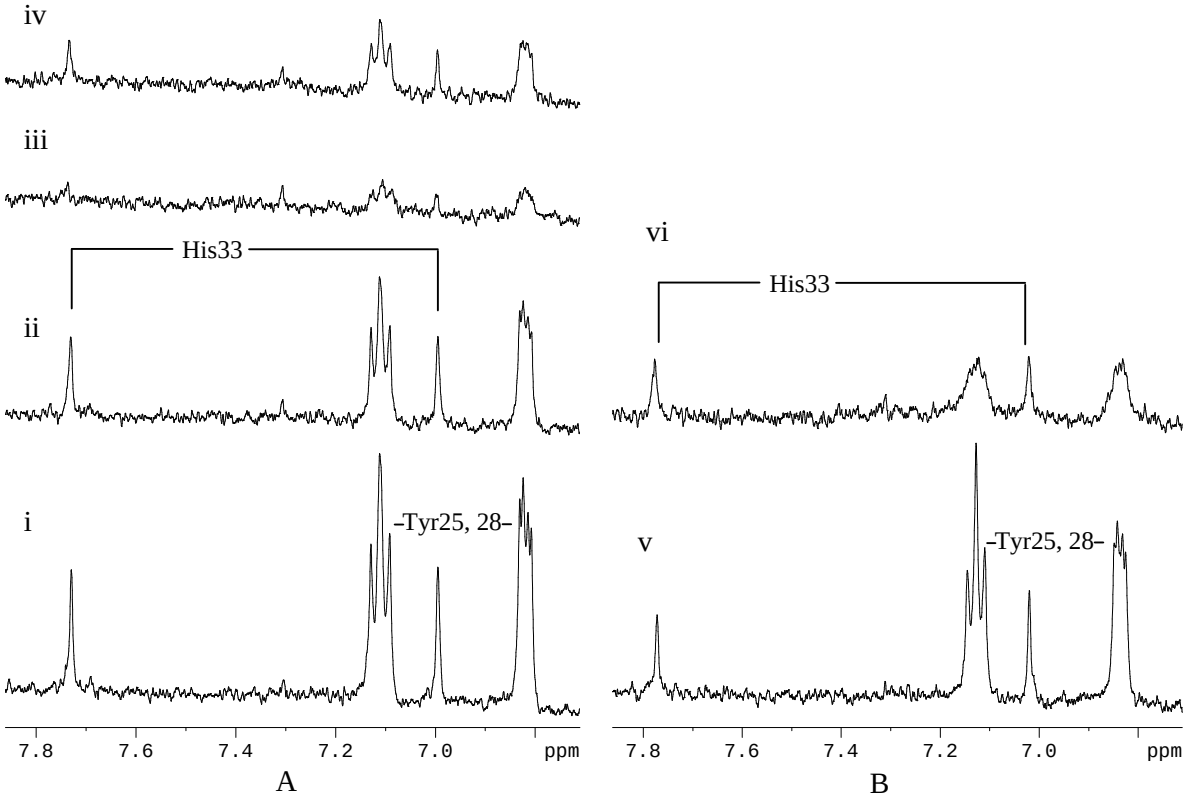

Figure 3.13 hcTnI 16-37 interacts with F-actin in the presence of hcTnI 36-52 and can also interact with F-actin in the presence of 0.1M KCl. ^{1}H MR of the aromatic region of the spectrum of 50µM hcTnI 16-37 (Ai) addition of 4µM F-actin (Aii) 15µM F-actin (Aiii) and addition of 15µM 36-52 (Aiv). ^{1}H MR of the aromatic region of the spectrum of 50µM hcTnI 16-37 in the presence of 0.1M KCl (Bv) addition of 25µM F-actin (Bvi), pH 7.2, T=298K.

Some reversal of the F-actin dependent reduction in intensity of hcTnI 16-37 was observed upon competition for F-actin binding by hcTnI 36-52 (Fig 3.13Aiv). The magnitude of the reversal was similar for both Tyr25, 28 and His33 and their signal intensities under these experimental conditions were used to obtain an estimate of the apparent K_d of ~90 ± 20 µM for hcTnI 16-37 binding to F-actin. The ability of hcTnI 36-52 to reduce the bound population of hcTnI 16-37 could be explained if the positive C-terminus of hcTnI 16-37 contributed to complex formation. The effect of an increase in ionic strength was therefore studied by titration of hcTnI 16-37 with F-actin in the presence of 0.1M KCl.

As seen from Figure 3.13B relaxation of the signals of both Tyr25, 28 and His33 was observed. However, the relaxation effects were notably different from those found at a lower ionic strength (Fig 3.13A). In the presence of 0.1M KCl significantly greater relaxation by F-actin was observed for the sidechain signals of Tyr25, 28 compared to that found for the sidechain signals of His33. This observation suggested that the mode of binding to F-actin had been altered by the increase in ionic strength such that the relaxation of His33 was less marked in the presence of 0.1M KCl, i.e. consistent with a reduction in the contribution of the C-terminal lysine cluster to complex formation. The data therefore confirmed the involvement of hcTnI residues 24-30 in the interaction with F-actin. The data also suggested that any potential contribution to this association with the F-actin surface due to the N-terminal arginine cluster was not ionic strength dependent at the salt concentration used. The data however still raised the question as to the extent to which the C-terminal lysine cluster was a significant 'player' in the association between the N-terminus of hcTnI and F-actin. This question was largely resolved by 'deletion peptide mimetics' and the subsequent study of hcTnI 16-29.

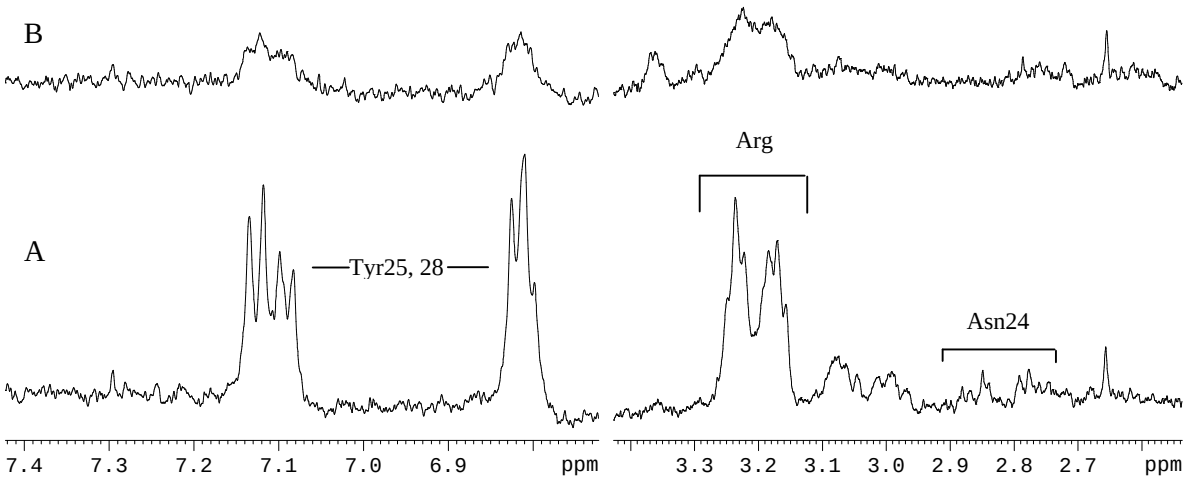

Figure 3.14 The shorter N-terminal peptide, hcTnI 16-29, interacts with F-actin. ^{1}H MR of the aromatic and the 2.6-3.4ppm regions of the spectrum of 50µM hcTnI 16-29 (A) addition of 4µM F-actin (B). Broadening of Arg19-21 and 26, Asn24 and Tyr25, 28 showed that the entire peptide length is involved in the interaction with F-actin, pH 7.2, T=298K.

Figure 3.14 shows parts of the spectrum of hcTnI 16-29 affected upon addition of 4µM F-actin (Fig 3.14B). The spectral regions shown here make use of Tyr25, 28 and the arginine residues (Arg 19-21 and Arg26) as reporters of F-actin interaction. The marked broadening of these signals indicated that the mobility of the entire length of the peptide was constrained and that the bound peptide was effectively 'pasted' on to the surface of F-actin. These observations on hcTnI 16-29 provided strong support for the determinants of F-actin binding by the N-terminus of hcTnI being localised with this 16-29 segment of the N-terminal extension.

3.5 Comparison of the F-actin interaction of hcTnI 16-29 with other actin binding sequences

Although the data described above strongly supported the specific nature of the interaction between hcTnI residues 16-29 with F-actin, the uniqueness of the location of the binding site on F-actin suggested by the competition experiments with the inhibitory

region needed to be further explored. The approach here was hampered by the limited data available that conclusively defined actin binding locations. Ideally, the approach to the definition of actin binding sites of the N-terminus of hcTnI should make use of a target peptide/protein that possessed an affinity comparable to or greater than that of hcTnI 16-29. High affinity actin targets such as DNase I or profilin however bind at actin monomer contacts not exposed on the F-actin filament [Holmes et al, 1990]. Use was therefore made of ß-thymosin, an actin monomer sequestering protein [Irobi et al, 2004] that binds actin with reasonably high affinity (K_d ~1µM, Webber et al, 1992). The nature of the interaction with actin by the N-terminal region of ß-thymosin had been defined by the crystallographic study of the complex between actin and ciboulot, a ß-thymosin homologue [Boquet et al, 2000, Hertzog et al, 2004] and is shown below.

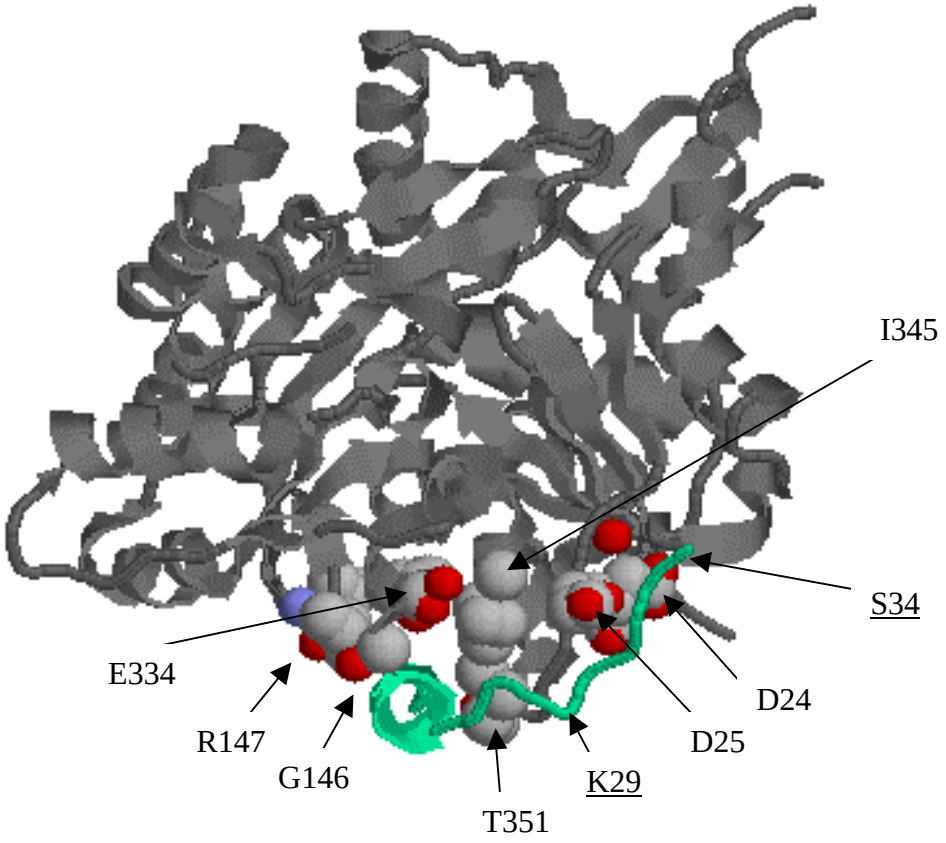

Figure 3.15 The binding of the N-terminus of Thymosin (Green, residues underlined) to actin (Grey). The picture was generated from pdb reference 1SQK using Rasmol.

3.5.1 The N-terminus of thymosin

Binding of the N-terminus of β-thymosin occurs across subdomain 1 and 3 of actin (Fig 3.15). The first half of the 24 residue peptide makes several contacts in the cleft between subdomains 1 and 3 while the second half is extended and makes primary electrostatic contacts with subdomain 1 (Asp24 and 25 of actin, Fig 3.15). Competition between β-thymosin residues 3-26 and hcTnI 16-29 was investigated by titration of hcTnI 16-29 into a 2:1 mixture of thymosin residues 3-26: F-actin (Fig 3.16).

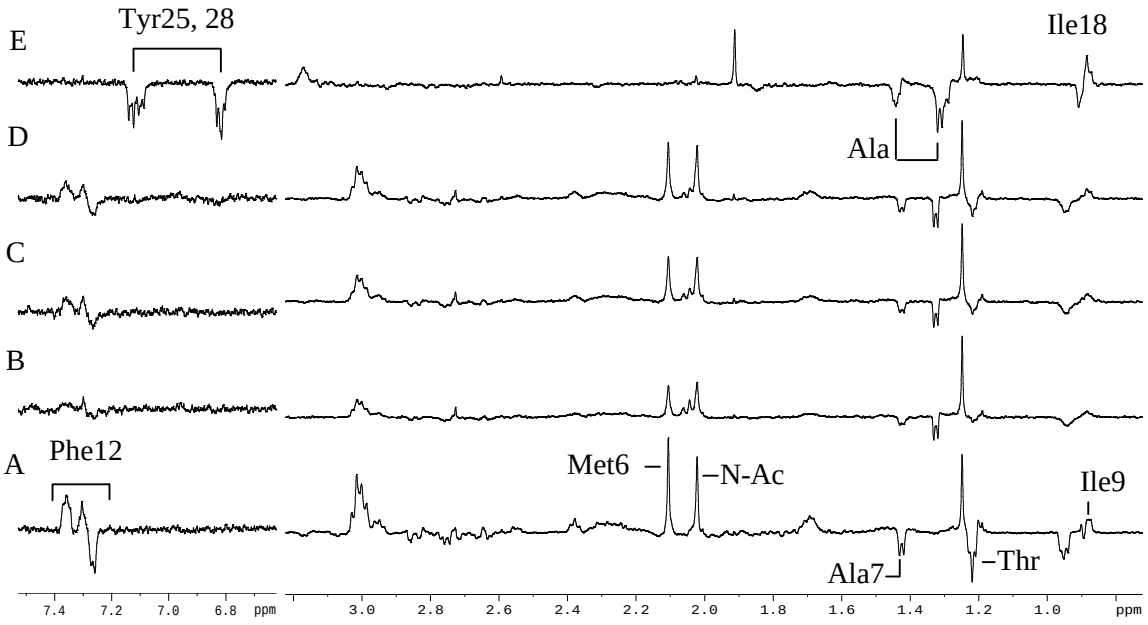

3-N-Ac-KPD**MA**E**I**E K**F**DKSKLKKT ETQEKN-26

Figure 3.16 hcTnI 16-29 interacts with F-actin in the presence of the N-terminus of human thymosin. ^{1}H MR of the of 50μM human thymosin 3-26 (A) addition of 25μM F-actin (B) addition of 24μM hcTnI 16-29 (C) addition of 50μM hcTnI 16-29 (D) compared to the spectrum of free 16-29 (E). Signals of hcTnI 16-29 are not observed in spectrum D at 50μM peptide indicating that they are broadened by interaction with F-actin even in the presence of the N-terminal peptide of thymosin, pH 7.2, T=298K.

Titration of hcTnI 16-29 showed that no signals from Tyr25, 28 were detected even at a final concentration equimolar to thymosin, (Fig 3.16D), i.e. the signals of hcTnI 16-29

remained broad and so did not provide any evidence of effective competition. This experiment again demonstrated the specificity of binding by hcTnI 16-29 and, also suggested that the site of interaction did not correspond to the cleft between subdomains 1 and 3, the site of interaction for β-thymosin.

In the context of a functional role for the interaction with F-actin by the N-terminal extension of hcTnI, it was relevant to continue to study any overlap in binding between this segment and the previously characterised second actin/Tm binding region common to all known isoforms of TnI. Figure 3.17 compares the binding of hcTnI 1-30 and that of a peptide comprising the second actin/Tm binding site. Binding of the second actin/Tm site was monitored via the effect of F-actin binding on the signal of His171.

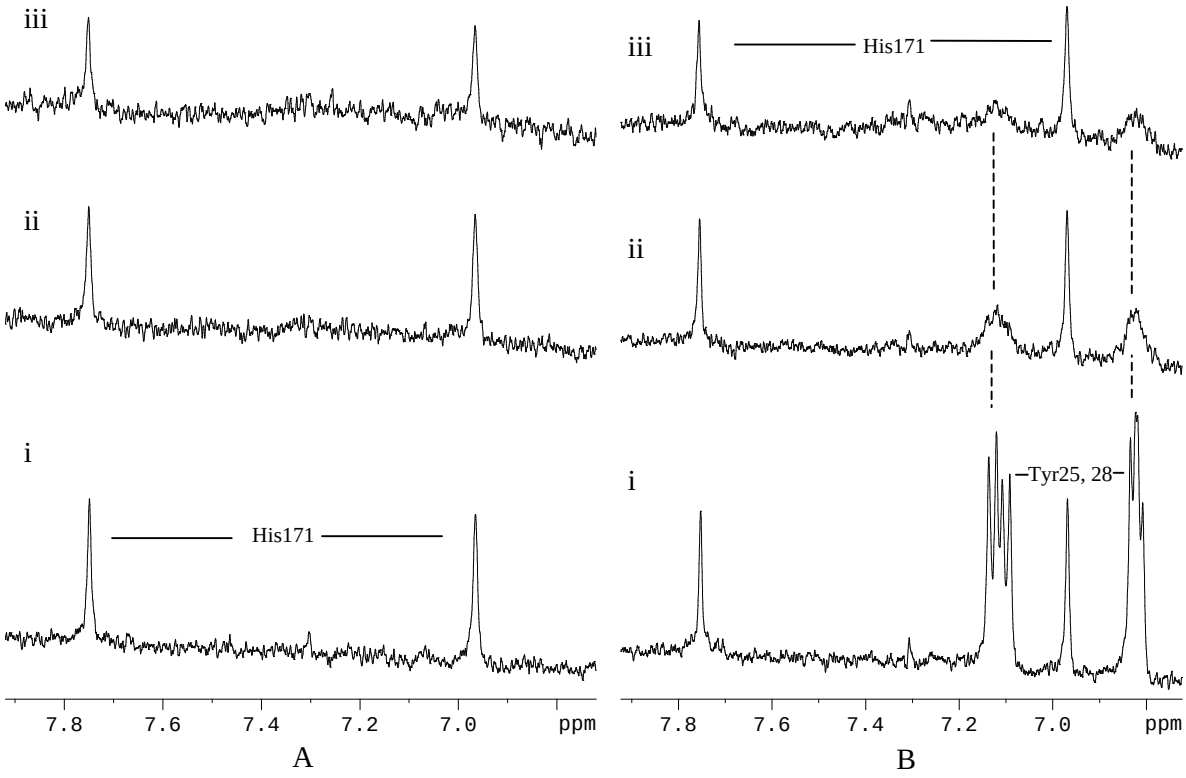

162-AKE<u>T</u>LDLRA**H**LKQVKKEDTEK-182

Figure 3.17 hcTnI 1-30 interacts with F-actin in the presence of hcTnI 162-182 (the second actin/Tm binding site, containing a Ser165 to Thr substitution). ^{1}H MR of the aromatic region of the spectrum of 50µM hcTnI 162-182 (Ai) addition of 7.5µM F-actin (Aii) 15µM F-actin (Aiii). ^{1}H MR of the aromatic region of the spectrum of 50µM hcTnI 162-182 in the presence of hcTnI 1-30 (Bi) addition of 7.5µM F-actin (Bii) 15µM F-actin (Biii), pH 7.2, T=298K.

The change in signal intensity that occurred with increasing concentration of F-actin was used to derive an estimated K_d of some 500 ± 100µM for the binding of the second site to F-actin. Within experimental error no change in the apparent K_d was found, as monitored by the intensity changes of His171 upon F-actin titration in the presence of equimolar unblocked hcTnI 1-30 (Fig 3.17B). The observation that the proportional change in intensity as a function of added F-actin was not markedly altered by the presence of hcTnI 1-30 suggested independent binding site locations on F-actin for the

two segments of hcTnI. The unblocked hcTnI 1-30 peptide was selected for use in this experiment due to its relatively low affinity, comparable to that observed for hcTnI 162-182. It was therefore of interest to discover from this experiment that the apparent K_d obtained for the binding of hcTnI 1-30 was ~50 ± 20μM, seemingly lower than reported above for the isolated peptide. This observation was not explored further but did support the conclusions that the two segments of hcTnI were not competing for the same site of binding on F-actin and, that they were able to interact simultaneously at the surface of F-actin.

3.6 Binding of the N-terminus of hcTnI to F-actin antagonised the ability of myosin loop regions to interact with F-actin

Implicated in the interaction between the myosin head and F-actin are the 'cardiomyopathy' loop (hcßM 398-414) and loop 2 of myosin (hcßM 622-646) that project away from the structure of the myosin head [Rayment et al, 1993]. Since these presumptive actin binding regions are exposed and do not make contacts with the rest of the myosin head, it was considered reasonable to undertake a peptide competition assay, in the presence of the N-terminal hcTnI segments, to explore the extent to which their binding sites on F-actin overlap. hcTnI 16-37 and hcTnI 16-29, were used for this mapping experiment. The viability of this study was enabled by the existence in the different sequences of residues whose signals could be uniquely monitored, so providing peptide-specific spectral reporters of the interaction with F-actin.

hcβM 398-414	398-N-Ac-GLC**H**PQVKVGNE**Y**VTKG-414
hcβM 622-646	622-N-Ac-AN**Y**AGADAPIEKGKGKAKKGSS**F**QT-646
hcTnI 16-37	16-N-Ac-APIRRRSSN**Y**RA**Y**ATEP**H**AKKK-37

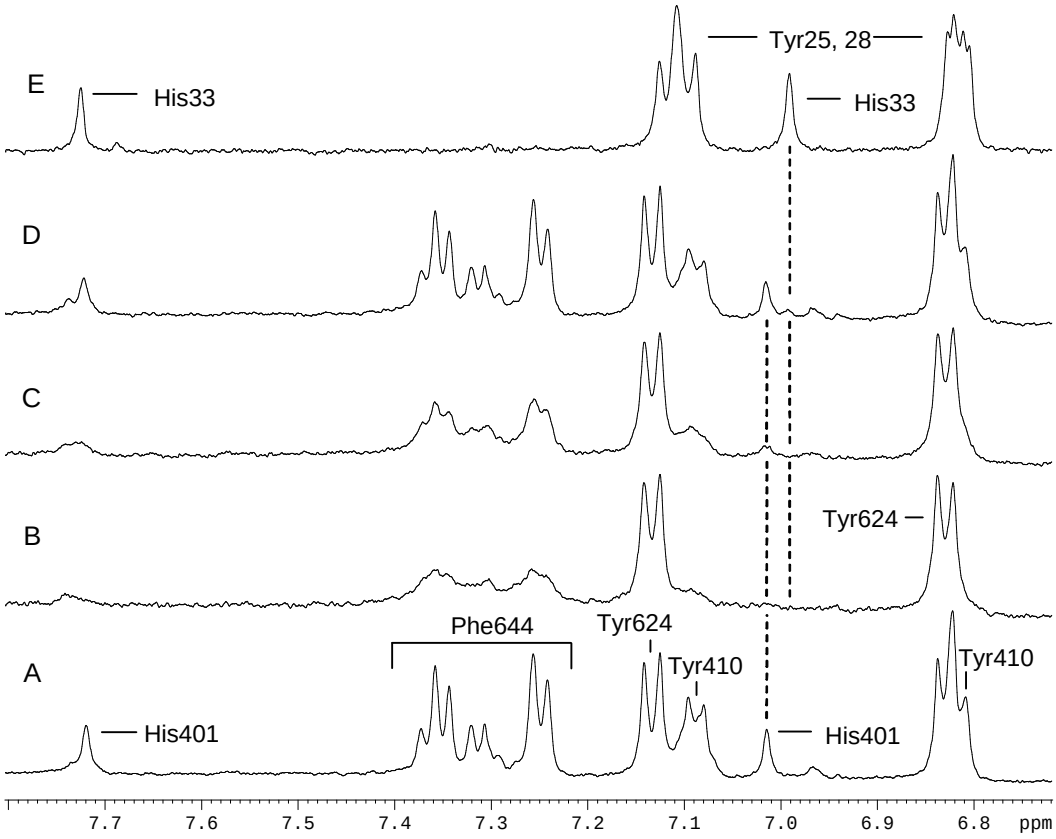

Figure 3.18 hcTnI 16-37 displaced both myosin loop peptides, hcβM 398-414 and hcβM 622-646 from F-actin. ^{1}H MR of the aromatic region of the spectrum of 70µM hcßM 398-414 and 70µM hcßM 622-646 (A) addition of 15µM F-actin (B) addition of 7.5µM hcTnI 16-37 (C) and addition of 15µM hcTnI 16-37 (D). Free hcTnI 16-37 is shown in (E), pH 7.2, T=298K. His401 at 7.01ppm and Tyr410 at 7.1ppm from hcßM 398-414 can be monitored and are shown to broaden in the presence of F-actin (B) with a return in signal intensity upon addition of 15µM hcTnI 16-37 (D). Phe644 of hcßM 622-646 was also found to broaden in the presence of F-actin (B) and its intensity returned upon addition of hcTnI 16-37 (C and D). The spectrum of free hcTnI 16-37 (E) showed where signals of His33 and Tyr25, 28 appear in the spectrum, confirming the absence of signal overlap with specific myosin loop sidechain signals.

Figure 3.18 shows the effect of F-actin on an equimolar mixture of the two myosin loop regions and the subsequent addition of hcTnI 16-37. As previously reported [Patchell et al, 2005], titration with F-actin led to the selective broadening of myosin loop 2 peptide resonances e.g. Phe 644 but not Tyr624 (Fig 3.18B). This indicated that the N-terminal region of hcßM 622-646 retained mobility independent of F-actin while it was bound to F-actin via its C-terminal residues. In contrast, resonances from groups along the

sequence of hcßM 398-414 (e.g. His401 and Tyr410, Fig 3.18B) were perturbed in the presence of F-actin indicating that this myosin sequence was ‘pasted’ onto the actin surface. The observation that progressive broadening effects on both peptides occurred at each stage of titration with F-actin confirmed the conclusion that the two peptides bound simultaneously and at different locations on F-actin [Patchell et al, 2005].

Reversal of the spectral broadening resulting from binding to F-actin was observed in the presence of hcTnI 16-37 (Fig 3.18). Titration with hcTnI 16-37 led to an increased recovery of the intensity of the signals of His401 and Tyr410 as well as for Phe644, even when hcTnI 16-37 was present at concentrations notably lower than those of the myosin peptides (3:1 molar excess of myosin peptides, Fig 3.18D). These observations indicated that the binding of hcTnI 16-37 to F-actin, confirmed by the broadening of signals of Tyr25, 28 and His33 (Fig 3.18C and D), led to the displacement of both myosin loop regions from the surface of F-actin. The conclusion from these data was that interaction of hcTnI 16-37 with F-actin occurred either at a region overlapping both myosin loop binding sites or, that its binding was relayed to effect a reduction in the affinity of both myosin loops for F-actin.

Given the observations reported earlier in this chapter that pointed to a contribution of the C-terminal lysine cluster of hcTnI 16-37 to its affinity for F-actin, the myosin loop competition assay was also carried out using hcTnI 16-29.

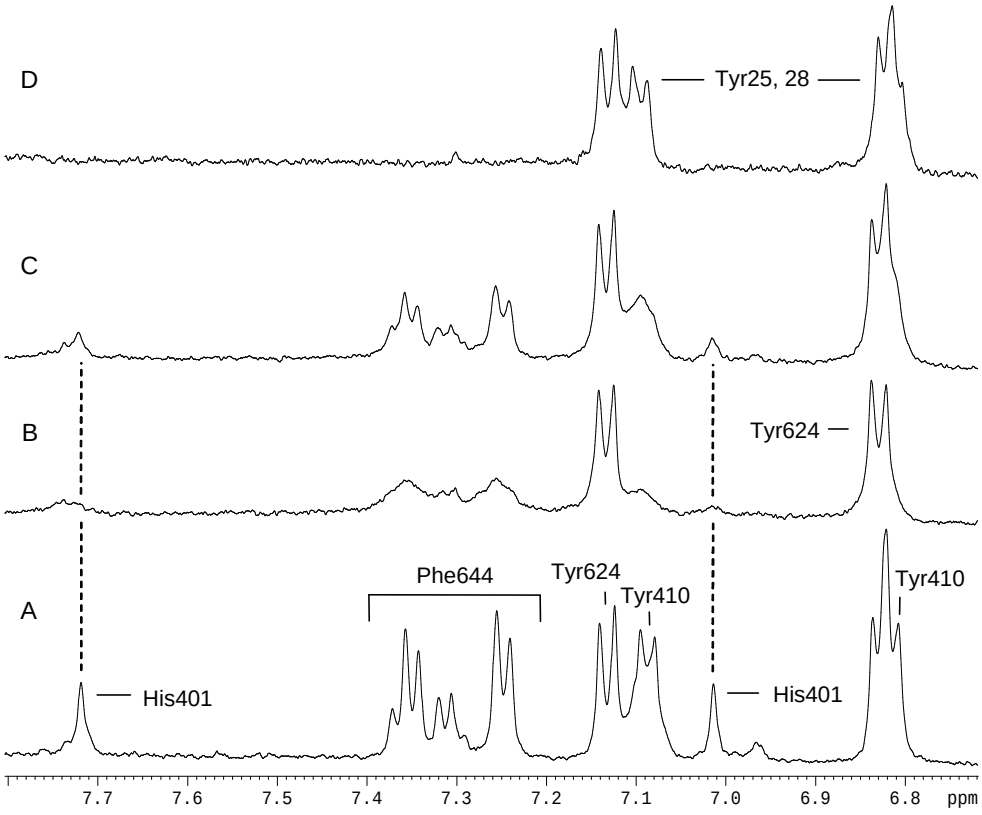

Figure 3.19 Differential displacement of the myosin loop peptides, hcβM 398-414 and hcβM 622-646 from F-actin by hcTnI 16-29. ^{1}H MR of the aromatic region of the spectrum of 70µM hcßM 398-414 and 70µM hcßM 622-646 (A) addition of 15µM F-actin (B) addition of 60µM hcTnI 16-29 (C). Free hcTnI 16-29 is shown in (E), pH 7.2, T=298K.
Again, His401 at 7.01ppm and Tyr410 at 7.1ppm from hcßM 398-414 are shown to broaden in the presence of F-actin (B) with a return in signal intensity upon addition of 60µM hcTnI 16-29 (C). Phe644 of hcßM 622-646 was also found to broaden in the presence of F-actin (B) and its signal recovered upon addition of hcTnI 16-29 (C). The spectrum of free hcTnI 16-29 (D) showed where signals of Tyr25 and 28 appeared in the spectrum and as in Figure 3.18, no overlap with specific myosin loop sidechain signals occurred for resonances of hcTnI 16-29.

The shorter length of hcTnI 16-29 compared to hcTnI 16-37 had not prevented the interaction of this region of the N-terminal extension of hcTnI with F-actin. It was of interest to see if the shorter length peptide, hcTnI 16-29, would be as effective at competing with the myosin loop peptides for F-actin as the longer hcTnI 16-37 peptide. Figure 3.19C demonstrates that hcTnI 16-29 antagonised the concurrent binding to F-actin by hcßM 398-414 and hcßM 622-646. The reversal of the linebroadening of His401, Tyr410 and Phe644 was readily apparent in the presence of hcTnI 16-29 into

solution. The differential displacement, more effective for hcβM 622-646 than for the cardiomyopathy loop (hcβM 398-414), will be considered again in chapter 4. A further difference between the results of this competition assay and that using hcTnI 16-37 was however observed. Namely, the concentration of hcTnI 16-29 required to cause comparable signal intensity reversal, an indication of the extent to which the population of the bound myosin peptides had decreased, was some 4-fold greater in the case of hcTnI 16-29 under these experimental conditions (cf. Fig 3.18D and Fig 3.19C). Notably, however, the highest concentration of hcTnI 16-29 used was still only equivalent to that of the myosin peptides and yet had resulted in a substantial (almost 50%) reversal in signal intensity (Fig 3.19C). The data therefore indicated the potency of hcTnI 16-29 as an antagonist and confirmed the specificity of the interaction of this region of hcTnI with F-actin. Further, the 'inhibitory effect' of the binding of hcTnI 16-29, given the length of the peptide, was also likely to have arisen from a relayed effect rather than by competitive binding at each of the two sites of interaction of the myosin loops with F-actin.

3.7 Chapter synopsis and Discussion

The studies described in this chapter aimed to explore the F-actin binding properties of the N-terminal region of hcTnI. The observations on a series of peptides covering the first 37 residues of hcTnI pointed to an association with F-actin that primarily involved contacts localised within the sequence spanning residues 16-30.

$_{1}$ADGSSDAAREPRPAPAPIRRRSSNYRAYATEPHAKKK$_{37}$

The $(Xaa\text{-}Pro)_4$ motif that precedes this region of the hcTnI sequence is a repeat also found in the N-terminus of the LC1 myosin light chain (Chapter 1). The X-P repeat

would be expected to possess an elongated structure given the steric constraints imposed the presence of proline [Schimmel and Florey, 1968]. The $(Xaa\text{-}Pro)_4$ motif, some 20Å long, would act to separate the N-terminal extremity of hcTnI from residues 18-30, potentially functioning to separate locales of interaction by hcTnI in a manner similar to the X-P repeats of LC1 that link different contacts made by the myosin light chain [Bhadari et al, 1986].

The hcTnI spacer segment and its preceding N-terminal residues did not participate in the interaction with F-actin. Rather, when present in the sequence of the hcTnI peptide assayed, residues 1-16 were observed to retain mobility independent of the complex formed between the peptide and F-actin. It is however likely that the binding of the N-terminus of hcTnI to F-actin would, as a consequence of localisation on the F-actin surface, impose a spatial constraint that orients the (entire) N-terminal region of hcTnI relative to the actin filament.

The binding specificity of the previously undiscovered interaction with F-actin involving the N-terminus of hcTnI was indicated by the data obtained in competition assays using several other F-actin ligands. The ability of hcTnI 16-29 to bind to F-actin in the presence of the thymosin peptide pointed to their possessing independent binding locations. A further indication of a specific binding locale for the N-terminal region of hcTnI came from the observation that hcTnI 1-30 bound to F-actin without competition from the so-named 2nd actin-Tm binding region, hcTnI 162-182, being detected. This suggested that, when in the context of the intact hcTnI molecule, both these regions of the protein could make independent contacts with the F-actin filament.

The specificity of binding by the N-terminus of hcTnI was also demonstrated by the observation that hcTnI 16-29 antagonised the association between F-actin and peptides based on two surface regions of human cardiac β-myosin. The two regions protrude from the S1 myosin head without making any intramolecular contacts [Rayment et al, 1993] and on this basis the hcβM peptides can be considered to be viable mimics of the F-actin interaction by these two myosin loops. While hcβM 622-646 (the loop 2 region) has been correlated with the weakly bound state of actomyosin, F-actin interaction with hcβM 398-414 (the cardiomyopathy loop) has been linked with the weak-strong transition of the crossbridge [Onishi et al, 2006]. Their separate binding sites on F-actin have been modelled and they were indeed here shown to bind concurrently to F-actin. It would have been incorrect to assume that the modelled interaction locations on F-actin corresponded to the binding sites taken up by the loops as isolated peptides. It was however justifiable to conclude that, since both peptides interacted with F-actin, their simultaneous displacement by different hcTnI peptides containing residues 16-29 provided direct evidence of the viability and specificity of the interaction between this region of hcTnI and F-actin.

One measure of any defined interaction is its equilibrium dissociation constant. The approach used here to estimate K_d made the assumption of an equilibrium involving 1:1 complex formation when analysing the changes in signal intensity that resulted from F-actin providing a 'relaxation sink'. In order to take account of the contribution of dynamics/'fuzziness' (either at the site of binding or, possible interchange between different modes of binding) the evaluation of K_d was in each case based on the ratio of (I_B/I_F) for several different hcTnI peptide resonances at different stages of each titration.

The titrations were carried out using increasing concentrations of F-actin and a fixed (50μM) hcTnI peptide concentration to report on the mole average of the peptide population in solution. A limitation here was the maximum concentration of F-actin that could be used during titration, typically 50μM, without resulting in dilution effects or introducing viscosity changes. This restricted the attainable concentrations of bound peptide as can be seen from the tabulation below that shows the calculated concentrations of the 1:1 complex formed for several different values of K_d.

		K_d μM			
		5	25	100	500
[hcTnI peptide] μM	[F-actin] μM	Corresponding [Complex] μM			
50	4	3.6	2.6	1.3	0.4
50	50	36.5	25	13.4	4.2

A roughly 10-fold increase in concentration of bound peptide is associated with a 100-fold increase in K_d under the experimental conditions used. Therefore, although meaningful in their own right, the range of K_d values as reported above for any given peptide are best used to inform of an order-of-magnitude comparison of the relative affinity of different hcTnI peptides for F-actin.

The relative K_d values for peptides comprising different spans of the hcTnI residue range 16-41 suggested that while hcTnI 16-29 contained the prime determinants for F-actin binding, the affinity of F-actin interaction with the N-terminal region of hcTnI was enhanced by the presence of residues 30-37. An adhesive contribution to binding by the basic cluster, Lys 37-39, was indicated by the greater F-actin concentrations required to induce comparable relaxation in the presence of salt (Figure 3.13) and, by the observation that under these solution conditions the relaxation resulting from binding to F-actin was greater for sidechain signals of Tyr25, 28 compared to that found for the

sidechain signals of His33. While the latter finding was an indication of reduced intimacy of contact with F-actin by the segment containing His-33, it also provided evidence of the retention of association by the region containing hcTnI residues 25-28.

The inferred predominant contribution to F-actin interaction from residues within hcTnI 16-29 needs to be considered in the light of the data relating to the interplay between by hcTnI 1-30 and the inhibitory region, hcTnI 128-153, binding to F-actin (Figures 3.7 and 3.8). Binding by the inhibitory region has previously been proposed to lead to conformational changes that are propagated to different locations on F-actin's surface even in the absence of tropomyosin [Patchell et al, 2002 and 2005]. The data presented in this Chapter suggested that while the binding of hcTnI 1-30 and hcTnI 128-153 occurred at non-overlapping locations, each peptide influenced the extent of F-actin binding by the other. This raised the possibility that the N-terminal region of hcTnI could affect the F-actin binding equilibrium of the inhibitory region. In the context of the function of the intact hcTnI molecule this interplay would endow the N-terminal extension of hcTnI with the ability to influence the calcium binding affinity of hcTnC via modulation of the equilibrium governing the exchange of the inhibitory region between F-actin and hcTnC.

This potential mechanism for regulating contractile activity in a manner specific to cardiac TnI is in keeping with the observation that deletion of mouse cTnI residues 2-11 left Ca^{2+} affinity unaffected [Sadayappan et al, 2008] while deletion of mouse cTnI residues 2-28 correlated with reduced Ca^{2+} affinity [Barbato et al, 2005]. The suggestion here is also consistent with the observation from studies of actomyosin ATPase activity inhibited by a series of mutations in the N-terminal extension of hcTnI

indicating that residues 16–29 are important to maintaining cardiac troponin in the high Ca^{2+} affinity state associated with ATPase activity [Ward et al, 2002]. The hypothesis here however needs to be considered in the light of the still ill-characterised interaction between the N–terminus of hcTnI and the N-domain of hcTnC [Sadayappan et al, 2008], an interaction inferred from the reduction in Ca^{2+} sensitivity associated with hcTnI phosphorylation. The observations shown in Figure 3.9 are of direct relevance. These data point to the inability of calcium-bound hcTnC to compete with F-actin for hcTnI 1-30 in contrast to the observed capacity of hcTnC to interact with the inhibitory region, hcTnI 128-153, under the same conditions (Figure 3.9). Any interaction between hcTnC and hcTnI 1-30 must therefore be rather weak and, in the presence of F-actin, the N-terminal extension of hcTnI is likely to be more closely associated with F-actin rather than with hcTnC. The resulting perspective of the equilibrium involving the N-terminus of hcTnI switching between F-actin and the N-terminal domain of hcTnC is shown schematically in Figure 3.20.

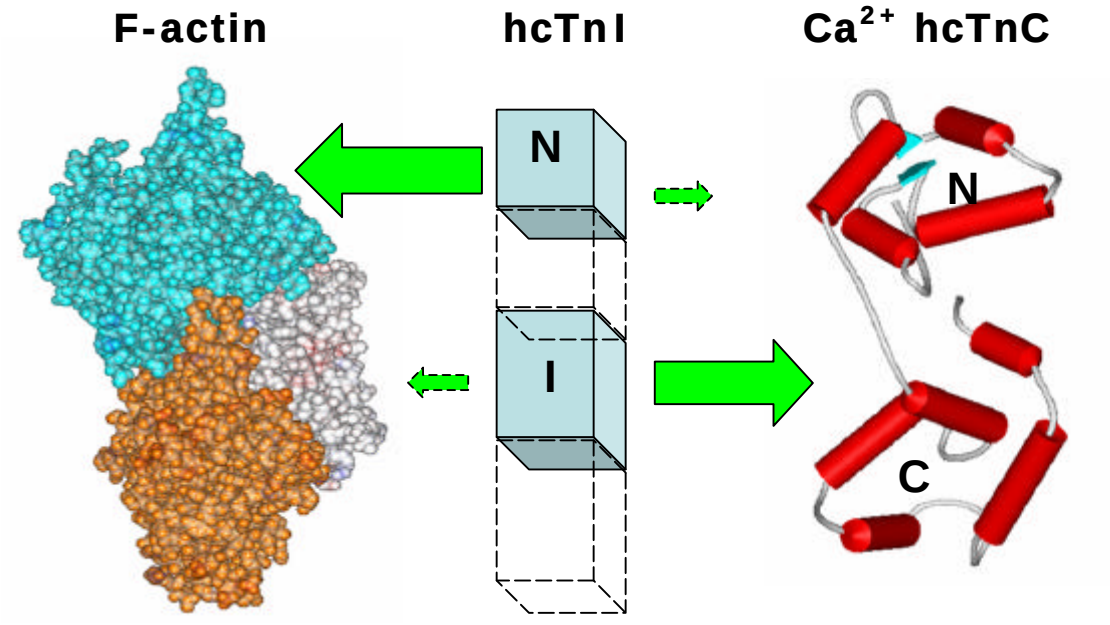

Figure 3.20 Representation of the equilibria in the presence of high Ca^{2+} involving the N-terminal extension of hcTnI. The short residence time on hcTnC and the relatively transient nature of this interaction compared to that involving F-actin are indicated. The interaction of the N-terminal extension of hcTnI with F-actin biases the inhibitory region (I) towards interaction with hcTnC. Figure not to scale.

In sum, even when taking into account the plausible interaction of the N-terminal extension of hcTnI with hcTnC, the impact of accessibility to F-actin would be to reduce the probability of association with hcTnC and thereby influence the stabilisation of Ca^{2+} affinity associated with interaction between the N-terminus of hcTnI and the N-terminal domain of hcTnC. Accessibility of the N-terminal extension of hcTnI to F-actin could also influence the Ca^{2+} affinity of hcTnC via modulation of the dynamic equilibrium involving binding of the inhibitory region to F-actin and to hcTnC. It was therefore of interest to go on to investigate the consequences of phosphorylation on the interaction between the N-terminus of hcTnI and F-actin.

4 Monophosphorylation of the N-terminus of hcTnI

Human cTnI contains two adjacent PKA phosphorylation sites at serine residues 22/23 within the N-terminal extension. Bisphosphorylation at these sites is associated with a decrease in Ca^{2+} sensitivity and the additive effect of sequential phosphorylation has been reported.

In cardiac muscle the N-terminal domain of cTnC contains a single Ca^{2+} binding site believed to be responsible for the initiation of cardiac muscle contraction. The observed decrease in Ca^{2+} sensitivity upon phosphorylation of the N-terminus cTnI has been suggested to be due to a change in the proposed interaction between the N-terminus of cTnI and the N-terminal domain cTnC. However work described in the previous chapter has shown the ability of the unphosphorylated region of 16-37 hcTnI to interact with F-actin in a manner that constrains the flexibility of residues throughout the peptide sequence including Ile18, Tyr25, 28 and His33. This interaction with F-actin therefore localises the sequence around the phosphorylation sites at Ser22/23 in the vicinity of the F-actin surface. Two possible versions of the monophosphorylated species were synthesised to give one monophosphorylated peptide with Ser22 phosphorylated ($S_{22}P$) and the other monophosphoryled species with Ser23 phosphorylated ($S_{23}P$) . The use of the two monophosphorylated peptides was intended to investigate the effect of each phosphorylation site on the F-actin binding capability of this 16-37 region of hcTnI.

The aims of the experiments described below were to:

1. Characterise the effect of the addition of a phosphate group at either location Ser22/23 on the conformation of the region of hcTnI comprised of residues 16-37.
2. Study the F-actin binding ability of these monophosphorylated peptides to determine the impact of phosphate incorporation. It was expected that comparison of the NMR data from F-actin titrations of unphosphorylated and monophosphorylated ($S_{22}P$ and $S_{23}P$) peptides would resolve if there are any observable differences in the interaction with F-actin.
3. Given the reported ability of positively charged species to catalyse actin polymerisation, test the ability of the unphosphorylated and monophosphorylated peptides to convert monomeric G-actin to F-actin using fluorescence spectroscopy to monitor the transition via alteration of the fluorescence emission of pyrene labelled G-actin.
4. Lastly, having established any detectable impact of phosphorylation, to make use of peptide probes to monitor competition for F-actin binding by the unphosphorylated and monophosphorylated hcTnI 16-37 peptides.

4.1 Comparison of the hcTnI 16-37 unphosphorylated and monophosphorylated peptides to assess the nature of any structural effect of phosphorylation

16-APIRRR**SS**NYRAYATEPHAKKK-37

The sequence shows the presence of two basic clusters at either end of the 16-37 peptide, namely the 19-21 region at the site preceding the sites of PKA phosphorylation

RRRSS and, a lysine cluster (KKK) at the C-terminus of the peptide, hcTnI residues 35-37.

Phosphorylation at Ser22 and/or Ser23 would be expected to alter the charge around the arginine cluster 19-21 (RRR) region and thereby influence the possible contribution of this segment to binding (or dissociation). The net charge of the unphosphorylated species is +3 and the addition of one phosphate group (containing two negative charges at pH 7.2) will give a net charge of +1.

Since the resonance position of each signal in the ^{1}H MR spectrum is determined by the local electron density at the nucleus, changes in chemical shift are indicators of an alteration in the electronic environment of the nucleus. Spectra of the unphosphorylated and monophosphorylated peptides are compared below (Fig 4.1) to illustrate the residues affected by phosphate incorporation. Subsequent alteration of the solution pH then provided a means of monitoring the extent to which the phosphate ionisation state was relayed to other regions of the peptide.

4.1.1 Comparison of the aromatic region of the spectra of the hcTnI 16-37 peptides

The aromatic region of the spectrum shows sidechain signals from Tyr25, 28 and His33. The chemical shifts of the signals of His33 were unaltered in the three peptides but changes were detectable for the C3,5H signals of Tyr25, 28 at 6.8ppm (Fig 4.1). Incorporation of the phosphate group thus caused only quite small changes in electron density, plausibly greater at the location of Tyr25 that is closer the phosphorylation site, $S_{23}P$.

Interestingly, the change was sensed by the protons at the extremity of the tyrosine ring with the C2,6H resonance less affected. This suggested the existence of an effectively long-range perturbation of the C3,5H shielding of both tyrosine residues.

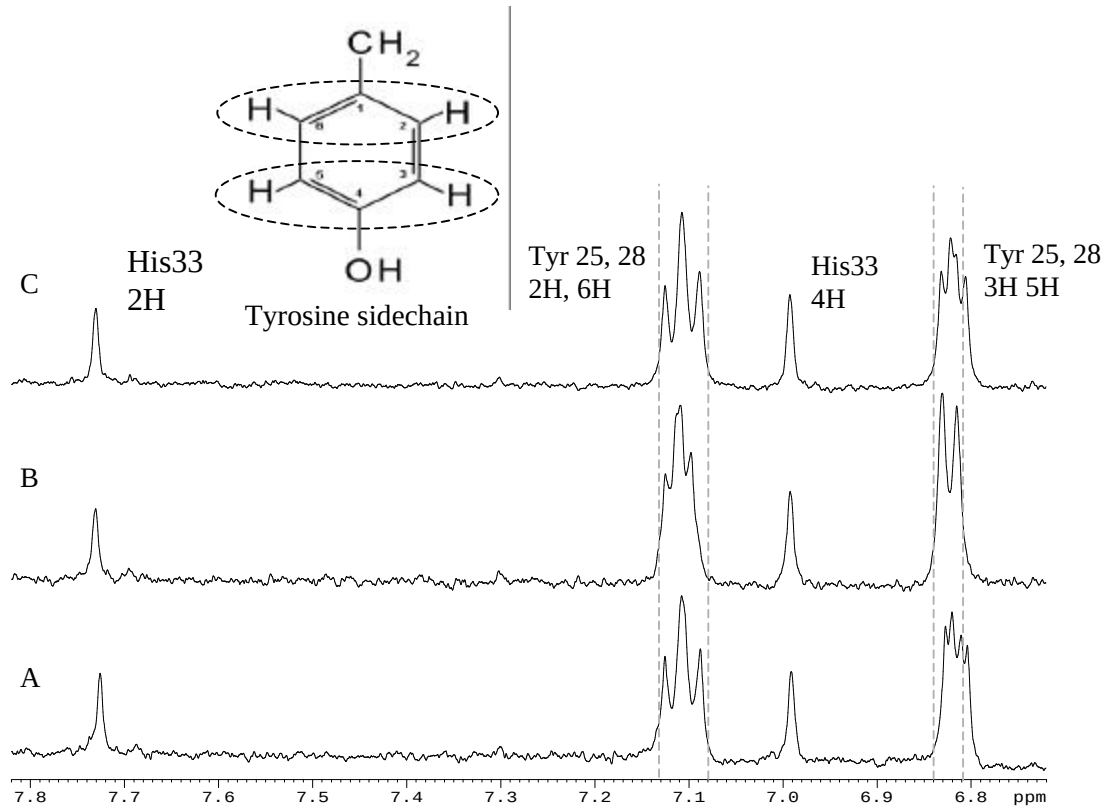

Figure 4.1 Aromatic region of the spectra of the hcTnI 16-37 peptides, pH 7.2 T=298K.
(A) unphosphorylated 16-37
(B) S23P monophosphorylated 16-37
(C) S22P monophosphorylated 16-37

4.1.2 Comparison of the Arginine and Lysine regions of the spectra of the hcTnI 16-37 peptides

The resonances of the dCH_2 groups of arginine and the eCH_2 groups of lysine occur in the range 2.95-3.05ppm (Fig 4.2). Differences in resonance energy for Arg dCH_2 signals were observed between the 3 peptides. This was not unexpected given the arginines of the PKA recognition motif (19-RRRSS-23).

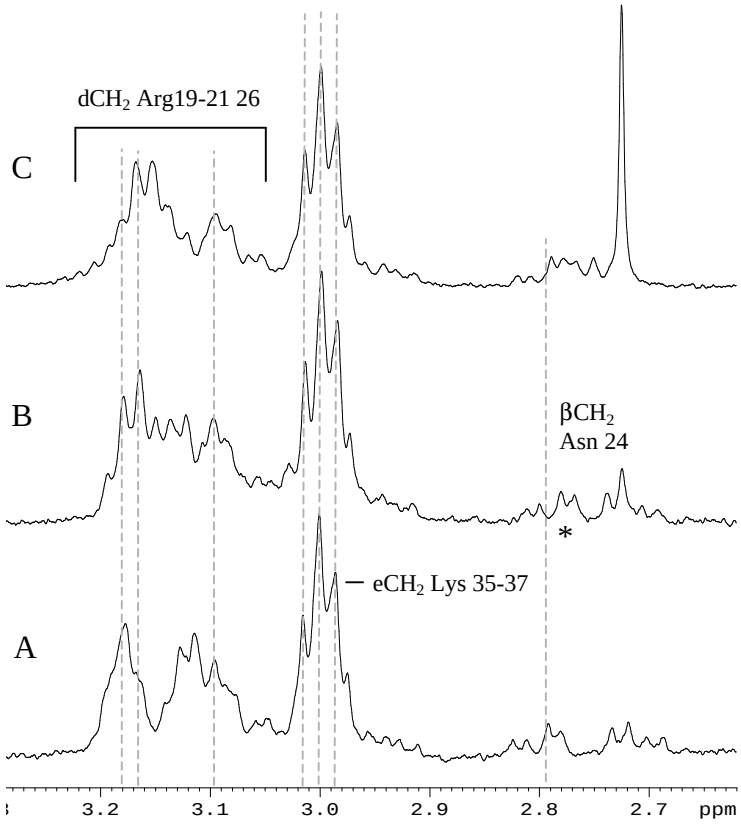

Figure 4.2 Comparison of the terminal groups of the sidechains of arginine and lysine of the hcTnI 16-37 peptides, pH 7.2 T=298K. * indicates the greater shift in the Asn24 signal of S23P.
(A) Unphosphorylated 16-37
(B) S23P monophosphorylated 16-37
(C) S22P monophosphorylated 16-37.

While the monophosphorylated peptides showed distinctive changes in the region of the terminal arginine sidechain signals, the sidechain signals of the lysines 35-37 at the other end of the peptide were unaltered by the introduction of phosphate group at either S22 or S23. This indicated the localised nature of the shielding change upon monophosphorylation. Consistent with this conclusion, the ßCH$_2$ signal of Asn24 was only sensitive to phosphate incorporation at S23 (Fig 4.2B *), reflecting localised changes in the electric field (electrostatic surface) around this region.

4.1.3 Comparison of the aliphatic region of the spectra of the hcTnI 16-37 peptides

The spectra shown below identify methyl signals of the ßCH_3 groups of alanine, the ?CH_3 signal of Thr30 and the signals of Ile18.

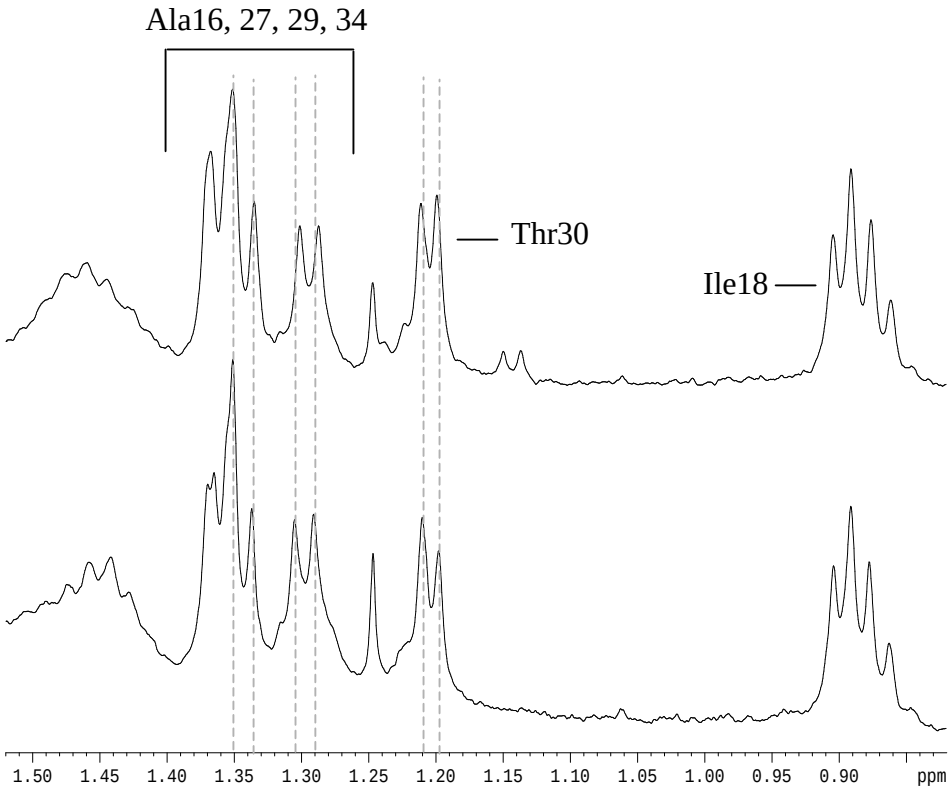

16-N-Ac-APIRRRSSNYRAYATEPHAKKK-37

Figure 4.3 Comparison of the methyl groups of the sidechains of alanine, Thr30 and Ile18 of hcTnI 16-37 peptides, pH 7.2 T=298K.
(A) Unphosphorylated 16-37
(B) S22P monophosphorylated 16-37.
The small shift differences seen are expanded upon in Figure 4.5

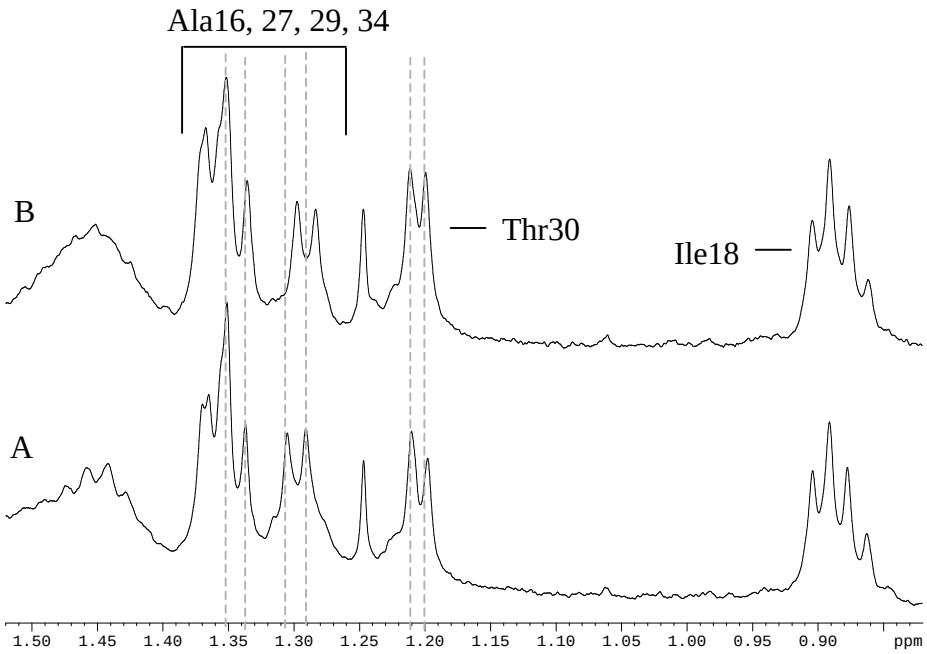

Figure 4.4 Comparison of the methyl groups of the sidechains alanine, Thr30 and Ile18 of hcTnI 16-37 peptides, pH 7.2 T=298K.
(A) Unphosphorylated 16-37
(B) S23P monophosphorylated 16-37.
This shows the sensitivity of a single alanine residue (1.3ppm) to phosphate incorporation at Ser23.

While the positions of the methyl group signals of Ile18 and Thr30 remain unaltered upon introduction of the phosphate group, an alteration in the chemical shift of a single alanine residue (1.3ppm) from Ala27 or 29, was readily observed between the unphosphorylated and the two monophosphorylated peptides (Fig 4.3-4.5).

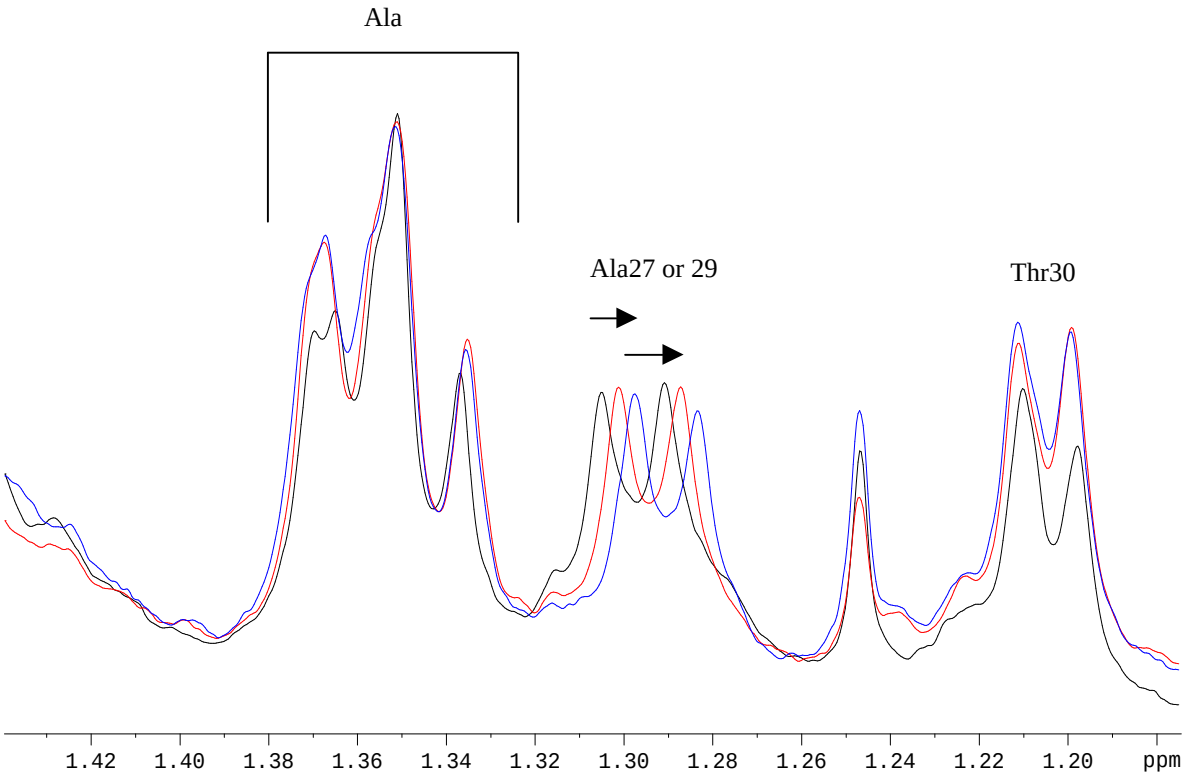

Figure 4.5 Comparison of the methyl group sidechains of alanine from the hcTnI 16-37 peptides, pH 7.2 T=298K.
Black - Unphosphorylated 16-37
Red - S22P monophosphorylated 16-37
Blue - S23P monophosphorylated 16-37.

So while phosphorylation effects were localised, consistent with the shift changes for Asn24, Tyr25 and 28, the phosphate-sensitive shift of the alanine signal could reflect an altered conformational average of Y25-R26-A27-Y28-A29 and/or simply a change in the electronic surface. This raised the question as to how the impact of phosphorylation may be generated. It was therefore pertinent to explore the effect of phosphate ionisation. The $S_{23}P$ monophosphorylated form of hcTnI 16-37 was the peptide selected for this study.

4.2 pH titration of S_{23}P hcTnI 16-37 raised possibility of long range electrostatic effects of phosphate incorporation

The comparison of the unphosphorylated and monophosphorylated peptide spectra indicated the localised changes in electronic shielding. Confirmation of the residues sensitive to introduction of the phosphate group was sought through study of the spectral response to variation of pH through the pKa of the phosphate, previously shown to be 5.25 in a hcTnI 16-42 monophosphorylated peptide [Keane et al, 1997]. Due to the possible overlap of the titration of the histidine sidchain through its pKa (~6), the effect of pH variation for an unphosphorylated peptide, hcTnI 16-41, was also studied. The spectra below (Fig 4.6) focus on the spectral region corresponding to signals of arginine dCH_2, lysine eCH_2 and the ßCH_2 of Asn24 (2.6-3.4ppm). The absence of any spectral change for these signals in the unphosphorylated peptide over the pH range 4.5-5.4 (Fig 4.6A) contrasted with the small but resolvable changes for Asn24, as well as with the alterations in the composite signals of arginine dCH_2 and lysine eCH_2, of S_{23}P hcTnI 16-37 (Fig 4.6B). The latter changes corresponded to altered environments for Lys35/36/37. Since the S_{23}P hcTnI peptide was C-terminally amidated, these observations raised the possibility that S_{23} phosphate ionisation was sensed by the basic residues at the C-terminal end of the peptide. The presence of a 'looped' conformation that involved the proximity of S_{23}P to the C-terminus of monophosphorylated hcTnI 16-37 was therefore one possible explanation suggested by these data.

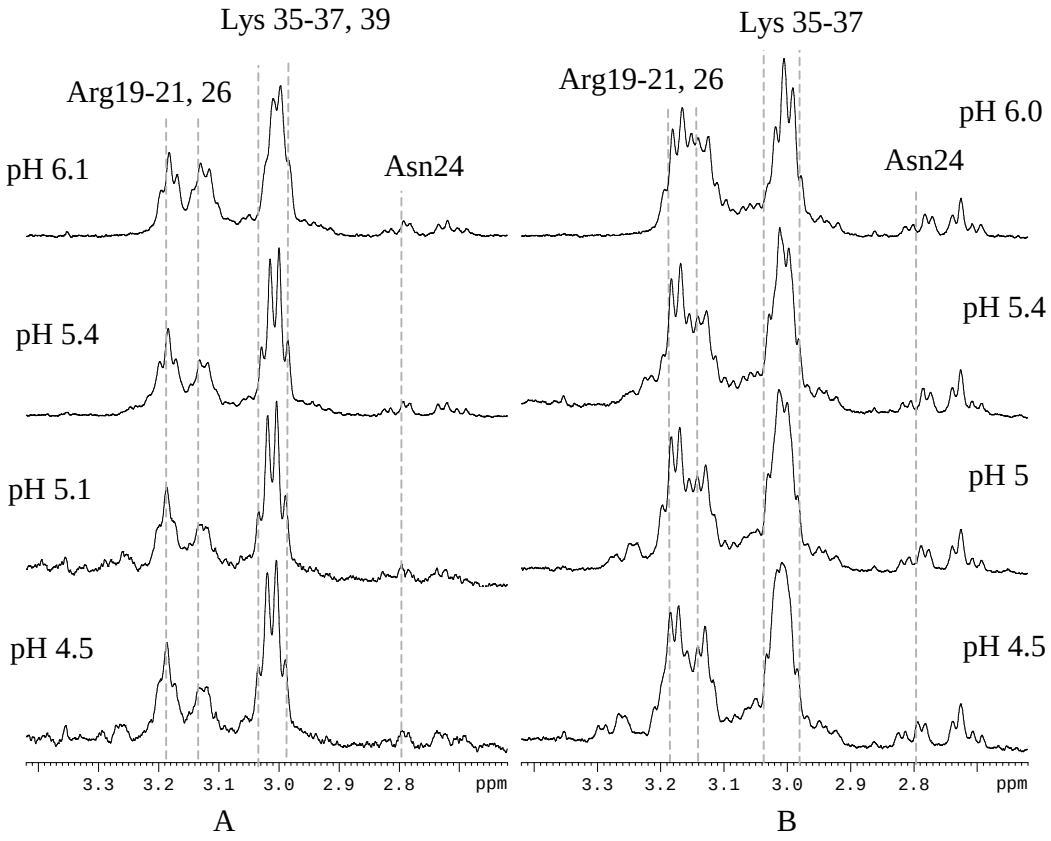

Figure 4.6 Comparison of the terminal groups of the sidechains of arginine, lysine and asparagine of hcTnI peptides during pH titration ranging from approximately 4.5-6. T=298K.
(A) Unphosphorylated 16-41
(B) S23P monophosphorylated 16-37

4.3 Both monophosphorylated peptides of hcTnI 16-37 retain interaction with F-actin

The detection of an interaction between F-actin and the hcTnI 16-37 peptides was achieved by the use of the spectral effects monitored using both Carr-Purcell (CP) and normal spectral acquisition approaches. As before, this was done in order to be able to obtain an estimate of the average relaxation rate experienced by different groups on the peptide molecules as a function of added F-actin.

The results shown below (Figs 4.7-4.10) present observations of the spectral effects during titration of each of the hcTnI 16-37 peptides with F-actin. Comparison of the F-

actin dependent effects, in the case of each peptide, was obtained by the use of the same molar concentration ratios of peptide to F-actin. F-actin was titrated into the 50μM peptide at concentrations of 4μM and 15μM. The reversibility of the binding of the hcTnI peptide(s) to F-actin was subsequently demonstrated by binding competition using a region of cTnI shown earlier to alter the binding between F-actin and 16-37.

For ease of representation the figures below display only the downfield, aromatic signal region of the spectra of hcTnI 16-37. The signals observed derive from residues uniquely identified and that are located in the segment of the N-terminus of hcTnI shown to associate with F-actin. Thus in the aromatic region of the unphosphorylated 16-37 hcTnI peptide the signals that can be monitored derive from Tyr25, 28 and His33. Figure 4.7 below illustrates that the population of the peptide molecules in solution are in fast exchange between being F-actin bound and being free. Sub-stoichiometric concentrations of F-actin led to marked relaxation of the signals of Tyr25, 28 and His33 observed in the two-pulse CP spectra as reductions in signal intensity. Although it could be assumed that the equilibrium between free and bound species involved only one unique mode of binding, the possibility of more than one bound form could not be discounted. Competition using hcTnI 36-52 was therefore studied based on the observation that this peptide had been found to be able to reduce the F-actin bound population of hcTnI 16-37 (Chapter 3).

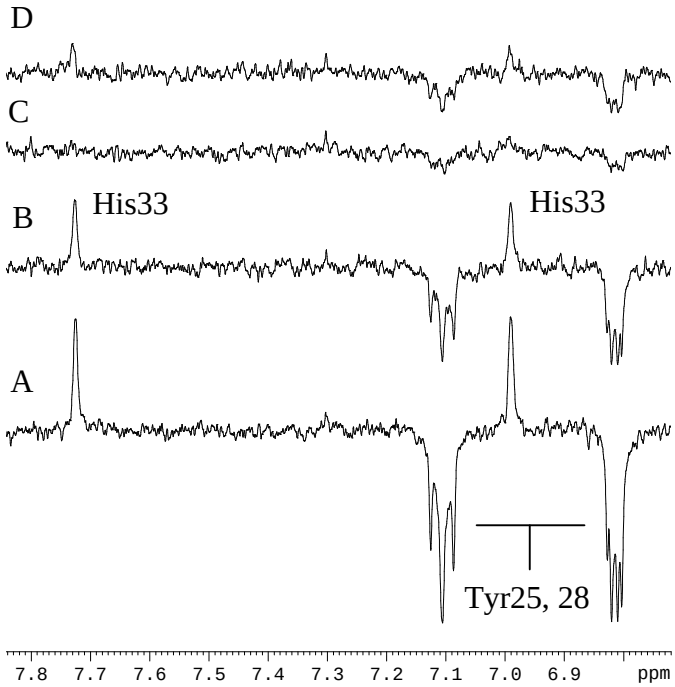

Figure 4.7 Interaction of unphosphorylated hcTnI 16-37 with F-actin causes relaxation of Tyr25, 28 and His33 indicative of the localisation of these sidechains on the surface of F-actin. Two pulse CP acquisitions of 50µM hcTnI 16-37 (A) in the presence of (B) 4µM F-actin and (C) 15µM F-actin and upon the addition of 15µM hcTnI 36-52 (D), pH 7.2 and T=298K.

The sequence of hcTnI 36-52 contains no aromatic residues and therefore no signals deriving from this peptide appeared in the aromatic region of the spectrum to mask the detection of effects on Tyr25, 28 and His33. Figure 4.7D illustrates that the presence of hcTnI 36-52 at a concentration equal to that of F-actin led to a small but observable increase in signal intensity for Tyr25, 28 and His 33. This observation indicated the reversibility of F-actin binding by hcTnI 16-37 but, since the magnitude of the signal intensity reappearance was relatively small (cf Fig 4.7A and 4.7D), suggested that the nature of the complex between hcTnI 16-37 and F-actin was not dominated by the contribution of the C-terminal basic residues of hcTnI 16-37 (as described in Chapter 3).

The impact of monophosphorylation on the interaction of hcTnI 16-37 with F-actin could be resolved by comparison of the spectral effects resulting from complex

formation with between F-actin and the unphosphorylated hcTnI 16-37 peptide. Figure 4.8B shows that addition of F-actin to S_{22}P hcTnI 16-37 led to broadening of the signals of Tyr25, 28 and His33 indicative of the retention of interaction with F-actin.

These data confirmed the ability of this monophosphorylated peptide of hcTnI 16-37 to interact with F-actin and implied that the addition of a phosphate group at S22 did not block the interaction between 16-37 and F-actin that still involved the region around Tyr 25 and 28.

One notable difference from the association of the unphosphorylated peptide with F-actin (Fig 4.8Aii) was that the relaxation of the sidechain signals of Tyr25, 28 of S_{22}P hcTnI 16-37 was relatively greater than that observed for the resonances of His33. Since relaxation derived from the intimacy of contact with the surface of F-actin, this suggested that the presence of the phosphate group on Ser22 had led to closer contact of Tyr25, 28 to F-actin compared to the sidechain of His33 to F-actin. This conclusion was supported by the observation that binding competition by hcTnI 36-52 was more effective in the case of S_{22}P hcTnI 16-37 where the competition of hcTnI 36-52 led to a more marked return of the tyrosine signals when compared to the unphosphorylated form of hcTnI 16-37 (Fig 4.8Aii and iv).

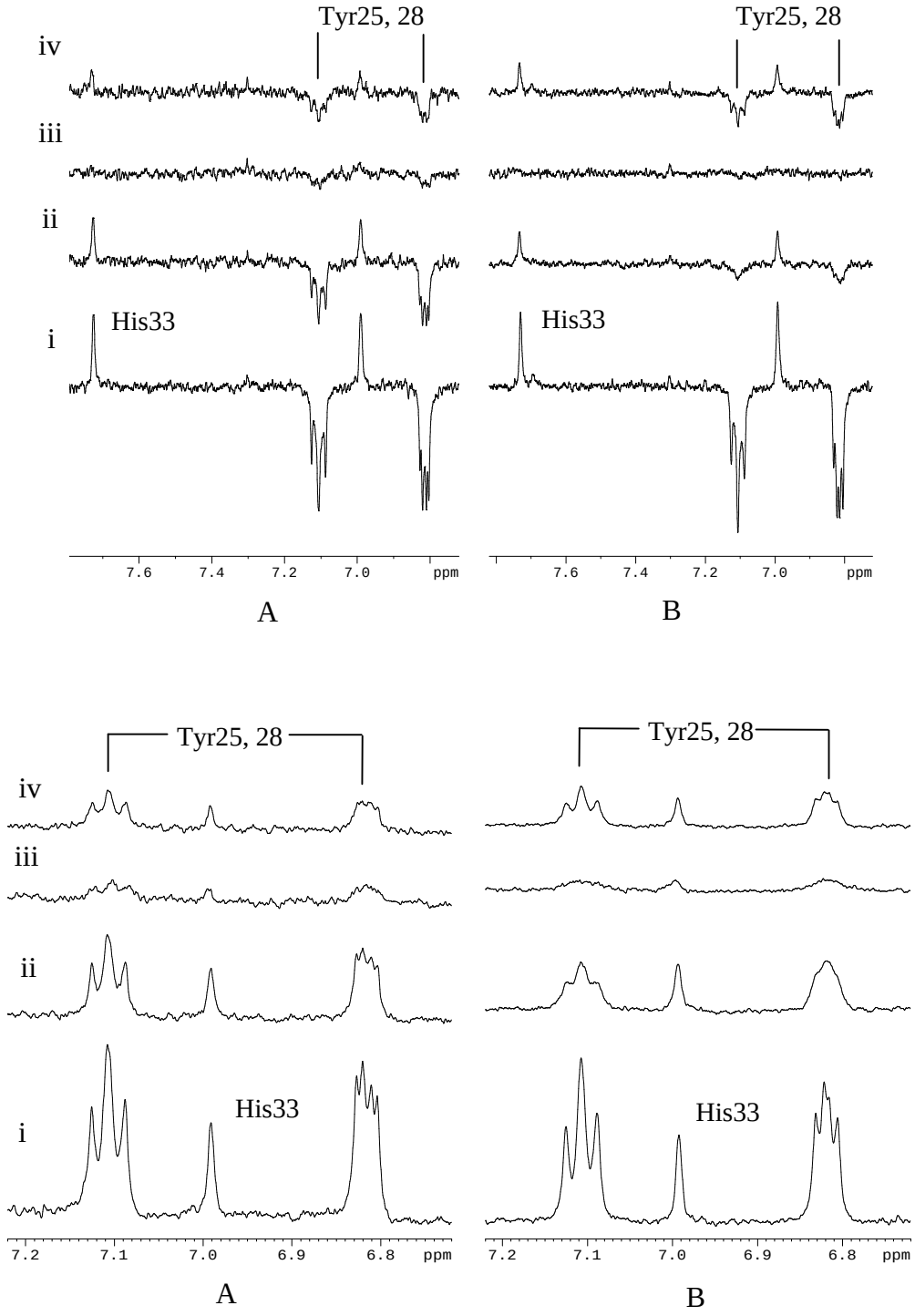

Figure 4.8 Binding to F-actin by hcTnI 16-37 (A) and S22P hcTnI 16-37 (B) involves the segment containing Tyr25, 28.
(A) Normal (lower traces) and two pulse (upper traces) spectra of 50µM hcTnI 16-37(i) obtained during titration with 4µM F-actin (ii) and 15µM F-actin (iii) and upon subsequent addition of 15µM hcTnI 36-52 (iv).
(B) Normal (lower traces) and two pulse (upper traces) spectra of 50µM $S_{22}P$ hcTnI 16-37, obtained during titration with 4µM F-actin (ii) and 15µM F-actin (iii) and upon subsequent addition of 15µM hcTnI 36-52 (iv), pH 7.2 and T=298K.

The possibility that phosphorylation at Ser22 influenced the mode of binding of hcTnI 16-37 to F-actin led to the expectation that the presence of the phosphate on Ser23 would be still more effective in interfering with any contribution to F-actin binding that is dependent upon the C-terminal basic residues of hcTnI 16-37 due to the phosphate group occurring closer to this part of the sequence. Figures 4.9 and 4.10 below compare the spectral effects of F-actin binding to S_{23}P hcTnI 16-37 with those found for the unphosphorylated peptide over a peptide to F-actin concentration ratio of 12:1 to 3:1.

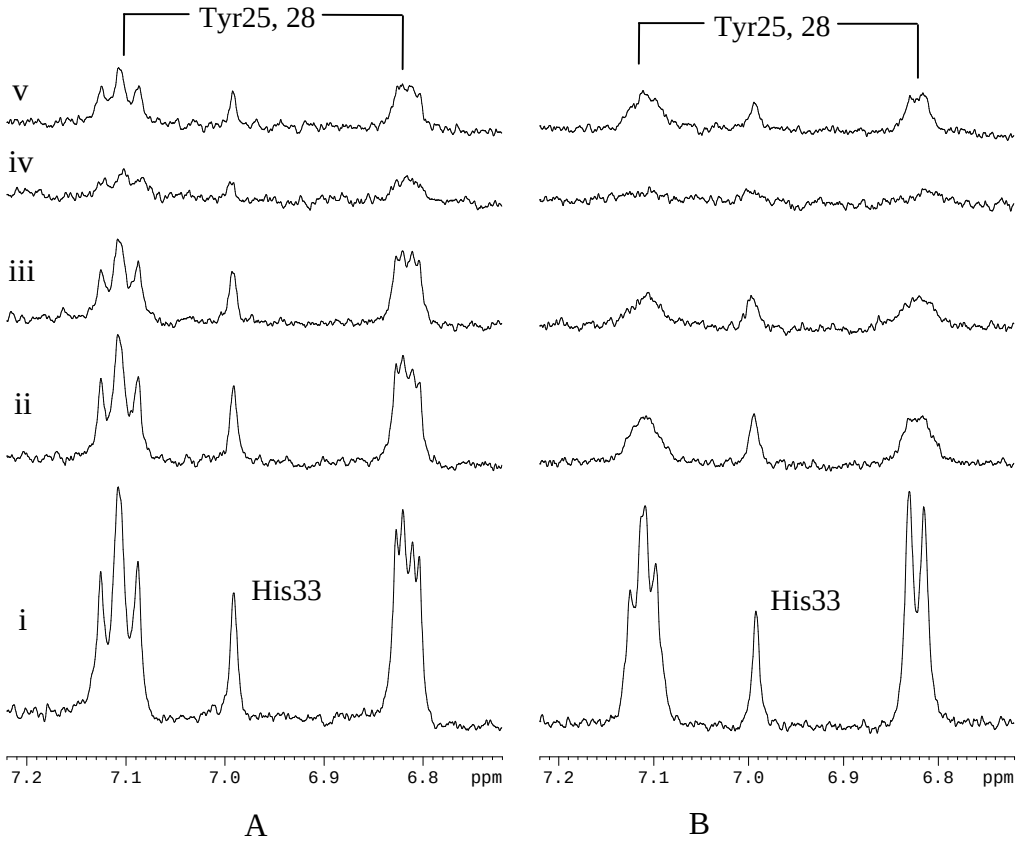

Figure 4.9 Binding to F-actin by hcTnI 16-37 (A) and S23P hcTnI 16-37 (B) involves the segment containing Tyr25, 28.

(A) 50µM hcTnI 16-37, obtained during titration with 4µM F-actin (ii),7.5µM F-actin (iii), and 15µM F-actin (iv) and upon subsequent addition of 15µM hcTnI 36-52 (v).

(B) 50µM S_{23}P hcTnI 16-37, obtained during titration with 4µM F-actin (ii),7.5µM F-actin (iii), and 15µM F-actin (iv) and upon subsequent addition of 15µM hcTnI 36-52 (v). pH 7.2 and T=298K.

The progressive increase in line broadening of Tyr25, 28 signals observed during titration (Fig 4.9) was confirmed by the relaxation time changes detected by two pulse CP acquisition (Fig 4.10). These observations directly led to the conclusion that complex formation with F-actin by both hcTnI 16-37 and S_{23}P hcTnI 16-37 still involved the association of the sidechains of Tyr25, 28 with the F-actin surface. The spectra obtained in the initial stages of the titration, i.e. at relatively low F-actin to peptide molar ratios, also suggested that complex formation between S_{23}P hcTnI 16-37 and F-actin led to significantly greater relaxation for the sidechain signals of Tyr25, 28 as compared to the ring protons of His33. This can be seen from the relative intensity of the corresponding resonances (Fig 4.9 and 4.10). Interestingly, competition by hcTnI 36-52 (Fig 4.9 trace v and Fig 4.10 trace iv) was not notably more effective in the case of S_{23}P hcTnI 16-37 compared to unphosphorylated hcTnI 16-37.

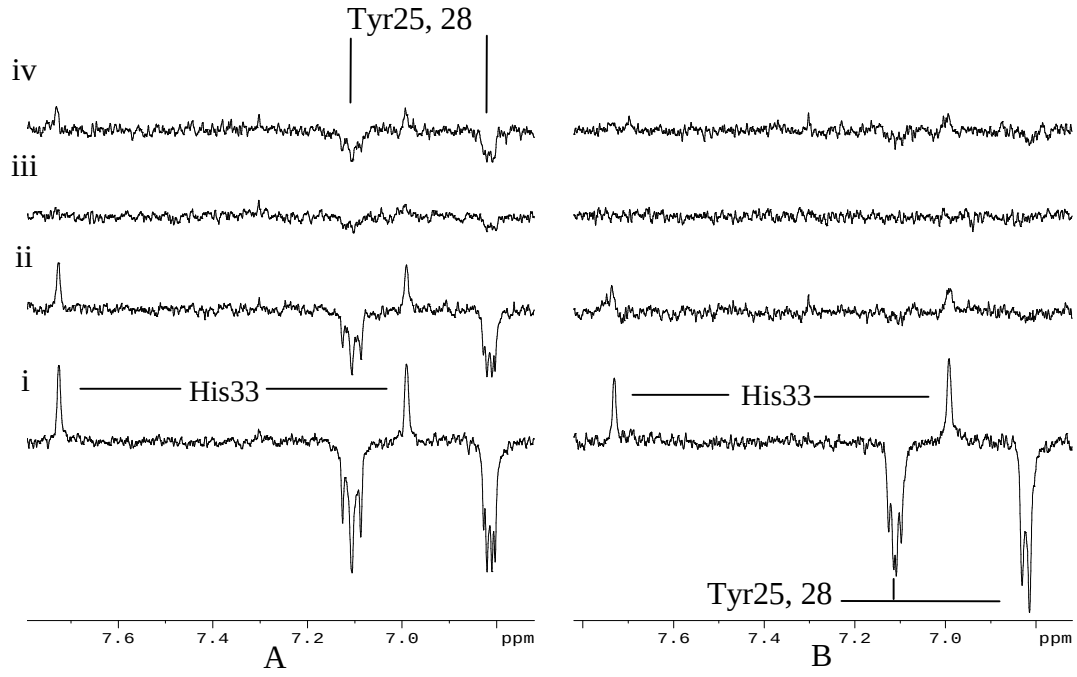

Figure 4.10 Binding to F-actin by hcTnI 16-37 (A) and S23P hcTnI 16-37 (B) in two pulse CP. (A) 50µM hcTnI 16-37, obtained during titration with 4µM F-actin (ii),15µM F-actin (iii), and upon subsequent addition of 15µM hcTnI 36-52 (iv).
(B) 50µM S_{23}P hcTnI 16-37, obtained during titration with 4µM F-actin (ii),15µM F-actin (iii), and upon subsequent addition of 15µM hcTnI 36-52 (iv), pH 7.2 and T=298K.

It seemed that there may be differences between the binding to F-actin by unphosphorylated hcTnI 16-37 and S_{23}P hcTnI 16-37. In order to compare the F-actin binding properties of hcTnI 16-37 and S_{23}P hcTnI 16-37, an equimolar mixture of these two peptides was titrated with F-actin. The ^{1}H MR spectra of the two peptides were virtually superimposable but, as illustrated in Figure 4.11, small chemical shift differences for certain residue types, e.g. Ala27 or 29 (1.3ppm), allowed resolution of the relative effects resulting from association of each peptide with F-actin. The distinctive resonances of Tyr25, 28 of the two peptides (Fig 4.12) allowed the observation of a more marked broadening of signals occurring for the unphosphorylated hcTnI 16-37 peptide. The inference of a greater extent of complex formation and, hence, higher affinity of hcTnI 16-37 for F-actin was confirmed by inspection of the distinguishable ßCH_3 methyl signal of alanine 27 or 29 (1.3ppm, Fig 4.11). This signal acted as a spectral reporter for hcTnI 16-37, appearing with a (right) upfield shift in the monophosphorylated peptide. This signal was observed to be broadened to a greater degree upon F-actin addition than the corresponding ßCH_3 resonance, arising from Ala 27 or 29 (1.3ppm), of S_{23}P hcTnI 16-37. Figures 4.11 and 4.12 also illustrate these differential actin-binding effects by the use of difference spectroscopy (denoted A minus B, top traces Figures 4.11 and 4.12) that highlighted the most perturbed signals as positive peaks in the difference spectrum.

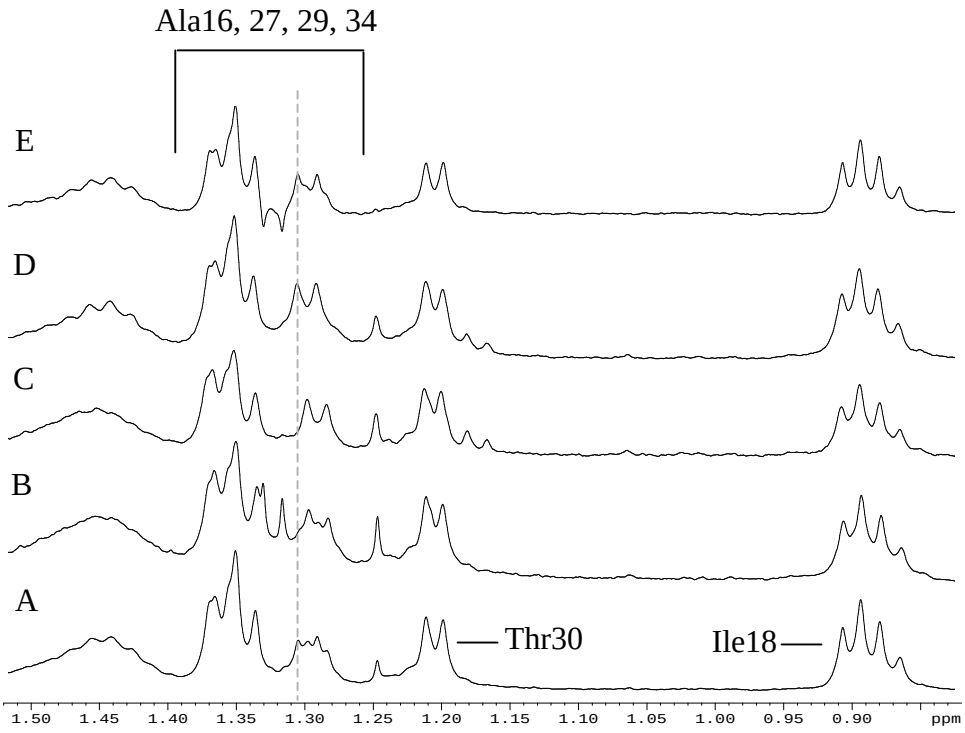

Figure 4.11 Observation of the methyl groups of a mixture of hcTnI 16-37 and S23P hcTnI 16-37 during titration of F-actin.
(A) Mixture of 50µM hcTnI 16-37 and 50µM S_{23}P hcTnI 16-37,
(B) Addition of 25µM F-actin
(C) Spectrum of 50µM free S_{23}P hcTnI 16-37
(D) Spectrum of 50µM free hcTnI 16-37
(E) Difference spectrum (spectrum A minus spectrum B) showing that the remaining positive signals (mainly Ala at 1.3ppm) are equivalent to unphosphorylated hcTnI 16-37, effectively subtracting the signals that remain at 25µM F-actin i.e. S_{23}P. Therefore S_{23}P hcTnI 16-37 is less involved in interaction with F-actin in spectrum B in the presence of the unphosphorylated 16-37 peptide, pH 7.2 and T=298K.

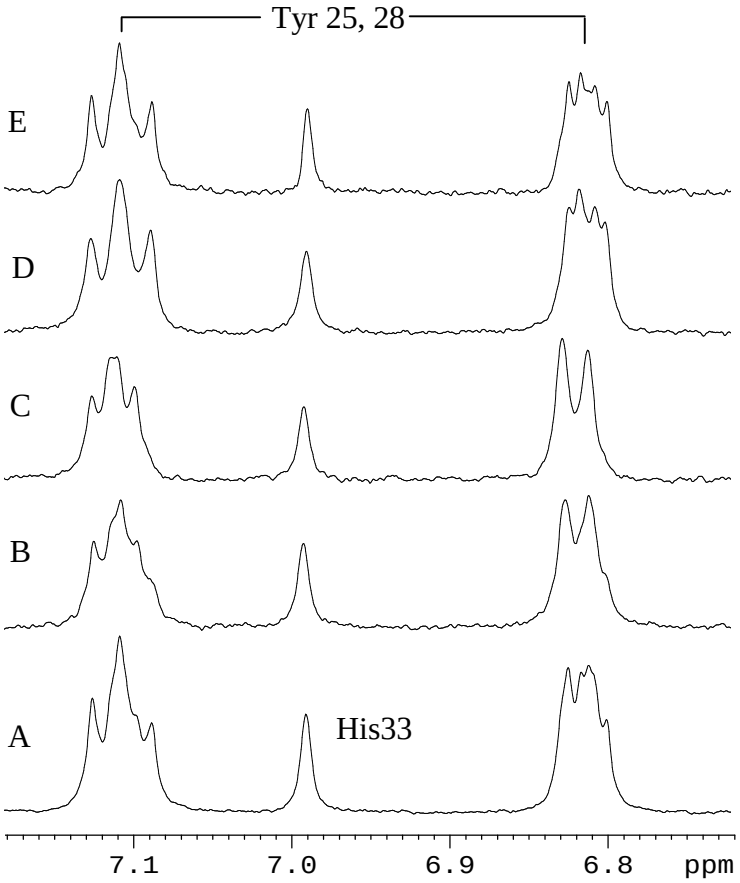

Figure 4.12 Observation of the aromatic region of a mixture of hcTnI 16-37 and S23P hcTnI 16-37 during titration of F-actin,
(A) Mixture of 50μM hcTnI 16-37 and 50μM S_{23}P hcTnI 16-37,
(B) Addition of 25μM F-actin
(C) Spectrum of 50μM free S_{23}P hcTnI 16-37
(D) Spectrum of 50μM free hcTnI 16-37
(E) Spectrum A minus spectrum B showing that the remaining signals are equivalent to unphosphorylated hcTnI 16-37. Note the similarities of Tyr25, 28 at 6.8ppm between B and C and, separately between D and E. Therefore S_{23}P hcTnI 16-37 is less involved in the binding with F-actin in spectrum B in the presence of the unphosphorylated 16-37 peptide, pH 7.2 and T=298K.

Clearly, therefore, phosphorylation at Ser23 reduced the affinity of hcTnI 16-37 for F-actin. However, consistent with the observations on S_{23}P hcTnI 16-37 alone (e.g. Fig 4.9), interaction with F-actin by both unphosphorylated and monophosphorylated (S_{22}P , S_{23}P) peptides involved association of the segment encompassing Tyr25, 28 with the surface of F-actin. Therefore it was considered relevant to confirm the contribution of charge to the binding of hcTnI 16-37 to actin.

4.4 Study of the contribution of charge of the N-terminus hcTnI to the interaction with actin

A fluorescence-based study of actin polymerisation was undertaken to investigate whether the binding contribution from basic residues of hcTnI 16-37 resulted from their direct interaction with acidic residues on actin.

It has been reported that G-actin polymerises to F-actin in the presence of short, positively charged peptide sequences and/or as a result of increasing ionic strength (Tang and Janmey 1996). The transition can be monitored using G-actin labelled at Cys374 with pyrene whose fluorescence increases upon polymerisation.

The effect of increasing time of after addition of 2mM $MgCl_2$ and 50mM KCl on the fluorescence spectrum of pyrene G-actin was used in an earlier chapter (methods, Chapter 2) as a 'proof of principle' illustration of the large (>100%) increase in fluorescence emission associated with the G- to F-actin transition and the time dependence of the process. Similar changes had been reported in the presence of the inhibitory peptide of hcTnI that has two clusters of positively charged residues (Patchell et al, 2002, Patchell and Cheung personal communication).

128-N-Ac-TQKIFDLRGKFKRPTLRRVRISADAM-153

This peptide was here used as a 'top-up' whose addition towards the end of the experiment was expected to lead to an increase in pyrene fluorescence and in this way to act as a check on the viability of the experiment. Figure 4.13 below shows the variability of the 385nm fluorescence emission maximum of 1µM pyrene G-actin with increasing concentrations of hcTnI 16-37 (0-10µM). A delay of some 30 minutes was

used between each titration step to allow the initiation of any polymerisation. No change in fluorescence emission was detectable. An overnight incubation of the solution led to an approximately 20% increase in emission (Fig 4.13) but no further change was observed upon subsequent addition of 5µM hcTnI 16-37. This suggested that the overnight alteration in emission may have resulted from a slow intrinsic (non-specific) polymerisation reaction. The fluorescence increase observed upon addition of relatively low concentration of hcTnI 128-153 (0.25µM-2µM) confirmed the inability of hcTnI 16-37 to drive the polymerisation reaction.

1µM Pyrene G-actin fluorescence response to hcTnI 16-37 (A) and subsequenct addition of hcTnI 128-153 (B)

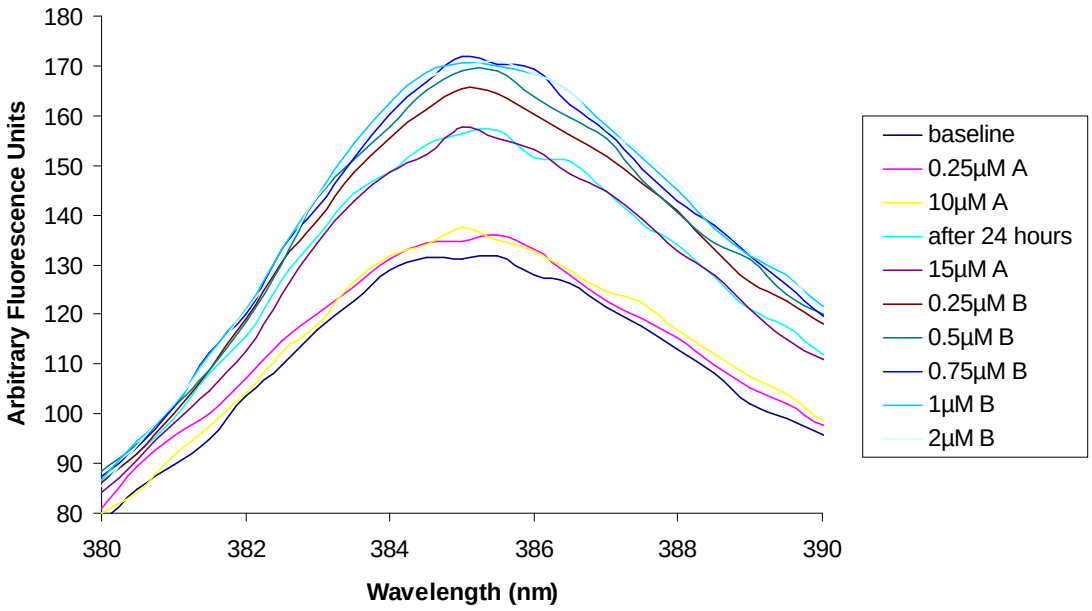

Figure 4.13 Fluorescence spectra showing emission of pyrene G-actin in a titration of unphosphorylated hcTnI 16-37 (A). Titration of unphosphorylated hcTnI 16-37 resulted in little increase in fluorescence emission, whereas titration of relatively low concentrations of the inhibitory peptide (hcTnI 128-153) (B) showed G-actin polymerisation confirming the inability of hcTnI 16-37 to drive polymerisation.

As a check on the inability of hcTnI 16-37 to behave as a catalyst for polymerisation, pyrene G-actin was first titrated with $S_{23}P$ hcTnI 16-37 with only the N-terminal

segment of the inhibitory region hcTnI 128-140 as the 'top up' species at the end of the titration. By 15µM $S_{23}P$ hcTnI 16-37 an increase of only some 10 Arbitrary Fluorescence Units (AFU) in the 385nm emission of pyrene G-actin was observed. Confirmation that fluorescence emission was indicative of catalysed polymerisation was obtained through the observation of a larger fluorescence change upon subsequent titration with hcTnI 128-140 (Fig 4.14). Twenty-four hours later a much bigger increase in fluorescence was seen but this could not be readily attributed to either peptide.

1µM Pyrene G-actin fluorescence response to hcTnI 16-37 S23P (A) and subsequent addition of hcTnI 128-140 (B)

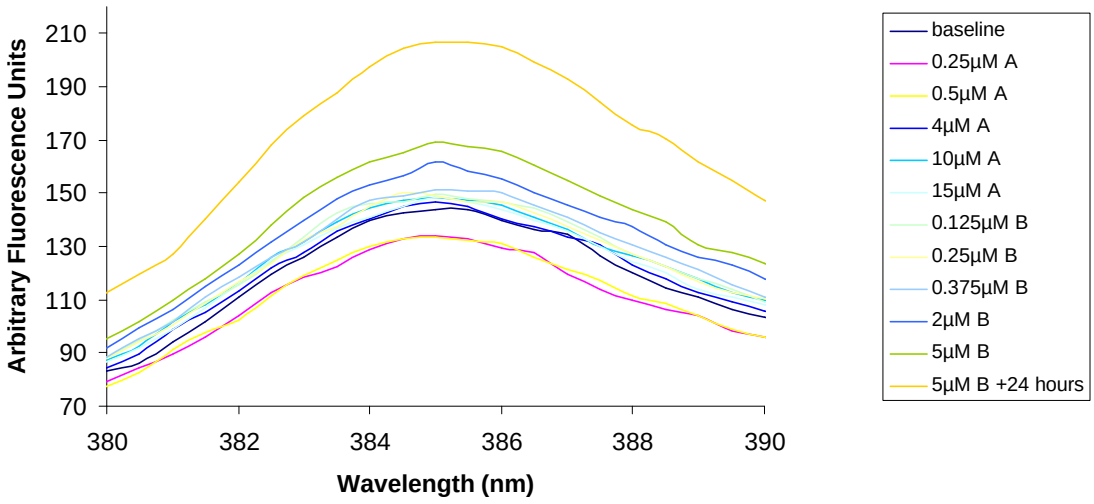

Figure 4.14 Fluorescence spectra of pyrene G-actin during titration of monophosphorylated 16-37 S23P (A) showed little increase in fluorescence emission, whereas titration of relatively low concentrations of the N-terminal segment of the inhibitory peptide hcTnI (128-140) (B) showed G-actin polymerisation confirming the inability of the monophosphorylated hcTnI 16-37 $S_{23}P$ to drive polymerisation.

Unlike hcTnI 16-37, both hcTnI 128-153 and hcTnI 128-140 separately proved effective mediators for the G-actin to F-actin transition. The apparent inability of hcTnI 16-37 to promote polymerisation strongly suggested either that its interaction with actin, here

G-actin, was not mediated by its positively charged residues or that its site of interaction was distinct from that of hcTnI 128-153. Given the observation above that hcTnI 36-52 was able to compete with hcTnI 16-37 for binding to F-actin, the ability of this peptide to promote polymerisation was also studied.

36-KKSKISASRKLQLKTLL-52

Titration of hcTnI 36-52 into 1µM pyrene labelled G-actin failed to elicit any change in fluorescence emission (Fig 4.15) even at a 6 fold molar excess of G-actin. As in the earlier experiments, the basic hcTnI inhibitory peptide (hcTnI 128-153) was subsequently added and was found to induce polymerisation of G-actin.

1µM Pyrene G-actin fluorescence response to hcTnI 36-52 (A) and subsequent addition addition of hcTnI 128-153 (B)

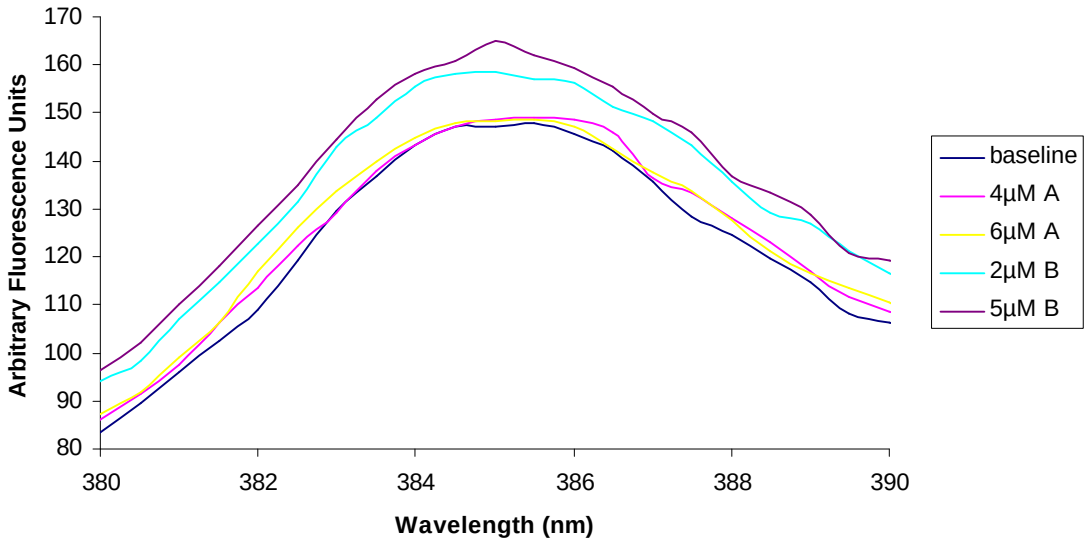

Figure 4.15 Fluorescence spectra of pyrene G-actin in a titration of hcTnI 36-52 (A) shows little increase in fluorescence emission. Again, titration of the inhibitory peptide hcTnI (128-153) (B) confirmed G-actin polymerisation. This also confirms that this peptide, hcTnI 36-52 is unable to drive polymerisation of G to F-actin.

Although it was possible that hcTnI 16-37 bound only to polymerised and not G-actin, taken together these fluorescence-based observations suggested that hcTnI 16-37

possessed a binding site on actin distinct from that occupied by hcTnI 128-153. This was consistent with the observations (Chapter 3) that the basic residues of hcTnI 16-37 did not dominate as the determinants of binding, a feature of the interaction explored in competition experiments using hcTnI 128-153.

4.5 hcTnI residues 128-153 compete with hcTnI 16-37 for F-actin binding

Since hcTnI 128-153 had previously been shown to simultaneously displace both myosin peptides from F-actin (Patchell et al, 2005) it was pertinent to assess the relative affinity for F-actin of this inhibitory region of hcTnI and hcTnI 16-37 peptides. Figure 4.16 compares the effect of titration with F-actin for separate equimolar mixtures of hcTnI 128-153 with either hcTnI 16-37 (A), or $S_{23}P$ hcTnI 16-37 (B), or $S_{22}P$ hcTnI 16-37 (C). It was readily apparent from the perturbation of the composite phenylalanine sidechain resonance of Phe132 and 138 from hcTnI 128-153 that the population of F-actin bound inhibitory region was greater if either of the monophosphorylated forms of hcTnI 16-37 were present in solution rather than unphosphorylated hcTnI 16-37. This was indicative of competition by hcTnI 16-37 even when monophosphorylated.

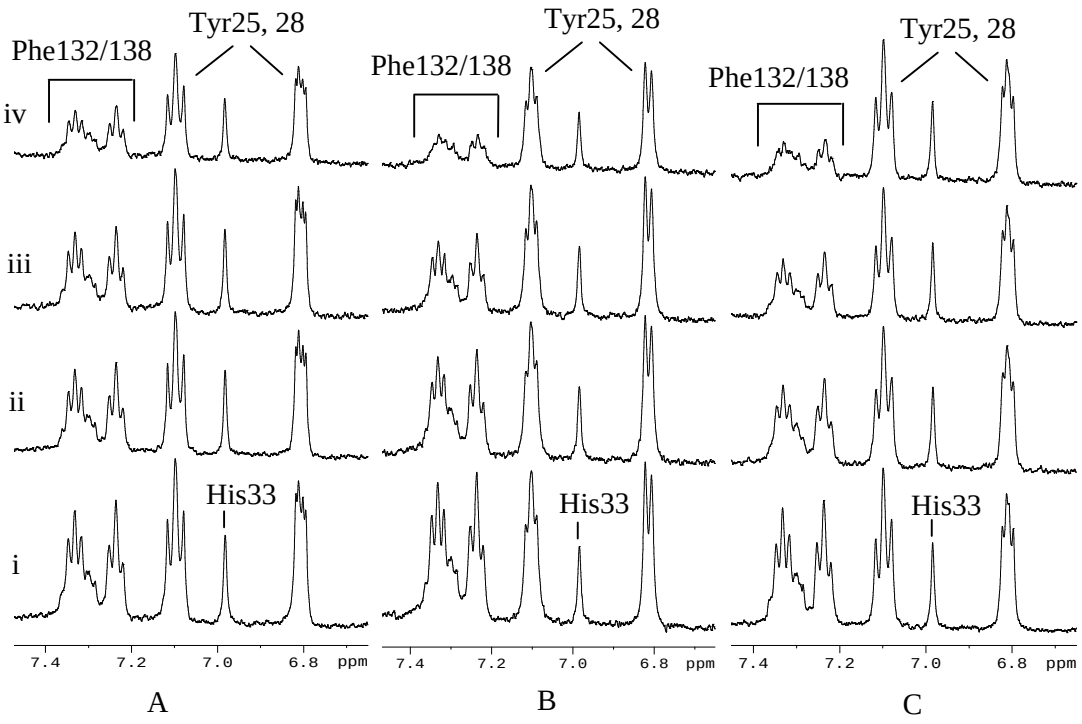

Figure 4.16 Spectrum of the aromatic region of a mixture of the inhibitory peptide hcTnI 128-153 and each of the hcTnI 16-37 peptides during titration of F-actin. Unphosphorylated hcTnI 16-37 (A) $S_{23}P$ hcTnI 16-37 (B) and $S_{22}P$ hcTnI 16-37 (C), pH 7.2 and T=298K.
(i) Mixture of 50µM hcTnI 128-153 and 50µM hcTnI 16-37 (A) $S_{23}P$ (B) $S_{22}P$ (C)
(ii) 4µM F-actin
(iii) 7.5µM F-actin
(iv) 15µM F-actin
The ability of the inhibitory peptide to antagonise binding between the hcTnI 16-37 peptides and F-actin can be seen by the reduced effect on Tyr25, 28, compared to that achieved in the absence of the inhibitory peptide hcTnI 128-153 (Figs 4.7-4.10). Phe132/138 of the inhibitory peptide hcTnI 128-153 broadened more with F-actin in the presence of $S_{23}P$ hcTnI 16-37 (Biv) than with the unphosphorylated hcTnI 16-37 peptide (Aiv).

The lower antagonism by the monophosphorylated peptides could have arisen from the reduced contribution of hcTnI 31-37 to binding by this region that contained a stretch of basic residues similar to the two clusters of positively charged groups of hcTnI 128-153. It was therefore necessary to establish that the presence of the hcTnI inhibitory region had not abolished binding by monophosphorylated hcTnI 16-37 to F-actin. The retention of binding to F-actin is demonstrated in Figure 4.17 A and B. Concurrent

perturbations were seen for the aromatic sidechain signals during titration with F-actin of equimolar mixtures of hcTnI 128-153 and hcTnI 16-37 (A) $S_{23}P$ hcTnI 16-37 (B).

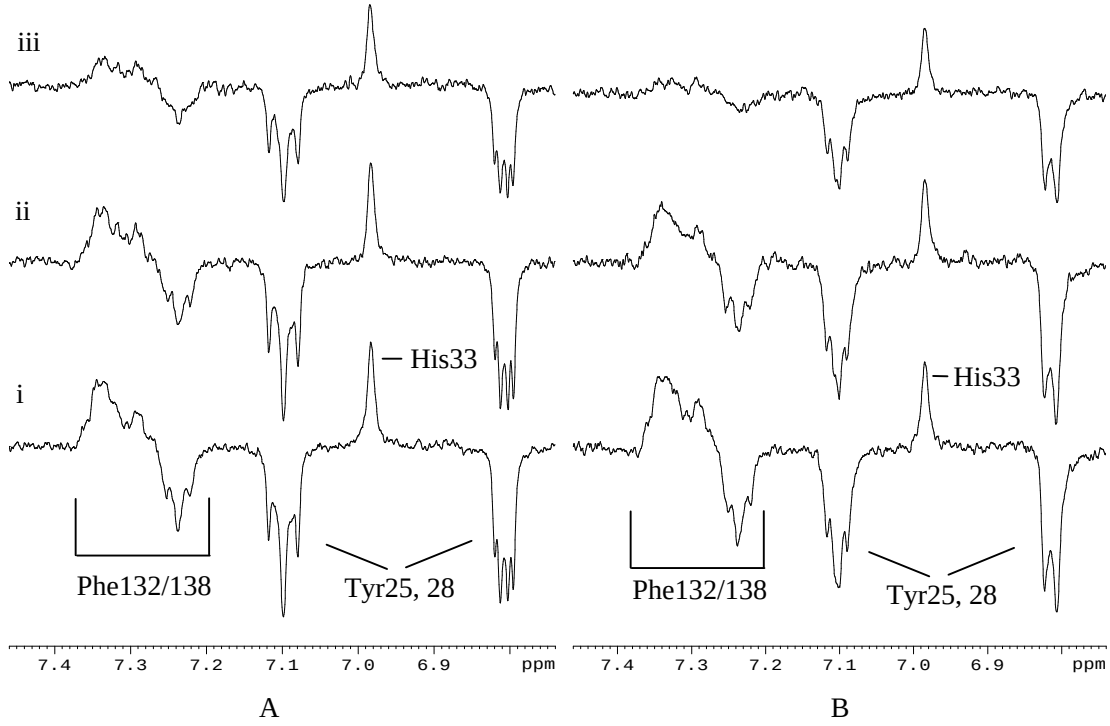

Figure 4.17 Two pulse CP spectrum of the aromatic region of a mixture of the inhibitory peptide hcTnI 128-153 and an hcTnI 16-37 peptide during titration with F-actin. Unphosphorylated hcTnI 16-37 (A) $S_{23}P$ hcTnI 16-37 (B), pH 7.2 and T=298K.
(i) Mixture of 50µM hcTnI 128-153 and 50µM hcTnI 16-37 (A) $S_{23}P$ (B)
(ii) 4µM F-actin
(iii) 15µM F-actin
Antagonism of the inhibitory peptide hcTnI 128-153 of the binding between the hcTnI 16-37 peptides and F-actin can be seen by the reduced effect on Tyr25, 28 than was achieved in the absence of the inhibitory peptide hcTnI 128-153 (Figs 4.7-4.10). Again, Phe132/138 of the inhibitory peptide hcTnI 128-153 broadened more with F-actin in the presence of $S_{23}P$ hcTnI 16-37 (Biii) than with the unphosphorylated hcTnI 16-37 peptide (Aiii).

4.6 The monophosphorylated Ser23P hcTnI 16-37 peptide displaced the myosin loop peptides from F-actin

Since $S_{23}P$ hcTnI 16-37 displayed a lower affinity for F-actin compared to the unphosphorylated peptide sequence, it was of interest to determine how this may affect its ability to influence the interaction of the myosin loops with F-actin. Competition by $S_{23}P$ hcTnI 16-37 for F-actin binding by hcßM 398-414 and hcßM 622-646 was

therefore studied. Figure 4.18 shows contrasting efficacy of hcTnI 16-37 and $S_{23}P$ hcTnI 16-37 as antagonists of F-actin binding by the myosin loop peptides. The spectra shown compare the effect of identical concentration ranges of unphosphorylated hcTnI 16-37 and $S_{23}P$ hcTnI 16-37. These experimental conditions allowed for a quantitative comparison of the relative affinity for F-actin of the phosphorylated and unphosphorylated peptides. A roughly 3 fold greater concentration of $S_{23}P$ hcTnI 16-37 was found under these experimental conditions to induce antagonism of myosin loop peptide binding matching that of the unphosphorylated hcTnI 16-37 that were observed to lead to a comparable reduction in the population of the myosin peptides bound to F-actin, as was judged by reversal of the line broadening of their signals (compare Fig 4.18 Aii with Fig 4.18 Biv) This observation pointed to less than an order of magnitude reduction in the affinity of hcTnI 16-37 for F-actin upon phosphate incorporation at Ser23. The likelihood that this reduction resulted from the effect of phosphorylation being relayed to the C-terminal segment of hcTnI 16-37 was confirmed by comparing the abilities of hcTnI 16-37 and hcTnI 1-30 to elicit displacement of the two myosin peptides below.

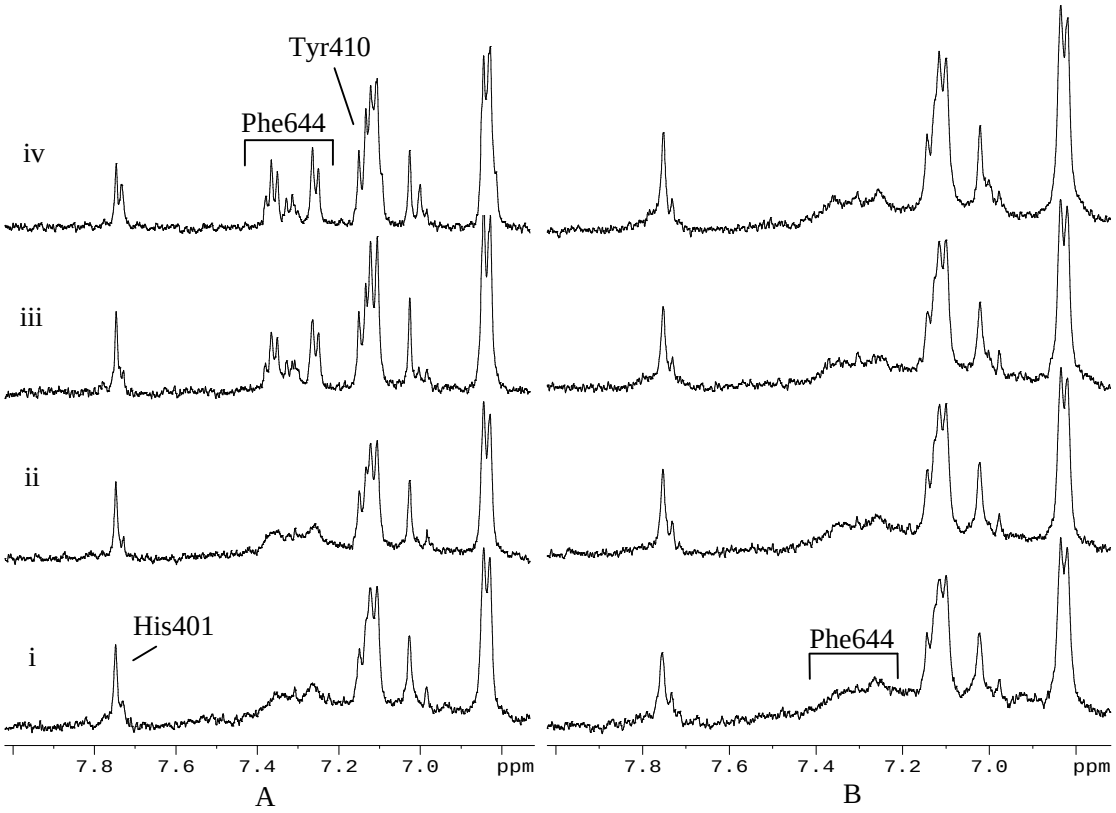

Figure 4.18 Demonstration of the reduction in efficacy of hcTnI 16-37 to displace two myosin loop peptides from F-actin as a consequence of phosphate modification of Ser23. (A) Titration of a mixture of 40µM hcßM 398-414 and 40µM hcßM 622-646 in the presence of 25µM F-actin (i) with increasing concentration of hcTnI 16-37 (ii-iv), pH 7.2 and T=298K.
(i) 0µM hcTnI peptide
(ii) Addition of 12µM hcTnI peptide unphosphorylated 16-37 hcTnI (A) S_{23}P hcTnI 16-37 (B)
(iii) Addition of 25µM hcTnI peptide unphosphorylated 16-37 hcTnI (A) S_{23}P hcTnI 16-37 (B)
(iv) Addition of 40µM hcTnI peptide unphosphorylated 16-37 hcTnI (A) S_{23}P hcTnI 16-37 (B)
The presence of hcTnI 16-37 resulted in the reversal of the broadening of the signals of both myosin peptides (e.g. His401, Tyr410 and Phe644) indicative of a reduction in the population of these peptides bound to F-actin. (B) Spectra as for A but with titration of S_{23}P hcTnI 16-37 as the competitor.

Figure 4.19 shows the progress of the titration of hcTnI 16-37 (A) and hcTnI 1-30 (B) into a mixture of the myosin peptides in the presence of F-actin. The concentrations of the competing hcTnI peptides are the same as those shown in Figure 4.18 with S_{23}P hcTnI 16-37. The less effective reversal of the F-actin induced perturbation of the myosin peptide resonances by hcTnI 1-30 closely matched that exhibited by S_{23}P hcTnI 16-37. Given that all three N-terminal hcTnI peptides were observed to separately bind

to F-actin in a manner that involved contact with the actin surface by residues 25-28, the results of the myosin loop competition assays supported the conclusion that association of this region with F-actin elicited displacement. A second conclusion was that the overall affinity for F-actin was mediated by the contribution of residues 31-37. Furthermore, the influence of the segment comprising hcTnI 31-37 $_{31}$EPHAKKK$_{37}$ plausibly altered either (or both) the on rate or off rate for complex formation. Of interest here was that this effect was modulated by the occurrence of phosphorylation at Ser23.

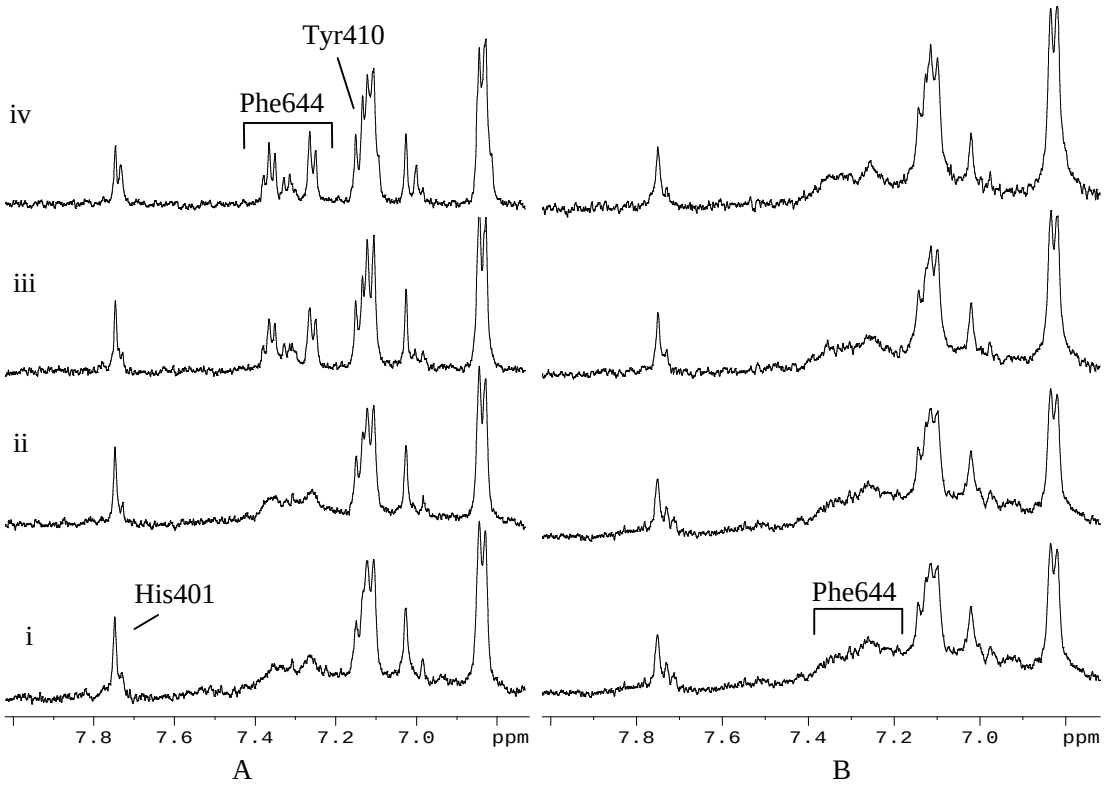

Figure 4.19 The reduced ability of hcTnI 1-30 to displace two myosin loop peptides from F-actin as a consequence of loss of residues 31-37. (A) Titration of a mixture of 40µM hcßM 398-414 and 40µM hcßM 622-646 in the presence of 25uM F-actin (i) with increasing concentration of hcTnI 16-37 (ii-iv), pH 7.2 and T=298K.
(i) 0µM hcTnI peptide
(ii) Addition of 12µM hcTnI peptide unphosphorylated hcTnI 16-37 (A) hcTnI 1-30 (B)
(iii) Addition of 25µM hcTnI peptide unphosphorylated hcTnI 16-37 (A) hcTnI 1-30 (B)
(iv) Addition of 40µM hcTnI peptide unphosphorylated hcTnI 16-37 (A) hcTnI 1-30 (B)
The presence of hcTnI 16-37 resulted in the reversal of the broadening of the signals of both myosin peptides (e.g. His401, Tyr410 and Phe644) indicative of a reduction in the population of these peptides bound to F-actin. (B) Spectra as for A but with titration of hcTnI 1-30 as the competitor.

Further assessment of whether displacement of both myosin peptides occurred during these competition assays was readily obtained by inspection of the upfield region of the spectra. This was because the uniquely identifiable methyl signals of hcßM 398-414 and hcßM 622-646 could be resolved (Fig 4.20). Using these signals as reporters, as was the case for displacement of the hcßM 622-646 myosin peptide (Fig 4.18A), the increased contribution of the hcßM 398-414 peptide signals indicated a reduced bound population. These changes allowed the conclusion that the region of hcTnI involving

residues 16-30 is able to compete with hcßM 398-414 for F-actin binding and, that the presence of hcTnI residues 31-37 available in the longer peptide enhanced overall affinity for F-actin and enabled displacement of hcßM 622-646.

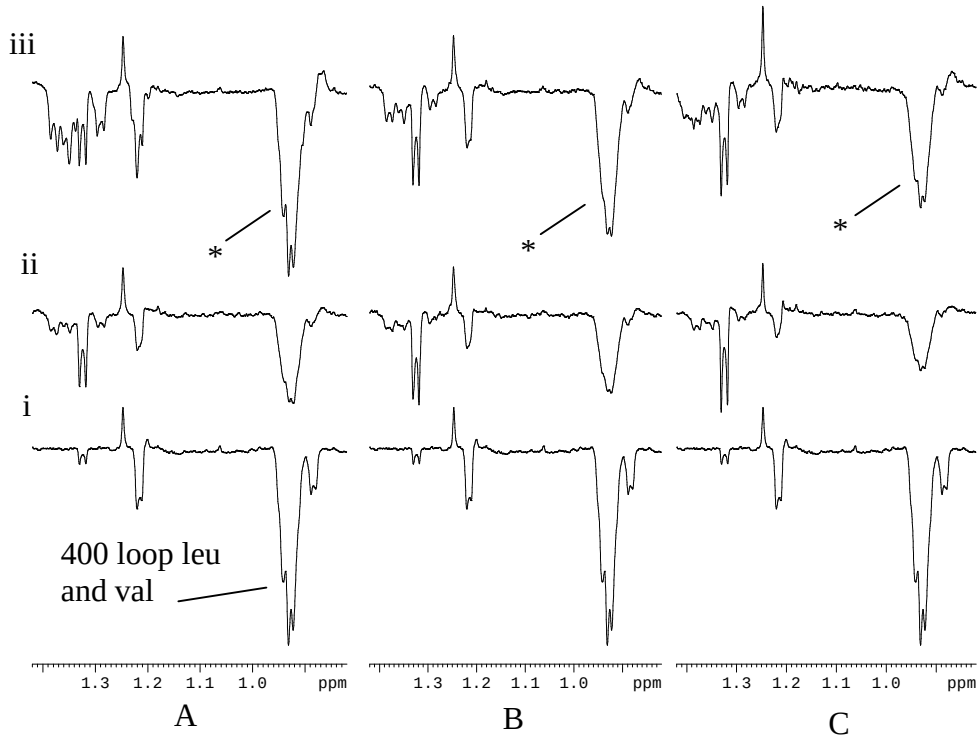

Figure 4.20 N-terminal peptides of hcTnI corresponding to hcTnI 16-37 (A) S_{23}P hcTnI 16-37 (B) and hcTnI 1-30 (C) are able to displace hcßM 398-414 myosin loop peptide from F-actin. The * represents the return of signals from hcßM 398-414 as judged by the uniquely identifiable signals of leucine and valine present only in hcßM 398-414 peptide, pH 7.2 and T=298K.
(i) 40µM hcßM 398-414
(ii) In the presence of 25µM F-actin and 40µM hcßM 622-646
(iii) Addition of 40µM hcTnI peptide unphosphorylated hcTnI 16-37 (A) S_{23}P hcTnI 16-37 (B) hcTnI 1-30 (C)
In the mixture of peptides used in this experiment hcßM 398-414 is the only sequence that contains leucines and valines. The corresponding CH_3 group signals appear inverted in these two-pulse spectra (trace i) and have resonance energies slightly downfield of the isoleucine methyl group signals that come from Ile631 of hcßM 622-646 and Ile18 of the N-terminal hcTnI peptides 16-37 and 1-30. In the presence of 25µM F-actin (trace ii) the methyl signals of hcßM 398-414 are found to have broadened upon interaction with F-actin. In all of the competition assays with the N-terminal hcTnI peptides (trace iii) there is an increase in the intensity of the inverted methyl signals at 0.93ppm (*) unique to the hcßM 398-414 peptide indicating its displacement by all of the N-terminal hcTnI peptides.

Therefore hcTnI 16-37 S_{23}P and 1-30 were both capable of displacing hcßM 398-414 from F-actin. Inspection of the extent of the changes in hcßM 398-414 signal intensity

resulting from competition however suggested that unphosphorylated hcTnI 16-37 was the most effective N-terminal peptide of hcTnI capable of displacing this myosin peptide.

A hypothesis to explain the observed difference in competition efficacy would be that the 'mode of binding' has changed in the $S_{23}P$ peptide with less 'direction' from the KKK region. This would be consistent with the observation that $S_{23}P$ binding to F-actin was less affected upon addition of 36-52 (Fig 4.9Bv). It would also be consistent with the observation that phosphate incorporation at Ser23 led to less effective displacement from F-actin of the hcßM 622-646 myosin loop peptide as judged by Phe644 (Fig 4.18).

4.7 hcTnI 16-37 S23P has a similar affinity for F-actin as hcßM 622-646

In order to inform of the F-actin affinity of $S_{23}P$ hcTnI 16-37, experiments were carried out at low concentrations of F-actin This was so as to obtain conditions under which F-actin was effectively fully bound. Titration of $S_{23}P$ hcTnI 16-37 into a mixture containing 50µM hcßM 622-646 and 7.5µM F-actin (Fig 4.21) showed that the presence of 50µM $S_{23}P$ hcTnI 16-37 (Fig 4.21D) effectively halved the population of bound hcßM 622-646. This conclusion could be seen from the contribution of the signals of Phe644 relative to the intensity of Tyr624.

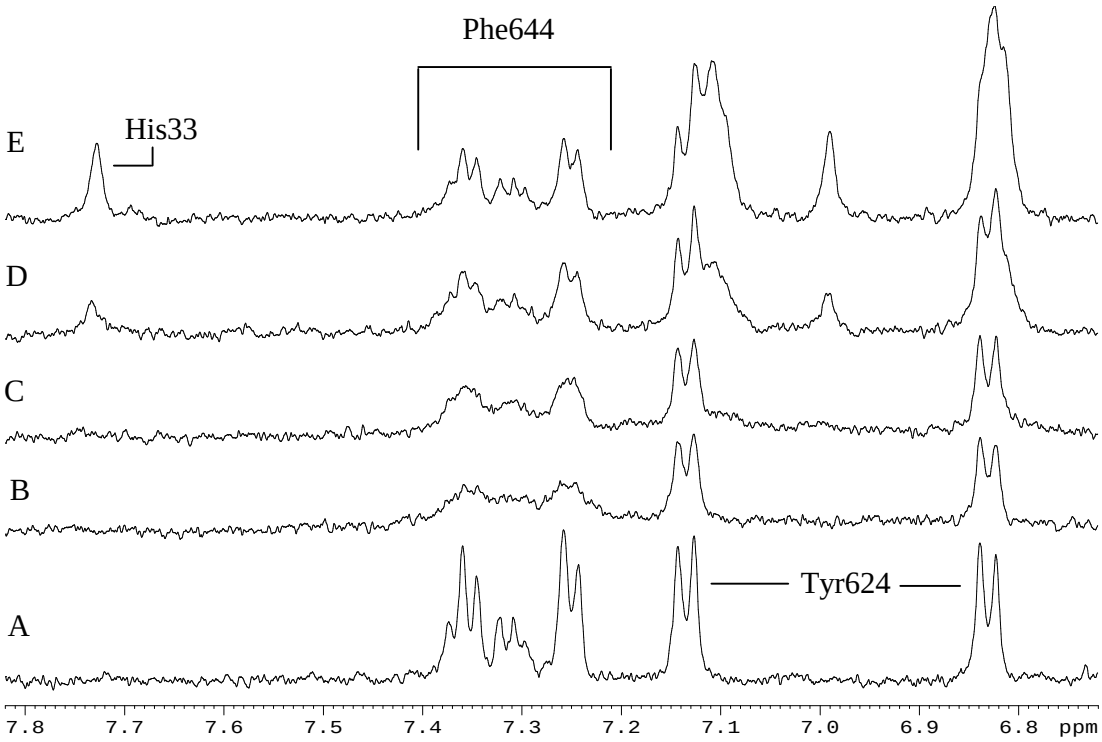

Figure 4.21 hcTnI 16-37 S23P displacement of the hcßM 622-646 loop peptide, pH 7.2 and T=298K.
(A) 50µM hcßM 622-646 loop peptide
(B) Addition of 7.5µM F-actin
(C) Addition of 15µM hcTnI peptide hcTnI 16-37 $S_{23}P$
(D) Addition of 50µM hcTnI peptide hcTnI 16-37 $S_{23}P$
(E) Addition of 80µM hcTnI peptide hcTnI 16-37 $S_{23}P$

Based on the equimolar peptide concentration present (Fig 4.21D) these data suggested roughly equal affinities for F-actin. The further addition of $S_{23}P$ hcTnI 16-37 (Fig 4.21E) resulted in continued displacement of hcßM 622-646.

The concentration range of $S_{23}P$ hcTnI 16-37 required to antagonise the binding by hcβM 622-646 was equivalent to that already observed upon competition with hcTnI 16-29 (Chapter 3). This was in keeping with the suggestion above that the contribution to F-actin binding by hcTnI residues 31-37 may be blunted by monophosphorylation. It was also in keeping with the conclusion that interaction with F-actin by hcTnI residues 16-29 was retained upon monophosphorylation.

In sum, antagonism of hcβM 622-646 binding to F-actin by unphosphorylated hcTnI 16-37 was more effective than that caused by S_{23}P hcTnI 16-37. The latter, monophosphorylated peptide was comparable to hcTnI 1-30 in displacing hcβM 622-646. The conclusion may thus be drawn that the 31-37 'EPHAKKK' region, absent in hcTnI peptides ending before residue Thr30, was minimally influential in the displacement of hcβM 622-646 by S_{23}P hcTnI 16-37

Figure 4.22 (a repeat of Fig 3.19) illustrated the selectivity of myosin loop peptide displacement by hcTnI 16-29 as shown in Chapter 3.

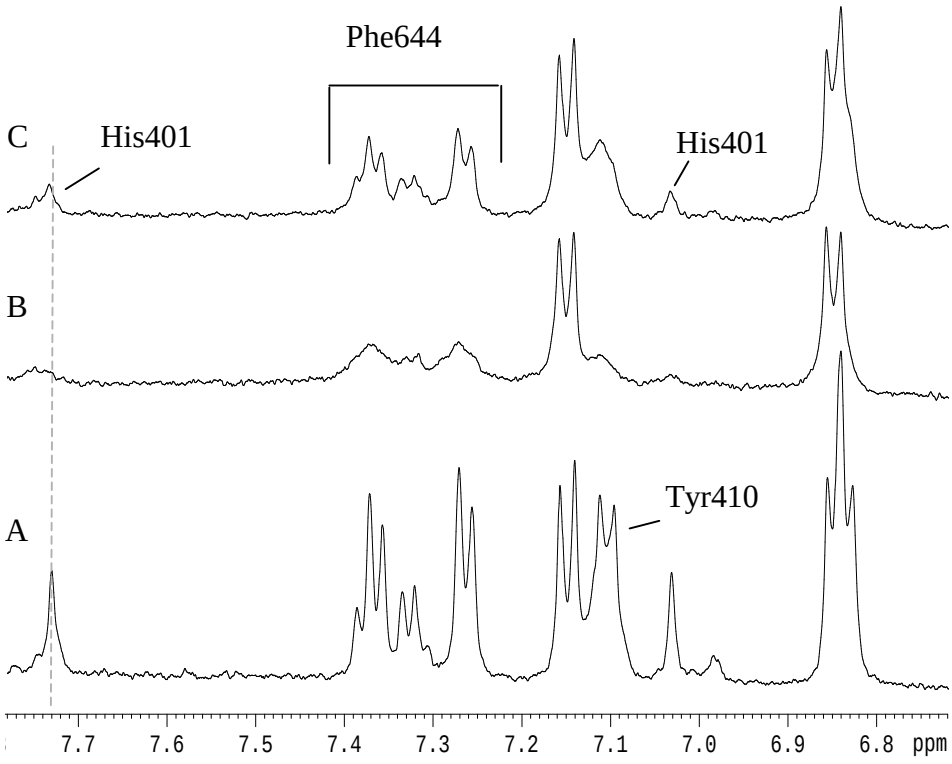

Figure 4.22 hcTnI 16-29 binding to F-actin led to displacement of the hcßM 622-646 myosin loop, pH 7.2 and T=298K.
(A) Mixture of 70µM hcßM 622-646 and 70µM hcßM 398-414 loop peptides
(B) Addition of 15µM F-actin
(C) Addition of 60µM hcTnI peptide hcTnI 16-29
Also note the confirmation of displacement by hcTnI 16-29 of hcßM 398-414 as judged by His401, although the competition by hcTnI 16-29 primarily disturbs binding by hcßM 622-646 as shown in chapter 3.

Competition by added hcTnI 16-29 reduced the extent of the population of hcßM 622-646 bound to F-actin (Fig 4.22C). The population of hcßM 398-414 bound to F-actin was however only slightly altered judged by the minor reversal in broadening effects on His401 (Fig 4.22C). These observations provided still further evidence for a distinctive binding site on F-actin for hcTnI 16-29.

Taken overall the data supported the notion that the segment comprising hcTnI 16-30 possessed the ability to bind to F-actin and, that the affinity enhancement enabled by hcTnI 31-37 was reduced by monophosphorylation.

4.8 Introduction of a Ser_{23} to Asp substitution in hcTnI 16-29 did not interfere with its F-actin interaction

As a means for modulating the charge of this short hcTnI peptide and, therefore, probing any electrostatic contribution to its F-actin binding, interaction of hcTnI 16-29 was compared with that of the peptide containing a Ser to Asp substitution at Ser23. This mutation was selected (rather than phosphate incorporation) so as to assess the impact of the smaller charge change resulting from the S –D substitution with aspartate containing only one negative charge at pH 7.2. This substitution, a commonly used phosphorylation mimic [e.g. Finley et al, 1999], provided a further control for establishing the viability of F-actin binding by this short segment of the N-terminal extension of hcTnI.

Figure 4.23 demonstrates the ‘immobilisation’ of Tyr25, 28 of each peptide judged by the broadening of their resonances. The data indicated that both hcTnI 16-29 and S23D hcTnI 16-29 bound F-actin with comparable affinity.

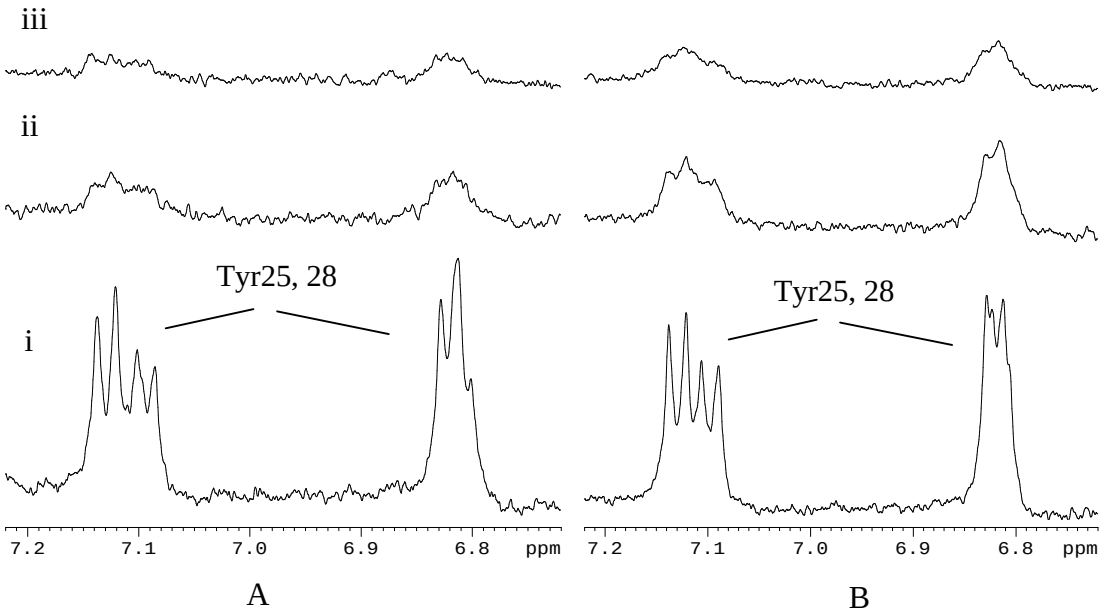

Figure 4.23 Aromatic region of 50µM hcTnI 16-29 (A) and 50µM hcTnI 16-29 S23D substitution (B) with a titration of F-actin showing the ability of the aspartate substituted peptide to interact with F-actin, pH 7.2 and T=298K.
(i) 50µM hcTnI 16-29 (A) and 50µM S23D hcTnI 16-29 (B)
(ii) 4µM F-actin
(iii) 7.5µM F-actin

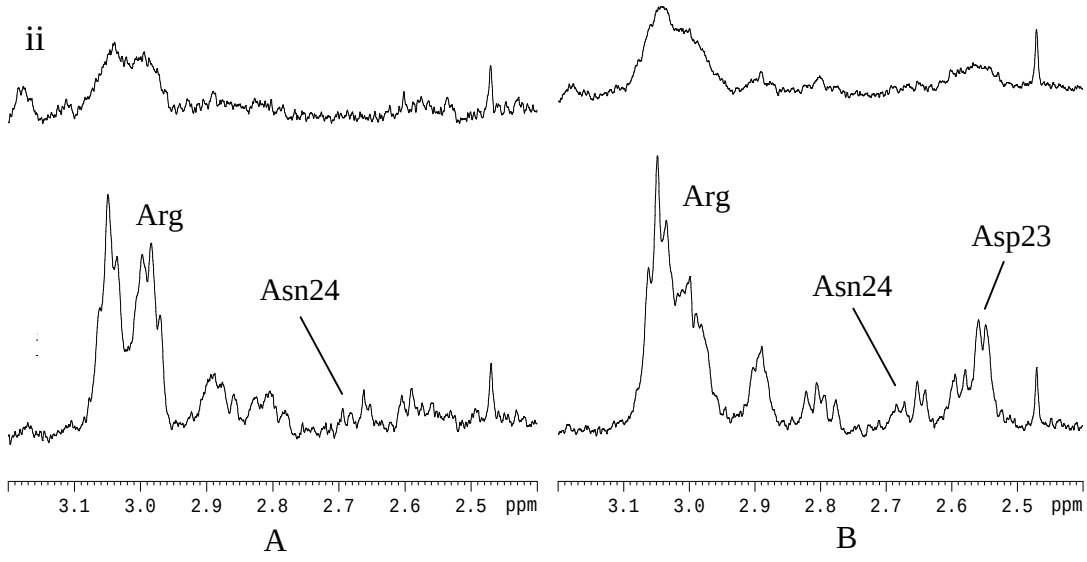

Figure 4.24 Spectra showing the aspartic acid sidechain signal of 50µM hcTnI 16-29 (A) and 50µM hcTnI 16-29 S23D substitution (B) with addition of F-actin showing the ability of the aspartic acid to interact with F-actin, pH 7.2 and T=298K.
(i) 50µM hcTnI 16-29 (A) and 50µM S23D hcTnI 16-29 (B)
(ii) 4µM F-actin
Note that the signals of Arg 19-21 and 26 as well as those of Asp 23 are broadened upon association of hcTnI 16-29 S23D with F-actin

The CH_2 region (2.4-3.2ppm) of the spectrum of both peptides (Fig 4.24) provided a window for the sidechain signals of arginine, asparagine and aspartate. The usefulness of the Asp substitution, introduced as Ser23 replacement, was that its signal could also be observed in the NMR spectrum (2.55ppm Fig 4.24). The signal of Asp23, along with the others of hcTnI 16-29, broadened upon association with F-actin. Thus, the substitution of aspartate at position 23 did not interfere with the ability of hcTnI 16-29 to interact with F-actin. Even in the presence of Asp23, hcTnI 16-29 remained 'pasted' on the surface of F-actin.

4.9 Chapter synopsis and Discussion

The data presented in this chapter provided a basis for suggesting how the effect of phosphorylation of the N-terminus region of hcTnI (Ser22 or Ser23) could impact upon the structure of this region and its interactions.

The introduction of the phosphate group at either Ser22 or Ser23 was observed to alter the electronic shielding environment of sidechain protons of downstream residues, e.g. Tyr 25 and 28 and Ala27 or 29. These alterations were barely detectable in the Ser23 to Asp substitution. Figure 4.25 shows that the alanine signal (1.3ppm) does not shift dramatically between spectrum A, hcTnI 16-29, and spectrum B, the S23D substitution, but moves to a noticeable extent between spectrum C, hcTnI 16-37, and D, $S_{23}P$.

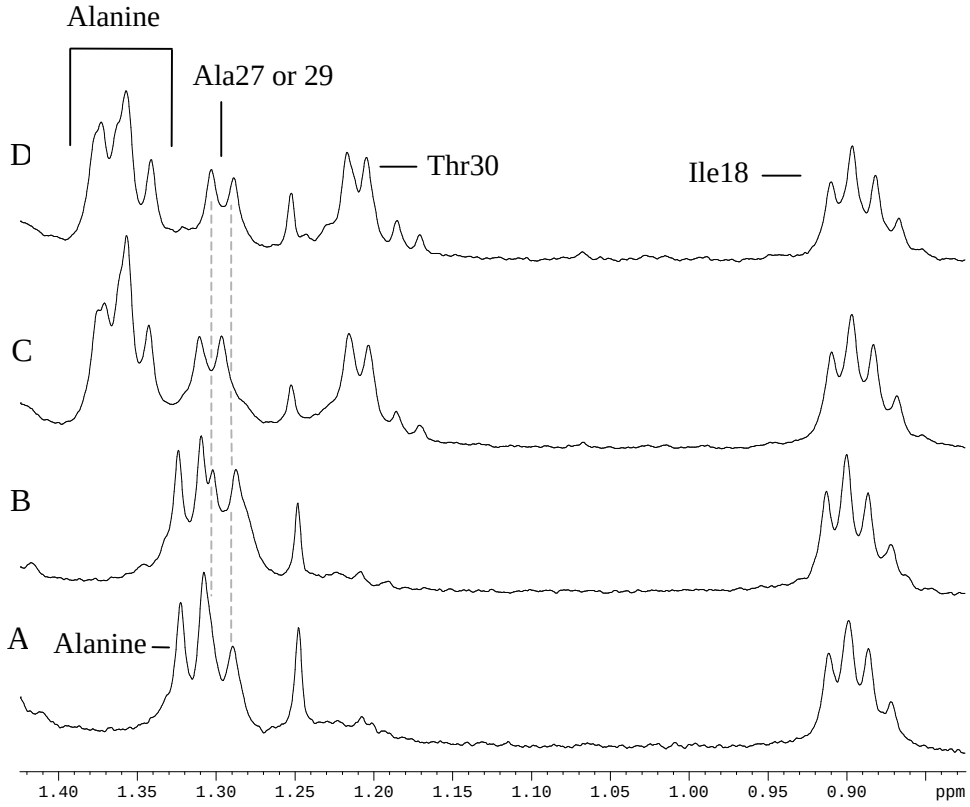

Figure 4.25 Spectra of the alanine region comparing N-terminal hcTnI peptides, pH 7.2 and T=298K.
(A) hcTnI 16-29
(B) hcTnI S23D 16-29 substitution
(C) hcTnI 16-37 unphosphorylated
(D) hcTnI S_{23}P 16-37
The 16-29 hcTnI peptides are not N-terminal acetylated or C-terminal amidated and the terminal alanines contained in these peptides are shifted upfield compared to the alanines present in the 16-37 peptides. However one of the alanine signals of the 16-37 peptide remains upfield (1.3ppm C and D) suggesting a structural preference. This alanine signal shifts upon monophosphorylation (C and D) and was shifted upfield to a greater extent in the 16-37 S_{23}P monophosphorylated peptide than S_{22}P. A small upfield shift in an alanine signal is observed between hcTnI 16-29 (A) and 16-29 S23D (B) indicating that the small charge change (-1) caused only a slightly increased electron density of this alanine signal.

This suggested an altered conformational average induced by phosphorylation that resulted from either the bulkiness and H-bonding possibilities of the phosphate group and/or, the greater charge of the phosphate compared to the carboxylate group of aspartate. The contribution of the charge on the phosphate mediating the conformational averaging in solution was confirmed by the spectral shifts observed

during pH titration through the phosphate pKa (of ~5.25). The observed shifts included those of arginine, asparagine and lysine of S_{23}P hcTnI 16-37 (Fig 4.6B). The contribution of ionisation from other charged groups (e.g. Glu31 or His33) over this pH range was considered unlikely given the absence of any similar shift changes having been observed for the unphosphorylated hcTnI 16-37 peptide (Fig 4.6A). Thus, the observation that the composite lysine sidechain signals of S_{23}P hcTnI was sensitive to the ionisation state of the phosphate group (Fig 4.6B) raised the possibility of a looped structure contributing to the conformational ensemble of S_{23}P hcTnI 16-37 with the C-terminal lysine cluster (Lys 35-37) localised in the vicinity of the phosphate group.

In such a looped conformation the positive charge of the lysine cluster would be shielded and any potential contribution of this basic tail to interaction by hcTnI 16-37 would therefore be reduced. This was indeed suggested above to be the case for F-actin interaction where the binding of S_{23}P hcTnI 16-37 was found to be some 3 fold weaker compared to hcTnI 16-37 while the contact of the segment containing residues Tyr25 – Thr30 was maintained in the association of both peptides with the surface of F-actin.

The retention of the localisation of this segment to the F-actin surface for hcTnI 16-37, hcTnI 1-30 and, hcTnI 16-29 can be taken to indicate that the electrostatic contribution to binding, demonstrated by the apparent ionic strength sensitivity of the binding of hcTnI 16-37, was not the dominant binding determinant (Chapter 3). This conclusion was supported by the inability of any of the hcTnI N-terminal peptides to induce polymerisation of G-actin in a manner typical of positively charged sequences (Fig 4.13).

The electrostatic contribution to F-actin binding by hcTnI 16-37 presumably originated from either the arginine cluster of the PKA motif and/or from the C-terminal lysine cluster of hcTnI 16-37. The possible involvement of the arginine cluster could not be discounted on the basis of the available data for F-actin binding by hcTnI 16-37, hcTnI 1-30, hcTnI 16-29 or, the two monophosphorylated hcTnI 16-37 peptides. The potential contribution of Arg19-21 and Arg26 will need further experiments. The observations enabled by the use of the myosin peptides as probes of F-actin interaction by the N-terminal hcTnI peptides, however, pointed to the effective contribution to F-actin affinity of the C-terminal lysine cluster. Both hcTnI 1-30 and S_{23}P hcTnI 16-37 were less potent inhibitors of myosin peptide binding than unphosphorylated hcTnI 16-37.

Taken overall, it can therefore be rationalised that the basic tail of hcTnI 16-37 enhanced the rate of association of hcTnI 16-37 with F-actin. This electrostatic enhancement of the rate of complex formation is akin to the reported contribution of the basic residues of hcβM 622-646 to its F-actin binding. Mutation of two lysine residues in this loop 2 region of the myosin head was found to result in reduced actomyosin interaction [Joel et al, 2001], while acetylation of the lysine residues of hcβM 622-646 completely abolished the ability of this peptide to bind to F-actin [Patchell et al, 2005]. A further contribution of the C-terminal basic cluster of hcTnI 16-37, via an influence on the peptide dissociation rate also cannot be discounted. Overall, however, the suggestion that incorporation of a phosphate group into hcTnI 16-37 results in shielding of the C-terminal lysine residues and hence less effective exposure of their basic charge, is consistent with the observation of lower affinity of S_{23}P hcTnI 16-37 for F-actin and with its reduced efficacy in inhibiting the binding of hcβM 622-646 to F-actin.

The implication of the suggested influence of phosphorylation in the context of the functional properties of the N-terminus of hcTnI is two pronged. The first relates to the ability of this region to interact with F-actin. The localisation on F-actin of the segment encompassing hcTnI residues 25-28 still occurred in either monophosphorylated form and in a manner that maintained its ability to displace hcβM 622-646 from F-actin as also demonstrated for hcTnI 16-29. Roughly equal affinities of $S_{23}P$ hcTnI 16-37 and hcβM 622-646 for F-actin were indicated by the competition data while introduction of aspartate for Ser23 did not detectably compromise the ability of hcTnI 16-29 to interact with F-actin.

The latter observation (Figures 4.23 and 4.24) also provided a suggestive clue as to the conformation of the bound peptide. If this segment of hcTnI was bound in a manner that involved docking contact by the sidechain of Ser23 then it would be reasonable that its replacement by aspartate would have led to altered contact(s). On the further assumption that the preceding arginine residue(s) may also have made docking contacts, plausibly with one or more acidic groups on F-actin, then the introduction of aspartate could have been expected to lead to repulsion. The observation of retention of interaction and the maintained relaxation of the resonances of arginine of hcTnI 16-29 S23D therefore suggested that the sidechain of residue 23 was oriented away from the surface of F-actin in the structure adopted by the bound peptide. The resulting rationalisation as to why the relaxation data indicated that hcTnI 16-29 was ‘pasted’ on F-actin is that interaction of its N-terminal region was directed by hydrophobic contact made by Ile18, with the C-terminal region docked via contacts involving Tyr 25 and 28.

In summary, therefore, the data presented indicate that for either monophosphorylated form of hcTnI it is likely that the association of the N-terminal extension of hcTnI with F-actin is able to influence the extent to which this region could associate with hcTnC. Such regulatory impact presumes the accessibility of the hcTnI N-terminal region to F-actin when hcTnI is complexed to hcTnC. The next chapter therefore focuses on the equilibrium between the hcTnC and F-actin bound forms of the N-terminus of hcTnI by making use of the model system, hcTnI 1-64/hcTnC complex, as a means of probing the accessibility of the N-terminus of hcTnI to F-actin when the cardiac-specific extension of hcTnI is localised to hcTnC.

5 The hcTnC complex

The data presented in the preceding chapters indicated that the a segment of the N-terminal extension of hcTnI (residues 16-30) can associate with F-actin and that this binding reduced the population of myosin loop regions interacting with F-actin. The latter property supported the possibility that the N-terminal extension of hcTnI may participate in the modulation of actomyosin ATPase activity associated with crossbridge cycling.

These data were however obtained using isolated hcTnI peptides. In order to begin to determine whether F-actin binding was a feature retained by the N-terminus of hcTnI when complexed with hcTnC we went on to the study of a more native model system based on the use of hcTnI residues 1-64. The hcTnI 1-64 construct contained the so-called hcTnC anchor sequence, hcTnI residues 42-64, as defined by inspection of the crystal structure of the partial cardiac troponin complex [Takeda et al, 2003]. This anchor region is docked on the C-terminal domain of hcTnC and forms a high affinity calcium dependent complex with the isolated C-domain of hcTnC and, with intact hcTnC (K_d ~10^{-8} M Ward et al, 2003). It was therefore possible to study the actin-binding properties of the N-terminal extension of hcTnI localised to hcTnC, in a 1-64 hcTnC complex, and to explore any constraints on the accessibility of the N-terminus imposed by anchoring hcTnI 1-64 on hcTnC. Furthermore, in order to explore any effect resulting from the N-terminal domain of hcTnC, the aim was to study the association with F-actin of two differing complexes (1) hcTnI 1-64 in complex with calcium bound C-domain hcTnC and (2) hcTnI 1-64 in complex with calcium bound intact hcTnC.

The results described in this chapter show the formation of the tightly bound complexes that were examined, hcTnI 1-64 calcium-bound C-domain hcTnC (hcTnI 1-64 C-domain) and hcTnI 1-64 calcium-bound hcTnC (hcTnI 1-64 hcTnC) and demonstrate the retention of the association between F-actin and hcTnI residues 18-30 that was also displayed by the isolated N-terminal peptides of hcTnI. As shown below the examination of these two hcTnI 1-64 complexes also shed new light on the structural consequences of docking the anchor region, hcTnI residues 42-64, to the C-domain of hcTnC.

5.1 Confirmation of complex formation between 1-64 hcTnI and the C-domain of hcTnC using native gel electrophoresis

Native gel electrophoresis was used to monitor complex formation of the C-domain of hcTnC with hcTnI 1-64. In the experiment illustrated in Figure 5.1, the result of the presence of hcTnI 1-64 on the migration of the separate N- and C-domains of hcTnC is shown. Comparison of lanes 1 and 5 showed the hcTnI 1-64 C-domain hcTnC complex with no free C-domain apparent (lane 1). The same complex could also be seen in lane 5 despite the presence of the hcTnC N-terminal domain in the sample. The hcTnC N-domain instead migrated by the same amount as it did when hcTnI 1-64 was not present (lane 3) indicating the absence of a tight complex with hcTnI 1-64 under these conditions. The free C-domain of hcTnC (lane 2) migrated much further along the gel than when in complex with hcTnI 1-64. This gel confirmed tight complex formation between hcTnI 1-64 and the C-domain hcTnC and the absence of a comparable affinity between hcTnI 1-64 and the N-domain of hcTnC.

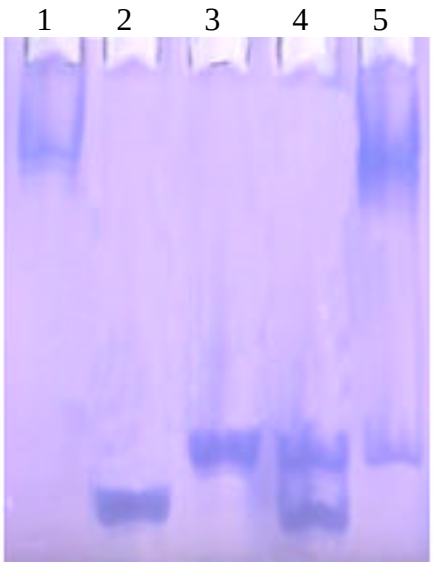

1 50µM hcTnI 1-64 and 50µM C-domain of hcTnC
2 50µM C-domain hcTnC
3 50µM N-domain hcTnC
4 50µM N-domain and 50µM C-domain hcTnC
5 50µM hcTnI 1-64 and 50µM N-domain and 50µM C-domain hcTnC

Figure 5.1 Native gel showing free C-domain cTnC·Ca^{2+} (lane 2) and complex formation with hcTnI 1-64 (lanes 1 and 5). Complex formation was not detected between hcTnI 1-64 and N-domain cTnC under these conditions. Samples were run in the presence of 1mM $CaCl_2$.

5.2 Binding of hcTnI 1-64 to the C-domain of hcTnC gave rise to a 'fuzzy' complex

The high affinity of hcTnI 1-64 for the C-domain of hcTnC meant that titration of the C-domain into hcTnI 1-64 was expected to lead to a progressively increasing amount of a long-lived complex. Consistent with its relatively low molecular mass, ~9kDa, the signals of the hcTnC C-domain were readily resolvable as illustrated, for example, by its methionine SCH_3 singlet resonances (1.93ppm, Fig 5.2B). Interaction with hcTnI 1-64, resulting in an overall molecular mass of ~16-17kDa, was not expected to induce marked relaxation. This was because the tumbling time of the complex, related to the molecular mass (Chapter 2) was only 2-fold greater than for the isolated hcTnC C-domain.

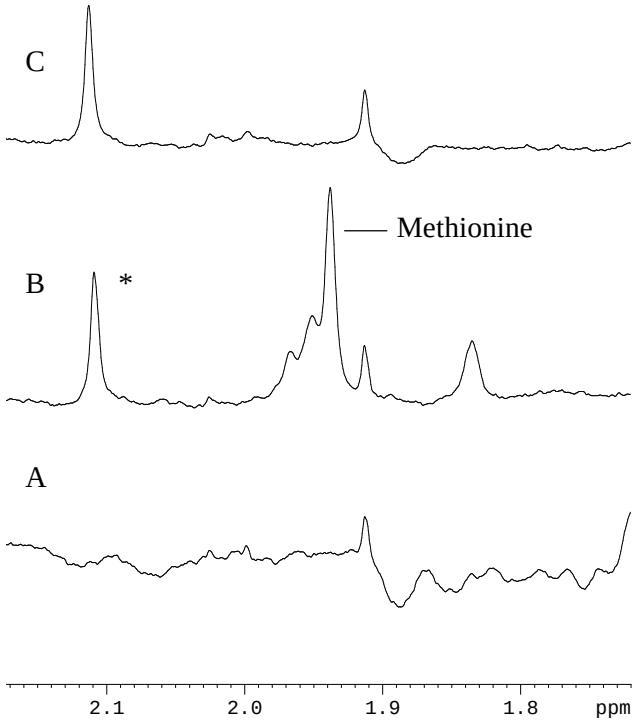

Figure 5.2 ^{1}H MR two pulse spin echo spectra of the 1.7-2.2ppm region of hcTnI 1-64 (A), C-domain hcTnC (B) and fully bound hcTnI 1-64 C-domain hcTnC complex (C) showing that the methionine signals from the C-domain hcTnC (B) broaden in complex with hcTnI 1-64 (C). * This is an impurity signal present in the C-domain hcTnC sample and acted as a reference signal by which to compare the gain of the spectra shown, pH 7.2 and T=298K.

It was therefore interesting to observe that these methionine signals of the hcTnC C-domain were significantly relaxed in the complex with hcTnI 1-64. These residues are located in the core of the C-domain and participate in the hydrophobic cleft that encloses the hcTnI anchor region (refer to figure 1.10, chapter 1) [Takeda et al, 2003; Vinogradova et al, 2005]. This defined location suggested that their relaxation must have arisen from 'interconversion' between different conformations of the binding surface and, hence, exchanging between different orientations of the residues making up the binding interface. In such a 'fuzzy' complex scenario it may be expected that other groups contributing to the structure of the binding cleft would also display conformational exchange. This was indeed was apparent from comparison of the spectrum of the free hcTnC C-domain with its resonances in the hcTnI 1-64 complex (Fig 5.3).

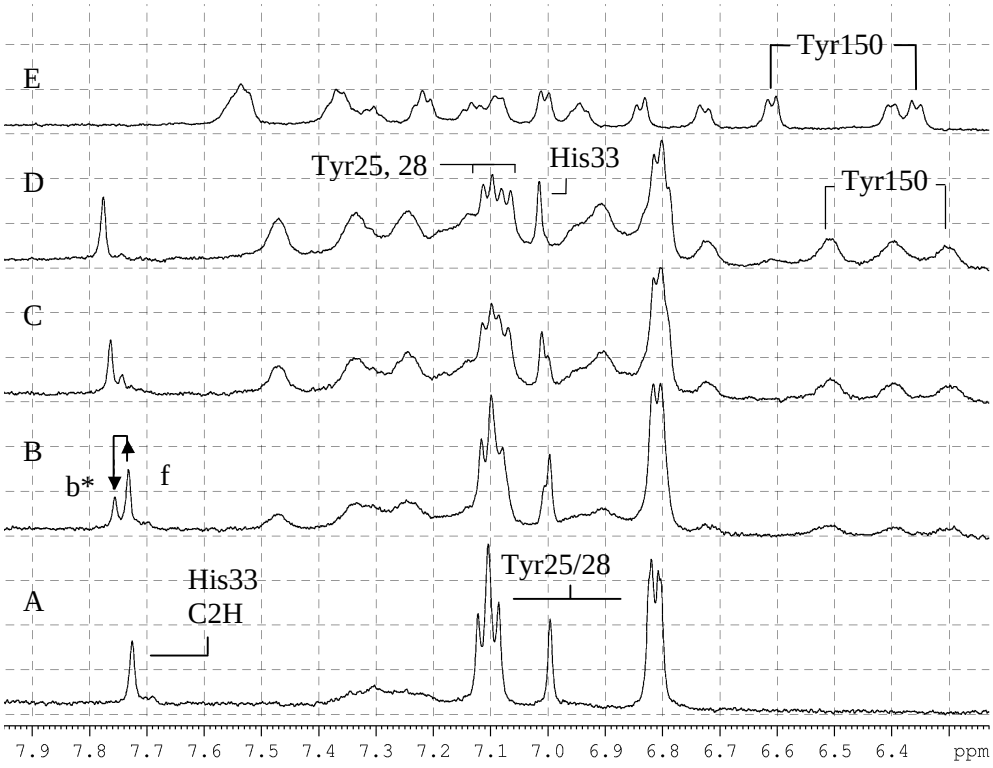

Figure 5.3 ^{1}H MR spectra of the aromatic region of hcTnI 1-64 at different stages of titration with C-domain hcTnC·Ca^{2+}. 50µM hcTnI 1-64 (A), upon addition of 25µM C-domain hcTnC (B), in the presence 50µM C-domain hcTnC (C) 75µM C-domain hcTnC (D) compared to free C-domain hcTnC (E). Note the location of the 2H His33 signal at 7.73ppm before addition of C-domain cTnC (f, free) and the new shifted downfield peak at 7.75ppm in the bound form (b*) (spectrum B), pH 7.2 and T=298K.

Inspection of the spectra shown in Figure 5.3 allowed the identification of the resonances of hcTnC Tyr150 (6.4ppm) and hcTnC phenylalanine sidechain signals (6.6ppm, 6.73ppm and 7.55ppm, BMRB entry 4994). Titration of hcTnC C-domain into hcTnI 1-64 showed the appearance of hcTnC C-domain peaks that increased in signal intensity with increasing concentrations of C-domain. Several of these differed in position from their corresponding signals of the free hcTnC C-domain and were notably broader than those of the isolated hcTnC C-domain (Fig 5.3D & 5.3E). Namely, upon titration there was no progressive change in the position of these bound C-domain signals and this provided the evidence for the slow exchange between bound and free forms on the timescale of the NMR experiment (Chapter 2). The increased

linewidth of the signals of the C-domain of hcTnC upon anchoring of hcTnI 1-64 was indicative of mobility within a bound structure, a 'fuzzy' complex.

5.3.1 The anchoring of residues 42-64 of hcTnI to the C-terminal domain of hcTnC resulted in an altered environment of residues within the N-terminal extension of hcTnI

The aromatic region of the spectrum of hcTnI 1-64 (Fig 5.3) showed the presence of the His33 C2H proton (7.73ppm) and C4H proton (7.0ppm) and, the sidechain groups of Tyr25, 28 C2,6H protons (7.1ppm) and C3,5H protons (6.8ppm). hcTnI 42-64 was the region expected to bind to the C-domain of hcTnC and therefore the spectrum shown (Fig 5.3) provided reporter signals by which to observe any effects of binding that may be relayed to the segment of 1-64 hcTnI protruding from the C-domain of hcTnC.

Upon initial addition of the C-terminal domain hcTnC·Ca^{2+} to hcTnI 1-64 (Fig 5.3B) two signals were observed from the His33 2H proton. The signal at 7.73ppm corresponded to the position seen for free (f) hcTnI 1-64 and, since hcTnC does not contain any histidine residues, the new downfield peak at 7.75ppm was presumably that of the bound (b*) form of hcTnI 1-64. This conclusion was supported by the observation that increasing concentration of the C-domain of hcTnC during the titration resulted in an increase in intensity of the signal at 7.75ppm (b*) and a corresponding reduction in the intensity of the residual signal at 7.73ppm (f). Thus, increasing the mole ratio of the C-domain of hcTnC to hcTnI 1-64 resulted in the observation of signal intensities corresponding to the bound and the free populations at each mole ratio. This slow exchange condition between free and bound forms of hcTnI 1-64 can be concluded to have come about from the high affinity of the complex and hence a slow off rate and,

importantly from the point of view of the conformation of the N-terminal extension, from distinct electronic shielding environments for the sidechain of His33 in the free and bound forms of hcTnI 1-64. As expected from the altered environment of the C2H of His33, it was also possible to observe the appearance, in slow exchange, of a downfield peak from the C4H proton (7ppm).

The chemical shift difference between the resonances of His33 in the free and bound forms of hcTnI 1-64, both sensing the same pH solution, suggested that in the bound species the sidechain of His33 was more deshielded i.e. the ionisation equilibrium of the histidine sidechain was shifted towards the more protonated form.

The C2H proton is known to be twice as sensitive to protonation of the histidine sidechain than that of the C4H proton [Wüthrich, 1986] . In this experiment an approximately two times larger downfield shift is observed for the C2H proton than for the C4H proton, consistent with the greater degree of protonation of the His33 sidechain in the bound form of hcTnI. Based upon the expected titration behaviour for the two sidechain resonances of histidine involving a single proton equilibrium (see chapter 2), the observed shift difference between bound and free forms of hcTnI 1-64 from 7.73 to 7.755ppm, a difference of 0.025ppm, corresponded to a modest but detectable increase in the pKa of His33 of some 0.05 pH units.

Also in keeping with the conclusion of slow exchange conditions, the signals of hcTnI 1-64 Tyr25, 28 2H and 6H protons (7.1ppm) appeared to give rise to separate signals as the level of complex formation with C-domain hcTnC increased during titration. The

observed upfield shift appeared to be greater for one of the tyrosine residues than for the other (Fig 5.3A-5.3D). Inspection of the spectrum of C-domain hcTnC showed that signal overlap from the C-domain was not the reason for the observed intensity increase of the C2,6H tyrosine signals (7.1ppm). It was therefore concluded that the C2,6H signals of either Tyr25, 28 hcTnI 1-64 reflected an altered environment of that residue when hcTnI 1-64 was anchored to the C-domain of hcTnC. As with the change of shielding environment for His33, this implied that the observed changes in Tyr25, 28 were due to an alteration in the conformation of the backbone of the segment protruding from the hcTnC C-domain as a consequence of complex formation.

The shielding environment change for the sidechains of Tyr25, 28 was not matched by apparent linewidth alterations of their resonances. As seen from Figure 5.3, the sidechain resonances of Tyr25 and 28 and His33 remained sharp in the spectrum of the complex. This was in contrast to the broadening seen for signals of aromatic groups of the hcTnC C-domain (cf. 5.3D and E). A consequence of the relatively broad sidechain signals of the C-domain of hcTnC bound to hcTnI 1-64 was that the contribution of these groups to the spectrum in the CP experiment was much reduced (Fig 5.4). This allowed for the now quite unambiguously detectable resonances of Tyr25, 28 and His33 of hcTnI 1-64 to be monitored. Upon anchoring to isolated C-domain hcTnC the intensity of the initially overlapping signals of Tyr25, 28 appears to have reduced (compare Fig 5.4A and 5.4D). While this may be inferred to be a consequence of increased relaxation, the shift separation of the tyrosines resonances induced by anchoring (above) is likely to have given rise to the more diffuse signal that would have unwittingly been perceived as broadening of the composite tyrosine sidechain resonance

of free hcTnI 1-64 if only spectra 5.4A and 5.4D were available. The spectra obtained during titration (Fig 5.4B-5.4D) showed the shift of the signals of Tyr25, 28 that resulted in their relative separation and an overall more diffuse tyrosine sidechain spectral envelope. The inference that anchoring residues 42-64 of hcTnI to the C-domain was sensed by the region around Tyr25, 28 and, resulted in an altered environment of His33, was then explored by inspection of spectral changes of other residues protruding from the C-domain of hcTnC.

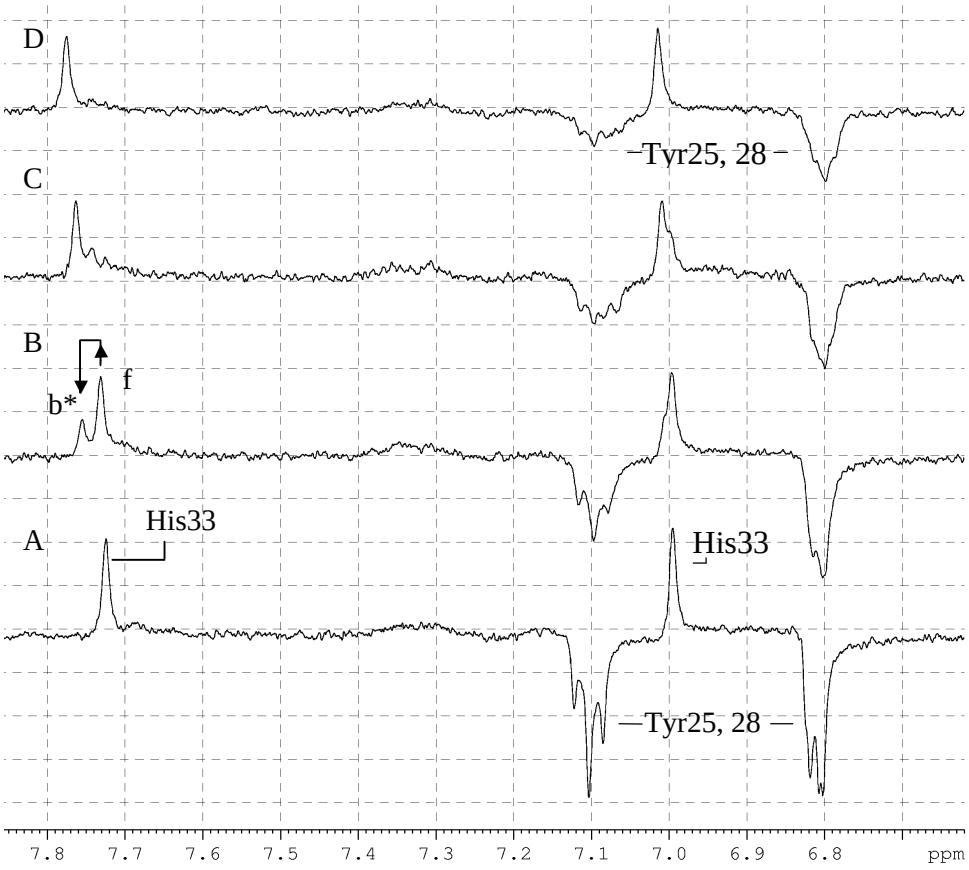

Figure 5.4 ^{1}H MR two pulse spin echo spectra of the aromatic region of hcTnI 1-64 in a titration with C-domain hcTnC. 50μM hcTnI 1-64 (A),upon addition of 25μM C-domain hcTnC (B), in the presence of 50μM C-domain hcTnC (C) upon 75μM C-domain hcTnC (D). Again the location of the 2H His33 signal at 7.73ppm (f, free) reduced with an increasing signal downfield at 7.75ppm in the (b*) bound form (spectrum B), pH 7.2 and T=298K.

5.3.2 The anchoring of residues 42-64 of hcTnI to the C-domain of hcTnC led to altered environments of a variety of residue types in the segment encompassing residues 18-40

Further corroboration of a conformational response adjacent to the protruding segment came from inspection of the Ala and Thr methyl signal region (1.50-1.55ppm) of the spectra obtained during C-domain hcTnC titration (Fig 5.5). This region of the spectrum contained signals of the two threonine residues, Thr30 and Thr50, of hcTnI 1-64. Based on comparison with the spectrum of hcTnI residues 16-41 and 36-52 (Chapter 3), the sidechain methyl signal of Thr50 in 1-64 could be identified as resonating at 1.23ppm with that of Thr30 appearing at 1.2ppm (Fig 5.5). During titration with C-domain hcTnC the resonance of Thr50 hcTnI 1-64 can be seen to have broadened completely, whereas the methyl signal of Thr30 was still observable in the spectrum of the complex (Fig 5.5). This was consistent with anchoring of region 42-64 leading to a greater relaxation effect on Thr50 within the anchor region while the decrease in mobility of Thr30 in the region adjacent to the protruding segment showed that anchoring to the C-domain hcTnC was relayed to residues away from the docked 42-64 segment. This adaptation of the conformation as a result of complex formation was also indicated by the signals of the alanine residues preceding the docked segment (Fig 5.5).

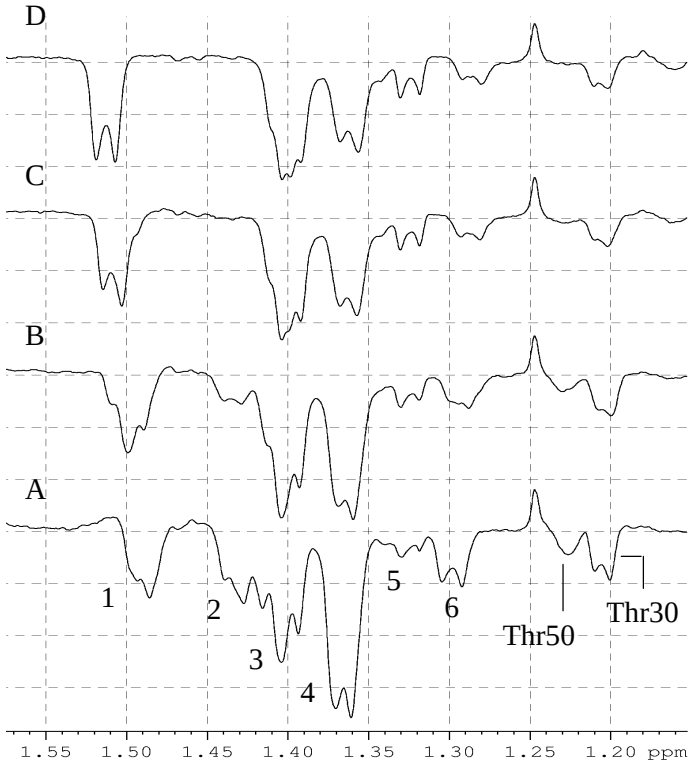

Figure 5.5 ^{1}H MR two pulse spin echo spectra of the methyl region of hcTnI 1-64 showing the alanine and threonine sidechain signals upon titration with C-domain hcTnC. 50μM hcTnI 1-64 (A) addition of 25μM C-domain hcTnC (B), in the presence of 50μM C-domain hcTnC (C) and in the presence of 75μM C-domain hcTnC (D). The signal at 1.33ppm (peak 5) was shown to derive from the C-domain hcTnC sample, pH 7.2 and T=298K.

The signals in the spectral region corresponding to alanine residues shown in Figure 5.5 (1.25-1.55ppm) are numbered in sequence from left to right, 1 through 6. The resonance positions observed for the hcTnI 1-30, hcTnI 16-41 and hcTnI 36-52 peptides allowed assignment of the remaining alanine signals to locations within the hcTnI sequence and are here described in the context of the response of the corresponding alanine residues to anchoring on the C-domain of hcTnC.

18-IRRRSSNYR**A**Y**AT**EPH**A**KKKSKI-40

For example, while peak 2, likely to derive from Ala42 that immediately precedes the anchored region, disappeared during titration (cf. Thr50 Fig 5.5), peaks 4 and 6 showed

less of a decrease in intensity (cf. Thr30 Fig 5.5), with a relatively smaller alteration observed for peak 3. Peak 1, that on the basis of the unblocked hcTnI 1-30 peptide spectrum includes the distinct downfield signal of Ala1, shifted and appeared better resolved in the bound form. (1.52ppm). Overall these observations suggested that the alanine residues of hcTnI 1-64 that were located within the region comprising hcTnI residues 1-18 retained resonance positions typical of this region in the free hcTnI 1-30 peptide. Those signals originating from and reporting on the adjoining segment of the sequence protruding from the anchor region (Ala27, 29 and 34), reflected altered environments imposed by the binding of hcTnI 42-64 to the C-domain of hcTnC as observed in Tyr25, 28 and His33.

The distribution of other particular residue types in the sequence of hcTnI 1-64 allowed further examination of the effects of anchoring on the region of hcTnI that jutted out from the C-domain of hcTnC.

18-IRRRSS**N**YRAYATEPHA**KKK**S**K**I-40

hcTnI 1-64 contains lysines at position 35-37, 39, 45, 49 and 57 and their composite eCH_2 signal was observed at 3.0ppm (Fig 5.6i). The changes in this signal upon complex formation with the C-domain of hcTnC could be monitored since there was little signal intensity at this resonance position detectable in the spectrum of the free C-domain hcTnC when acquired using the two pulse experiment (Fig 5.6v). During titration with C-domain hcTnC a notable reduction in signal intensity of the composite lysine sidechain signal of hcTnI 1-64 was observed, partly due to an increase in the dispersion of the contributing resonances. Lysine residues involved in the anchor region of hcTnI 1-64 (Lys45, 49 and 57) were likely to have relaxed more than those

located at the protruding segment (Lys 35-37 and 39). The observed chemical shift changes for the signals of the lysine residues that were detectable in the complex (Fig 5.6iv) were therefore consistent with an altered conformational average of the corresponding region of the sequence that contains a cluster of these residues, Lys35-37 and 39.

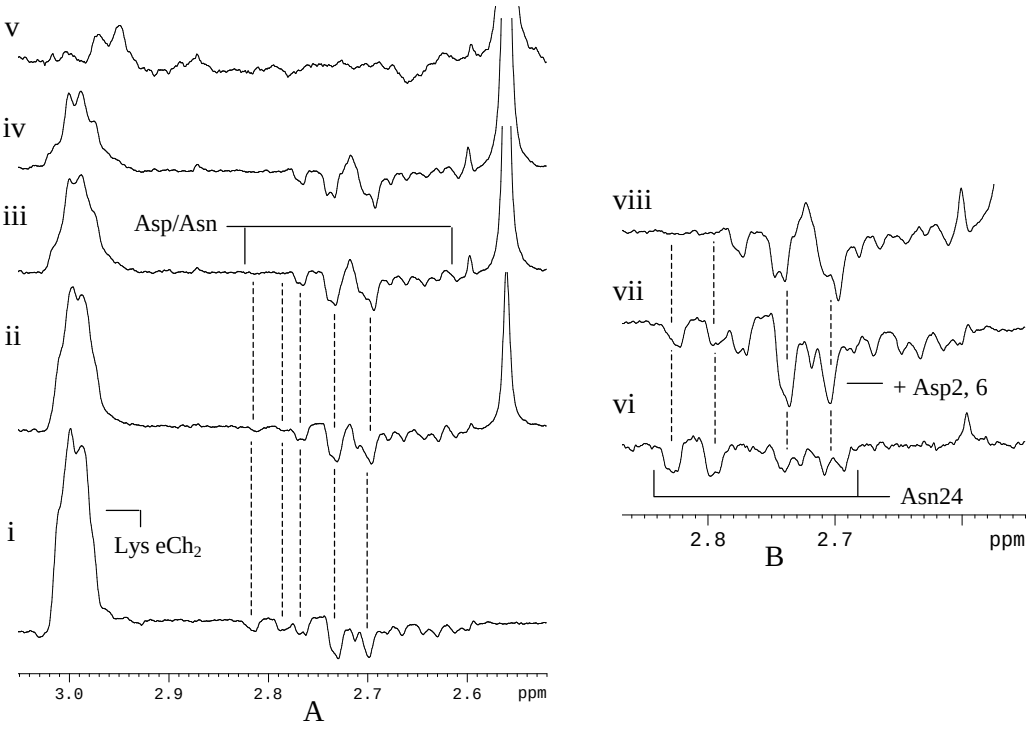

Figure 5.6A ^{1}H MR two pulse spin echo spectra of the 2.5-3.1ppm region of hcTnI 1-64 showing the sidechain signals of lysine eCH_2, aspartate (asp) and asparagine (asn) upon titration with C-domain hcTnC. 50µM hcTnI 1-64 (i), upon addition of 25µM C-domain hcTnC (ii), in the presence of 50µM C-domain hcTnC (iii), in the presence of 75µM C-domain hcTnC (iv) compared to free C-domain hcTnC (v). Identification of aspartate and asparagine is shown. Fig. 5.6B ^{1}H MR two pulse spin echo spectra of the 2.5-2.9ppm region containing aspartate (Asp) and asparagine (Asn) sidechain signals comparing hcTnI 16-37 (vi) hcTnI 1-64 (vii) and hcTnI 1-64 in complex with C-domain hcTnC (viii). Asn24 signals are uniquely identifiable at 2.8 and 2.83ppm as seen in hcTnI 16-37 with Asn24 being the only sidechain with this resonance position (vi). Asn24 completely broadened in the hcTnI 1-64 hcTnC complex (viii), pH 7.2 and T=298K.

The last set of unique residues of hcTnI 1-64 that were used as reporters for the region that is believed to protrude from the anchor were Asn24 and, towards the extreme

N-terminus, Asp2/6. The CP acquisition experiment was most useful in enabling resolution of these reporter resonances since hcTnC C-domain signals that resonated in the asparagine and aspartate region (2.6-2.9ppm) were too broad to be detected (Fig 5.6). Consistent with the corresponding resonance positions in the hcTnI 1-30 and hcTnI 16-37 peptides, the CP spectrum of free hcTnI 1-64 (Fig 5.6B) showed the presence of Asn24 doublet signals at 2.8 and 2.83ppm and Asp signals at 2.70, 2.74 and 2.77ppm, with overlapping Asp and Asn signals between 2.7-2.74ppm. Upon complex formation with C-domain hcTnC, signals from Asn24 (2.8 and 2.83ppm) are seen to have broadened beyond detection (Fig 5.6Bviii). However the sidechain signals of Asp2 and 6 (2.70 and 2.74ppm) remained sharp. This was in keeping with the observations described above for the other residue types whose signals reported on hcTnI residues 16-40. The spectral data obtained for the hcTnI 1-64 C-domain hcTnC complex therefore gave the impression that the extreme N-terminus (1-15) retained mobility independent of the complex and that the segment of hcTnI encompassing residues 24-33 adjacent to the protruding region (34-42) adjusted in response to the anchoring of hcTnI 1-64 to the C-domain of hcTnC. The extent to which docking to the C-domain may have constrained exposure of the protruding segment was then probed by monitoring the accessibility of this region to F-actin.

5.4 hcTnI residues 25-28 remained accessible to F-actin in the 1-64 hcTnI C-domain complex – interaction of this region with F-actin may be relayed to the C-domain

The observations below are presented using both direct and two pulse spectra that allowed distinction between resonances attributable to the hcTnC C-domain from those originating from hcTnI 1-64. Spectrum A (Fig 5.7) shows the aromatic region of the

1-64 hcTnI C-domain hcTnC complex with the 2H and 4H signals of hcTnI of His33 at 7.77ppm and 7.01ppm respectively. Tyr25, 28 could be resolved via the C2,6H protons (7.1ppm) and C3,5H (6.8ppm). During titration with F-actin (Fig 5.7B to D) broadening was observed for the signals of Tyr25, 28 (7.1ppm and 6.8ppm). The broadening of the signals Tyr25, 28, consistent with F-actin interaction, was relatively greater than was observed for the signals of His33. This suggested that His33 was less closely associated with the F-actin surface in the 1-64 hcTnI C-domain hcTnC complex.

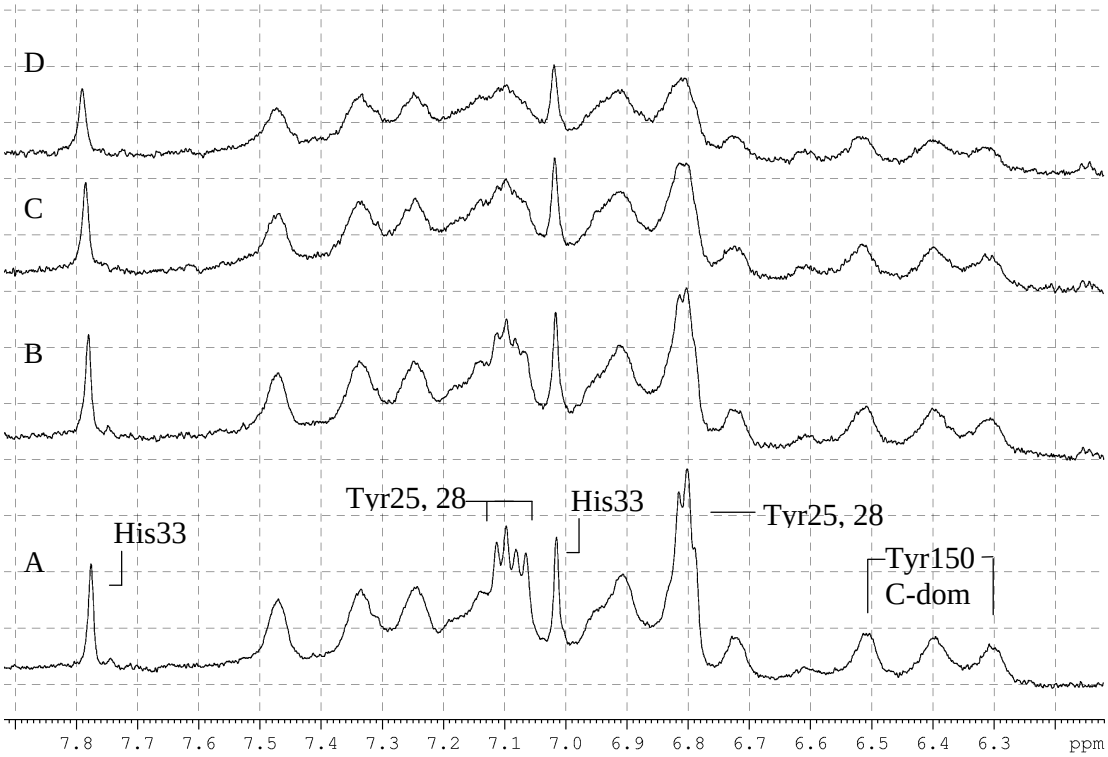

$_{18}$-IRRRSSN**Y**RA**Y**ATEP**H**AKKKSKI-$_{40}$

Figure 5.7 ^{1}H MR spectra of the aromatic region of hcTnI 1-64 C-domain hcTnC·Ca^{2+} complex. 50µM hcTnI 1-64 C-domain hcTnC·Ca^{2+} complex *(excess C-domain hcTnC ~75µM)* (A) addition of 7.5µM F-actin (B) addition of 15µM F-actin (C) and addition of 25µM F-actin (D). The signals of His33 were observed to shift progressively downfield during titration. The relative shift of the C2H and C4H signals, ~2 fold larger for the C2H proton, suggested that this shift change may have resulted from a small decrease in pH upon F-actin addition although the possibility of a slightly increased pKa in the presence of F-actin could not be discounted, pH 7.2 and T=298K.

Interestingly some hcTnC C-domain signals were also perturbed upon F-actin interaction with hcTnI 1-64 anchored to the C-domain of hcTnC e.g. signals at 6.3ppm and 6.4ppm (Fig 5.7A to D). The possibility that these changes were due to a direct interaction between the C-domain of hcTnC and F-actin was considered unlikely. This was because association would have resulted in more widespread resonance broadening for the hcTnC C-domain given contact between these molecules. Furthermore, the two aromatic resonances for which changes (downfield shift and broadening, 6.3 and 6.5ppm, Fig 5.7) were most readily detectable were assignable to Tyr150 of hcTnC (BMRB entry 4994). This residue participates in the hydrophobic core of the hcTnC C-domain and is therefore unlikely to be accessible to interaction with F-actin. The conclusion here therefore is that the region around Tyr25, 28 hcTnI was able to interact with F-actin and that this interaction could be communicated to or sensed by the C-domain of hcTnC. It therefore appeared that the binding of the N-terminus of hcTnI to F-actin led to an indirect effect on the C-domain hcTnC, presumably relayed through the anchor region of cTnI 42-64 (see supplementary figure I.1, Appendix I).

5.5 Study of the extent of the surface of interaction between the protruding region of hcTnI 1-64 and F-actin

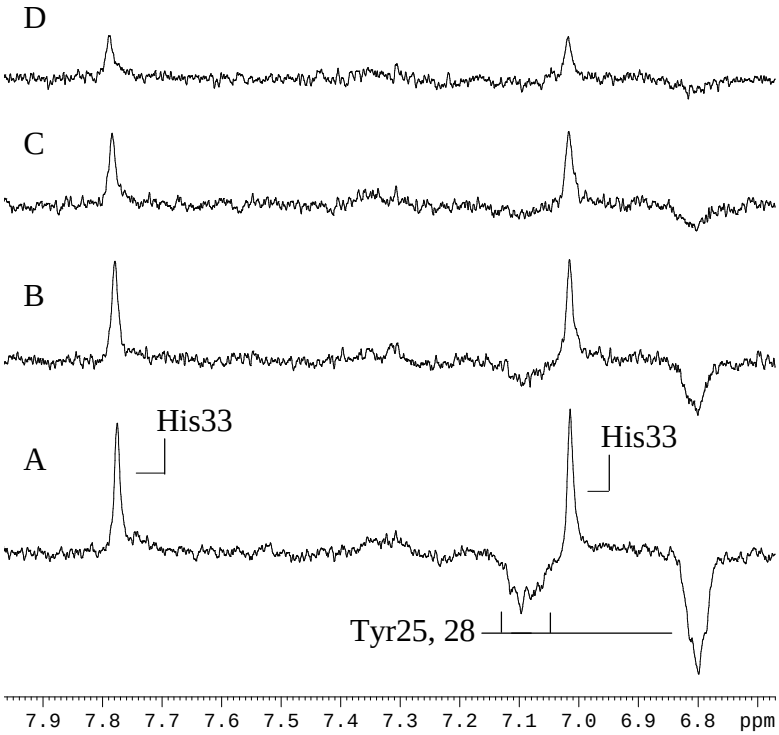

Figure 5.8 ^{1}H MR two pulse spin echo spectra of the aromatic region of hcTnI 1-64 C-domain hcTnC·Ca^{2+} complex. 50μM hcTnI 1-64 C-domain hcTnC·Ca^{2+} complex *(excess C-domain hcTnC ~75μM)* (A) upon addition of 7.5μM F-actin (B) in the presence of 15μM F-actin (C) in the presence addition of 25μM F-actin (D), pH 7.2 and T=298K.

The difference in the response to F-actin binding reported by the relative broadening of the signals of Tyr25, 28 and His33 (above) was confirmed by two pulse acquisitions (Fig 5.8) obtained during F-actin titration into the hcTnI 1-64 C-domain hcTnC complex. The greater relaxation of Tyr25, 28 compared to that observed for His33 was consistent with the relative broadening effects seen for these residues of Ser23P hcTnI 16-37 (Chapter 4) and this prompted inspection of the F-actin dependent effects for signals of other residues in the sequence of hcTnI 1-64 when bound.

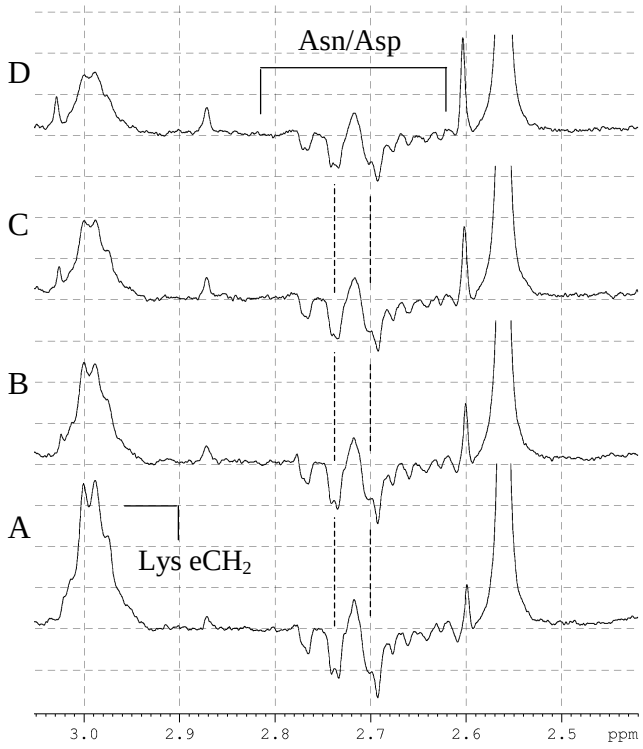

$_{18}$-IRRRSSNYRAYATEPHA**KKK**S**K**I-$_{40}$

Figure 5.9 ^{1}H MR two pulse spin echo spectra of the 2.4-3.1ppm region of hcTnI 1-64 C-domain hcTnC·Ca^{2+} complex. 50μM hcTnI 1-64 C-domain hcTnC·Ca^{2+} complex (A) addition of 7.5μM F-actin (B) in the presence of 15μM F-actin (C) and in the presence of 25μM F-actin (D). Broadening was observed on the signals from lysine at 3.0ppm with minimal effect observed on the asp signals at 2.7 and 2.74ppm, pH 7.2 and T=298K.

Inspection of the aspartate region of the two-pulse spectral acquisition of the 1-64 hcTnI C-domain cTnC complex during the course of the titration with F-actin (2.6-3.1ppm Fig 5.9) showed that the signals of Asp2 and Asp6 remained relatively sharp. Also shown in these spectra (3.0ppm) is the residual signal from the eCH_2 signals of Lys35-37 and Lys39 in the protruding segment upstream of the anchor region. The lysine resonance is seen to have been affected by interaction with F-actin but the intensity change in the two pulse spectrum that reports alteration in relaxation indicated that the corresponding residues were not in intimate contact with F-actin (Fig 5.9).

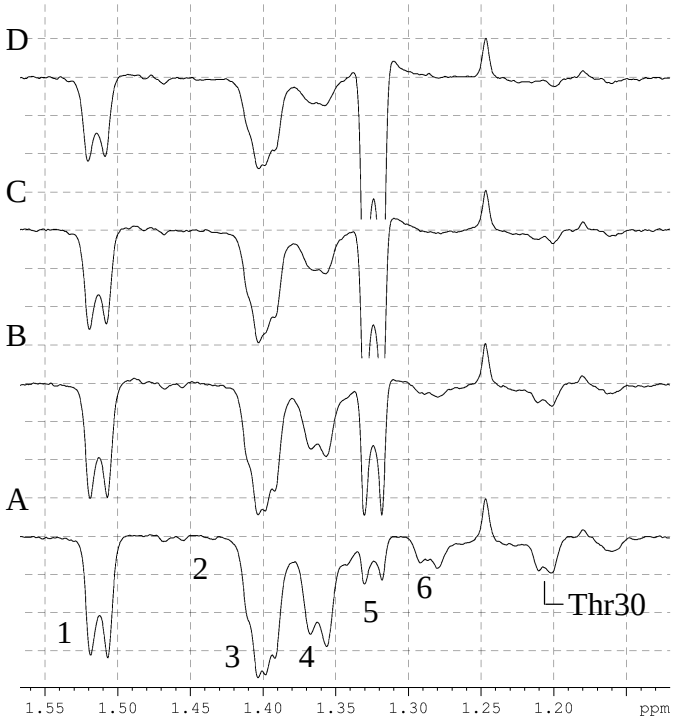

$_{18}$-IRRRSSNYR**A**Y**AT**EPH**A**KKKSKI-$_{40}$

Figure 5.10 ^{1}H MR two pulse spin echo spectra of the 1.15-1.55ppm region of hcTnI 1-64 C-domain hcTnC·Ca^{2+} complex showing signals from the sidechain of alanine and threonine. 50µM hcTnI 1-64 C-domain hcTnC·Ca^{2+} complex (A) addition of 7.5µM F-actin (B) in the presence of 15µM F-actin (C) and in the presence of 25µM F-actin (D). Peak 2 broadened or shifted upon complex formation with C-domain hcTnC. Peak 5 is an impurity (ethanol) from the C-domain hcTnC and F-actin samples. Titration of F-actin caused broadening in Thr30 and a number of alanine signals, pH 7.2 and T=298K.

The final set of residues that could be monitored were alanine and threonine between 1.15-1.55ppm. Inspection of Figure 5.10 shows that the Thr30 sidechain signal at 1.2ppm had broadened upon F-actin titration indicative of its proximity to the surface of F-actin. There were also changes detected in specific signals from alanine. The signal intensity of peaks 3 and 4 (1.40 and 1.36ppm) upon complex formation (Fig 5.10A) suggested that this is a subset of the alanine residues in the protruding segment. Peaks 1 and 3 (1.51 and 1.40ppm) are not as markedly affected by the presence of F-actin as the alanine signals of peaks 4 and 6 (1.36ppm and 1.27ppm) ascribed to Ala27 and Ala29.

The observed broadening of Ala27, 29 and Thr30 is consistent with the binding of the region 25-28 hcTnI given the relaxation induced by F-actin for the sidechain resonances of Tyr25, 28. Therefore the interaction between F-actin and hcTnI 1-64 in the C-domain complex spans at least hcTnI residues 25-30.

Localisation of the broadening effects was indicated by the relaxation of hcTnI residues in the range 24-30 caused by F-actin binding being greater for this region than for residues either side. This suggested that the extreme N-terminus (residues 1-15) and the region of hcTnI that protruded from the C-domain (residues 33-42) (and the C-domain itself) had mobility that was not as constrained by docking to F-actin as was the case for the 24-30 hcTnI bound region. Attachment to F-actin with hcTnI residues 24-30 acting as a hook was then explored in the complex of hcTnI 1-64 with intact hcTnC (for a model of hcTnC and hcTnI 1-64, see supplementary figure I.2, Appendix I).

5.6 Analysis of the extent to which the N-terminus of hcTnI was shielded when hcTnI 1-64 was anchored to intact hcTnC

The studies described above, using hcTnI 1-64 in complex with the calcium-bound C-domain hcTnC, indicated that the N-terminal region of the hcTnI construct remained accessible to interaction with F-actin. It was anticipated that, when hcTnI 1-64 was in complex with calcium-saturated intact hcTnC, any association between the N-domain of hcTnC and the N-terminus of hcTnI 1-64 may antagonise or modulate the accessibility of hcTnI to F-actin. This possibility was of further interest since the study of the hcTnC C-domain complex with hcTnI 1-64 also suggested that docking of hcTnI 42-64 led to

changes in the conformational average adopted by the segment encompassing Tyr25, 28 and His33 that was expected to jut away from the anchored region.

As with the C-domain of hcTnC, native gel electrophoresis was used to confirm the association of hcTnI 1-64 with calcium saturated intact hcTnC. The gel below (Fig 5.11) shows the altered migration of hcTnC in the presence of hcTnC 1-64 (compare lanes 1 and 3). The complex was not disrupted in the presence of F-actin as seen from lane 5 (Fig 5.11). These observations showed that interaction with F-actin could be studied without fear of dissociation of the hcTnI 1-64 complex with hcTnC.

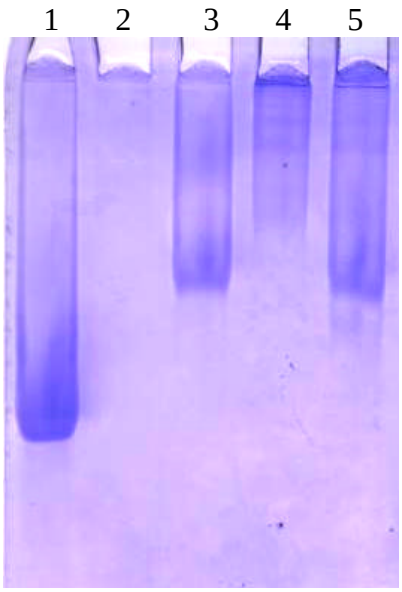

1 50µM hcTnC
2 50µM hcTnI 1-64
3 50µM hcTnI 1-64 hcTnC complex
4 25µM F-actin
5 50µM hcTnI 1-64 hcTnC complex 25µM F-actin

Figure 5.11 Native gel showing free cTnC·Ca^{2+} (lane 1) and complex formation with hcTnI 1-64 (lanes 3 and 5). Complex was not disrupted in the presence of F-actin as observed by the lack of any free hcTnC in lane 5. The samples loaded on each well are shown in the Figure 5.text. Free hcTnI 1-64 did not run into the gel (lane 2), probably due to its isoelectric point, theoretical pI 10.48. Samples were run in the presence of 1mM $CaCl_2$.

^{1}H MR spectral comparison of hcTnI 1-64, calcium saturated hcTnC and, the complex formed (Figure 5.12A) illustrates the initial analysis of the complex. The study focussed on the spectral differences of aromatic sidechain resonances resulting from complex formation between hcTnI 1-64 and calcium-bound hcTnC. In the case of hcTnC, the positions of the signals reflected the relative orientation of the

corresponding aromatic groups that gave rise to distinctive ring current shifts as a result of the packing of the individual sidechains in the tertiary fold of the N- and C-terminal domains of hcTnC (e.g. the signals of Tyr150 identified in the figure). In the case of hcTnI 1-64, the readily identifiable signals of Tyr25, 28 and His33 acted as reporters of any change in the electron shielding environment (and hence, chemical shift position) and mobility of the corresponding sidechains.

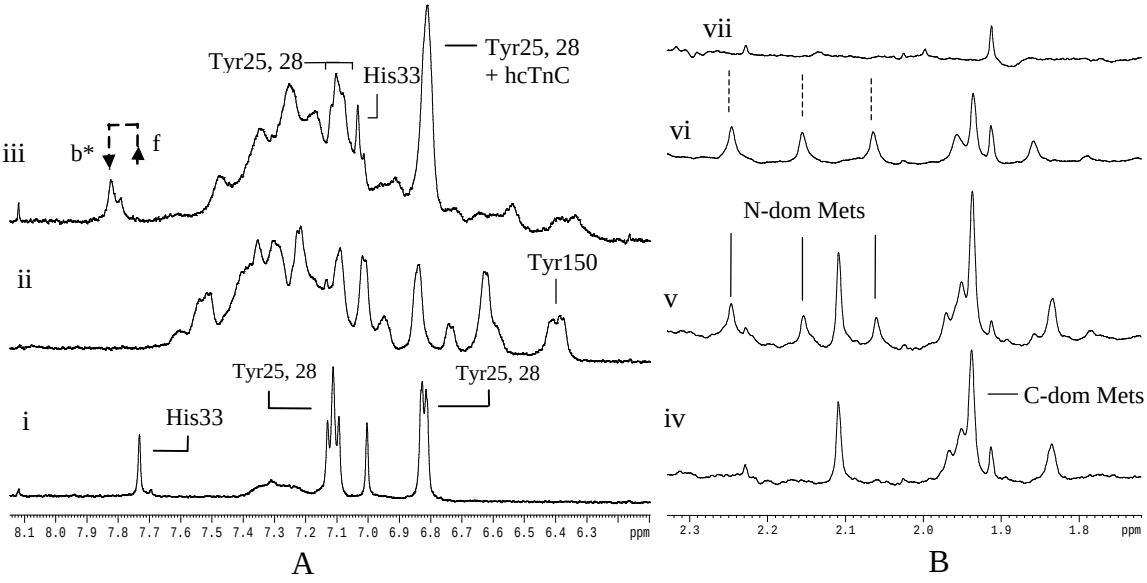

Figure 5.12A ^{1}H MR spectra of the aromatic region of hcTnI 1-64 (i) free hcTnC·Ca^{2+} (ii) and 50μM 1-64 hcTnI hcTnC·Ca^{2+} (iii). Note the location of the 2H His33 signal at 7.73ppm before addition of hcTnC (f, free) and the new shifted downfield peak at 7.75ppm in the (b*) bound form (spectrum ii), pH 7.2 and T=298K.
Figure 5.12B ^{1}H MR two pulse spin echo spectra of the 1.7-2.3ppm region of hcTnC·Ca^{2+} and its domain constructs. C-domain hcTnC·Ca^{2+} (iv) Separate C- and N- domains hcTnC·Ca^{2+} (v), intact hcTnC·Ca^{2+} (vi) and, hcTnI 1-64 hcTnC·Ca^{2+} complex (vii). Upon complex formation between hcTnI 1-64 and intact hcTnC, the methionine signals originating from the N-domain hcTnC broadened (vii) , pH 7.2 and T=298K.

As seen from Figure 5.12A, upon complex formation between hcTnI 1-64 and calcium-saturated hcTnC, many of the aromatic sidechain signals of hcTnC have shifted and broadened. The increase in linewidth occurred for several of the ring current shifted signals (e.g. 6.4ppm, 6.6ppm and 7.5ppm in Fig 5.12Aii) originating from the

hydrophobic core of the protein. This observation was consistent with the broadening found for the hcTnC signals in the C-domain of hcTnC upon complex formation with hcTnI 1-64. An increased linewidth was also apparent for the methionine sidechain signals of hcTnC when anchored to hcTnI 1-64 (Fig 5.12Bvii). Both aromatic and methionine residues participate in the hydrophobic core of each of the domains of hcTnC and, while some also make contact with the anchor region of hcTnC, others occur at the cleft on the N-terminal domain into which the switch peptide region of hcTnI binds. It was surprising therefore that anchoring of hcTnI 1-64 at the C-domain resulted in the observation of effectively global broadening effects for signals of residues in both domains of hcTnC (N and C terminal methionine signals, Fig 5.12Bvi and vii). Notably, as described below, signals originating from the N-terminal protrusion of hcTnI 1-64 (e.g. His33) did not mirror the same magnitude of linewidth increase as those signals of hcTnC. This indicated that the protruding segment of hcTnI 1-64 remained unaffected by the relaxation process that gave rise to the observed broadening in hcTnC. Since hcTnI 1-64 was on its own not a sufficiently large molecule to act as a relaxation sink, such linewidth changes would be expected to arise from the fluctuating conformations of hcTnC in the complex. While dynamics within the C-terminal clamp for the anchor region hcTnI 1-64 had been a feature observed for the hcTnC C-domain complex (above), the observations here suggested that the anchoring on the C-domain also resulted in ‘fuzziness’ (fluctuating conformations) of the N-domain of hcTnC.

5.7 Characterisation of the N-terminal extension of hcTnI in the hcTnC hcTnI 1-64 complex

Comparison of the aromatic region of the spectra of free hcTnI 1-64, free hcTnC and the complex between 1-64 hcTnI and hcTnC (Fig 5.12) showed that the C2H resonance of His33 (7.8ppm in the complex, Fig 5.12Aiii) was broader than the C4H proton of His33 (7.03ppm). This difference is unlikely to have resulted from the interaction of His33 with hcTnC since this would plausibly have constrained the mobility of the sidechain and resulted in similar relaxation changes for both sidechain protons. The cause for the shift in the His33 signals is likely to be due to an increase in its pKa, consistent with the increase in pKa suggested from the observations upon complex formation of hcTnI 1-64 with the C-domain hcTnC (above). However the shift in the His C2H proton appeared to be more than twice of that for the C4H proton upon complex formation between hcTnI 1-64 and intact hcTnC, and was also accompanied by broadening of the C2H proton (Fig5.12A). This would have come about from a change in the local environment of the His33 sidechain when 1-64 hcTnI was in complex with intact hcTnC. The possibility of a conformational change in the preceding N-terminal segment of hcTnI 1-64 was explored by inspection of the sidechain signals of Tyr25, 28.

Inspection of the sidechain signals originating from Tyr25, 28 of hcTnI 1-64 (Fig 5.12A) showed that the C3,5H (6.8ppm) composite resonance contributed more intensely to the spectrum of the complex than the signal of the C2,6H protons (7.1ppm). This observation was inconsistent with the spectrum of the complex being formed as a simple arithmetic sum of the spectra of the component molecules. Rather, the spectrum observed for the complex mirrored the spectrum obtained for Tyr25, 28 in the C-domain

complex with hcTnI 1-64 (Fig 5.7 and 5.8). Namely, the apparent loss of resolution for the C2,6H signals of Tyr25, 28 (7.1ppm) was likely due to an upfield shift of one of the 'doublet' signals that gave rise to two less overlapping resonances. This conclusion was supported by the observed of 'shoulders' of the C2,6H signals of Tyr25, 28 (Fig 5.12A). Similarly, what appeared to be a relatively smaller change in apparent intensity for the C3,5H composite signal of Tyr25, 28 (6.8ppm) compared to the change observed for their C2,6H signals was inconsistent with the mobility of the tyrosine rings being constrained by interaction with hcTnC. It was also inconsistent with the more extensive broadening of hcTnI 1-64 and hcTnC signals involved in the interaction between the two proteins. The observed changes could, however, be ascribed to a smaller (or absent) change in electron shielding environment for the C2,6H protons upon complex formation, again consistent with the observations made for hcTnI 1-64 in the hcTnC C-domain complex (above). It was therefore likely that the observed changes in these tyrosine signals upon complex formation with intact cTnC were the result of an altered environment of Tyr25, 28 upon anchoring residues 42-64 hcTnI to the C-domain of intact cTnC and were not necessarily indicative of an interaction between the N-domain of cTnC and the N-terminus of 1-64 hcTnI.

The implication from these observations was that complex formation of hcTnI 1-64 with intact hcTnC did not seemingly result in effective association of the N-terminus of hcTnI with hcTnC. Thus, the N-terminus of hcTnI may interact only transiently with the N-domain of hcTnC. A further inference from these data was that linkage to the hcTnC C-domain via residues 42-64 of hcTnI resulted in the structural adaptation of the segment encompassing hcTnI 25-33. It was therefore relevant to go on to look at any

changes in other spectral 'windows' in the sequence of the N-terminal extension of hcTnI that were able to report on the consequences of the association between hcTnI 1-64 and hcTnC.

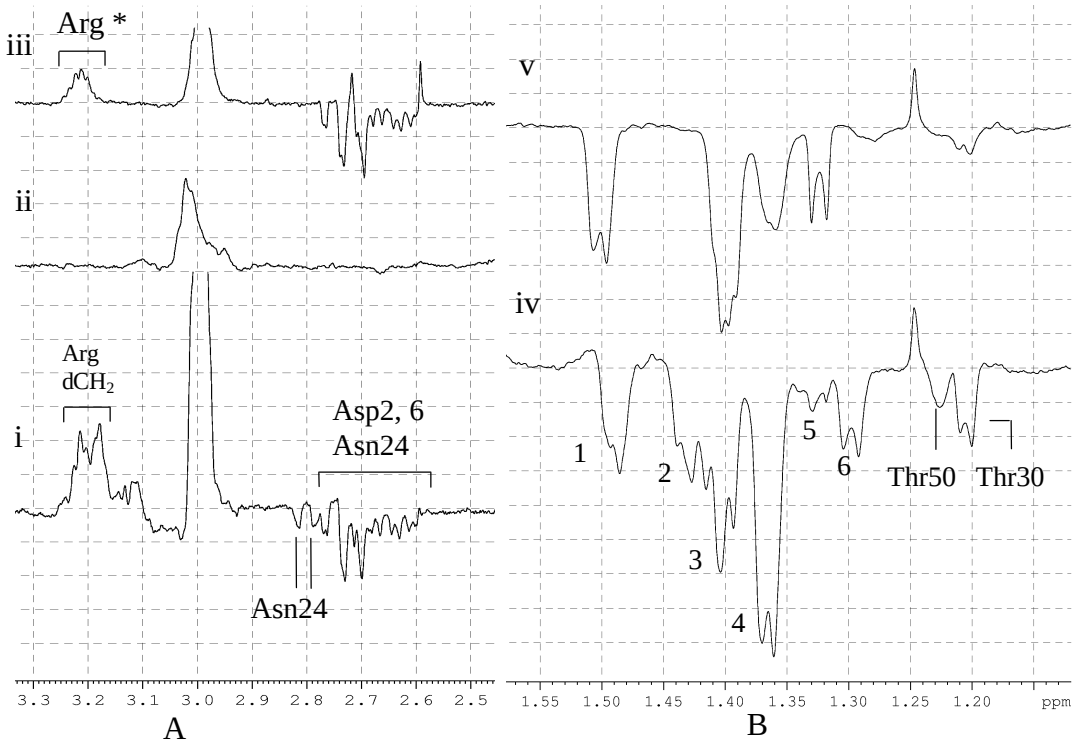

Figure 5.13A ^{1}H MR two pulse spin echo spectra of the 2.1-4.1ppm region of the spectra of hcTnI 1-64 (i) free hcTnC·Ca^{2+} (ii) and, hcTnI 1-64 hcTnC·Ca^{2+} (iii). Changes have occurred in the 3.15-3.3ppm region of the spectrum where signals of the dCH_2 sidechain signals of arginine appear. There are no signals in this region from hcTnC (ii) and the residual arginine resonance (*) observed upon complex formation plausibly derives from arginine residues of hcTnI 1-64 located in the extreme N-terminus (e.g. 1-15), pH 7.2 and T=298K.
Figure 5.13B ^{1}H MR two pulse spin echo spectra of the methyl region showing the alanines and threonine sidechain signals of hcTnI 1-64 (iv) and hcTnI 1-64 in complex with hcTnC·Ca^{2+} (v). The changes observed between free hcTnI 1-64 and when in complex with intact hcTnC are comparable to those observed between free hcTnI 1-64 and the hcTnI 1-64 hcTnC C-domain complex (Fig 5.5), pH 7.2 and T=298K.

Figure 5.13A shows the 2.5-3.3ppm range of the two pulse spectra of hcTnI 1-64, hcTnC and their complex that included resonances of hcTnI 1-64 Asp2 and 6 and Asn24. The assignment of the sidechain signals for these residues was obtained by spectral comparison of different hcTnI segments with signal-to-residue identification

based upon the distinctive chemical shifts of the ßCH_2 resonances of Asp2 and 6 and that of Asn24 (2.79 and 2.82ppm). The ßCH_2 signal of Asn24 was observed to be broadened beyond detection in the hcTnI 1-64 hcTnC complex. The sidechain signals from Asp2 and 6 at 2.6-2.77ppm had, however, remained relatively sharp (Fig 5.13Aiii). The intensity retained by the signals of Asp2 and 6 in both the hcTnC and hcTnC C-domain complexes (Fig 5.13Aiii and Fig5.6Bviii) confirmed that the extreme N-terminus of hcTnI 1-64 possessed unrestricted mobility in both bound forms. This was also suggested by the observation of selective broadening of arginine dCH_2 signals (Fig 5.13Aiii) that appear in the range 3.1-3.3ppm. The residual arginine signals of hcTnI 1-64 detectable in the spectrum of the complex hcTnC were plausibly derived from arginine 9 and 12 (assignment based on the free N-terminal hcTnI peptides described in Chapter 3).

Inspection of the alanine and threonine region of the spectra observed upon complex formation between hcTnI 1-64 and hcTnC (Fig 5.13B) showed changes in these signals that were comparable to those found upon complex formation with the isolated C-domain hcTnC. Namely, the alanine ßCH_3 resonance, peak 1, had shifted while peak 2 had broadened completely leaving signals 3 and 4 relatively unaffected, as was observed in the hcTnI 1-64 C-domain hcTnC complex (Fig 5.5). Significantly also, broadening effects on the methyl signals of Thr30 (1.2ppm) and Ala27 (1.3ppm) upon complex formation with intact hcTnC (Fig 5.13B) were comparable to those observed upon interaction with the C-domain of hcTnC (Fig 5.5).

Taken overall, the observations described above suggested that the spectral changes for residues along the sequence of the segment of hcTnI that extends/protrudes away from its hcTnC anchor were comparable in both hcTnC C-domain and intact hcTnC complexes. From this perspective, anchoring gave rise to an altered conformation of the region of hcTnI 25-33, while any potential interaction with the N-domain of hcTnC did not give rise to detectable changes in the mobility of the N-terminal extension of hcTnI. In this regard it was therefore interesting to consider the linebroadening changes observed for the methionine signals that derive from the N-domain of hcTnC. Since the 1-64 hcTnI peptide was too small to act as a relaxation sink and, did not display effective interaction with hcTnC other than through its C-terminal anchor region, such broadening could only have come about from exchange between different conformations (i.e. fuzzy complex) and, hence, interconversion between states associated with different chemical shift positions of these groups. The distinct resonance positions for these methionine residues in the spectrum of free hcTnC were a consequence of ring current shifts resulting from proximity and orientation relative to aromatic sidechains within the hydrophobic core of the N-domain hcTnC. The observation here of exchange-broadened signals indicated that the packing of these sidechains became more ‘fluid’ (i.e. greater degree of interconversion between different conformational states). This may be due to a direct interaction between a region of 1-64 hcTnI and the N-domain hcTnC that was not reflected in the spectral properties of the protruding residues of hcTnI 1-42, or may be due to changes relayed to the N-domain of hcTnC upon anchoring between hcTnI 1-64 and hcTnC.

5.8 The N-terminal region of hcTnI in the hcTnC hcTnI 1-64 binary complex remains accessible to interaction with F-actin

The ability to monitor signals of the N-terminal region in the spectrum of the hcTnC hcTnI 1-64 complex meant that it was possible to study whether this region of hcTnI remained exposed or whether it was shielded from F-actin by hcTnC. Titration of F-actin into the complex showed a reduction in the intensity of signals of Tyr25, 28 that contribute to the spectrum at 6.8 and 7.1ppm (Fig 5.14A).

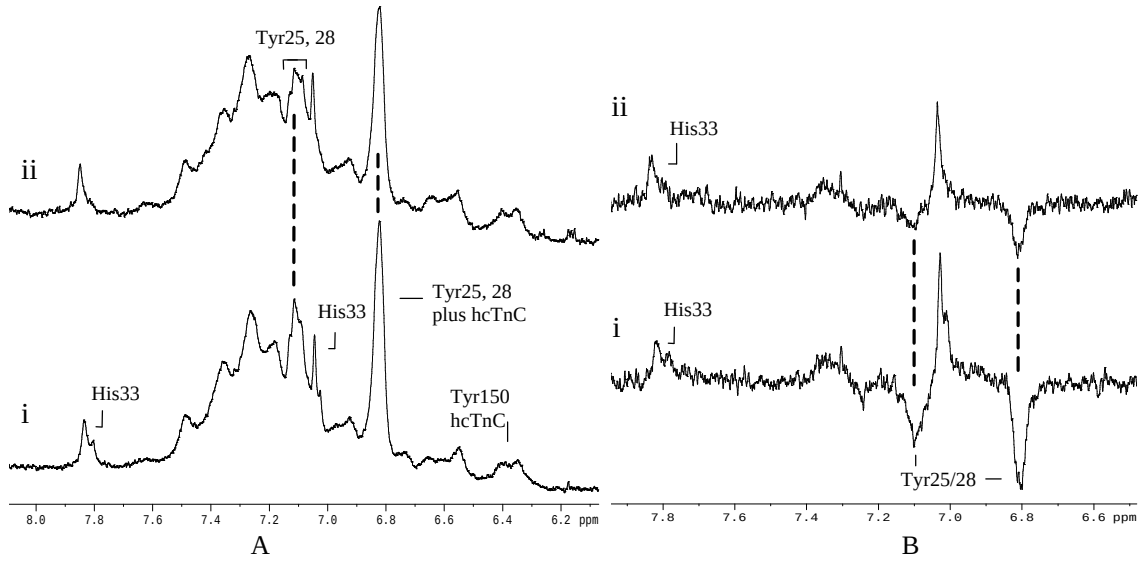

Figure 5.14A ^{1}H MR spectra of the aromatic region of 50μM hcTnI 1-64 hcTnC·Ca^{2+} complex (i) and upon addition of 25μM F-actin (ii). Broadening was observed on signals at 6.8ppm and 7.1ppm from sidechain signals of Tyr25, 28 with seemingly less effect on His33 signals at 7.03 and 7.8ppm.
Figure 5.14B ^{1}H MR two pulse spin echo spectra of the aromatic region of 50μM hcTnI 1-64 hcTnC·Ca^{2+} complex (i) and addition of 25μM F-actin (ii). Broadening was again observed on signals at 6.8ppm and 7.1ppm from sidechain signals of Tyr25, 28 with seemingly less effect on His33 signals at 7.03 and 7.8ppm, pH 7.2 and T=298K.

Similar perturbations were not detectable for signals of hcTnC. These observations suggested that complex formation with hcTnC had not inhibited the interaction with F-actin involving the segment encompassing hcTnI Tyr25, 28. They also suggested that hcTnC retained mobility independent of the F-actin filament. The ability to move independently of F-actin required flexibility of the hcTnI region separating the actin

binding site from hcTnC. Support for this came from the observation that signals of hcTnI His33 were less perturbed than those of Tyr25, 28 upon interaction with F-actin (Fig 5.14).

Inspection of Figure 5.15 identifies that F-actin induced relaxation was detectable for the methyl group signals associated with Ala27 or 29 and Thr30 while the resonance of Ala1 (peak 1) remained sharp indicative of unconstrained mobility for that N-terminal residue.

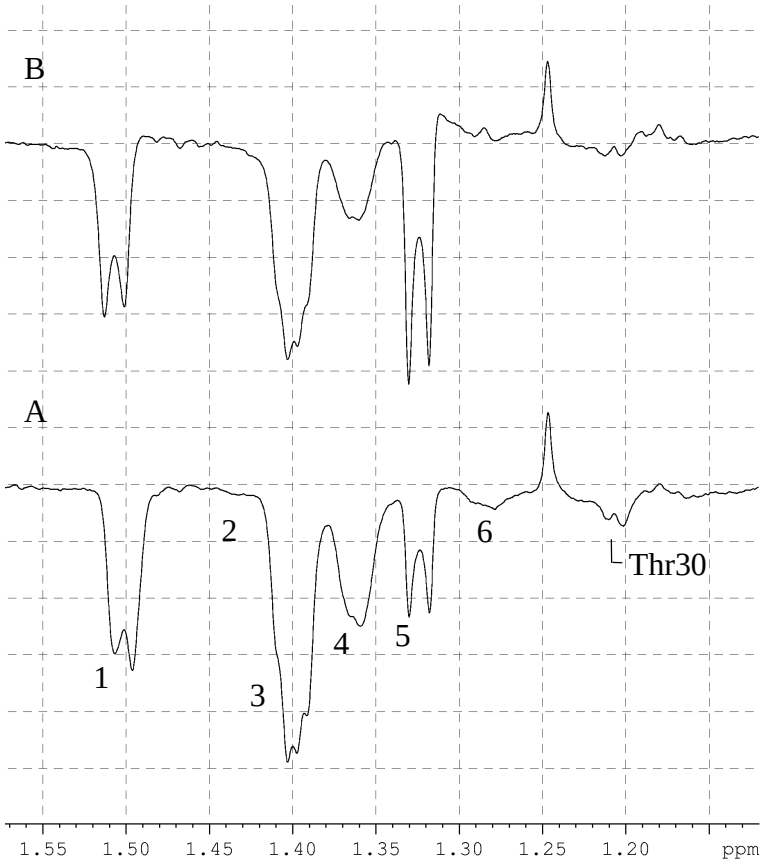

Figure 5.15 ^{1}H MR two pulse spin echo spectra of the 1.15-1.55ppm region of hcTnI 1-64 hcTnC·Ca^{2+} complex showing signals from the sidechains of alanine and threonine. 50µM hcTnI 1-64 hcTnC·Ca^{2+} complex (A) and upon addition of 25µM F-actin (B). Peak 2 broadened or shifted upon complex formation with hcTnC. Peak 5 is an impurity (ethanol) from the hcTnC and F-actin sample, pH 7.2 and T=298K.

These observations gave the impression that actin binding to the complex did not involve close association of F-actin with the 34-42 residue segment of hcTnI, consistent with the residual flexibility of this region when hcTnC/hcTnI 1-64 interacts with F-actin.

The conclusion that the specific region, around residues 25-30, of the N-terminus of hcTnI was accessible to F-actin interaction, presumably due to any association between hcTnC and the hcTnI N-terminus being only transient, could plausibly have come about because the switch peptide region of hcTnI (residues 149-158, [Takeda et al, 2003]) was not bound to the N-domain of hcTnC under the experimental conditions used. The possibility existed that hcTnI switch peptide binding to hcTnC could influence the conformation of the N-domain hcTnC causing any interaction with the N-terminus of hcTnI to be longer lived. This was explored by comparison of the F-actin binding response of an equimolar mixture of hcTnI 147-180 and calcium saturated hcTnC (Fig 5.16) with that observed using a mixture of hcTnI 147-180 and the hcTnC hcTnI 1-64 complex (Fig 5.17).

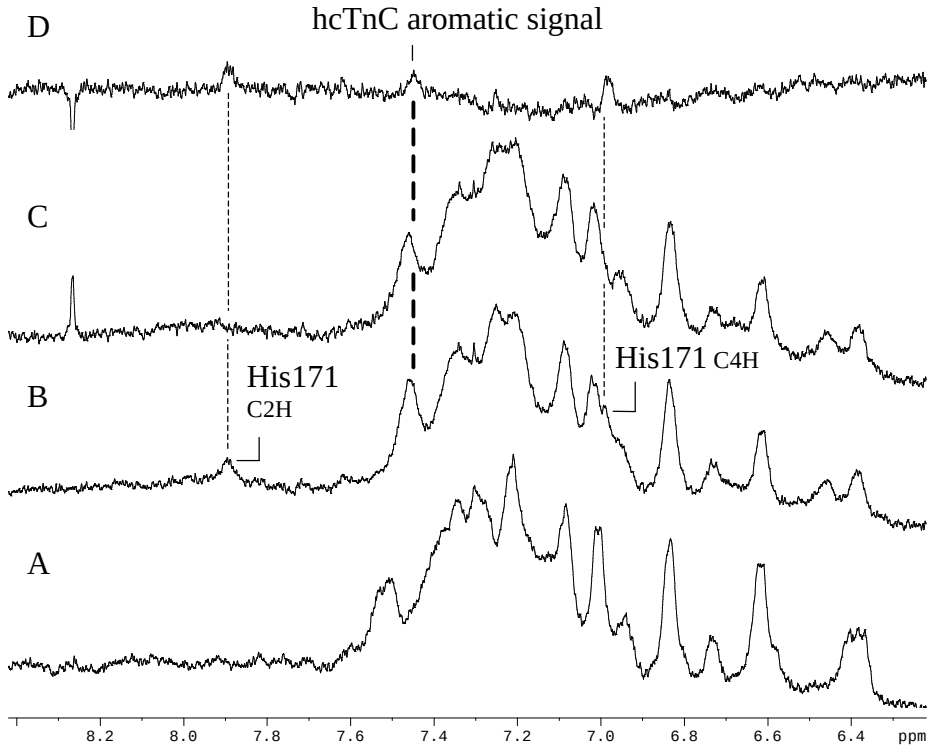

Figure 5.16 ^{1}H MR spectra of the aromatic region of 50µM free hcTnC·Ca^{2+} (A) upon addition of 50µM hcTnI 147-180 (B) and then in the presence of 50µM F-actin (C). The difference spectrum (D) before and after F-actin addition (B minus C) showed changes in hcTnC signals upon addition of F-actin plausibly due to saturation transfer from hcTnI 147-180 (see text), pH 7.2 and T=298K.

Figure 5.16 shows that a subset of aromatic signals of hcTnC had shifted upon interaction with hcTnI 147-180 (i.e. fast exchange between the peptide – bound and peptide – free forms of hcTnC). This observation was consistent with the association of the switch peptide and hcTnC involving hydrophobic contacts between the peptide and the hydrophobic cleft of the N-domain hcTnC. 'Fuzziness' of the bound complex between hcTnC and hcTnI 147-180 was suggested by the linebroadening seen for the shifted hcTnC resonances and, by the broad signal of the C2H of His171 of hcTnI 147-180 observed in the presence of hcTnC (Fig 5.16B).

Subsequent titration with F-actin identified a very specific set of spectral changes readily resolved by difference spectroscopy (Fig 5.16C and D). The resonances perturbed by the presence of F-actin included the C2H and C4H of His171 of hcTnI 147-180 as expected since, when bound to F-actin, the resonances of hcTnI 147-180 were virtually fully relaxed (Chapter 3). Also clearly observed in the difference spectrum was a signal originating from hcTnC. No perturbation of any hcTnC resonance had however been detected in a control experiment monitoring the effect of F-actin on the spectrum of isolated hcTnC. The most likely possibility from these observations is that hcTnI 147-180 was in equilibrium between different bound forms, i.e. exchanging between F-actin interaction and association with hcTnC. So, when associated with hcTnC, the hcTnI 147-180 peptide could provide a relaxation mechanism for hcTnC groups that are in the immediate vicinity of the region comprising those residues of the peptide that had made contact with F-actin. Such saturation transfer (whose physical origin was outlined in Chapter 2) therefore accounts for the broadening observed in the signal from specific groups of hcTnC as a consequence of hcTnI 147-180 ‘flitting’ between being bound to hcTnC and being bound to F-actin.

The observation of linebroadening induced by F-actin in only a single signal in the spectrum of hcTnC when associated with hcTnI 147-180 (Fig 5.16D) confirmed that non-specific association of hcTnC with F-actin had not occurred, a conclusion relevant to the experiment described below. Figure 5.17 shows the spectral changes which resulted from the titration of F-actin into the mixture of hcTnI 147-180 and the hcTnC complex with hcTnI 1-64.

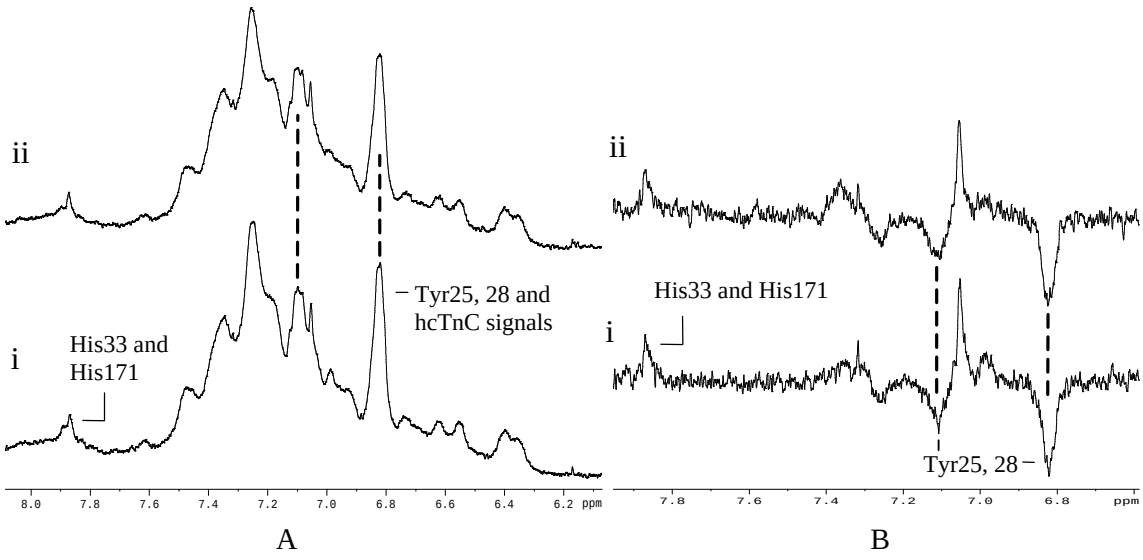

Figure 5.17A ^{1}H MR spectra of the aromatic region of 50µM hcTnI 1-64 hcTnC·Ca^{2+} complex in the presence of 50µM hcTnI 147-180 (i) and upon addition of 25µM F-actin (ii).
Figure 5.17B ^{1}H MR two pulse spin echo spectra of the aromatic region of 50µM hcTnI 1-64 hcTnC·Ca^{2+} complex in the presence of hcTnI 147-180 (i) and upon addition of 25µM F-actin (ii), pH 7.2 and T=298K.

The presence of F-actin led to perturbations of the resonances of Tyr25, 28 showing that the N-terminus of hcTnI was still accessible to F-actin under these conditions. Thus even in this solution scenario, with the switch region of hcTnI bound to hcTnC, interaction of the N-terminus of hcTnI with both hcTnC and F-actin was retained. This led to the conclusion that the N-terminus of hcTnI is accessible to F-actin under all the experimental conditions studied (as discussed, 5.9 and refer to figure 5.18, page 167).

5.9 Chapter synopsis and Discussion

The aim of the work described in this Chapter was to discover whether the interaction with F-actin by the isolated N-terminal extension of hcTnI was maintained when hcTnI 1-64 was localised on hcTnC. Comparison of the consequence of anchoring to the hcTnC C-terminal domain and to intact hcTnC was undertaken in an attempt to identify

the influence of interaction between the N-terminus of hcTnI and the N-domain of hcTnC.

Structure-focussed studies of the association between hcTnI and the isolated C-domain of hcTnC had not previously been carried out and so titration of hcTnI 1-64 with the hcTnC C-domain was undertaken. Consistent with the high affinity of the binary hcTnI 1-64 -cTnC·Ca^{2+} complex (Kd ~6nM, Ward et al, 2003) slow exchange was observed between free and bound forms of hcTnI 1-64. The line widths of resonances originating from residues of the N-terminus of hcTnI remained significantly sharper than those of the C-terminal domain hcTnC·Ca^{2+}. The signals of Tyr25, Tyr28 and His33 of hcTnI 1-64 however showed shifts under conditions of slow exchange. It therefore appeared that these residues experienced an altered environment when hcTnI residues 42-64 were anchored [Takeda et al, 2003]. This suggested that docking to the C-terminal domain hcTnC was relayed to the protruding N-terminus of hcTnI.

The segment of hcTnI 1-64 encompassing Tyr25 and Tyr28 remained accessible to interaction with F-actin. However, unlike the observations on the hcTnI 16-37 peptide (Chapter 3), significant changes in the signal linewidth of His33 were not detected in the presence of F-actin. This indicated that the mobility of His33 was not constrained by F-actin in the ternary complex formed. The data obtained with the hcTnI N-terminal peptides suggested that this difference can be accounted for by the absence of a contribution to F-actin binding from residues C-terminal to the segment encompassing hcTnI 16-29. Namely, anchoring of hcTnI 1-64 on the C-terminal domain could have resulted in a conformational change of this segment (above) so that its contribution to F-

actin binding by hcTnI 16-29 was ineffective and/or, this segment may be shielded from F-actin by virtue of proximity to the anchored region.

Although titrations of hcTnI 1-64 with hcTnC were not carried out, the electronic shielding environment of Tyr25, Tyr28 and His33 were found to have altered in a similar fashion when hcTnI 1-64 was anchored to intact hcTnC. This observation, while consistent with the crystallographic data that identify the proximity of residues 34-41 to the N-terminal domain hcTnC [Takeda et al, 2003], however suggested that the C-terminal anchoring of hcTnI 1-64 is likely to have contributed to the conformation adopted by the protruding segment.

The addition of increasing concentrations of F-actin to the complex of hcTnC and hcTnI 1-64 showed that the segment of hcTnI 1-64 encompassing Tyr25 and Tyr28 remained accessible to interaction with F-actin. As was observed for the hcTnI 1-64 complex with the C-domain, comparatively minor changes in the signal linewidth of His33 were found to have occurred as a result of binding to F-actin. Thus, anchoring of hcTnI 1-64 on hcTnC could be concluded to not have compromised the ability of the N-terminal region to associate with F-actin, an interaction localised by these experiments as involving the segment encompassing Tyr25 and Tyr28.

The N-terminus of hcTnI preceding the protrusion from the C-terminal domain hcTnC, specifically the region between residues 18-30 [e.g. Ward et al, 2004], is widely associated as interacting with the N-terminal domain cTnC. The studies carried out in this work were however unable to unambiguously detect any cross-relaxation of signals

of hcTnC resulting from the binding of the anchored hcTnI 1-64 to F-actin. This could have been because of the spectral overlap in the aliphatic region that contains the sidechain group types associated with surface regions of hcTnC. Alternatively, the region of interaction with hcTnC may involve hcTnI residues C-terminal to Tyr28 that were not in intimate contact with F-actin and so could not provide a cross-relaxation mechanism as seen with hcTnI 147-180. The extent to which common residues of hcTnI interact with cTnC and F-actin therefore still remains to be established.

The demonstration from the studies in this Chapter that the N-terminal region of hcTnI was capable of association with F-actin when hcTnI 1-64 was anchored to hcTnC supported the existence of exchange of the hcTnI N-terminal between both proteins. The possibility of switching between F-actin and the N-terminal domain of cTnC is shown schematically in Figure 5.18.

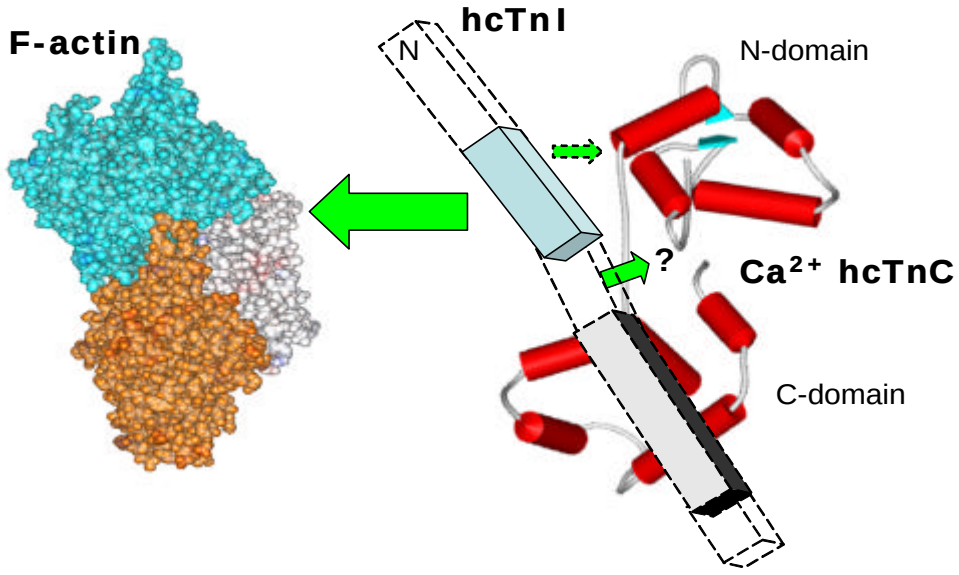

Figure 5.18 shows the ability of a specific region (~16-30) of the N-terminus of cTnI (blue) to interact with F-actin while the anchor cTnI (residues 42-64, shaded) is bound to cTnC. A portion of the protruding segment of cTnI from the C-domain of cTnC appeared to be less accessible to F-actin in the complex, the region containing His33. Figure not to scale.

The region encompassing Tyr25 and Tyr28 is shown as being in equilibrium between F-actin and its potential site on the N-terminal domain of hcTnC. One consequence of F-actin interaction by the N-terminus of hcTnI would then be to reduce the probability of its association with hcTnC and hence to reduce the stabilisation of Ca^{2+} affinity commonly associated with the interaction between the N-terminus of hcTnI and N-terminal domain of hcTnC. This regulatory scenario for the 'head' of the hcTnI molecule is discussed further in Chapter 7 along with the F-actin binding properties of its C-terminal tail that are addressed in the next chapter.

6 The C-terminus of hcTnI

This final chapter of the work undertaken describes studies on the second 'loose end' of hcTnI, the C-terminal tail sequence of the molecule. Unlike the unique N-terminal extension of hcTnI, the C-terminal ~30-40 residues have a sequence that is highly homologous across TnI isoforms (Chapter 1). The reference here to the C-terminal tail of hcTnI as a 'loose end' comes about because of the relatively ill-defined functional properties of this region. This segment has been shown to possess mobility unconstrained by incorporation of (fast skeletal, fs) TnI within a troponin complex comprised of fsTnC and fsTnT residues 165-263 [Murakami et al, 2005, Blumenshein et al, 2006]. This so-called 'mobile domain' of TnI extends from fsTnI residues 131-182 (hcTnI residues 164-209) that begins with the sequence identified as the second actin-Tm binding region of TnI just beyond the switch peptide segment whose Ca^{2+} dependent binding to the N-domain of TnC is associated with triggering the movement of the inhibitory region of TnI away from F-actin. Proteolytic deletion of the last 17 residues of hcTnI has been reported to result in slower rates of contractile activation and relaxation kinetics as well as an increase in calcium sensitivity [Narolska et al, 2006]. These observations prompted exploration of the F-actin and the F-actin/tropomyosin binding properties of the C-terminal tail of hcTnI using defined peptides spanning overlapping regions of the sequence (Fig 6.1).

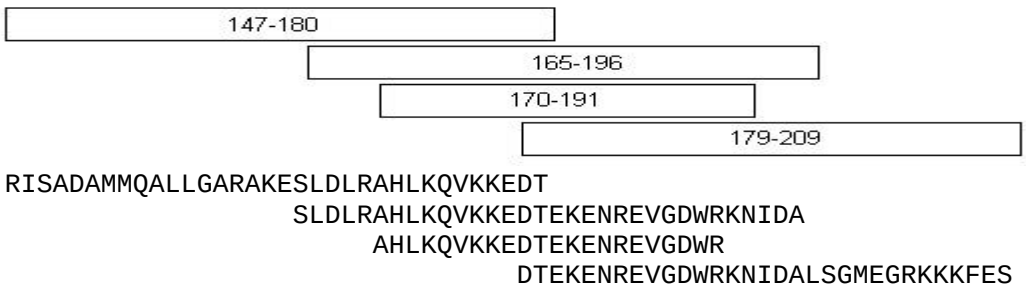

Figure 6.1 Comparison of the C-terminal peptides of hcTnI used in this chapter and the manner in which these peptide sequences overlap.

The studies were intended to (1) enable resolution of any structural predisposition exhibited by the isolated peptide sequences as reportable via resonance energy position differences and, (2) identify the residue span of any interaction site with F-actin and the extent to which such interaction localised the flanking sequences to the F-actin surface and thereby influenced their rotational freedom. The order of the work described below therefore begins with the peptide hcTnI residues 147-180 spanning the linked switch region and the proposed second actin/Tm binding site and, then explores the structural and actin binding properties of the remainder of the C-terminal tail of hcTnI.

6.1 The N-terminal portion of hcTnI 147-180 is involved in interaction with F-actin

The previous chapter showed the ability of hcTnI 147-180 to cause cross relaxation of hcTnC upon addition of F-actin. This could only have come about as a result of the binding to hcTnC by a region also localised to the surface of F-actin and so was possibly due to the presence of a common binding region within hcTnI 147-180 for hcTnC and F-actin. Since the region suggested as comprising the second actin/Tm binding site was clearly linked to but distinct from the TnC-binding switch peptide sequence, it was therefore of interest to investigate the nature of the interaction between hcTnI 147-180 and F-actin in the absence of hcTnC. There are readily observable residues throughout this peptide; the N-acetyl group, Met153, 154 at its N-terminus and His171 and Thr180 towards the C-terminus (Fig 6.2). Although several leucine and alanine residues are present, these residues occur in the first two thirds of the sequence while lysine residues act as reporters for the C-terminal third of the molecule.

Notable in the peptide spectrum are distinct methyl group signals from the different alanine residues in the sequence, indicative of different conformational averaging giving rise to altered electron environments. The relative intensities of the three ßCH_3 doublet signals of alanine (with a ratio of 2:3:1 intensity left to right 1.5-1.3ppm) suggested that one alanine resonance was furthest upfield, experiencing the greatest shielding. Also observed were shielding differences for the leucine/valine methyl sidechains with one residue resonating furthest upfield. These observations are consistent with local structural preferences adopted by this peptide in solution.

$_{147}$-**N-Ac**-RISADA**MM**QALLGARAKESLDLRAHLKQVKKED**T**-$_{180}$

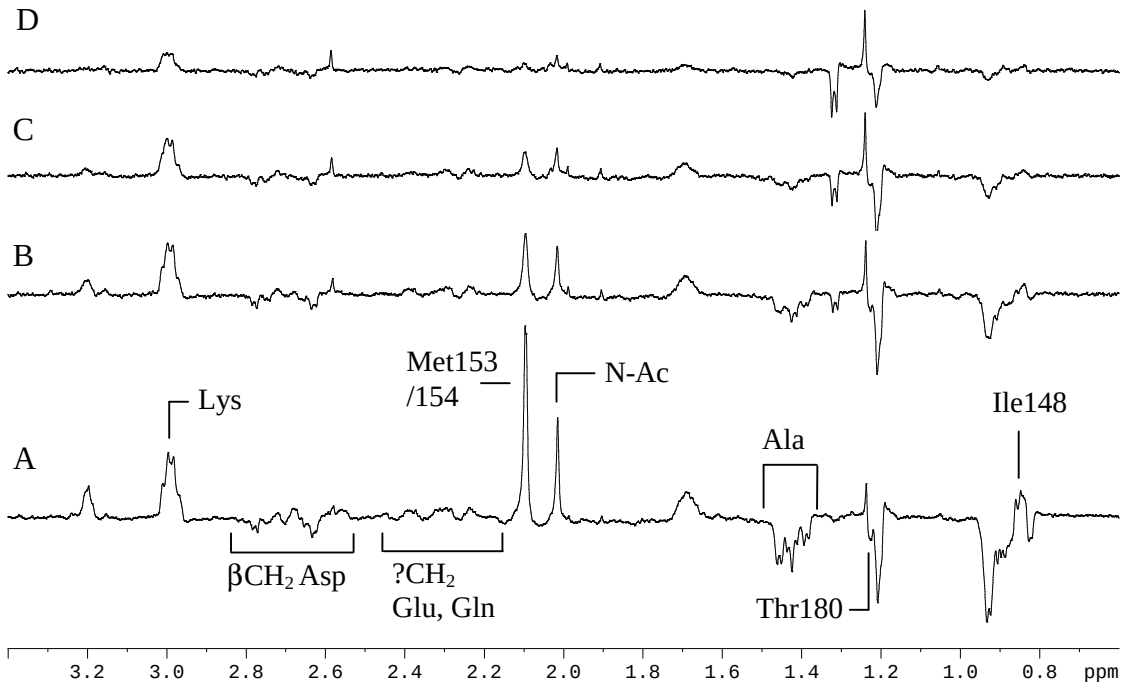

Figure 6.2 ^{1}H MR two pulse spin echo spectra of the aliphatic region of 50µM hcTnI 147-180 (A) and in the presence of 4µM F-actin (B) 7.5µM F-actin (C) and 15µM F-actin (D), pH 7.2 and T=298K.

Titration of hcTnI 147-180 with F-actin demonstrated that binding to F-actin constrained the mobility of the N-terminal (switch peptide) segment more noticeably than for the C-terminal region of the peptide. Addition of 4uM F-actin into hcTnI

147-180 (Fig 6.2B) CP shows that the relaxation observed for the N-Ac (2.1ppm) and Met153/154 methyl groups (2.0ppm) are more affected (~>50% reduction) than that detected for the methyl signal from Thr180 (1.23ppm) (~<20%). The lysine signals at 3.0ppm of which three out of four appear at the C-terminus of the peptide seem also to be less affected (~<20%) than signals from the N-terminus of the peptide.

$_{147}$-N-Ac-RISADAMMQALLGARAKESLDLRA**H**LKQVKKEDT-$_{180}$

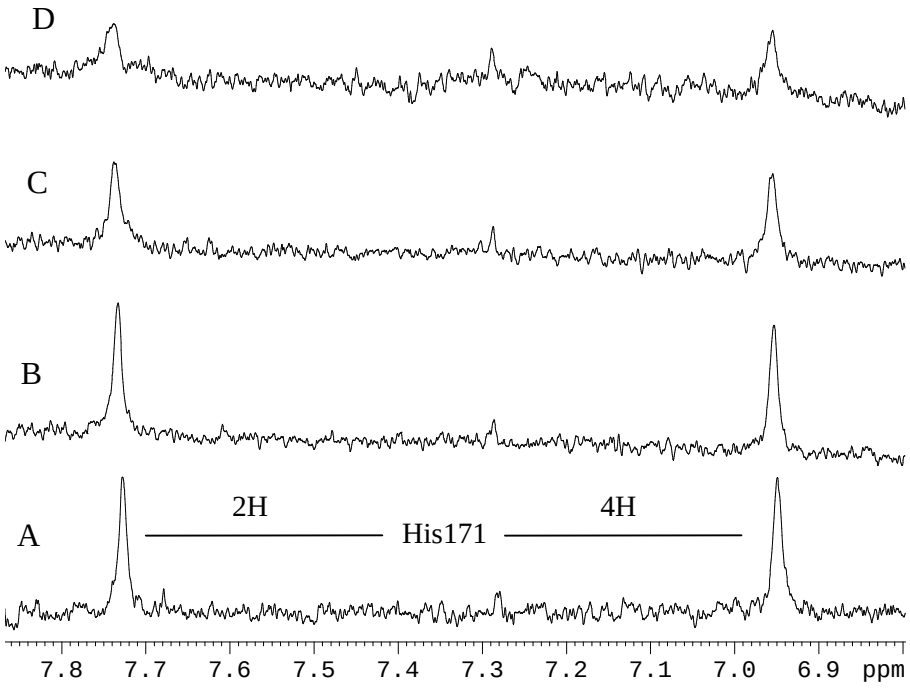

Figure 6.3 ^{1}H MR spectra of the aromatic region of 50µM hcTnI 147-180 (A) and in the presence of 4µM F-actin (B) 7.5µM F-actin (C) and 15µM F-actin (D), pH 7.2 and T=298K.

The relative relaxation effects for the different residue types along the sequence of hcTnI 147-180 suggested that the peptide was localised to the surface of F-actin via the N-terminal and central portion of the sequence. This can be inferred from the initial changes observed during the titration with F-actin (Fig 6.2A & B) in combination with the linewidth changes for the readily detectable signal in the aromatic region of the spectrum from His171, the only aromatic residue in this peptide (Fig 6.3). The observation that signals of His171, along with the composite Leu/Val CH_3 resonance

and the alanine CH_3 signal were more notably perturbed by F-actin binding than signals from the extreme C-terminus of the peptide (lysine residues, Thr180) is in reasonable agreement with the proposed second actin/Tm binding site up to residue 148 in fast skeletal TnI homologous to residue 180 of cardiac TnI, based on peptide mapping studies of fast skeletal TnI [Tripet et al, 1997]. More recently the second actin/Tm binding site has been reported as comprising hcTnI residues 173-181 [Gomes et al, 2005].

The attempt here is to analyse this interaction by monitoring specific residues of the hcTnI 147-180 peptide and the observations indicate that this peptide interacts with F-actin in a manner that restricts the mobility of residues at the N-terminal portion (i.e. 147-172) while less constraint on segmental mobility was observed for the extreme C-terminus of the peptide (residues 173-180) that were less intimately associated with the F-actin surface. This inference was open to examination through study of the actin binding properties of an overlapping sequence of hcTnI, residues 165-196, after considering its structural properties.

6.2 Sequence-context structural preferences within the C-terminal 'tail' of hcTnI

The studies of the N-terminal segments of hcTnI provided evidence of the flexibility of the structure adopted by the N-terminus as judged by the absence of significant signal dispersion. This contrasted with the resonance spread observed for hcTnC associated with the relatively well-defined tertiary fold of its two domains (Chapter 1). It was therefore of interest to note that the overlapping peptides spanning hcTnI residues 165-209, the region corresponding to the 'mobile domain', possessed specific sequence

locations whose resonance energies were different to those expected for unstructured regions. The following section of this chapter illustrates and discusses some of the chemical shift evidence for the sequence-context dependent structural preferences characterising particular regions of the C-terminal tail of hcTnI.

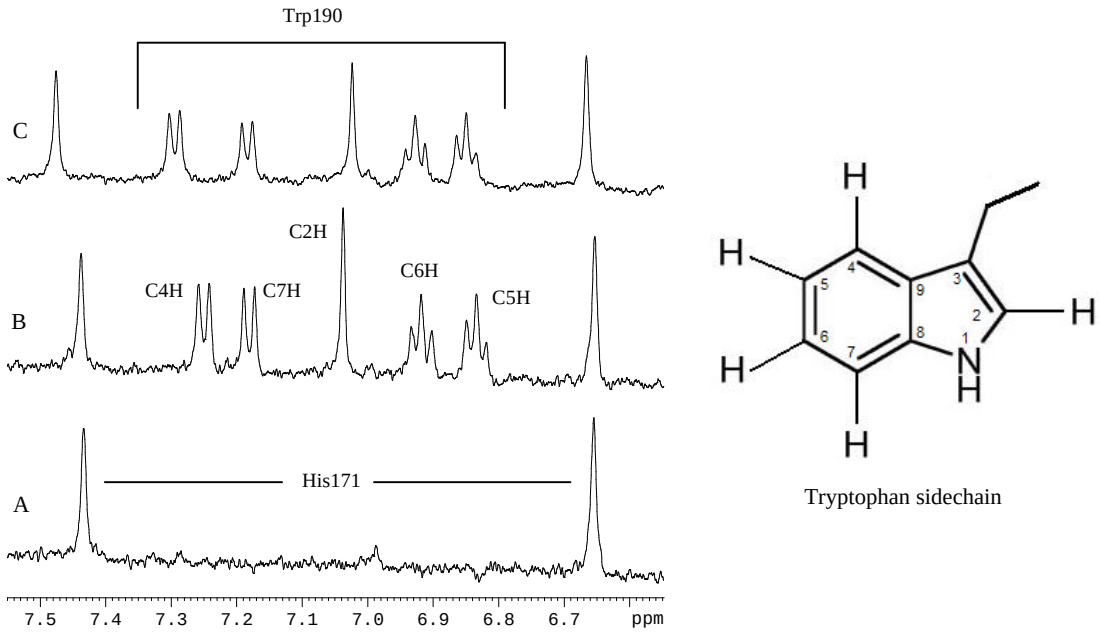

Figure 6.4 ^{1}H MR spectra of the aromatic region comparing three C-terminal hcTnI peptides. hcTnI 147-180 (A), hcTnI 165-196 (B) and, hcTnI 170-191 (C), pH 7.2 and T=298K.

Figure 6.4 compares the aromatic region of the spectra of hcTnI 147-180, 165-196 and 170-191. The C4H and C2H signals of the sidechain of Trp190 show significant deviations from their random coil positions (Fig 6.4B and C). The different shift changes for these two protons, ~0.1ppm upfield for the C4H and ~0.1ppm downfield for the C2H signal, and the absence of chemical shift deviation for the other sidechain resonances, were indicative of a preferential orientation of the Trp sidechain relative to the peptide backbone rather than a consequence of proximity to a neighbouring sidechain. The retention of this conformational preference for the segment encompassing Trp190 in hcTnI 170-191 and, the further deviation from their random

coil position for both signals in hcTnI 165-196, were indicative of a restricted backbone conformation.

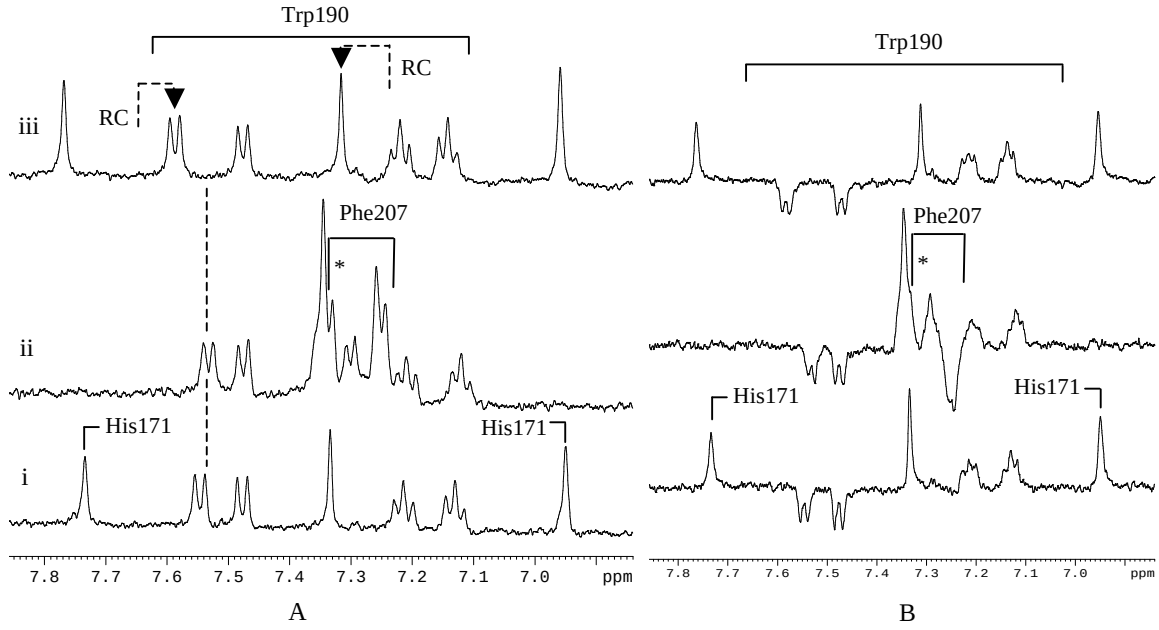

Figure 6.5 ^{1}H MR spectra (A) and ^{1}H MR two pulse spin echo spectra (B) of the aromatic region comparing the 3 C-terminal hcTnI peptides:- hcTnI 165-196 (i), hcTnI 179-209 (ii), and hcTnI 170-191 (iii). * The Phe207 triplet signal overlaps here with a Trp190 singlet signal (ii), pH 7.2 and T=298K.

Comparison with the shifts in another peptide containing Trp190, hcTnI 179-209, also showed the shifted positions of the Trp190 sidechain (Fig 6.5). The most likely cause of the electronic shielding differences was a preferred orientation relative to a peptide carbonyl group (Chapter 2). Protons located in the region above the centre of the C=O double bond experience electronic shielding while those located beyond the oxygen atoms are deshielded (see Figure 6.6).

The diagram (Fig 6.6A) shows the three sidechain orientations (rotamers g-, g+ and t) available to the tryptophan ring.

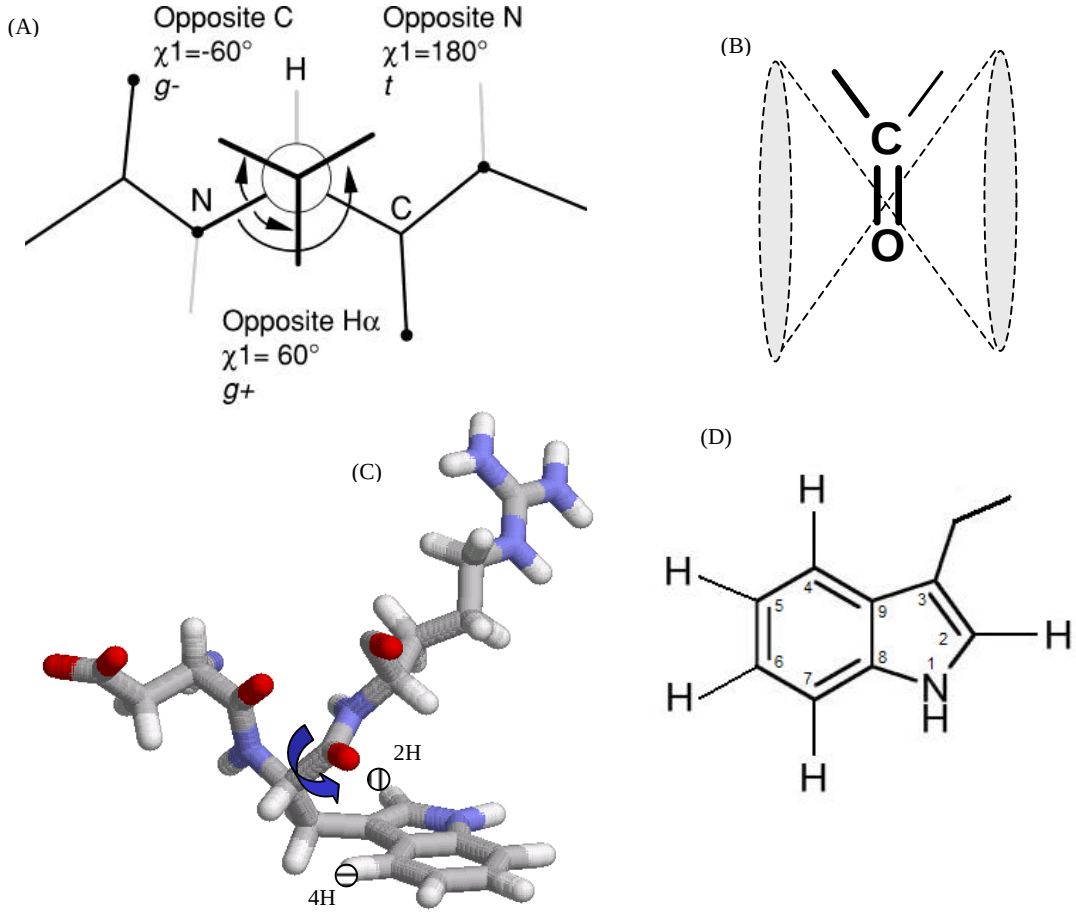

Figure 6.6 Demonstration of the different possible conformations of a peptide g-, g+ or t (A) (Martin et al, 2003). The shifted Trp190 signals suggest a preference for the g+ orientation (B). Model conformation for the homologous DWR sequence of the peptide showing the upfield shift for the C4H and downfield shift of the C2H that would be as a consequence of orientation relative to the carbonyl of Trp190 (C). The sidechain of tryptophan (D), pH 7.2 and T=298K.

In order to account for the observed shifts of the C2H and C4H there must exist a preference for the g+ orientation where the ring is located closer to the plane of the C=O group. The shielding resulting from the carbonyl group is shown in Figure 6.6B. The + sign indicates the shielding (upfield shift) for any proton located within the cone. Figure 6.6C shows a model conformation for the DWR sequence that would result in the upfield shift for the C4H and downfield shift of the C2H as a consequence of orientation relative to the carbonyl of Trp190. Restricted rotation about the Tryptophan Ca-C backbone bond must occur in order to give rise to the conformational preference

reflected by the shifts on the Tryptophan ring protons. This constraint imposes a direction to the projection of the peptide backbone as illustrated by the arrow in Figure 6.6C.

The influence of a temperature increase on the chemical shift position of the C4H and C2H signals of Trp190 was investigated and a reversal of the shielding effects was observed (i.e. return towards random coil resonance positions). This indicated the existence of a defined backbone structure in the vicinity of Trp190 (Fig 6.7).

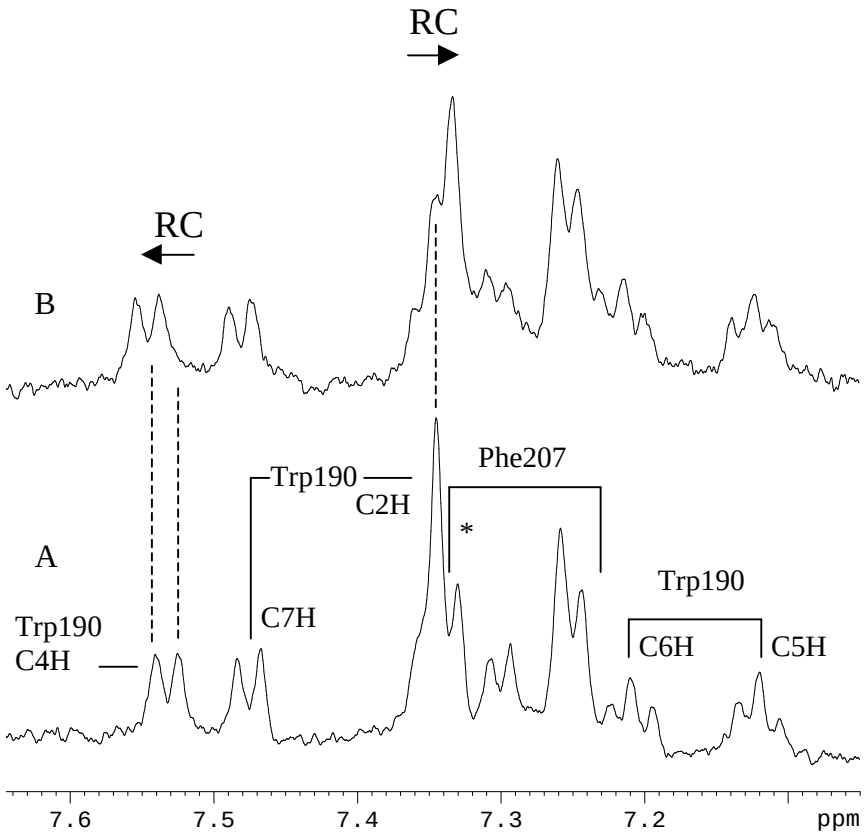

Figure 6.7 ^{1}H MR spectra of the aromatic region of hcTnI 179-209 298K (A) and 318K (B). At the higher temperature Trp190 signals move towards the position where the signals would be expected to appear in a random coil peptide, pH 7.2. * A Phe triplet signal at 7.345ppm is overlapping with a Trp singlet signal at the same ppm.

Thus, the most likely origin of the observed shift for the resonances of Trp190 was orientation of the sidechain relative to the backbone carbonyl group of Trp190 (Fig 6.7).

Although disposition with respect to other carbonyl groups could not be discounted, the distinctive environment of the C4H and C2H protons indicated a defined rotamer preference that came about from the sequence context of Trp190, $_{188}$-GDWR-$_{191}$. Another conformational preference observed was indicated by the dependence on sequence context of the chemical shift of the His171 C2H sidechain resonance that was different in hcTnI 170-191 when compared to the shifts seen for His171 of hcTnI 165-196 (Fig 6.5). This suggested that the sidechain's environment was influenced by the presence of the residues preceding His171. Comparison of the resonance energy separation between the C2H and C4H sidechain protons of His171 observed in the spectra of hcTnI 147-180, 165-196 and 170-191 (Fig 6.4) showed that the sidechain of His171 of hcTnI 170-191 experienced a distinctive environment in hcTnI 170-191 compared to the other hcTnI peptides. Since the peptide was acetylated at its N-terminal alanine residue, the change in shielding experienced by the His171 sidechain was likely to result from an altered structural preference characteristic of the sequence $_{169}$-RAHLK-$_{173}$. Support for this came from the chemical shift of Ala170 that precedes His171 and was the sole alanine residue in hcTnI 170-191 making it uniquely assignable (Fig 6.8).

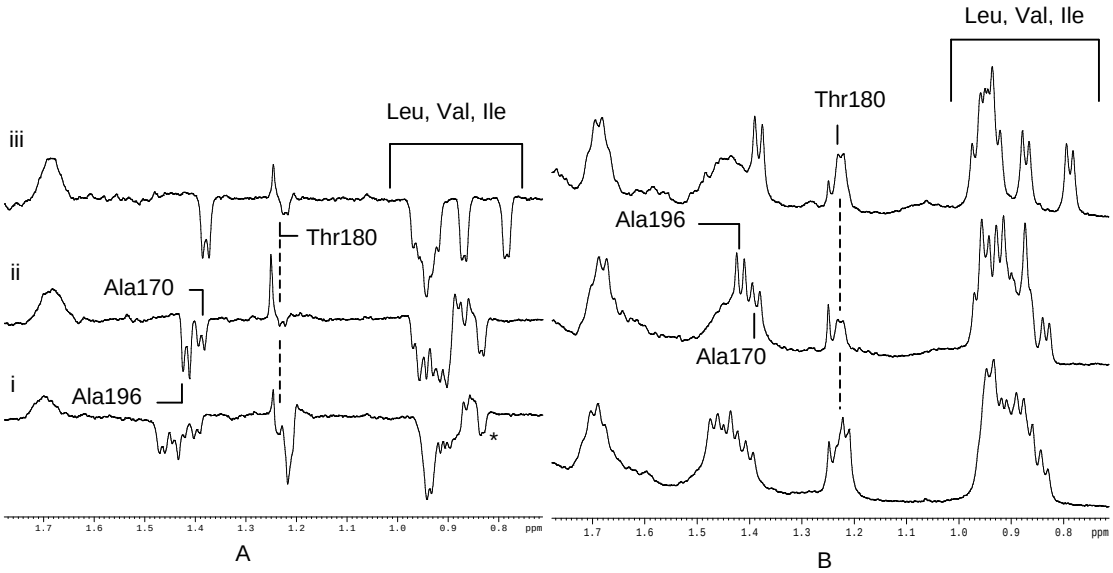

Figure 6.8 ^{1}H MR two pulse spin echo spectra (A) and ^{1}H MR spectra (B) of the aliphatic region comparing overlapping C-terminal hcTnI peptides. 50μM hcTnI 147-180 (i), 50μM hcTnI 165-196 (ii), 50μM hcTnI 170-191 (iii). * Leu172, pH 7.2 and T=298K.

Consistent with a sequence-context dependent conformational preference in this region of the C-terminus of hcTnI the relaxation properties of the methyl group of Ala170 showed that this group possessed restricted mobility in hcTnI 165-196 and hcTnI 147-180. This was indicated by the Ala170 methyl group signal intensity in the spin echo experiments (Fig 6.8A). This mobility difference could be clearly seen in the spectrum of hcTnI 165-196 that has only two alanine residues, Ala170 and Ala196, resonances that were separately resolved and consequently, easily identifiable (Fig 6.8Aii and 6.8Bii).

The conclusion of the existence of structural constraints for the two segments in the C-terminus of hcTnI $_{169}$-R<u>AHL</u>K-$_{173}$ and $_{187}$-VGD<u>W</u>R-$_{191}$, was also supported by the observation of the marked upfield shift for a pair of methyl groups in the spectrum of hcTnI 170-191 (Fig 6.8Aii). Such a shift was to be expected from proximity to an aromatic ring, here His171 and Trp190. The distribution of the single leucine and two

valine residues in the sequence that could give rise to these upfield shifted signals suggested that these resonances originated from either Leu172 or Val187. The magnitude of the upfield shift observed in the spectra of hcTnI 147-180 and 165-196 was smaller (Fig 6.8i & 6.8ii compared to 6.8iii) and affirmed the dependence of the local structural preference on its sequence context.

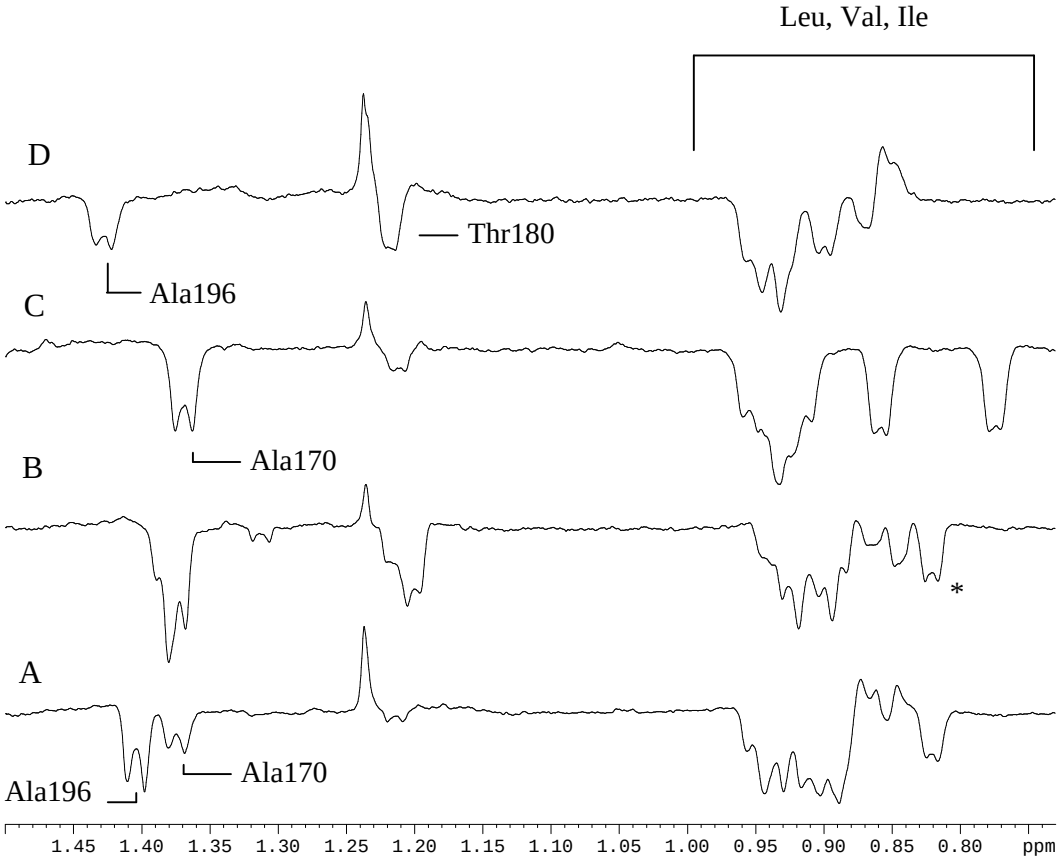

Figure 6.9 ^{1}H MR two pulse spin echo spectra of the aliphatic region comparing three C-terminal hcTnI peptides. hcTnI 165-196 (A), hcTnI 162-182 (containing a Ser165 to Thr substitution) (B), hcTnI 170-191 (C), and hcTnI 179-209 (D), pH 7.2 and T=298K.. * A shifted methyl (CH_3) signal present in peptides starting before residue 170 and up to residue 182 (see text).

These shifted methyl resonances were also observed in the spectrum of hcTnI 162-182 (Ser165 Thr substitution) (Fig 6.9B) that also contains the $_{169}$-RAHLK-$_{173}$ sequence but is missing Val187. It was, therefore, reasonable to conclude that the signals observed here (0.82ppm) derived from Leu172 and, hence, that the $_{169}$-RAHLK-$_{173}$ segment

displayed a structural preference that disposed the sidechain of Leu172 above the plane of the ring of His171. Thus, two relatively structured 'elbow joints' occur in the C-terminus of hcTnI $_{169}$-RAHLK-$_{173}$ and $_{187}$-VGDWR-$_{191}$.

The span of 13 residues between K_{173} and V_{187} linking these two structural segments is very hydrophilic and contains 4 basic and 5 acidic residues. The observation of restricted mobility of the methyl group of Thr180 located in the middle of this linker was therefore of interest. The signal intensity for the ?CH_3 of Thr180 resolved in the two pulse experiment could be directly compared to that of the distinguishable single methyl group of Ala170 in the spectrum of hcTnI 170-191 (Fig 6.9C). The notably lower intensity of Thr180 indicated an environment for its ?CH_3 group that imposed constraints on its mobility relative to the rotational freedom for Ala170. The constrained flexibility of Thr180 was even more apparent in the spectra of hcTnI 165-196 (Fig 6.9A). Overlap with an impurity signal unfortunately precluded any reliable conclusion being drawn for the environment experienced by Thr180 in the spectrum of hcTnI 147-180 (Fig 6.8A). Overall, however, the data for the hydrophilic intervening segment, residues 173-186 of hcTnI, suggested a relatively well defined conformation as may be expected on grounds of charge attraction/repulsion and as could also be inferred from the resonance dispersion for the sidechain signals of negatively charged residues of glutamate and aspartate observed in hcTnI 147-180 (Fig 6.2). Furthermore, as described below, the conformational preferences along the C-terminal tail of hcTnI reported via the chemical shift of specific residues were unaffected in the presence of 0.1M KCl (below) suggesting their stability at this higher ionic strength.

6.3 The region of hcTnI spanning residues 165-196 interacts with F-actin in a manner that involves its N-terminus

Since the interaction between F-actin and hcTnI 147-180 did not seem to involve intimate contact of the extreme C-terminus of the hcTnI peptide, it was of interest to investigate the F-actin binding capability of a peptide containing an extended sequence. hcTnI 165-196 was the sequence selected aiming to identify the contribution of the central segment of the hcTnI 147-180 sequence to F-actin binding as well as the involvement of the residues downstream of His171. Readily observable sidechain signals were resolved in the aromatic region of hcTnI 165-196, His171 (6.95 and 7.74ppm) and Trp190 whose signals span 7.1-7.6ppm (Figure 6.10). Compared to the spectral perturbations induced by F-actin for hcTnI 147-180 (Figures 6.2 and 6.3) notably higher concentrations of F-actin were required to give rise to significant linebroadening of signals of hcTnI 165-196 reflecting the lower affinity of hcTnI 165-196. The residues of hcTnI 165-196 involved in interaction with F-actin could be demarcated by the finding that the resonances of His171 were more perturbed than the sidechain signals of Trp190. The greater line broadening observed for the resonances of His171 compared to the signals of Trp190 during titration with F-actin can be seen in the spectra shown in Figure 6.10. These relative changes were an indication that the sidechain of Trp190 hovers over the surface of actin with hcTnI 165-196 being tethered to actin via the N-terminal region of the peptide.

$_{165}$-N-Ac-SLDLRA**H**LKQVKKEDTEKENREVGD**W**RKNIDA-$_{196}$

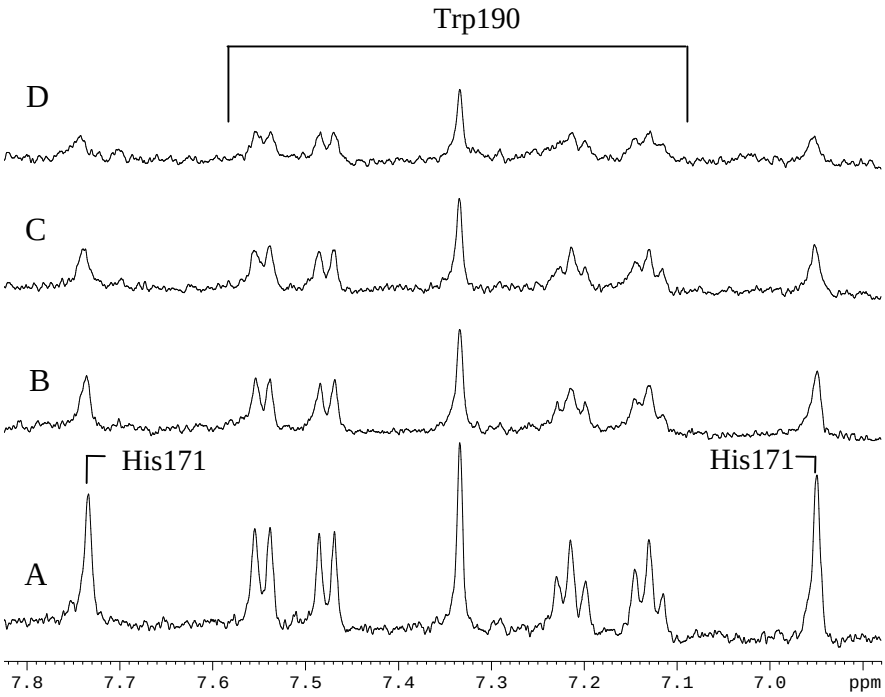

Figure 6.10 ^{1}H MR spectra of the aromatic region of hcTnI 165-196 upon addition of F-actin. 50µM hcTnI 165-196 (A) and in the presence of 15µM F-actin (B), 25µM F-actin (C) and, 50µM F-actin (D), pH 7.2 and T=298K.

Further evidence of contact between F-actin and the N-terminus of hcTnI 165-196 could be seen from the region of the spectra containing the methyl signals of the N-Acetyl group, Ala170, Thr180 and Ala196 (Fig 6.11). During F-actin titration the signals of the N-Acetyl group (2.05ppm) and the βCH_3 group of Ala170 (1.37ppm) were more perturbed than the βCH_3 group signal of Ala196 (1.4ppm).

$_{165}$-**N-Ac**-SLDLR**A**HLKQVKKED**T**EKENREVGDWRKN**I**D**A**-$_{196}$

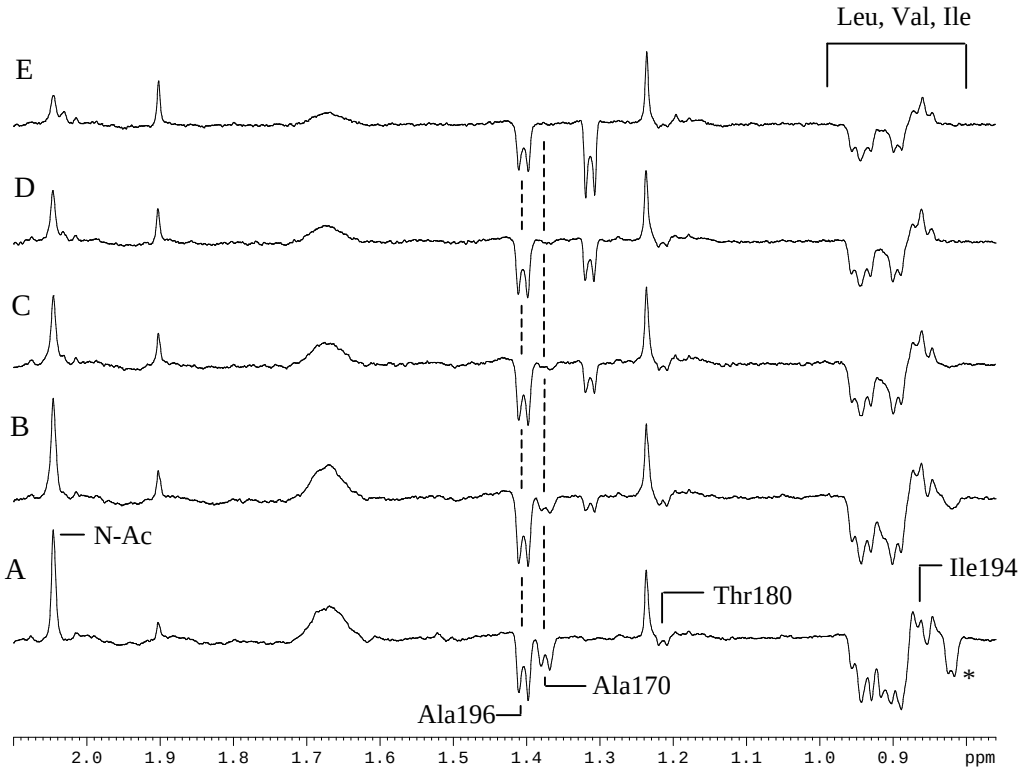

Figure 6.11 ^{1}H MR two pulse spin echo spectra of the aliphatic region of hcTnI 165-196 upon addition of F-actin. 50µM hcTnI 165-196 (A) and in the presence of 7.5µM F-actin (B), 15µM F-actin (C), 25µM F-actin (D) and, 50µM F-actin (E). * This shifted methyl signal assigned to Leu172. The intensity of Ala196 can be used to identify that two methyl groups other than those of Ile194 contribute to the residual signal at 0.9ppm observed at high actin concentration (E). These are likely to arise from Val187, pH 7.2 and T=298K.

As described earlier, the Thr180 methyl signal of hcTnI 165-196 (1.21ppm) was comparatively broad prior to F-actin addition and hence not easily detectable in the CP experiment shown in Figure 6.11.

The spectra shown in Figure 6.12 however clearly demonstrated that the reduction in signal intensity for Thr180 was markedly smaller than for Ala170. Consistent with this was the observation of a dramatic effect on the methyl group signal at 0.81ppm that,

given its shifted position, had been ascribed above to Leu172, located in the sequence next to His171.

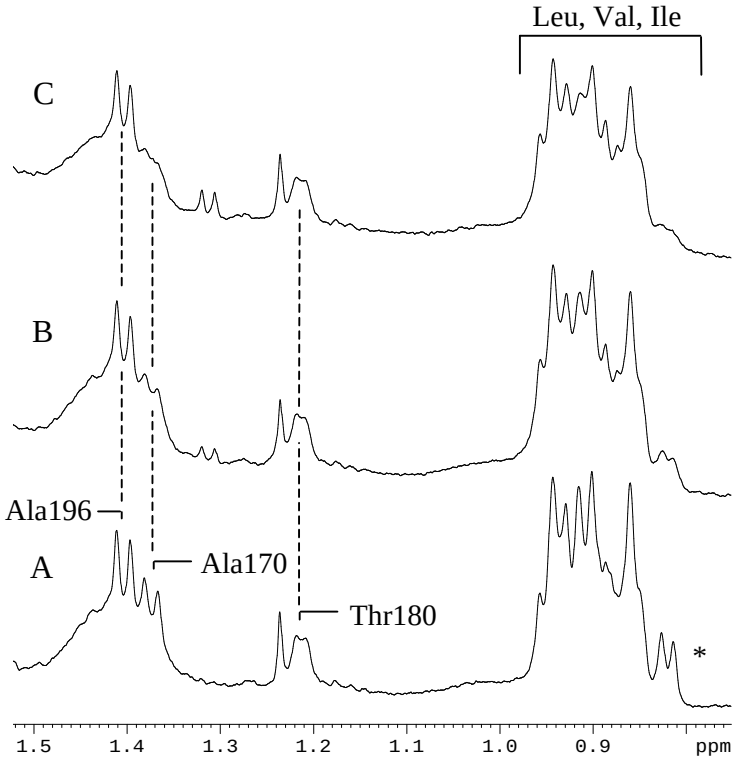

Figure 6.12 ^{1}H MR spectra of the aliphatic region of hcTnI 165-196 upon addition of F-actin. 50μM hcTnI 165-196 (A) and in the presence of 7.5μM F-actin (B) 15μM F-actin (C). * Leu172, pH 7.2 and T=298K.

Further, the relative lack of any perturbation for the methyl group of Ile194 (Fig 6.11), together with the observation of retained signal intensity even at high concentrations of F-actin from Lysine eCH_2 (Fig 6.13) and Leu/Val CH_3 groups (Fig 6.11 and 6.12), pointed to a gradation of relaxation effects along the peptide.

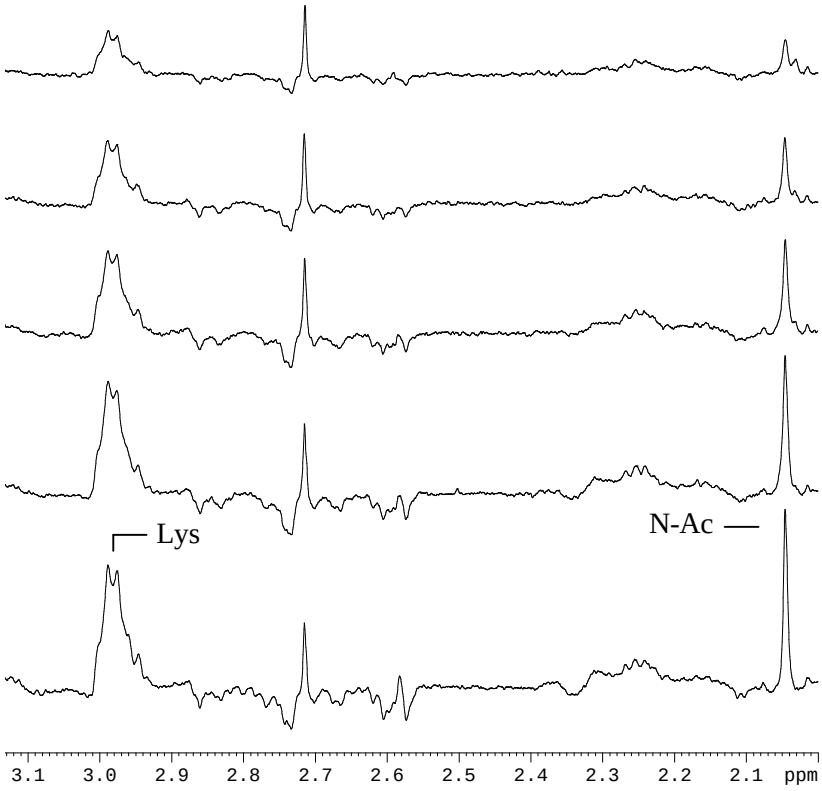

Figure 6.13 ^{1}H MR two pulse spin echo spectra of hcTnI 165-196 of the region 2-3.0ppm of upon addition of F-actin. 50µM hcTnI 165-196 (A) and in the presence of 7.5µM F-actin (B) 15µM F-actin (C) 25µM F-actin (D) and 50µM F-actin (E), pH 7.2 and T=298K.

The relaxation increase along the sequence of hcTnI 165-196 and its reduction for the residues in the C-terminus of the peptide allowed a physical representation of the bound peptide consistent with the seemingly lower affinity of hcTnI 165-196 compared to hcTnI 147-180. The peptide was docked via its N-terminus and this attachment, augmented in the case of hcTnI 147-180 by residues preceding Ser165, enabled the localisation of the remainder of the sequence. Confirmation of this mode of binding came from studies on hcTnI 170-191.

6.4 The 170-191 peptide hcTnI displays minimal interaction with F-actin

The aromatic region of the spectrum of hcTnI 170-191 comprised two signals from His171 located at the N-terminus of the peptide along with signals from Trp190 located

at its C-terminus. As can be seen in the spectra shown in Figure 6.14, there was very little perturbation of the signals from either of these residues during titration with F-actin, even when the concentration ratio of F-actin to peptide was increased to equimolar and above (Fig 6.14C, D). There was therefore little observable interaction of hcTnI 170-191 with F-actin.

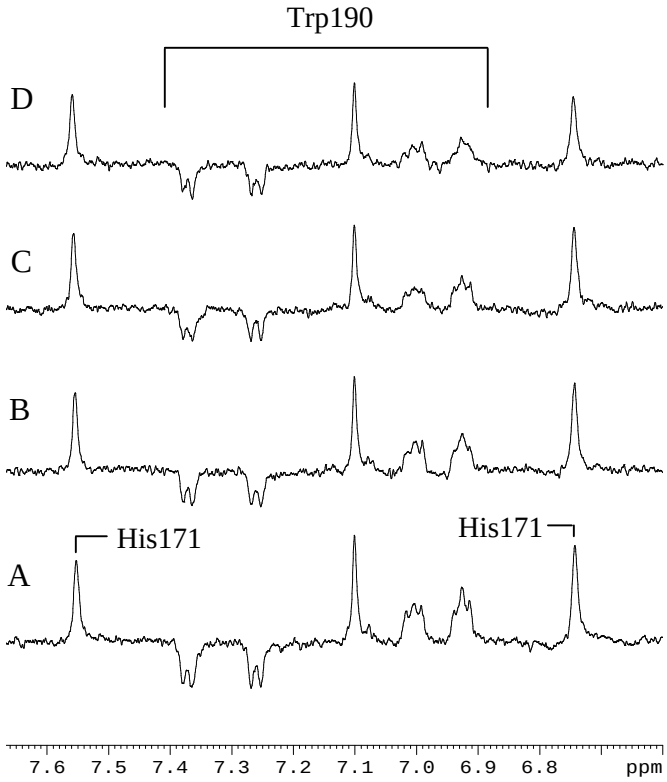

Figure 6.14 ^{1}H MR two pulse spin echo spectra of the aromatic region of hcTnI 170-191 upon addition of F-actin. 50µM hcTnI 170-191 (A) and in the presence of 25µM F-actin (B), 50µM F-actin (C) and, 75µM F-actin (D). These spectra illustrate the absence of any marked relaxation for the signals of His171 and Trp190 in the presence of F-actin, pH 7.2 and T=298K.

Close inspection of the methyl region of the CP spectrum (Fig 6.15) showed that some loss of intensity was detectable for the signal from the sidechain of Ala170, while there was little observable change in the methyl group signal of Thr180. A slight reduction in signal intensity of the two shifted methyl group sidechains at 0.57 and 0.64ppm was also detectable at the higher concentrations of F-actin (Figure 6.15). Leu172, Val175

and Val187 are the residues that could given rise to these signals. The similar relaxation effect on these two shifted signals compared to the lack of alteration in the remaining CH_3 resonances suggested that they originated from a single residue. This was likely to be Leu172 given the correlation based on chemical shift position described earlier but the available data did not permit their definite assignment. The assignment of these resonances to a particular residue in the sequence of hcTnI 170-191 was not pursued since the observed spectral changes for the peptide occurred at high F-actin concentrations (equimolar to peptide and above) and indicated that the hcTnI residue region of 170-191 is far less capable of interacting with F-actin compared to the peptide comprising hcTnI residues 165-196.

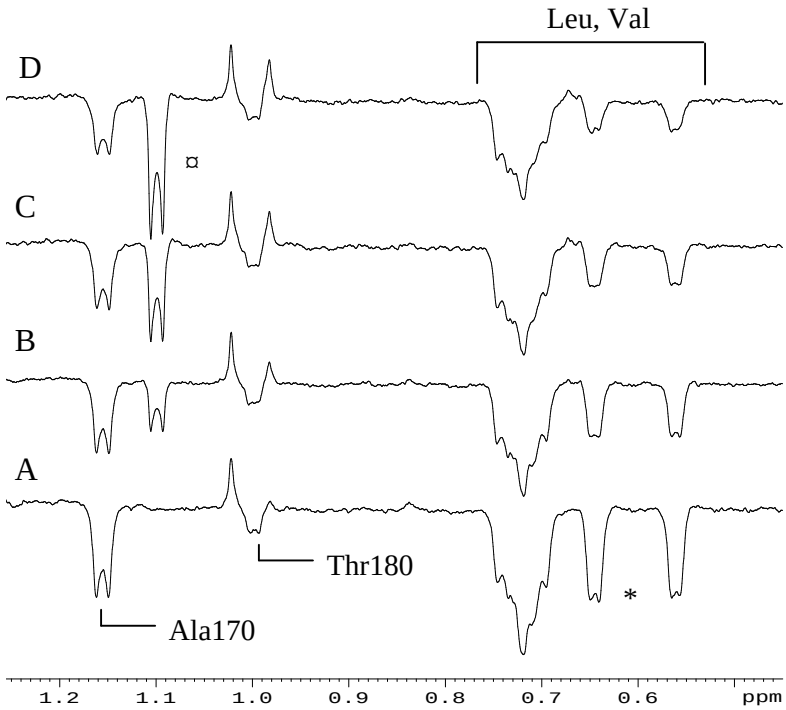

Figure 6.15 ^{1}H MR two pulse spin echo spectra of the aliphatic region of hcTnI 170-191 upon addition of F-actin. 50µM hcTnI 170-191 (A) and in the presence of 25µM F-actin (B), 50µM F-actin (C) and, 75µM F-actin (D) showing some but minimal effect on the two shifted methyl signals that may derive from Leu172 (*) and on the signal of Ala170 in the presence of F-actin. ¤ Impurity from the F-actin sample (ethanol), pH 7.2 and T=298K.

Since the N-terminus of hcTnI 165-196 was more affected upon F-actin addition than the C-terminus, it might be suggested that the loss of the first few residues of hcTnI 165-196 (i.e. 165-169) led to the disruption in the F-actin binding properties of hcTnI 170-191. The further conclusion based on the assay of the F-actin binding properties of hcTnI 170-191 to bind to F-actin is the observed absence of a well-defined interaction (Fig 6.15). This therefore supported the suggestion above, that F-actin interaction involving residues ~165-175 ensured the 'hover' or localisation of residues ~180-195 in the vicinity of the F-actin surface. The extent to which the extreme C-terminal region of hcTnI was able to jut away from the actin surface was therefore studied using the overlapping peptide, hcTnI 179-209 that contained the extreme C-terminal sequence of hcTnI.

6.5 F-actin interaction with hcTnI 179-209 involved the C-terminal residues of hcTnI

hcTnI 179-209 provided several unique reporter groups for different regions along the sequence while the absence of Leu/Val/Ile from the C-terminal ~12 residues and the N-terminal ~8 residues meant that the corresponding CH_3 signals could also be used as windows for any interaction detected between the central segment of hcTnI 179-209 and F-actin.

$_{179}$-**N**-**Ac**-D**T**EKENREVGD**W**RKN**I**D**A**LSG**M**EGRKKK**F**ES-$_{209}$

The aromatic region of the spectrum of hcTnI 179-209 (Fig 6.16) shows the signals that derive from the sidechains of Trp190 and Phe207. Addition of F-actin led to progressive broadening of all these sidechain signals indicative of the interaction of hcTnI 179-209 with F-actin. The relative change in signal intensity seen in Figure 6.16, with greater perturbation of the ring proton signals of Phe207 compared to those of

Trp190, suggested involvement of the C-terminus of the peptide in the interaction with F-actin.

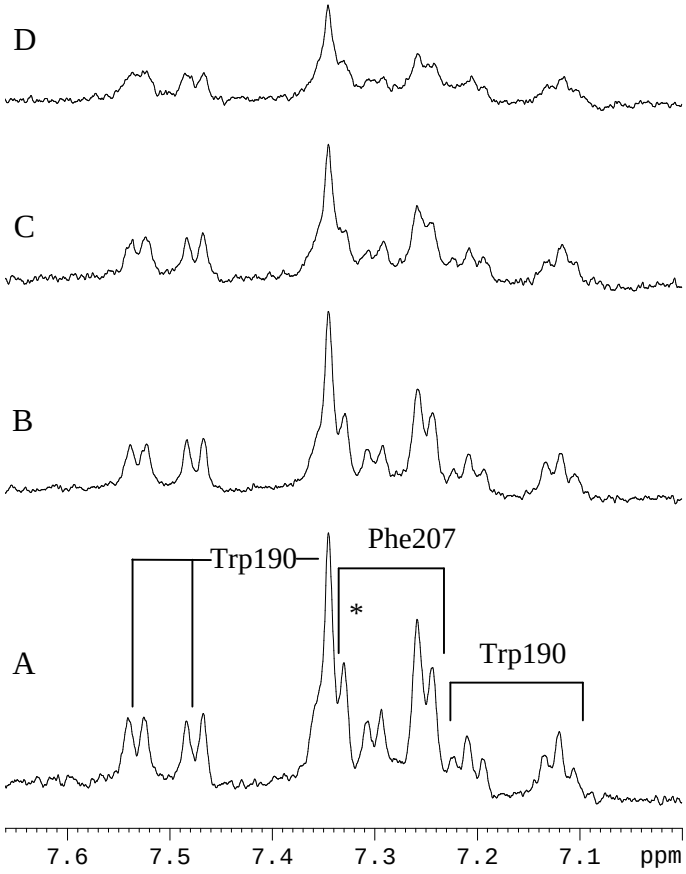

Figure 6.16 ^{1}H MR spectra of the aromatic region of hcTnI 179-209 upon addition of F-actin. 50µM hcTnI 179-209 (A) and in the presence of 7.5µM F-actin (B), 15µM F-actin (C) and, 25µM F-actin (D) with relatively more effect on signals of Phe207 compared to those of Trp190 observed in the presence of F-actin. * Phe signal overlapping with Trp signal, pH 7.2 and T=298K.

Further analysis of the nature of binding was enabled by inspection of the methyl region of the spectra of hcTnI 179-209 acquired during the titration with F-actin.

The region of the spectrum that spans 0.8-2.1ppm (Fig 6.17) shows the signals from the N-acetyl group, and the sidechain signals of Thr180 (1.2ppm), Ile194 (0.84ppm), Ala196 (1.4ppm) and Met200 (2.02ppm). The sequence of CP spectra acquired during titration (Figure 6.17) illustrated that addition of F-actin led to progressive broadening

of Met200 to an extent that was markedly greater than was observed for the remaining readily identifiable signals. This was best illustrated by the undetectable spectral change for the N-acetyl resonance and the small change in the signal of Thr180 ?CH_3, which are both localised at the N-terminus of the peptide (Fig 6.17).

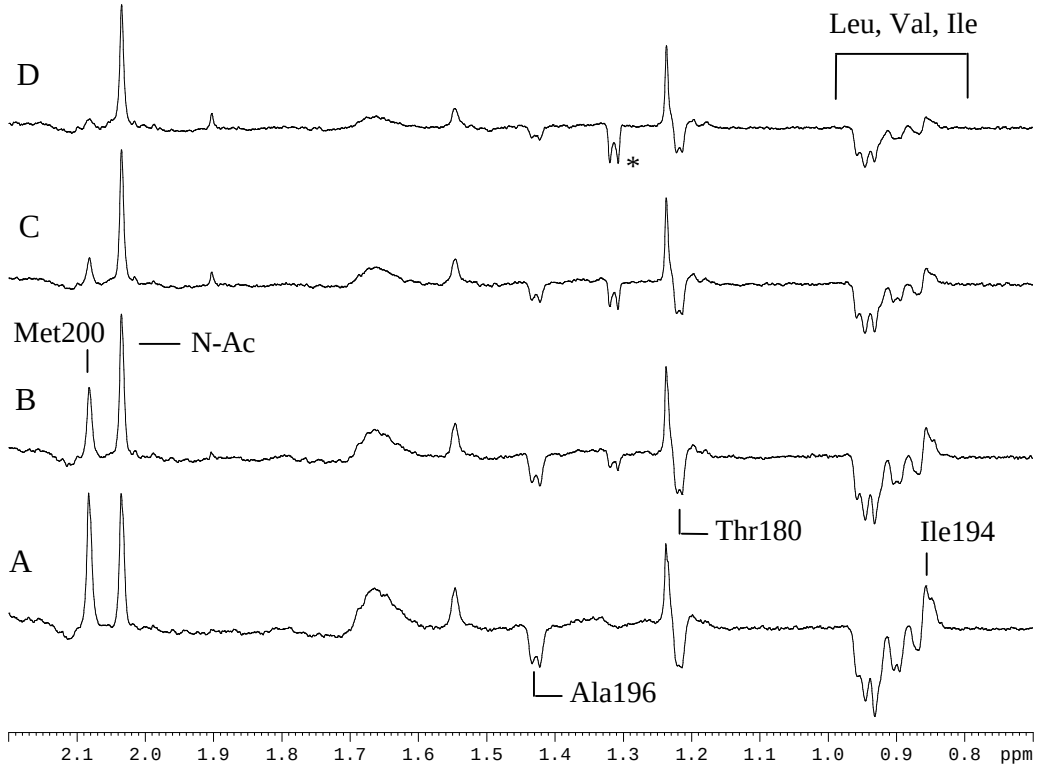

Figure 6.17 ^{1}H MR two pulse spin echo spectra of the aliphatic region of hcTnI 179-209 upon addition of F-actin. 50µM hcTnI 179-209 (A) and in the presence of 7.5µM F-actin (B), 15µM F-actin (C) and, 25µM F-actin (D) with a dramatic effect on Met200 compared to no change in the N-acetyl signal in the presence of F-actin, suggesting that the interaction involved the C-terminus of the peptide. * Impurity signal present in the F-actin sample (ethanol), pH 7.2 and T=298K.

The observation of a progressive reduction in signal intensity of the SCH_3 signal of Met200 during titration indicated that association with F-actin entailed rapid equilibrium (fast exchange) between free and bound forms of the peptide. Further, distinguishably different relaxation changes for signals of various groups of the peptide resulted from F-actin interaction. Signals of residues in the N-terminal half of the peptide were still readily resolvable towards the end of the titration (Fig 6.17C, D):-,

Ala196, Ile194, Leu/Val, Thr180 and the N-Acetyl. This complex formation presumably involved better contact between the C-terminal end of the peptide than was felt by the N-terminus, whose signals remained relatively unaffected by the association of the peptide hcTnI 179-209 with F-actin.

Putting together the observations on the three overlapping peptides spanning hcTnI residues 165-209 identified two distinct zones of interaction. The first of these encompasses the region previously identified as the 'second actin/Tm binding site'. The finding that an F-actin binding site was also localised at the C-terminal extremity of hcTnI was a novel observation. This binding region contains a cluster of basic residues whose contribution to binding was explored by titrations with F-actin carried out a higher ionic strength (0.1M KCl). The presence of salt in solution at the outset of each titration also enabled any ionic strength dependent chemical shift changes to be monitored for the free peptide. This provided a means for testing the effect of ionic interactions in the stabilisation of the 'elbow joint' segments of the C-terminus. The experiments described below present the data obtained for hcTnI 165-196 in the presence of salt before focussing on the ionic strength dependence observed for the binding of hcTnI 179-209 to F-actin.

6.6 hcTnI 165-196 retained interaction with F-actin in the presence of 0.1M KCl

Figure 6.18 shows the aromatic region of the spectrum of hcTnI 165-196 in the absence (A) and presence of 0.1M KCl (B). No alteration in chemical shift was detectable for the resonances of His171 or Trp190 in the presence of 0.1M KCl (Fig 6.18B) or Ala170 (Fig 6.19B). Changes in the relaxation properties (and hence mobility) of the methyl

group of Ala170 were also not detectable (Fig 6.19). The presence of 0.1M KCl did not therefore disturb the sequence-correlated conformational preference of the segments encompassing these residues.

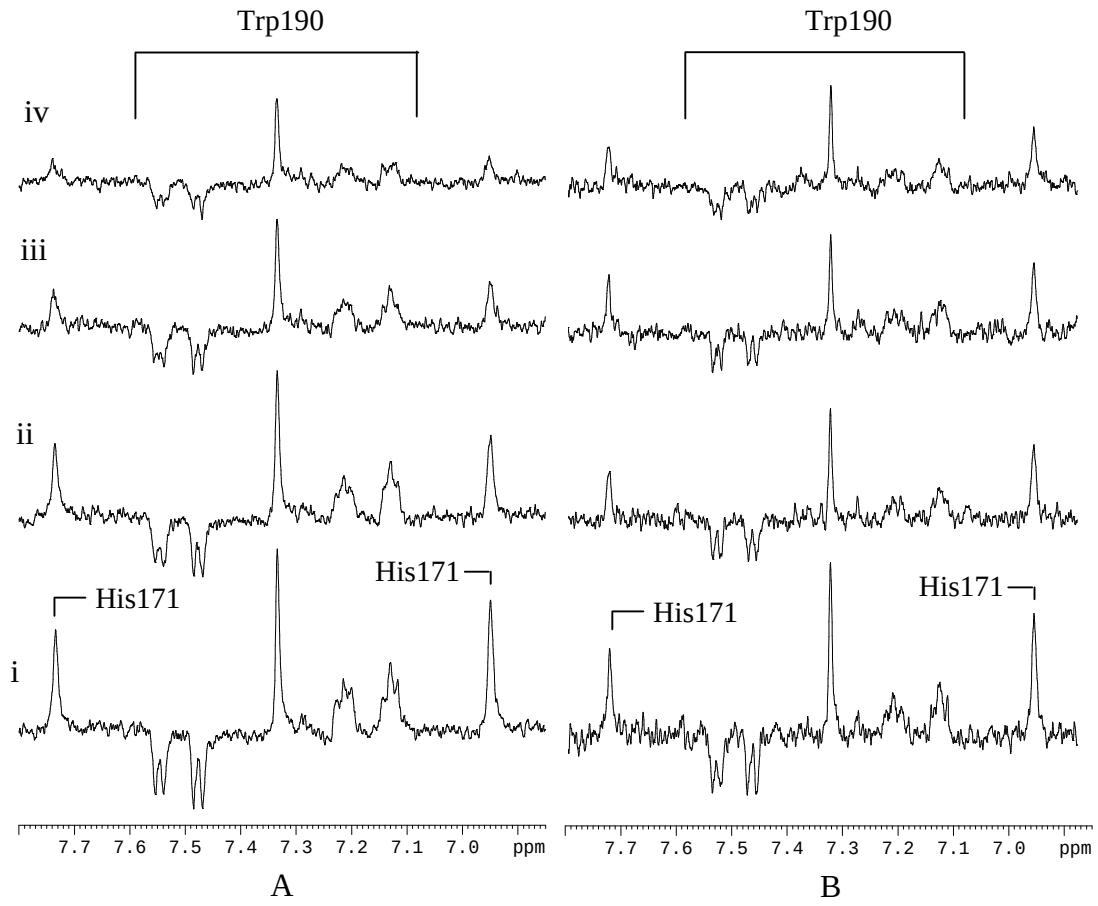

Figure 6.18 ^{1}H MR two pulse spin echo spectra of the aromatic region of hcTnI 165-196 in the absence (A) and presence (B) of 0.1M KCl upon addition of F-actin. 50µM hcTnI 165-196 (i) and in the presence of 7.5µM F-actin (ii), 15µM F-actin (iii) and, 25µM F-actin (iv) , pH 7.2 and T=298K.

Comparison of the relaxation effects resulting from association with F-actin ± 0.1M KCl showed the occurrence of greater line broadening on His171 in the absence of KCl (Fig 6.18ii). The methyl resonance of Ala170 was also found to be slightly less perturbed at equivalent concentrations of F-actin in the presence of 0.1M KCl (Fig 6.19).

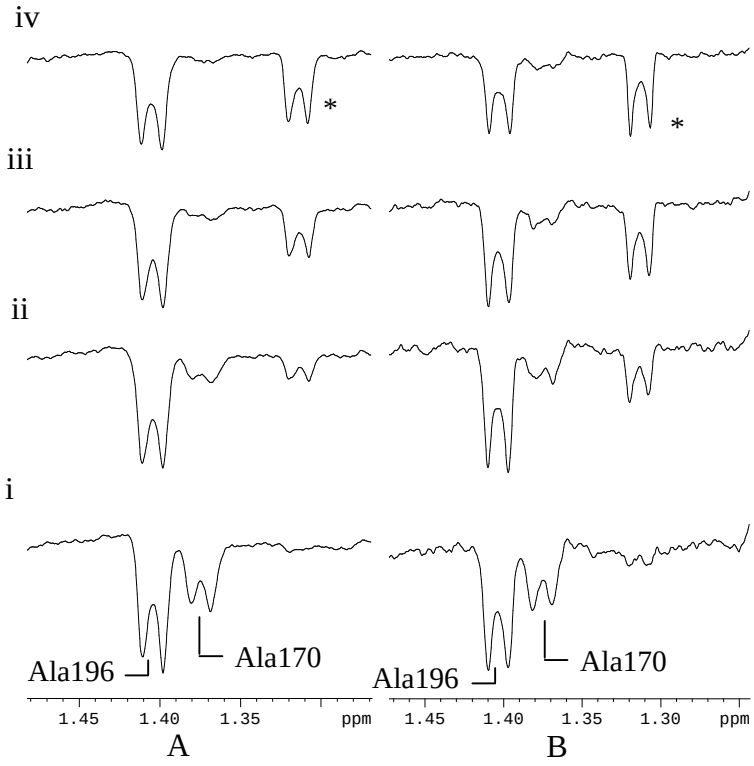

Figure 6.19 ^{1}H MR two pulse spin echo spectra of the alanine region of hcTnI 165-196 in the absence (A) and presence of 0.1M KCl (B) upon addition of F-actin. 50µM hcTnI 165-196 (i) and in the presence of 7.5µM F-actin (ii), 15µM F-actin (iii) and, 25µM F-actin (iv). * Impurity from the F-actin sample (ethanol), pH 7.2 and T=298K.

The differences in the response to F-actin binding observed for the signals of Ala170, His171 and Ala196 in the presence and absence of 0.1M KCl are presented in the graph shown in Figure 6.20.

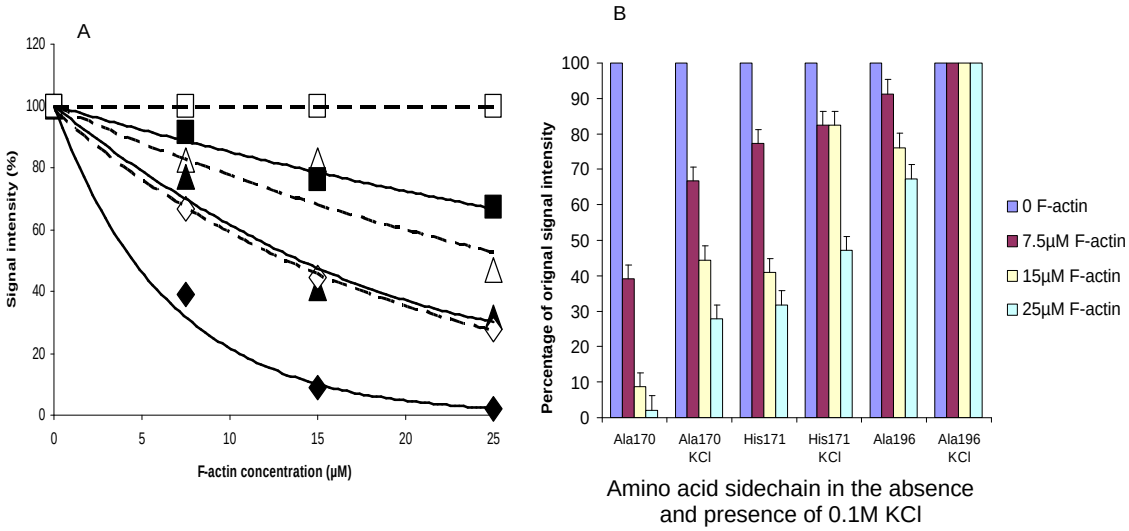

Figure 6.20 (A) Interaction of hcTnI 165-196 with F-actin was reduced by the presence of KCl as shown by the altered signal intensity observed in two pulse spin echo experiments. The signals in the N-terminus of hcTnI Ala170 ◆ His 171 (2H) signal ▲ were more affected in the presence of F-actin than signals in the C-terminus Ala196 ■ showing that the N-terminus of hcTnI 165-196 was more involved in the interaction with F-actin than the C-terminus. Ala170 in the presence of 0.1M KCl ◇. His171 (2H) in the presence of 0.1M KCl △. Ala196 in the presence of 0.1M KCl □. (B) Bar graph showing the change in signal intensity from specific sidechain signals upon the addition of F-actin in the absence and presence of 0.1M KCl. The slightly weaker affinity in the presence of 0.1M KCl apparent from the F-actin concentration dependence of the spectral perturbations was consistent with a primarily non-ionic association.

As already described for hcTnI 165-196, complex formation with F-actin involved the N-terminal segment and this association with the surface of F-actin resulted in the C-terminal portion of the peptide displaying mobility determined by the complex. As seen from the otherwise comparable changes during the titration, this peptide maintained the ability to interact with F-actin in the presence of 0.1M KCl suggesting that more than purely electrostatic interactions contributed to the interface with F-actin.

6.7 hcTnI 179-209 interaction with F-actin was retained in the presence of 0.1M KCl

In contrast to the nature of the residues shown to be involved in the binding by hcTnI 165-196 to F-actin, the interaction site on hcTnI 179-209 was demonstrated to

encompass charged residues at the C-terminus $_{200}$-MEGRKKKFES-$_{209}$. It was therefore of interest to test the ability of this peptide to interact with F-actin in the presence of 0.1M KCl. Figure 6.21 compares the aromatic spectral region of hcTnI 179-209 during titration with F-actin in the absence (A) and presence of 0.1M KCl (B).

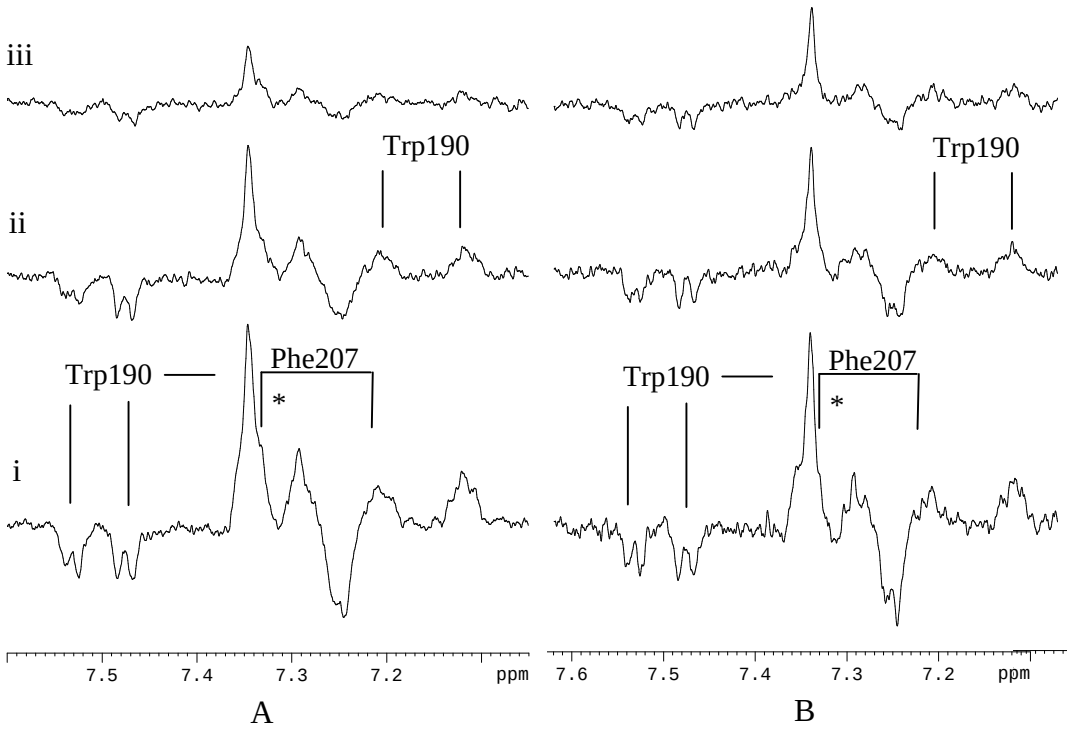

Figure 6.21 ^{1}H MR two pulse spin echo spectra of the aromatic region of hcTnI 179-209 in the absence (A) and presence of 0.1M KCl (B) upon addition of F-actin. 50µM hcTnI 179-209 (i) and in the presence of 7.5µM F-actin (ii), 15µM F-actin (iii), pH 7.2 and T=298K.

Inspection of these spectra showed that signals attributable to the sidechain of Phe207 were apparently a little less perturbed at equivalent concentrations of F-actin in the presence of salt (Fig 6.21). Significantly, however, interaction with F-actin was retained and still led to the mobility of the N-terminal segment of hcTnI being reduced by the anchoring to F-actin via the C-terminus of the peptide. This inference, derived from inspection of the signals of Trp190 (Figure 6.21), was readily confirmed by inspection of the aliphatic group region of the spectrum (Fig 6.22) where signals from the N-acetyl group, Thr180, Ile194, Ala196 and Met200 could be identified. The

change in signal intensity of these groups upon addition of F-actin was found to be reduced in the presence of 0.1M KCl, but the relative perturbations for the different reporter signals were not detectably altered (Fig 6.22and 6.23).

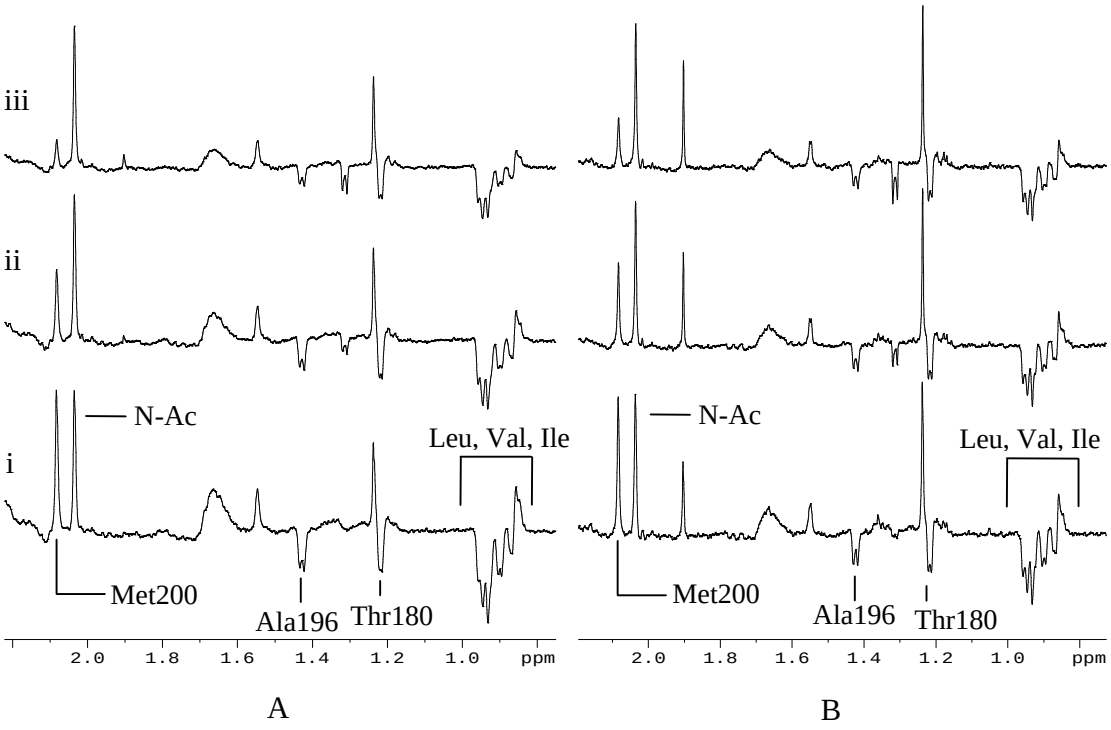

Figure 6.22 ^{1}H MR two pulse spin echo spectra of the aliphatic region of hcTnI 179-209 in the absence (A) and presence (B) of 0.1M KCl upon addition of F-actin. 50µM hcTnI 179-209 (i) and in the presence of 7.5µM F-actin (ii), 15µM F-actin (iii), pH 7.2 and T=298K.

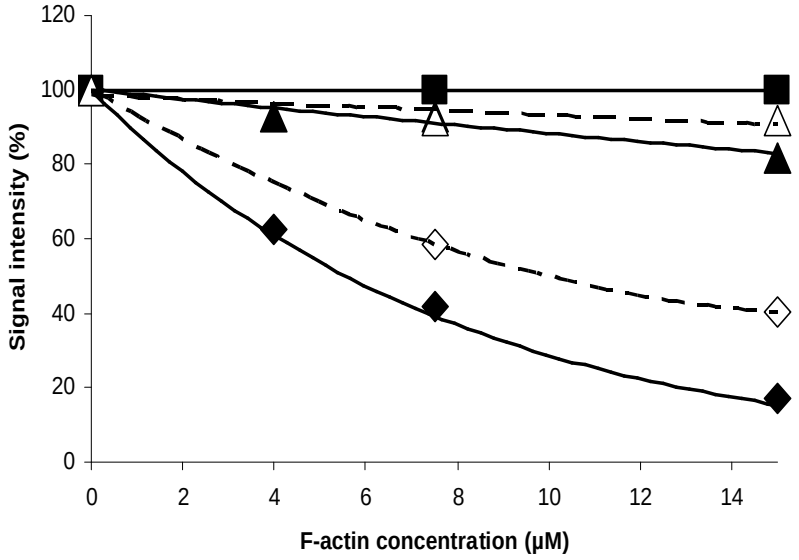

Figure 6.23 Interaction of hcTnI 179-209 with F-actin was reduced by the presence of 0.1M KCl as shown by the altered signal intensity observed in two pulse spin echo experiments. The signals in the C-terminus of hcTnI 179-209 Phe207 and Met200 ◆ were more affected in the presence of F-actin than signals from the N-terminus, Thr180 ▲ N-Ac ■ showing that the C-terminus of hcTnI 179-209 was more involved in the interaction with F-actin than the N-terminus. Phe207 and Met200 in the presence of 0.1M KCl ◇. Thr180 in the presence of 0.1M KCl △. The N-Ac signal did not change in the absence or presence of KCl upon addition of F-actin.

As illustrated from the comparison of the relaxation induced by F-actin in the absence and presence of 0.1M KCl (Fig 6.23), this peptide was therefore still able to interact with F-actin. The mode of binding involved the C-terminus of hcTnI 179-209, judged by Met200 and Phe207, but this attachment resulted in only slight reduction of the rotational freedom of its N-terminus as judged by the signal of Thr180 (Fig 6.22).

The observed interaction of the extreme C-terminus of hcTnI with F-actin was a novel finding and its persistence in the presence of other actin binding events required further study. This was first investigated using F-actin/Tropomyosin. Comparison of the aromatic region of hcTnI 179-209 upon titration with F-actin alone (Fig 6.24A) and titration with F-actin/Tropomyosin (Fig 6.24B) showed similar relative relaxation

effects for the sidechain resonances of Trp190 and Phe207, These observations implied that the interaction between F-actin and hcTnI 179-209 was maintained in the presence of tropomyosin.

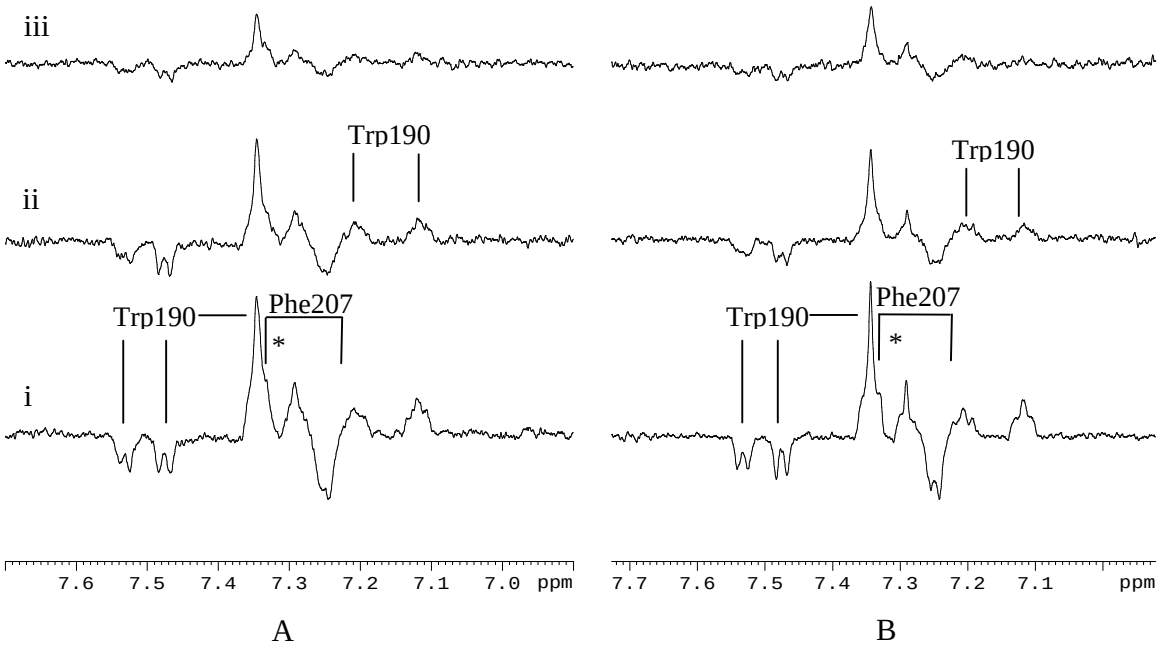

Figure 6.24 ^{1}H MR two pulse spin echo spectra of the aromatic region of hcTnI 179-209 upon addition of F-actin (A) and F-actin Tropomyosin (B). 50µM hcTnI 179-209 (Ai) and in the presence of 7.5µM F-actin (Aii) and 15µM F-actin (Aiii). 50µM hcTnI 179-209 (Bi) 7.5µM F-actin/Tm (Bii) 15µM F-actin/Tm (Biii) . Showing that hcTnI 179-209 maintains the ability to interact with F-actin in the presence of Tm, pH 7.2 and T=298K.

6.8 The C-terminus of hcTnI (200-209) retained interaction with F-actin in the presence of hcTnI 147-180 and, in the presence of the inhibitory region

The impression gained from the studies described above was that the extreme end of hcTnI C-terminal to inhibitory and switch peptide sequences contained two regions that interact with F-actin. In order to study whether these segments could bind concurrently to distinct sites on F-actin and to characterise their relative affinities, an equimolar mixture of hcTnI 147-180 and hcTnI 179-209 was first titrated with F-actin. The binding of each peptide could be followed by monitoring signals specific to residues of

each peptide – Met153 and 154, His171, Leu172 and, Trp190, Met200 and Phe207 – whose distinguishable spectral location was readily determined by comparison with the individual peptide spectra (Fig 6.25). The ability to observe these distinctive reporter groups meant that it was possible to monitor the relative relaxation effects induced by interaction with F-actin. The initial F-actin titration point shown in Figure 6.25C illustrates that quite marked spectral changes were observed for signals of both peptides even when only a relatively low concentration of 4μM F-actin had been added into the solution containing 50μM of each peptide. The prevailing molar concentration ratio of ~1:12:12, F-actin to each of the peptides was in the range where it was expected that the F-actin binding sites would be fully saturated. The observation that groups on both peptides were subject to relaxation by F-actin under these conditions suggested the existence of non-overlapping binding sites on the surface of F-actin for these two actin-binding regions of hcTnI.

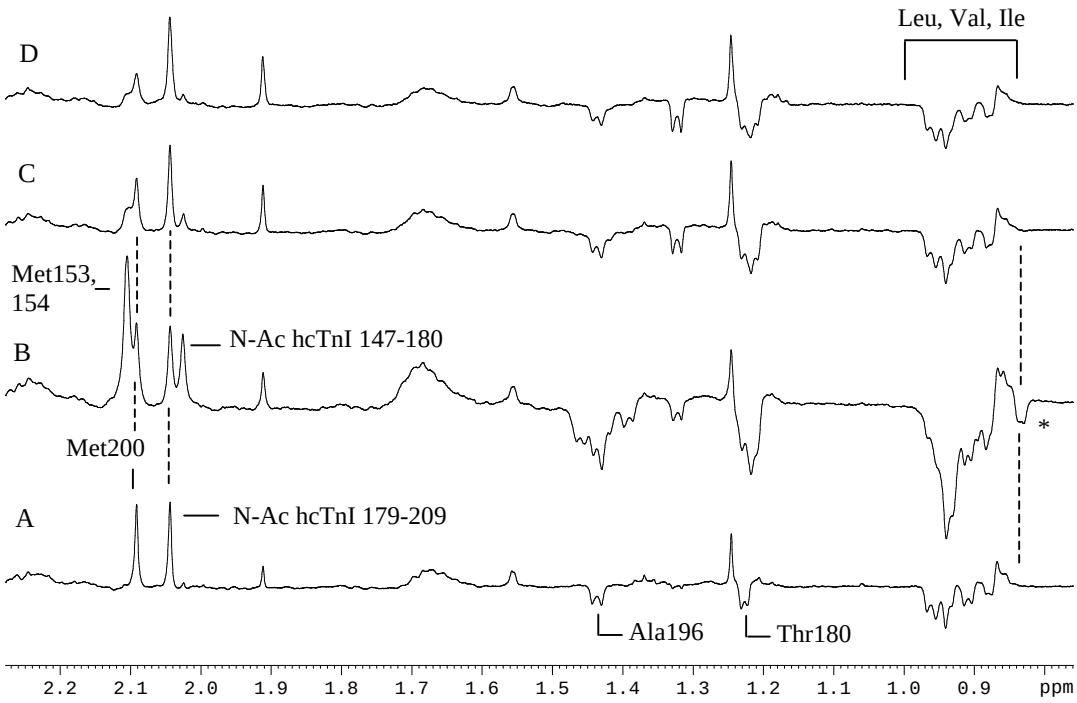

Figure 6.25 ^{1}H MR two pulse spin echo spectra of the aliphatic region of 50μM hcTnI 179-209 (A) and in a mixture with 50μM hcTnI 147-180 (B) upon addition of 4μM F-actin (C) and 7.5μM F-actin (D). The spectral changes observed demonstrated the ability of both peptides to interact with F-actin at the same time. The mode of binding to F-actin for hcTnI 179-209 still involved its C-terminus, judged by Met200 with less perturbation of its N-terminus as judged by the N-Ac. hcTnI 147-180 interaction with F-actin can be seen from the relaxation of the signals of the N-Ac, Met153/154, Leu172 (*) in the presence of hcTnI 179-209, pH 7.2 and T=298K.

The specific and distinctive F-actin binding sites of hcTnI 179-209 and hcTnI 147-180 were also indicated by the observed relaxation of the signals of both His171 and Phe207 upon F-actin addition (Fig 6.26iii and iv). Both sets of resonances appeared to show equivalent rates of relaxation changes induced by F-actin. These findings supported the inference that the two peptides were bound simultaneously and also suggested their comparable affinity for F-actin.

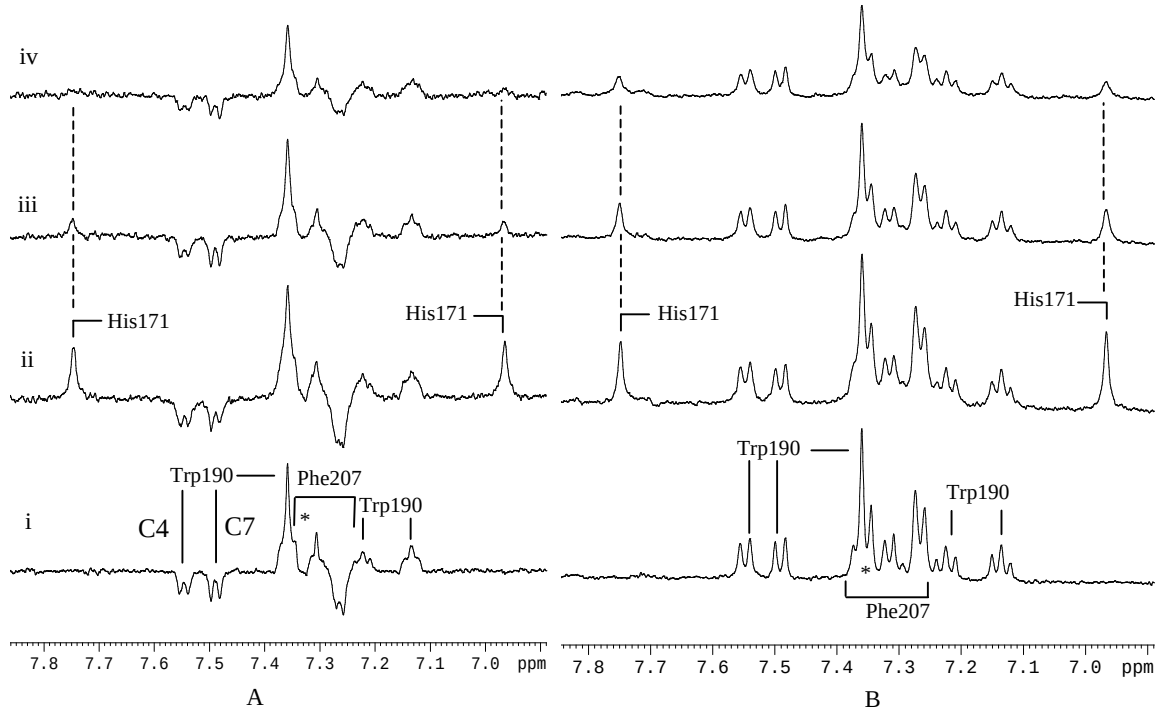

Figure 6.26 ^{1}H MR two pulse spin echo spectra (A) and ^{1}H MR spectra (B) of the aromatic region of hcTnI 179-209 (i) and in a mixture with hcTnI 147-180 (ii) upon addition of 4μM F-actin (iii) and 7.5μM F-actin (iv). * The Phe207 triplet signal at 7.36ppm overlapped with the Trp190 singlet signal, pH 7.2 and T=298K.

The aromatic region of the spectra shown in Figure 6.26 are presented in order to provide further evidence that, upon interaction with F-actin, the region of hcTnI 179-209 surrounding Trp190 was effectively tethered to the actin surface rather than making direct contact with actin. This could be seen from the extent to which fine structure was retained by the signals of the C4H proton (7.55ppm) and C7H proton (7.49ppm) of the sidechain of Trp190 (Fig 6.26iv A & B) in contrast to the line broadening for the sidechain of Phe209 (7.25-7.35ppm). Also observed was the greater perturbation of the signal from the C4H proton compared to the signal from the C7H proton of Trp190 (Fig 6.26iv). This was inconsistent with the equivalent relaxation that would have resulted from the docking of the tryptophan sidechain onto F-actin.

The extreme N-terminus of hcTnI 179-209 retained mobility unaffected by the attachment of the peptide to F-actin. This was observed by the absence of any perturbation of the N-acetyl group which reported on the N-terminus of the peptide (Fig 6.25). In similar fashion, the segment of hcTnI 147-180 constrained by interaction with F-actin could be resolved from the changes observed for its N-acetyl group, Met153, 154 and Leu172. The determinants of interaction on each peptide were therefore unaffected by their simultaneous attachment to F-actin. Taken overall these observations indicated the existence of distinct binding locations on the F-actin surface for hcTnI 147-180 and 179-209 and, that each surface location was not shielded by the exposed, yet, tethered regions at the C-terminus of hcTnI 147-180 and at the N-terminus of hcTnI 179-209.

Since the F-actin interaction of the C-terminal region of hcTnI likely involved the cluster of basic residues at the extreme end of the molecule, the possibility existed that its site of interaction on F-actin could be the same as for the similarly basic 'inhibitory' region. This possibility was tested by the study of any competition by the inhibitory region for the binding to F-actin by hcTnI 179-209. The line-broadening observed for the phenylalanine sidechain signals shown in Figure 6.27 indicated that both hcTnI 179-209 and hcTnI 128-153 interacted with F-actin when at a relative mole ratio of 3:1:1 C-terminal peptide to inhibitory region to F-actin (Fig 6.27C). The presence of higher concentrations of the inhibitory peptide (Fig 6.27D) indicated some degree of displacement of hcTnI 179-209 but the data suggested that the two regions are likely to target distinct actin binding locations.

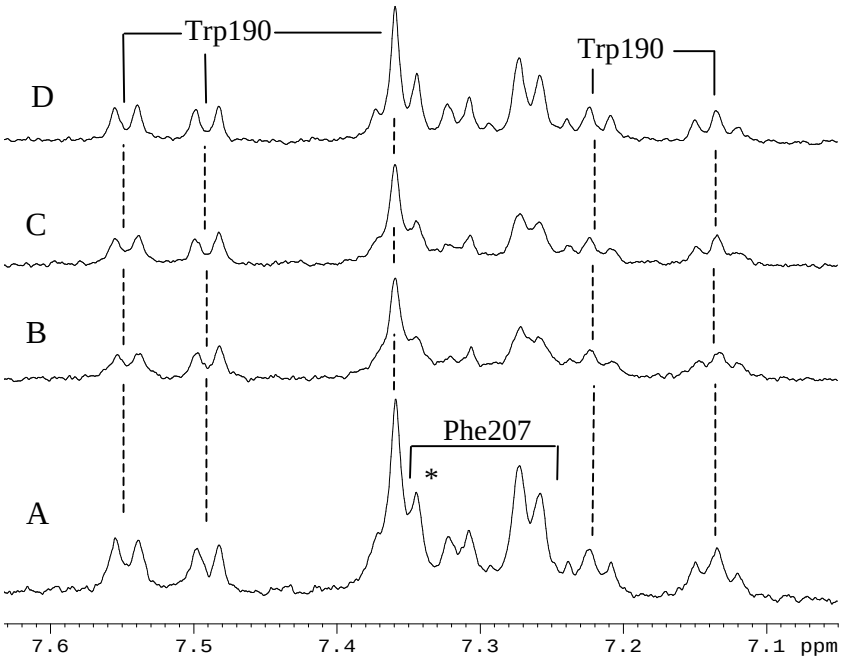

Figure 6.27 ^{1}H MR spectra of the aromatic region of 50µM hcTnI 179-209 (A) in the presence of 15µM F-actin (B) and on addition of 15µM hcTnI 128-153 (C) and in the presence of 30µM hcTnI 128-153 (inhibitory peptide) (D). The spectral changes shown indicated that the binding of hcTnI 179-209 occurred in the presence of the inhibitory peptide (C) although the extent of interaction between hcTnI 179-209 and F-actin was reduced when the concentration of inhibitory peptide exceeded that of F-actin (D). * Overlapping Phe and Trp signals. Note that some of the Phe signals from hcTnI 128-153 between 7.25 and 7.39ppm may be appearing in (C) and (D) , pH 7.2 and T=298K.

6.9 The segment of hcTnI encompassing residues ~180-196 projects away from the actin surface upon attachment of its flanking segments

In order to investigate the possibility of overlap on the surface of actin for the regions of hcTnI identified as actin interaction sites, titration experiments were also carried out using an equimolar mixture of hcTnI 165-196 and the inhibitory peptide, hcTnI 128-153. Fig 6.28B below illustrates the higher affinity of the inhibitory peptide. This was judged by the notable line broadening of the sidechain signals of Phe132 and 138 observed in the titration with F-actin in contrast to the changes in the resonances of His171 which altered more gradually with increasing concentration of F-actin (Fig 6.28Bii).

As seen from Figure 6.28A below, the data also indicated that attachment to F-actin via the N-terminus of hcTnI 165-196 tethered its C-terminal residues and resulted in constrained rotational mobility of the region that encompassed Trp190. The F-actin binding characteristics displayed by hcTnI 165-196 and hcTnI 179-209 therefore indicated that the segment linking the actin binding sites at the N- and C- termini of these overlapping peptides projected away from the surface of F-actin.

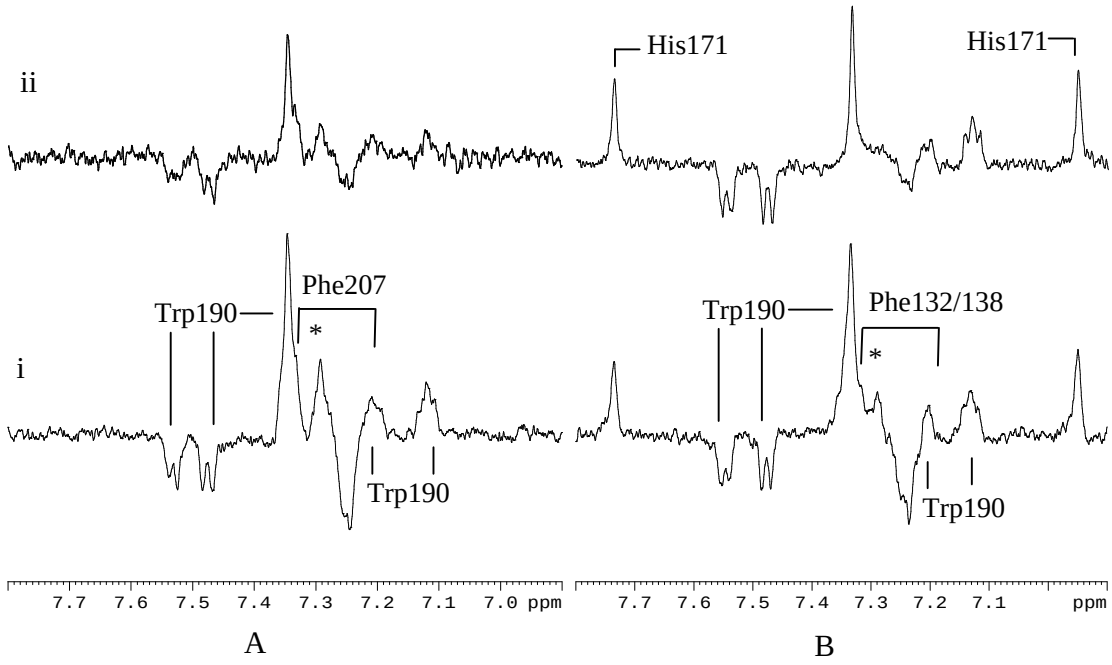

Figure 6.28 ^{1}H MR two pulse spin echo spectra of the aromatic region of hcTnI 179-209 (A) and an equimolar (50μM) mixture of hcTnI 165-196 and hcTnI 128-153 (B). The upper spectra in each panel are those obtained upon addition of 15μM F-actin (ii). * The Phe triplet signals at 7.36ppm overlap with the Trp190 singlet signal, pH 7.2 and T=298K.

An indication of the affinity of F-actin for the inhibitory region hcTnI 128-153, relative to that for the hcTnI C-terminus was obtained from the relative intensity changes between the spectra shown in Figures 6.28A and B. The spectra show the effect of F-actin addition to hcTnI 179-209 (Fig 6.28A) and to an equimolar mixture of hcTnI 165-196 and hcTnI 128-153 (Fig 6.28B). The peptide sequences selected for this

comparison meant that the relative broadening of signals of Trp190 and Phe207 of hcTnI 179-209 (Fig 6.28) could be assessed against the relative broadening of Trp190 of hcTnI 165-196 and Phe132, 138 of the inhibitory region. The extent of the line broadening observed for signals of Phe207 of hcTnI 179-209 at a 3:1 peptide to F-actin ratio was comparable to that seen for the signals of Phe132 and 138 of the inhibitory peptide (hcTnI 128-153) at the same relative concentration of peptide to F-actin (6.28ii A and B). These findings implied that the binding affinity of the inhibitory peptide for F-actin was comparable to the binding affinity of hcTnI 179-209 for F-actin.

6.10 Myosin loop peptides, hcβM 398-414 and hcβM 622-646 interact with F-actin in the presence of hcTnI 179-209

The distinctive location of the hcTnI C-terminal binding site on F-actin indicated above was explored further by use of the myosin loop peptides as probes of the interaction with F-actin. Figure 6.29 shows that the concurrent binding to F-actin by hcßM 398-414 and hcβM 622-644 was unaffected by the presence of hcTnI 179-209 at a relative molar ratio of ~7:1:1 of myosin peptide: F-actin: hcTnI 179-209. In contrast, the subsequent addition of the inhibitory peptide at a concentration equimolar with F-actin and hcTnI 179-209 substantially antagonised the binding of the myosin peptides (Figure 6.29D). The displacement of the myosin peptides upon addition of the inhibitory segment was clearly identifiable by the reversal of the linebroadening of Tyr410, His401 and Phe644. The interaction of the inhibitory region with F-actin did not, however, detectably perturb the signals that originated from hcTnI 179-209 (Fig 6.29D).

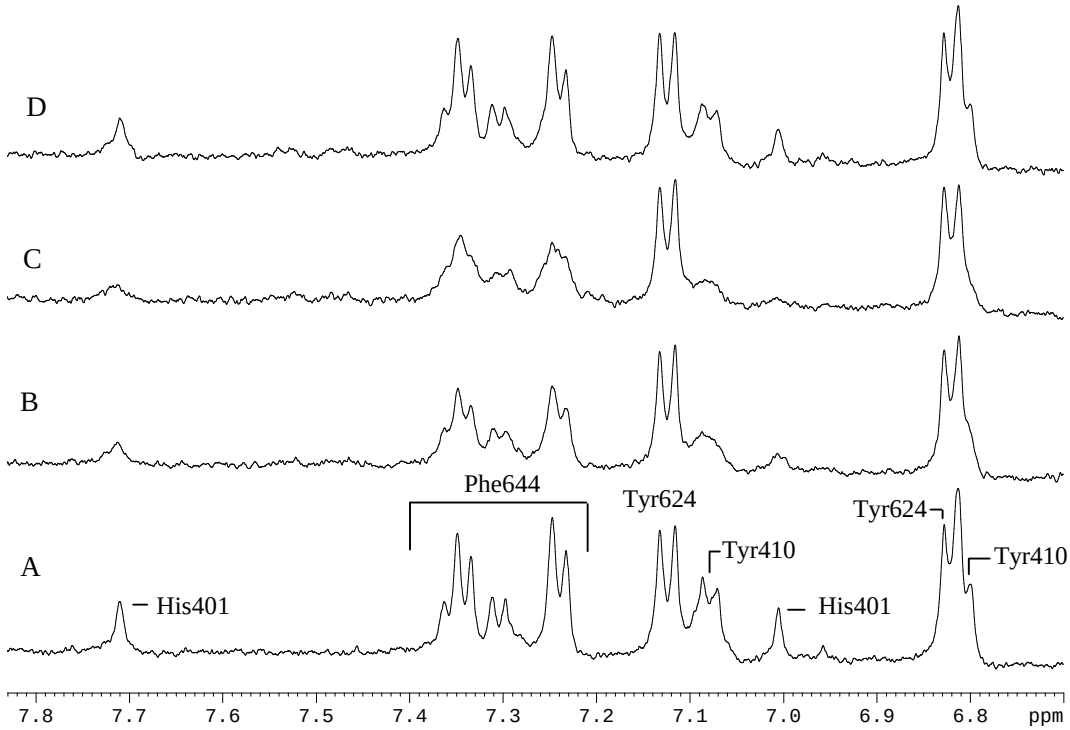

Figure 6.29 ^{1}H MR spectra of the aromatic region of a mixture of 50μM hcβM 398-414 and 50μM hcβM 622-646 (A) with addition of 4μM F-actin/hcTnI 179-209 (B) and 7.5μM F-actin/hcTnI 179-209 (C) subsequent addition of 7.5μM hcTnI 128-153 (D). The effect of the addition of the inhibitory peptide was to displace both the myosin loops from F-actin, , pH 7.2 and T=298K.

6.11 Interaction between hcTnI and F-actin involves multiple sites of attachment

The ability of the inhibitory peptide to antagonise F-actin binding of the two myosin peptides supported the suggestion of independent actin locations for interaction by hcTnI 128-153 and hcTnI 179-209, given that the myosin peptides interactions with F-actin were unaltered in the presence of hcTnI 179-209. Combined with the observation that the second actin/Tm binding region of hcTnI (residues 161-181) also lacked the ability to influence the interaction of the myosin loops with F-actin [Patchell et al, 2002], the different sets of data presented in this chapter on the C-terminal region of hcTnI suggested the occurrence of multi –site attachment to F-actin by distinct segments of hcTnI residues 128-209.

In the light of these observations, and the demonstrated ability of the N-terminus to interact with F-actin (Chapters 3-5), it was relevant to begin to explore whether the binding to F-actin by the C-terminal tail of hcTnI could influence interaction with F-actin by the N-terminal region of hcTnI. Given the observed antagonism by hcTnI 128-153 between hcTnI 1-30 and F-actin (Chapter 3), it was of interest to extend this investigation by carrying out an experiment in the presence of hcTnI 179-209. Therefore the aim here was two fold. Firstly it was to see whether hcTnI 1-30 could interact with F-actin in the presence of the C-terminal region hcTnI 179-209. Secondly to examine the ability of hcTnI 128-153 to compete with hcTnI 1-30 for F-actin in the presence of hcTnI 179-209.

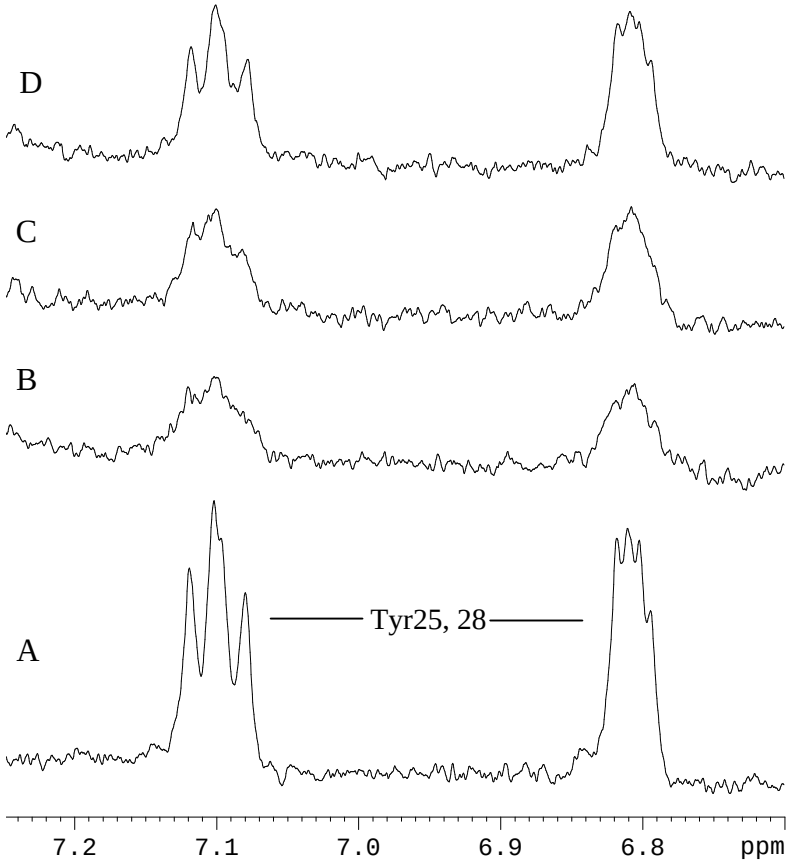

Figure 6.30 ^{1}H MR spectra of the aromatic region of 50µM hcTnI 1-30 (A) with addition of 4µM F-actin/hcTnI 179-209 (B). Addition of 2µM inhibitory peptide hcTnI 128-153 (C) and 4µM Inhibitory peptide hcTnI 128-153 (D) displaces hcTnI 1-30 from F-actin, pH 7.2 and T=298K.

Figure 6.30 shows that, at a 12:1 mole ratio of hcTnI 1-30 to an equimolar mixture of F-actin and hcTnI 179-209, the N-terminal peptide was able to interact effectively. The concentrations used in this experiment took into account the comparable K_d estimated above for F-actin interaction by hcTnI 128-153 and hcTnI 179-209. Since at this mole ratio of 'competitor' peptide:F-actin hcTnI 128-153 affected binding of hcTnI 1-30 the data in Figure 6.30 suggested that both the N-terminal and C-terminal segments of hcTnI were able to bind concurrently to F-actin. The inability of hcTnI 179-209 to antagonise binding by hcTnI 1-30 was supported by the observation that subsequent addition of comparable concentrations of hcTnI 128-153 (Figures 6.30C and D) caused displacement of hcTnI 1-30 consistent with the antagonism reported in Chapter 3. This difference between the effect of binding of hcTnI 128-153 and hcTnI 179-209 is taken up in the discussion below and in the overview of the data presented in Chapter 7.

6.12 Chapter synopsis and discussion

The F-actin binding assays described in this Chapter made use of a series of overlapping peptides that covered residues 147-209 at the C-terminus of hcTnI (equivalent and 73% identical to residues 116-182 of human fast skeletal TnI as shown in the FASTA-derived homology alignment below). Some 10 hydrophobic residues (shown in italics) make up the switch region of hcTnI that adopt a helical conformation when bound to hcTnC [Takeda et al, 2003 and Chapter 1] and that precede the second actin/Tm binding site which extends to ~ hcTnI residue 180.

```
       147        158                   180                 198        209
hcTnI  RI*SADAMMQALL*GARAKESLDLRAHLKQVKKEDTEKEN--REVGDWRKNIDALSGMEGRKKKFES
       :.:::::..:::::. :  .:::::.:::::::::::::   :.:::::::::.  :::::::: :::
hfsTnI RMSADAMLKALLGSKHKVCMDLRANLKQVKKEDTEKERDLRDVGDWRKNIEEKSGMEGRKKMFESES
       116                                                                182
```

The extreme C-terminal region of hcTnI, residues~ 198-209 underlined above, was here demonstrated to be capable of binding to F-actin at a location that was suggested by these studies to be distinct from the sites of F-actin interaction with the hcTnI inhibitory region (Figure 6.27) and hcTnI 147-180 (Figure 6.26) that included the so-named second F-actin/Tm binding site. The identification of this novel binding site was of interest since the C-terminal region of hcTnI does not make any contacts within the troponin complex [Murakami et al, 2005, Blumenschein et al, 2006] yet, deletion of residues 192-209, as detected upon myocardial stunning, increased cross-bridge cycling kinetics and led to an increase in myofilament Ca^{2+} sensitivity [Tachampa et al, 2008].

The binding data described above indicated that the interaction with F-actin by hcTnI179-209 involved both hydrophobic and electrostatic contributions to the association of the C-terminal region of the peptide with F-actin. Binding did not involve contact with the F-actin surface by the preceding segment (residues ~ 179-195). This region was however found to possess restrained mobility upon complex formation rather than showing rotational freedom independent of the tumbling of F-actin. This observation was consistent with the suggestion of structural predisposition that was made on the basis of the chemical shifts of particular residues of the free peptides spanning hcTnI residues 165-196.

The chemical shift of the resonance of any group is the average over the entire population of molecules and the deviation from ‘random coil’ values (Appendix II) reflects the proportion of the population that possesses well-defined structure. Significant deviation from these values and/or the observation of distinctive resonance

energies for nuclei of the same groups present in the same residue type located at different positions along the peptide sequence is as an indication of local conformational preferences (Chapter 2). Chemical shifts untypical of freely flexible peptides were observed for residues in two regions of the C-terminus of hcTnI, 169-RAHLK-173 and 187-VGDWR-191. It is not possible to define their structure on the basis of the shift data alone. The inference of sequence-context conformational preference for separate parts of the hcTnI C-terminal region preceding Met200 was however supported by the observation of constrained sidechain mobility for particular residues (Ala170 and Thr 180, above) and suggested that the structure of the C-terminal region of hcTnI was segmented and contained several 'joints' linking the separate actin binding patches. With this in mind it can be rationalised that docking of the extreme C-terminus to F-actin would result in the correlated motion of the preceding sequence as was observed for hcTnI179-209.

The contribution of both hydrophobic and electrostatic interactions to the association of the extreme C-terminus of hcTnI with F-actin was indicated by the nature of the sidechains found to make intimate contact with F-actin (Met200, Phe207) and the decrease in affinity of interaction in the presence of salt (K_d up ~2 fold to some 600μM as indicated by the I_B/I_F ratios, Figures 6.21 and 6.22). The free energy difference deriving from the presence of salt, ~2 kJ mol^{-1} ($\Delta G=-RT\ln K$), amounted to roughly 10% of the free energy change that characterised the binding of hcTnI179-209 to F-actin. The association of the C-terminal extremity of cTnI with F-actin may therefore be 'steered' by ionic attraction but is likely to be 'embedded' by hydrophobic contacts. The distinctive location of this association on F-actin was suggested by the absence of

binding competition from the two myosin loop peptides and from the second actin/Tm binding region.

In sum, the ability of the C-terminal region to act as a 'anchor', thereby localising the hcTnI 'tail' on the surface of F-actin, occurred also when the inhibitory and 2nd actin site regions of hcTnI were bound to F-actin and, was not antagonised by the presence of tropomyosin. These observations point to the existence of several actin-binding patches located within hcTnI residues 147-209. The inferred mechanistic contribution of the extreme C-terminal patch identified in this study is that it aids/directs the re-attachment of the inhibitory region to the thin filament upon its dissociation from TnC (Figure 6.31).

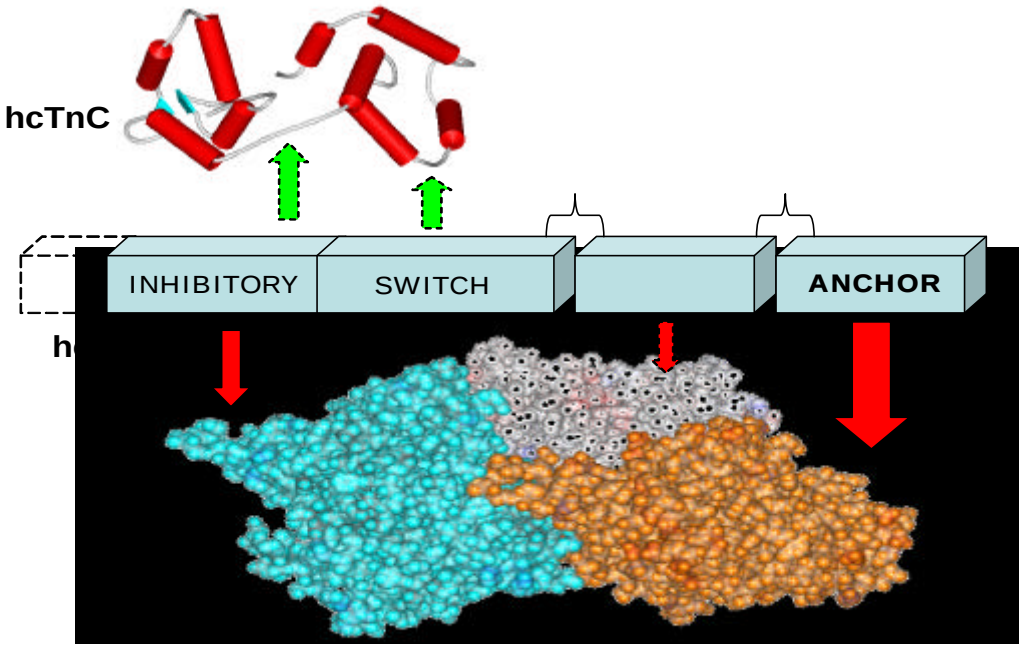

Figure 6.31 Schematic representation of the patches of interaction between the C-terminus of hcTnI and F-actin. The segmented structure of the C-terminal region is identified by inclusion of brackets along the sequence to illustrate the location of hcTnI 169-RAHLK-173 and 187-VGDWR-191. The anchor function of the extreme C-terminal of hcTnI is illustrated as contributing to the relocation of the inhibitory region back on to F-actin. The second actin/Tm binding site is here shown as aiding in this anchoring role.

This suggestion is in keeping with the increased cross-bridge cycling kinetics resulting from deletion of this tail contact [Tachampa et al, 2008]. Discussion of the functional implications of F-actin interaction by the hcTnI C-terminal extremity is taken up in the final Chapter.

7 Overall Discussion

The key outcome from the studies described in this thesis is the identification of two previously uncharacterised sites of interaction between hcTnI and F-actin. While the C-terminal association of hcTnI with F-actin is pertinent to all TnI isoforms, the association by a region on the N-terminus of hcTnI is of relevance to the functional properties specific to the cardiac isoforms of TnI. This discussion attempts to provide a structural perspective for the part played by the 'head' and 'tail' of hcTnI in the thin-filament based regulation of cardiac muscle.

7.1 General considerations of structural linkage

The functional contribution of any interaction with F-actin can be related to the residence time of the bound 'ligand' since this lifetime reflects the availability of the ligand to other interactions and, the influence of binding to the maintenance of F-actin in a given 'state'.

Three major states of the thin filament (blocked, closed and open) [McKillop and Geeves 1993; Gordon et al, 2001; Pirani et al, 2006] have been put forward as important to the description of the contraction/relaxation cycle and relate to the accessibility to actin by the myosin head and associated actomyosin crossbridge ATPase activity. The interconversion required between these states implies hopping along a free energy profile that resembles relatively flat ripples and this suggests the opportunity for the population of any given state to be modulated by an 'effector' such as troponin-I. One aspect of such modulation is the dynamics of effector interaction.

As indicated by the observations in Chapter 5 on the docking of hcTnI to the C-terminal domain of hcTnC, mobility can exist at the interface between ligand and receptor. Hydrophobic contacts predominate in the case of hcTnI binding to the hcTnC C-domain and the 'fuzziness' observed here for the complex suggests that this mobility was associated with swivelling within a structured cavity. Accessibility to such a cavity can be regulated by binding at a different site, e.g. by Ca^{2+} as in the case of the switch region of hcTnI binding to the N-domain of hcTnC, for example. The implication is that the protein contacts 'wriggle' and, that binding events can therefore be relayed via structural linkages. An example of such interactive relay mediated by only a few sidechain contacts can be seen from the proximity of the N-terminal of the inhibitory region of TnI to a calcium liganding sidechain, Glu152, on TnC (Figure 7.1).

The figure, obtained after inspection of the available crystal structures of the cardiac and the fast skeletal troponin complexes (PDB identifiers 1J1E and 1YTZ), shows this structural linkage between the inhibitory region and the calcium ligand as found for each troponin complex.

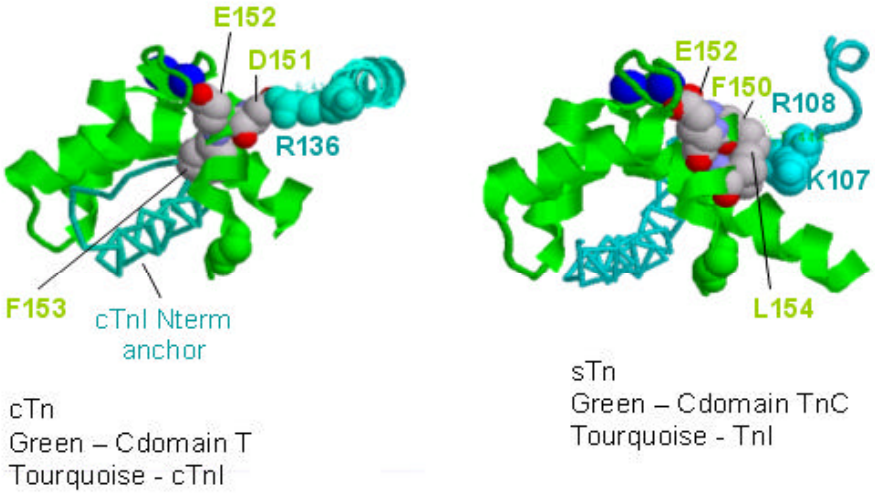

Figure 7.1 Views of the cardiac (left) and fast skeletal (right) TnI anchor region (turquoise, helical backbone representation) bound to the C-domain of TnC (green, with bound calcium ions shown in blue) also showing the contacts made by the N-terminal of the inhibitory region of TnI (turquoise, appearing on the right of each picture). Views obtained using the Rasmol graphics software and PDB entries 1J1E and 1YTZ.

In hcTnC the orientation of Glu152 is influenced by the interaction of a neighbouring sidechain, Asp151, with Arg136 of the hcTnI inhibitory region. Also, as shown in Figure 7.1, hcTnI residues 42-60 that are anchored to the hcTnC C-domain lie in the cavity shaped by the bound calcium. Sidechain contacts between Phe153 of hcTnC and Leu 54 of hcTnI contribute to the interface between hcTnC and the hcTnI anchor region. The sequence of hcTnC comprising Asp151-Glu152-Phe153 therefore acts as a 'hub' that connects 3 different inputs – Ca^{2+}, hcTnI anchor region and, binding by the hcTnI inhibitory segment.

Further inspection of the structure revealed that the sidechain of Leu54 of hcTnI was packed against the sidechains of hcTnC residues Phe153, Met157 and Val160 that all lie on the same face of the helix at the C-terminus of hcTnC. This suggested the possibility of a relay pathway linking the 3 inputs with the site of the Gly159Asp (G159D) dilated cardiomyopathy associated mutation that is located next to Val160 on this C-terminal helix of hcTnC. The G159D mutation has been reported to blunt myofilament desensitisation associated with phosphorylation of the N-terminal extension of cTnI [Biesiadecki et al, 2007] and it has since been proposed that the uncoupling of the relationship between phosphorylation and Ca^{2+} sensitivity could be the cause of the dilated cardiomyopathy phenotype [Dyer et al, 2009]. The structural linkage identified here between the C-terminal helix of hcTnC and the anchor region of hcTnI provides a plausible mechanism for the connection between the mutation and its functional consequences.

Docking of hcTnI on the C-domain of hcTnC resulted in an altered conformation of the segment protruding from the bound hcTnI anchor region (Chapter 5). The dynamics within the binding cavity suggest the potential for modifying the bound conformational 'ensemble' without the need for an unduly large expenditure of energy input. The G159D mutation could be accommodated by sidechain reorientation on the C-terminal helix of hcTnC. A domino-like response would be relayed to alter the conformational average of the bound anchor region that would consequently be reflected in the conformation adopted by the protruding N-terminal region of hcTnI. This hypothesis, open to experimental investigation using approaches such as those used in this study, is supported by the observation [Baryshnikova et al, 2008] that the affinity of complex formation between hcTnI 34-71 and hcTnC was reduced ~10-fold upon introduction of the G159D mutation indicative of less effective anchoring.

The extensive hydrophobic contacts at the hcTnI anchor-hcTnC interface therefore provide overall stability while enabling localised dynamics that can respond to and be relayed by structural linkages as that described above. The hcTnI molecule has the additional capacity of binding at several other locations and to different thin-filament protein targets. These characterised interactions within troponin and with F-actin/Tm are associated with the role of troponin-I in promoting the blocked state of the thin filament. The part played by the region of the troponin-I sequence comprising the last ~ 20 residues of hcTnI that follow the second F-actin/Tm binding site is however not well characterised [Galinska et al, 2010]. Mutations in this region of hcTnI that hangs free from the troponin complex (e.g. R192H, S199G, G203S and K206Q [Chang et al, 2008]) are implicated in both hypertrophic and restrictive cardiomyopathy while C-

terminal truncation of cardiac TnI has been reported to be associated with myocardial stunning following transient bouts of ischemia [Van Eyk et al, 1998]. While affinity chromatography and ultracentrifugation studies of a deletion construct missing the last 17 residues of hcTnI showed that the interactions with cTnT, cTnC or actin-Tm "were not grossly altered" [Foster et al, 2003], faster crossbridge cycling and a decrease in Ca^{2+} affinity of troponin was observed when the truncated protein was reconstituted into thin filaments [Tachampa et al, 2008].

The N-terminal extension of hcTnI, recently shown to contain a dominant dilated cardiomyopathy mutation, K36Q [Carballo et al, 2009], is the other region of the protein sequence studied here and that is associated with an influence on Ca^{2+} sensitivity although the details by which this effect is manifested are also not well resolved [Saddayappan et al, 2008]. The following consideration of the relevance of F-actin interaction by different regions of hcTnI will focus first on the the hcTnI tail in the light of the function suggested in this thesis that its interaction restrains the C-terminus of hcTnI from being unleashed from F-actin. The more dynamic role of the N-terminal head and the impact of its phosphorylation will then be discussed.

7.2 Multiple actin-binding patches at the C-terminus of cTnI are tacked down on the F-actin-tropomyosin filament and modulate myofilament Ca^{2+} activation

The binding data (Chapter 6) demonstrated the presence of a distinctive F-actin binding site at the extreme C-terminal residues of hcTnI. This interaction, enabled by both hydrophobic and electrostatic contributions, was retained when the inhibitory and 2nd actin site regions of cTnI were bound to F-actin. The C-terminal extremity can

therefore be considered as anchoring cTnI to F-actin, binding that was observed to localise the preceding segment (hcTnI residues ~ 179-195) to the surface of F-actin without involving direct interaction. The 'anchor' interaction was retained in the presence of tropomyosin but with an overall affinity of hcTnI residues 179-209 for F-actin/Tm not detectably different from that observed for F-actin alone. This indicated that the relatively exposed protrusion of residues ~ 179-195 from the surface of F-actin acts as a linker between distinct F-actin binding patches but may not contribute significantly to stabilisation of the F-actin/Tm complex.

The association between the coiled coil tropomyosin strands and F-actin is known to contribute to the overall stability of the actin filament [Cooper et al, 2002] and vice versa [Singh and DeGregori, 2009]. The association has been described as being 'shape-driven' and based upon matching surface contours [Holmes and Lehman, 2008]. Of the seven, almost-equivalent, sequence repeats that are distributed along the 284-residue tropomyosin primary structure, it is the central region of the molecule, residue range ~130-190 within repeats 4 and 5, that has been shown to interact with both actin and troponin [Sakuma et al, 2006; Singh and DeGregori, 2007]. Located in this central region are residues 165–185 that have been described as essential for actin binding [Singh and DeGregori, 2007 and 2009]. Further, fsTm residue 146 has recently been found to crosslink to fsTnI 157-163 (equivalent to hcTnI $_{186}$EVGDWRK$_{192}$) but only at low Ca^{2+} concentrations [Mudalige et al, 2009]. This site of crosslinking occurs at the residue span containing the R192H cardiomyopathy mutation and shown in Chapter 6 to act as a structured joint, a 'wrinkle' that demarcates a boundary between the preceding sequence comprising the inhibitory region, cTnC-binding switch segment

and the adjacent 2nd F-actin/Tm binding site and, the extreme C-terminal ~ 20 residues shown by this study to contain a further ‘anchor’ to F-actin (Figure 6.31).

A segmented topology for the C-terminal region was suggested by the locally structured joints comprising hcTnI 169-RAHLK-173 and 187-VGDWR-191 with the ‘retainer’/‘anchor’ function of the extreme C-terminus of hcTnI contributing to the efficiency of the relocation of the inhibitory region back on to F-actin at low Ca^{2+} with the second F-actin/Tm binding site aiding in this anchoring role by acting as a ‘fastener’.

Support for the proposed anchor role of the extreme C-terminus of hcTnI comes from the EM reconstruction of the average location of tropomyosin on F-actin filaments bound to cardiac troponin incorporating truncated hcTnI1-192 that was reported as this thesis study was coming to an end [Galinska et al, 2010]. Removal of the anchor tail region resulted in alteration of the position of tropomyosin to expose more of the predicted myosin binding site(s) on F-actin than was observed for the blocked state of the filament typified by low Ca^{2+}.

This view of the part played by the C-terminal region of hcTnI can be placed in the context of calcium mediated contractility that entails the short adhesive patches of hcTnI, the ‘activating regions’, on the F-actin-tropomyosin filament assembly being recruited by hcTnC, the ‘activation target’ (Figure 7.2).

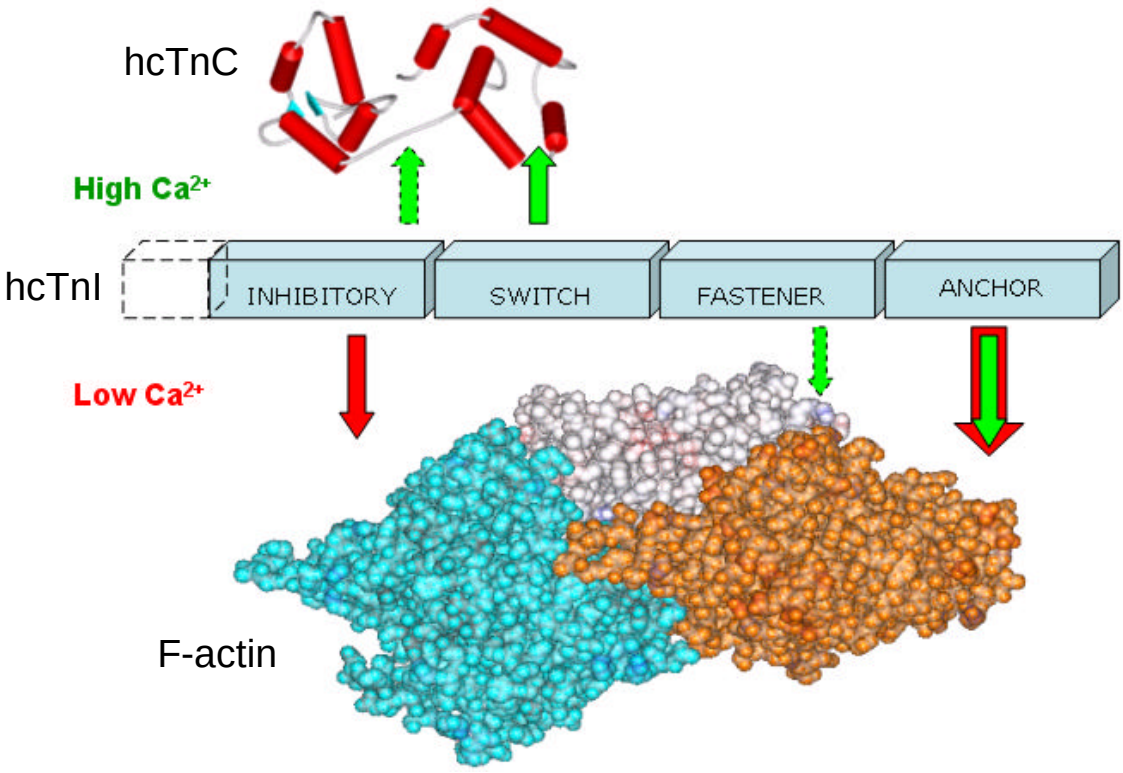

Figure 7.2 Representation of the Ca^{2+}-mediated multi-sited attachment between the C-terminus of hcTnI and F-actin. The combination of fastener and anchor regions enables the adhesion of hc-TnI in a defined orientation and possible restraint over tropomyosin migration. This adhesive constraint would be released when the inhibitory and switch regions associate with Ca^{2+}-cTnC when the extreme C-terminus of hcTnI now acts as the anchor linkage that could also influence the extent of tropomyosin migration (see text).

Namely, the transition between different states of the thin-filament associated with the shift of tropomyosin on the F-actin filament observed in response to Ca^{2+} binding and release by hcTnC can be viewed as involving contact patches of hcTnI whose adhesion to F-actin can thereby be relayed along the F-actin filament. Upon activation by Ca^{2+}, tropomyosin migration would be less constrained by the region that links the fastener and anchor segments of hcTnI while the C-terminal anchor would expedite the return of the thin-filament assembly to its inhibited state. This facilitation by the hcTnI C-terminal anchor and the contribution from Lys204-206 to its F-actin affinity (Chapter 6) would, for example, account for the observation that the K206Q cardiomyopathy

mutation led to an increase in the maximum actoS1-ATPase activity [Deng et al, 2003]. From the perspective put forward here, hcTnI acts as an inhibitor to block actin-myosin interaction locally and, by mediating the positioning of tropomyosin, also acts indirectly to facilitate its regulatory role. High Ca^{2+} would be expected to shift the region preceding the 'anchor' towards hcTnC with the ‘anchor’ ensuring that the reversal of this change is directed since orientation/disposition and proximity would be effectively retained. The interaction identified in this study between the C terminus of hcTnI and the F-actin filament may therefore modulate myofilament Ca^{2+} activation.

7.3 Modulation of myofilament Ca^{2+} activation by the N-terminus of hcTnI

Ca^{2+} sensitivity of the cardiac myofilament is also modulated by β-adrenergic stimulated PKA phosphorylation of the isoform-specific N-terminus of troponin-I. The change in Ca^{2+} sensitivity upon cTnI phosphorylation has been linked to the increase in Ca^{2+} dissociation kinetics that is generally assumed to result from altered interaction between the N-terminus of cTnI and the regulatory N-terminal domain of cTnC. The nature of this interaction is still unresolved. NMR spectroscopic studies [Abbott et al, 2001; Ward et al, 2004a; Baryshnikova et al, 2008], binding studies [Ward et al, 2004a] and deletion mutagenesis [Ward et al, 2002] have led to the suggestion that hcTnI residues in the range 19-30 contain the region of interaction between the N-terminus of cTnI and the N-terminal domain of cTnC.

The data presented in Chapters 3 and 5 identified a competing partner target opportunity, interaction with F-actin, shown to involve hcTnI residues 16-29 even when hcTnI1-64 was complexed with hcTnC. As seen from the ability of the inhibitory

region of troponin-I to alternate between hcTnC and F-actin in a Ca^{2+}-dependent manner, similar promiscuity of binding by the N-terminal region of hcTnI is not implausible. The opportunity available to the N-terminus of hcTnI for switching between F-actin and the N-terminal domain of cTnC (Figure 5.18) would therefore entail a dynamic equilibrium involving association between F-actin and its potential site on the N-terminal domain of hcTnC [Mitchell et al, 2007].

A consequence of F-actin interaction by the N-terminus of hcTnI is that the extent of its association with hcTnC would decrease. Accessibility to F-actin would therefore be expected to result in a reduced population of hcTnC states whose Ca^{2+} affinity was stabilised by the binding of the N-terminus of hcTnI. Upon Ca^{2+} activation, however, the inhibitory region would, along with the switch region, be localised on hcTnC with consequent enhancement of Ca^{2+} affinity (Figure 7.2). The interactivity observed between the binding to F–actin by the hcTnI N-terminal and by the hcTnI inhibitory region (Chapter 3) and, the relative affinity of the inhibitory region for hcTnC and F-actin (Figure 3.9) are of relevance here. These observations indicate that, at activating Ca^{2+} levels, the interaction of the hcTnI N-terminal with F-actin would aid the repopulation of hcTnC from which the inhibitory region had dissociated in favour of F-actin and thereby sustain increased Ca^{2+} affinity [Mitchell et al, 2008].

Thus, while reduction in the prevailing Ca^{2+} concentration would encourage release of the switch region, reassociation of the inhibitory region with F-actin and the release of the N-terminal region of hcTnI from F-actin, the accessibility of the N-terminal extension of hcTnI to F-actin enabled at activating Ca^{2+} concentrations is likely to

influence the Ca^{2+} affinity of hcTnC via modulation of the dynamic equilibrium involving binding of the inhibitory region to F-actin and to hcTnC. From this perspective, the modulation of Ca^{2+} affinity via phosphorylation of the N-terminal region of hcTnI can be rationalised by the reduced F-actin binding affinity of the phosphorylated species (Chapter 4).

The equilibrium population of the hcTnI16-37 peptide bound to F-actin was shown in Chapter 4 to be altered upon monophosphorylation at either Ser22 or Ser23. The difference in F-actin affinity for this peptide was ascribed to the altered contribution within hcTnI residues 30-37 in the S22P hcTnI16-37 peptide and more so for the S23P hcTnI16-37 peptide. Two other findings are directly relevant in this regard. The first is the observed ability of hcTnI16-29 to interact effectively with F-actin even upon substitution of Ser22 by aspartate. The second is that, as detected by the hcTnI segment containing Tyr 25 and Tyr 28, this interaction with F-actin was retained in the hcTnI1-64 complex with hcTnC (Chapter 5). Here, as for the monophosphorylated hcTnI16-37 peptides, the region of interaction with F-actin did not extend as far as His33 of hcTnI, suggesting shielding of the surrounding sequence upon docking to hcTnC. Consistent with the observed disposition of hcTnI 35-40 relative to the N-domain of hcTnC that was resolvable in one of the two structures per unit cell found in the partial cardiac troponin structure [Takeda et al, 2003], a possible explanation was that the shielding of His33 arose due to interaction of the surrounding sequence with hcTnC. This explanation would also account for the observation [Carbalo et al, 2009] that the charge change present in the dilated cardiomyopathy K36Q mutant led to reduced thin filament Ca^{2+} affinity. Further, given that the nature of the structural change resulting from

phosphate incorporation resulted in less effective exposure of the charge on Lys34-36 (Chapter 4), it can be inferred that phosphorylation is relayed to this region of hcTnI. Such relay could impact on the association of Ca^{2+} with the N-domain of hcTnC and, may also affect the association of Ca^{2+} with the hcTnC C-domain via the linkage mediated by the docked hcTnI residues 42-60 (above).

A final point relates to the relative population of the hcTnI N-terminal bound to F-actin and its associated dependence on the equilibrium between kinase and phosphatase activity.

Preliminary experiments have confirmed the original observations of Jacquet et al [Jaquet et al, 1995] of roughly equivalent rates of dephosphorylation of Ser22 and Ser23 by a phosphatase preparation isolated from heart muscle. When placed in the context of the PKA phosphorylation kinetics [Quirk et al, 1995 and preliminary experiments] and the prevalence of Ser22P monophosphorylated hcTnI in mass spectrometry-based analysis of heart tissue [Zabrouskov et al, 2008], it is possible to obtain some insight into the different phosphorylated forms of hcTnI that may be present on the thin-filament assembly in the healthy human heart (Figure 7.3).

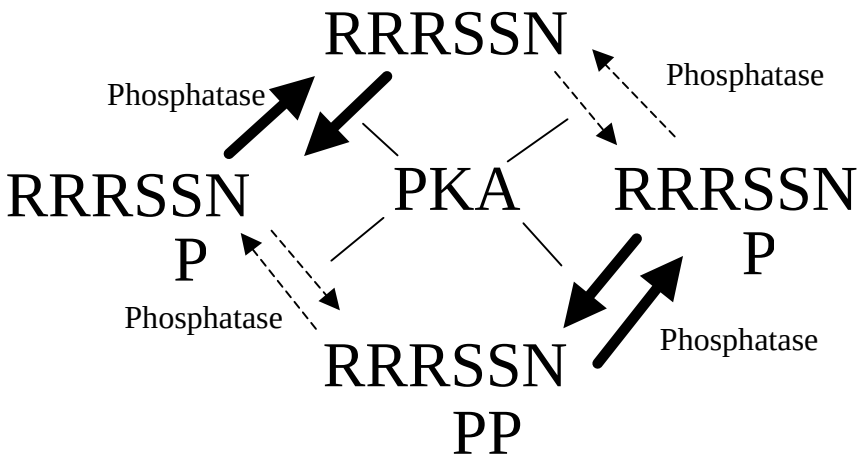

Figure 7.3 Phosphorylation at position Ser23 may be the more important switch. This region of hcTnI may be monophosphoylated at $S_{22}P$ due to dephosphorylation of the bisphosphorylated form with switching between monophosphorylated $S_{22}P$ and bisphosphorylated forms may occur in the healthy heart.

Hopefully apparent from the observations described in this thesis is that both the head and the tail of hcTnI contribute to the modulation of myofilament Ca^{2+} activation. Further work is required to elaborate on the contribution of these ends of the hcTnI molecule along with exploration of the functional capability of the extreme N-terminal region of hcTnI and the involvement of troponin-T and of tropomyosin if one is to adequately place the observations made in this study in the context of the thin filament protein assembly. Much relevant guidance towards this can be derived from the published work of Professor S V Perry.

Appendix I

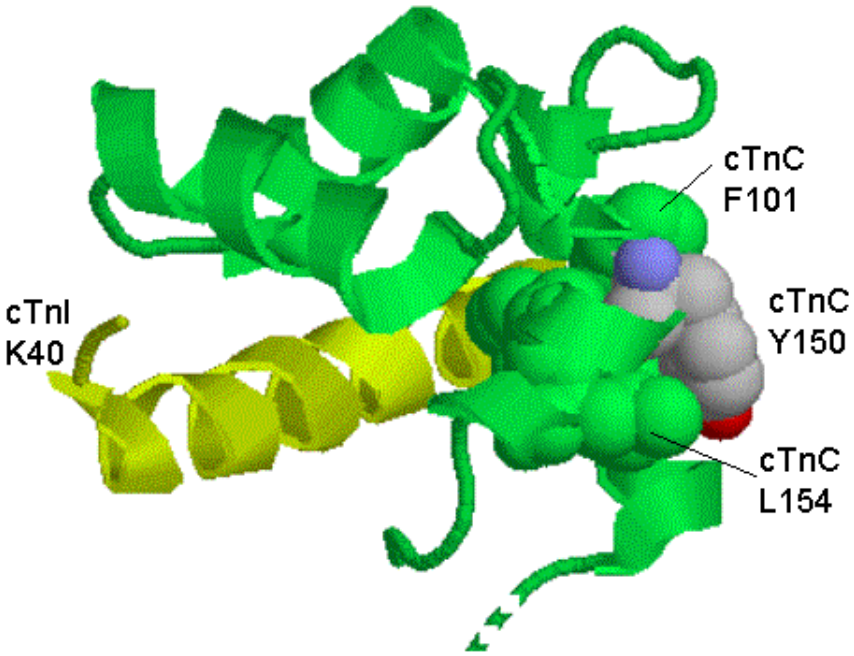

Figure I.1 C-terminal domain of cTnC (green) bound to the anchor region of cTnI as determined in the crystal structure of the partial cardiac troponin complex [Takeda et al, 2003]. The hydrophobic neighbours of cTnC Tyr 150 are shown in spacefill format.

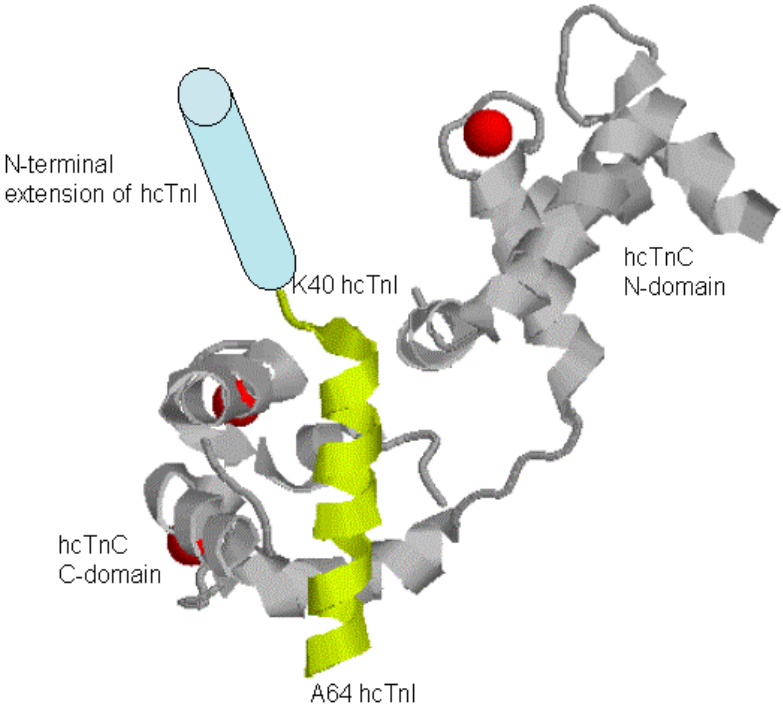

Figure I.2 Partial human cardiac troponin crystal structure showing hcTnC (grey), bound Ca^{2+} (red), hcTnI residues 40-64 (yellow) [Takeda et al, 2003], and the N-terminal extension of hcTnI (blue) shown as a protruding segment.

Appendix II

^{1}H chemical shifts observed in small (random coil) peptides [Bundi and Wütrich 1986] for sidechain groups of the different amino acid residues referred to in this study. Shifts are quoted in ppm relative to the reference signal used by Bundi and Wütrich.

Residue				
Ala			βCH_3	1.39
Val			gCH_3	0.97, 0.94
Ile			gCH_3	0.95
			dCH_3	0.89
Leu			dCH_3	0.94, 0.90
Pro	βCH_2	2.28, 2.02	gCH_2	2.03, 2.03
			dCH_2	3.68, 3.65
Ser	βCH_2	3.88, 3.88		
Thr			gCH_3	1.23
Asp	βCH_2	2.84, 2.75		
Glu	βCH_2	2.09, 1.97	gCH_2	2.31, 2.28
Lys			eCH_2	3.02, 3.02
Arg		1.89, 1.79	dCH_2	3.32, 3.32
Asn	βCH_2	2.83, 2.75		
Gln	βCH_2	2.13, 2.01	gCH_2	2.38, 2.38
Met			eCH_3	2.13
Trp	βCH_2	3.32, 3.19	2H	7.24
			4H	7.65
			5H	7.17
			6H	7.24
			7H	7.50
Phe	βCH_2	3.22, 2.99	2,6H	7.30
			3,5H	7.39
			4H	7.34
Tyr	βCH_2	3.13, 2.92	2,6H	7.15
			3,5H	6.86
His	βCH_2	3.26, 3.20	2H	8.12
			4H	7.14

Bundi, A. and Wüthrich, K. (1979) *Biopolymers* 18**,** 285–297. ^{1}H NMR parameters of the common amino acid residues measured in aqueous solutions of the linear tetrapeptides H–Gly–Gly–X–L-Ala–OH

Appendix III

Approach taken to the derivation of K_d from the F-actin binding assays using the intensity change of ^{1}H NMR resonances of a peptide ligand

Background

The individual resonances typically observed in an NMR spectrum for each nucleus in the molecule report on the shielding environment and relaxation properties of the corresponding groups averaged over the entire population of molecules in solution. The averaging occurs because of rapid interconversion between different conformational states. Similarly, when the peptide and F-actin association and dissociation are very rapid then each peptide signal that is observed reports on the mole-fraction weighted average of the NMR parameters of the free and bound states [Fisher & Jardetzky, 1965; Sarazin et al, 1972; Roberts, 1993] and is given by [Fielding, 2007]

$$M_{obs}=X_{L(free)}M_{L(free)}+X_{L(bound)}M_{L(bound)}$$

where M_{obs} is the NMR observable, $X_{L(free)}$ and $X_{L(bound)}$ are the mole fractions of free and bound ligand, and $M_{L(free)}$ and $M_{L(bound)}$ are the NMR relaxation parameters of the peptide ligand in its free and bound states, respectively.

The occurrence of rapid interconversion on the NMR timescale between free and F-actin bound forms of the hcTnI peptides can be inferred from the relaxation observed a variety of signals each of which originate from a single group of the entire peptide population and, the progressively greater broadening effects that were seen in the presence of increasingly higher concentrations of F-actin. These observations are characteristic of exchange of peptide molecules between free and bound states that is fast on the NMR timescale.

The analysis of the effects of exchange processes on NMR observed binding curves [Feeney et al, 1979; Roberts, 1993] illustrated that,for a nucleus on a ligand that is in fast exchange between free (F) and bound (B) sites, the observed transverse relaxation rate, $1/T_{2obs}$, and hence the resulting resonance linewidth (linewidth = $1/\pi T_{2obs}$), is given

$$1/T_{2obs} = X_{L(B)}/T_{2(B)} + X_{L(F)}/ T2_{(B)} + \{X_{L(B)} (X_{L(F)})^2\}\ t_B\ 4\pi^2\ \Delta\delta^2$$

where $\Delta\delta$ is the shift difference between the free and bound nuclear resonance and t_B is the lifetime of the bound state (equivalent to $1/k_{off}$). The last term is the exchange contribution whose value reduces to zero in the case of very fast exchange [Feeney et al,

1979; Roberts, 1993]. The assumption of this exchange condition is commonly made on the evidence of experimentally-observed progressive signal perturbations [Roberts 1993; Fielding 2007] and is also made in this study. The linewidth parameter observed can then be taken to be proportional to the mole fraction weighted average of the bound and free states (above and Chapter 2).

Derivation of relationship for K_d in terms of the signal intensity at constant hcTnI peptide concentration in the presence of increasing concentrations of F-actin

For a 1:1 binding equilibrium

F-actin (A) + hcTnI peptide (P) ? F-actin·hcTnI peptide (AP)

the dissociation equilibrium constant, $K_d = [A]_F[P]_F / [AP]$ *Equation 1*

and, the fraction of bound peptide, f_B, is given by

$$f_B = [AP] / ([AP] + [L]_F)$$

that can be expressed in terms of K_d using Equation 1 to gives

$$f_B = (1 + K_d/[A]_F)^{-1}$$ *Equation 2*

To enable reference to the total (T) peptide concentration present, $[P]_T$, the terms involving $[P]_F$ and [AP] were expressed in terms of $[P]_T$ given that

$$[A]_T - [A]_F = [AP] = [P]_T - [P]_F \text{ and hence } [P]_F = [P]_T - [A]_T + [A]_F$$

Replacement of $[P]_F$ and [AP] in Equation 1 yields the following expression for Kd :

$$K_d = [A]_F ([P]_T - [A]_T + [A]_F) \div ([A]_T - [A]_F)$$

that can then be rearranged (upon 'cross-multiplication') into a quadratic equation :

$$([A]_F)^2 + ([P]_T - [A]_T + K_d)[A]_F - K_d[A]_T = 0$$

before solving formally for $[A]_F$ as

$$[A]_F = -½ \{([P]_T - [A]_T + K_d) \pm \text{sqrt}\{([P]_T - [A]_T + K_d)^2 + 4K_d[A]_T\}$$ *Equation 3*

with any numerical solution of equation 2 taking only the positive square root into consideration.

Substitution of the (positive square root, √) solution for $[A]_F$ into Equation 2 for f_B gives :

$$f_B = 1 / \{ 1 + (2K_d \div \{([P]_T - [A]_T + K_d) + \sqrt{}\{([P]_T - [A]_T + K_d)^2 + 4K_d[A]_T\} \}$$

that can be rearranged to give (*Equation 4*)

$$f_B = 1 / \{ 1 + \{2K_d / ([P]_T - [A]_T + K_d)\}\{\underline{\sqrt{} (1 + 4K_d[A]_T/([P]_T - [A]_T + K_d)^2)} -1\}^{-1}$$

where the underlined term is dealt with below.

Appendix III

The somewhat unwieldy expression for f_B can be simplified for use in the case of the studies described in this thesis that typically made use of F-actin concentrations that were significantly higher than those of the hcTnI peptide (eg for experimental data obtained when mole ratios of hcTnI peptide to F-actin were in the range 12:1 to 7:1).

When $[P]_T > [A]_T$

the value of the term $4K_d[A]_T/([P]_T - [A]_T + K_d)^2$ that occurs within the sqrt tends to zero. This allowed the approximation of the expression underlined above using an expansion based upon the Taylor power series : $\sqrt{(1 + x)} = 1 + x/2 - x^2/8 + x^3/16 - \ldots\ldots$

and ignoring the italicised terms in the Taylor expansion.

In this way the underlined square root term above, $\{\sqrt{(1 + 4K_d[A]_T/([P]_T - [A]_T + K_d)^2)}\}$ could be simplified to $1 + \{ 2K_d / ([P]_T - [A]_T + K_d) \}$

Substitution of this approximation into equation 4 gives a less unwieldy formulation for f_B that involves K_d and the experimentally measurable $[A]_T$ and $[P]_T$

$$f_B = (1 \div \{1 + \{([P]_T - [A]_T + K_d)/[A]_T\} \}$$

which simplifies to the readily applied relationship for f_B

$$f_B = [A]_T \div ([P]_T + K_d) \qquad \textit{Equation 5}$$

Under conditions of fast exchange between hcTnI peptide and F-actin, the peptide signals report on the mole-fraction weighted average of the corresponding signal linewidths in the free and F-actin bound states, υ_F and υ_B. The signal intensity in the free peptide spectrum, I_F , and the signal intensity observed for the peptide sigal in the presence of F-actin, I_B , can then be related to the signal linewidths and, the fraction of free (f_F) and bound (f_B) peptide by the expression [Sarazin et al, 1972; Fielding 2007]

$$I_B/I_F = \upsilon_F \div (f_F\upsilon_F + f_B\upsilon_B) \qquad \textit{Equation 6}$$

Since the aim is to link to equation 5 for f_B, this expression for the ratio I_B/I_F needed to be rearranged to eliminate the inclusion of the fraction of free peptide, f_F, in the equation. This was achieved by recalling that $f_F = 1\text{-}f_B$ and then considering an alternative variable, ρ, defined as $(1 - I_B/I_F)$, so as to reorganise equation 6 into terms involving only ρ, f_B and υ_B/υ_F

$$\rho = (1 - I_B/I_F) = 1 - \{\upsilon_F \div (f_F\upsilon_F + f_B\upsilon_B)\} = 1 - \{\upsilon_F \div (f_F + f_B\upsilon_B/\upsilon_F)\}$$

and so

$$\rho = 1 - \{\upsilon_F \div (1 - f_B + f_B\upsilon_B/\upsilon_F)\} = 1 - \{1 \div (1 + f_B\{ (\upsilon_B/\upsilon_F) - 1\}\} =$$

Finally, simplifying the equation by rewriting $\{(\upsilon_B/\upsilon_F) -1\}$ as a constant, c,

the substitution of equation 5 into this formula for ρ leads to

$$\rho = 1 - \{1 \div \{1 + c([A]_T \div ([P]_T + K_d)\ \}$$

that allows evaluation of K_d for the complex between F-actin and a peptide of hcTnI by relating the fraction of bound peptide to the observed change in NMR signal height via

$$\mathbf{I_B/I_F = 1 \div \{1 + c[F\text{-}actin]_{total}/([P]_{total} + K_d)\ \}} \qquad \textbf{Equation 7}$$

where the constant c can be evaluated by inspection of the signals in the spectrum of the free peptide and by assuming that the linewidth of the bound peptide approximates the linewidth of F-actin. As described in Chapter 2, the observed linewidths of the free peptide signals, υ_F were ~ 7 Hz while the linewidth of the resonances of F-actin, υ_B was ~200 Hz [Prochniewicz et al, 1999] leading to a value of c ~ 30 that was used for the purpose of any calculation of K_d.

Appendix IV- List of Abstracts

European Muscle Conference, Oxford 2008, UK

Interactions of the N-terminus of cardiac troponin-I and their role in myocardial contractility

W.W.A. MITCHELL, V.B. PATCHELL, D.G. WARD, B.A. LEVINE, I.P. TRAYER and S.V. PERRY, (2008) J Muscle Res Cell Motil, 29: 276

Cardiac contractility is regulated by the interplay between Ca^{2+} and phosphorylation. The lusitropic effect of β-adrenergic stimulation is modulated by PKA phosphorylation at the isoform-specific N-terminal extension of the inhibitory subunit of the cardiac troponin complex (cTnI). The molecular mechanism by which cTnI phosphorylation elicits an increase in crossbridge kinetics and a lower Ca^{2+} sensitivity of force is however still unresolved. We are therefore exploring possible associations of the N-terminus of human cTnI with thin filament proteins in order to define what interaction(s) could contribute to the modulation of the contractile cycle. We have identified a phosphorylation-sensitive association with F-actin encompassed within residues 18-30 of the N-terminus of human cTnI. This interaction is observed to inhibit the attachment to F-actin by myosin loop 2 that is associated with the weak-binding step of crossbridge formation. Since direct contact between cTnC and the N-terminal extension of cTnI has been suggested to mediate the mechanism for phosphorylation-dependent Ca^{2+} sensitivity we investigated the interaction with F-actin using cTnI residues 1-64 complexed with calcium-bound cTnC. These studies demonstrate retention of the association with F-actin by the cTnI N-terminus at a segment upstream of the region of cTnI interacting with cTnC. The implications of these data will be discussed in the context of the regulation of myocardial Ca^{2+} sensitivity by phosphorylation.

Appendix IV

European Muscle Conference, Stockholm 2007, Sweden

The interaction of the N-terminal of cardiac troponin I with F-actin may contribute to the modulation of calcium sensitivity by phosphorylation

W.W.A. MITCHELL, B.A. LEVINE, D.G. WARD, S.V. PERRY, V.B. PATCHELL,
(2007) J Muscle Res Cell Motil, 28: 447-448

Phosphorylation at the N-terminus of cardiac troponin I (cTnI) has been shown to regulate contractile activity in the myocardium with Ca^{2+} sensitivity decreasing upon mono- and bisphosphorylation. The molecular role of the N-terminal region in the regulatory function of cTnI is however still unclear. Our studies of human cTnI using proton magnetic resonance and fluorescence spectroscopy to localise regions of interaction have identified the association of the N-terminal of cTnI with F-actin. The use of defined fragments of human cTnI (hcTnI) showed that interaction involves residues 16-52 that contain the phosphorylation sites (Ser-22 and 23). Experiments carried out with overlapping sequences demonstrated that residues 16-29 play a significant role in F-actin interaction. We further observed that complex formation between the N-terminus of hcTnI and F-actin inhibited the association of F-actin with human cardiac β-myosin residues 398-414 and 623-660, myosin loop interactions correlated with actomyosin activity. Since cTnI in resting heart is predominantly monophosphorylated and dual phosphorylation upon β-adrenergic stimulation is associated with an increase in heart rate, we investigated how phosphorylated hcTnI peptides affect these actin-myosin contacts. Our results suggest that myocardial Ca^{2+} sensitivity may be modulated by cTnI interaction with actin.

Appendix IV

YPS – Cations in Physiological Signalling, Manchester 2008, UK

The role of the N-terminal extension of cardiac troponin-I in myocardial contractility

W.W.A. MITCHELL, B.A. LEVINE, D.G. WARD, S.V. PERRY, V.B. PATCHELL,

Cardiac contractility is regulated by the interplay between Ca^{2+} and phosphorylation. The lusitropic effect of β-adrenergic stimulation is mediated by PKA phosphorylation at the N-terminus of the inhibitory subunit (TnI) of the cardiac troponin complex. This facilitates relaxation but also increases the calcium requirement for contraction since the phosphorylation of cardiac TnI leads to a decrease in Ca^{2+} sensitivity of cardiac troponin-C (cTnC), an increase in the rate of the contractile cycle and therefore heart rate. Thereby the inotropically stimulated heart can fill during sympathetic stimulation when increased heart rate shortens diastole.

Ca^{2+} binding associated with activation occurs at the N-terminal domain of cTnC which only has a single Ca^{2+} binding site (unlike the fast skeletal isoform where two Ca^{2+} binding sites are involved in triggering contraction). The mechanism by which cTnI phosphorylation reduces Ca^{2+} sensitivity of force is not well understood. Direct interaction by the N-terminus of cTnI with cTnC has been suggested. We are interested in the possible associations of the N-terminus of TnI with thin filament proteins in order to define what molecular interaction(s) could be the basis for the modulation in the contractile cycle. We have studied the interaction between cTnI and F-actin that underlies the ability of troponin to inhibit actomyosin ATPase activity. We find that the N-terminus of cTnI interacts with F-actin while the region downstream of this cardiac specific sequence associates with cTnC. We present a model for a potential mechanism for the regulation of Ca^{2+} sensitivity by phosphorylation.

Appendix IV

Alternative Muscle Conference Leeds 2008, UK

The role of the N-terminal extension of cardiac troponin-I in myocardial contractility

W.W.A. MITCHELL, B.A. LEVINE, D.G. WARD, S.V. PERRY, V.B. PATCHELL,

Cardiac contractility is regulated by the interplay between Ca^{2+} and phosphorylation. Ca^{2+} binding associated with activation occurs at the N-terminal domain of cardiac troponin C (cTnC). β-adrenergic stimulation triggers PKA phosphorylation at the isoform-specific N-terminus of the inhibitory subunit (TnI) of the cardiac troponin complex. This facilitates relaxation but also increases the calcium requirement for contraction since the phosphorylation of cardiac TnI leads to a decrease in Ca^{2+} sensitivity of cTnC, an increase in the rate of the contractile cycle and therefore heart rate. Thus the inotropically stimulated heart can fill during sympathetic stimulation when increased heart rate shortens diastole. The mechanism by which cTnI phosphorylation reduces Ca^{2+} sensitivity of force is however not well understood. Direct interaction by the N-terminal 30 residues of cTnI with cTnC has been suggested. Our interest is the possible associations of the N-terminus of TnI with thin filament proteins in order to define what molecular interaction(s) could be the basis for the modulation in the contractile cycle. We have studied the interaction between cTnI and F-actin that underlies the ability of troponin to inhibit actomyosin ATPase activity. We suggest a potential mechanism for the regulation of both Ca^{2+} sensitivity and crossbridge cycling by phosphorylation.

Appendix IV

Alternative Muscle Conference, London 2007, UK

Interactions of the N-terminal region of cardiac troponin-I

Mitchell Wayne, Gallon Clare, Levine Barry, Perry Sam, Patchell Val (2007)

The N-terminal tail of cardiac troponin-I (cTnI) contains a sequence unique to the cardiac isoform of this inhibitory component of the troponin complex. PKA phosphorylation at Ser22 and Ser23 of the N-terminal extension of cTnI regulates Ca^{2+} sensitivity and hence myocardial contractility. No interaction with other components of the troponin complex or F-actin has been observed for the extreme N-terminal region. Using peptides spanning cTnI residues 16-52 (16-29, 16-41 and 36-52) it has been possible, with proton magnetic resonance and fluorescence spectroscopy, to study whether any part of this region of cTnI associates with F actin. It was found that residues 16-41 and 36-52 interact with F-actin. The overlapping segment in these peptides allowed competition experiments which showed that the region comprising residues 16-41 has a higher affinity for F actin. These data suggest that an extended span of residues on the N-terminus of cTnI interacts with F actin. This segment also contains the sites for phosphorylation. Because of this it was of interest to see whether the interaction of the N-terminus of cTnI was able to influence interaction of F actin with myosin. This was initially explored by observing whether the N-terminus of cTnI can displace specific regions of myosin bound to F actin, which has been demonstrated for the inhibitory region of cTnI (Thr128 Met153). The ability of the N-terminal tail of cTnI to modify the interaction of F actin with human cardiac β myosin residues 398-414 and 622-646 raises the possibility that phosphorylation of the cTnI N-terminal can influence actomyosin ATPase activity.

References

Abbott, M. B., Dong, W. J., Dvoretsky, A., DaGue, B., Caprioli, R. M., Cheung, H. C., and Rosevear, P. R. (2001) Modulation of cardiac troponin C-cardiac troponin I regulatory interactions by the amino-terminus of cardiac troponin I. Biochemistry 40, 5992-6001.

Barbato, J. C., Huang Q. Q., Hossaint M. M., Bond M. and Jin J. P. (2005). Proteolytic N-terminal truncation of cardiac troponin I enhances ventricular diastolic function. Journal of Biological Chemistry. 280, 6602-6609.

Bartegi A, Roustan C, Chavanieu A, Kassab R and Fattoum A. (1997) Interaction of F-actin with synthetic peptides spanning the loop region of human cardiac beta-myosin heavy chain containing Arg403. Eur J Biochem. 250, 484-91.

Baryshnikova, O. K., Robertson I. M., Mercier P. and Sykes B. D. (2008). Dilated cardiomyopathy G159D mutation in cardiac troponin C weakens the anchoring interaction with troponin I. Biochemistry. 47, 10950-10960.

Baryshnikova, O. K., Li, M. X., and Sykes, B. D. (2008) Modulation of cardiac troponin C function by the cardiac-specific n-terminus of troponin I: Influence of PKA phosphorylation and involvement in cardiomyopathies. Journal of Molecular Biology 375, 735-751.

Berjanskii, M.V. and Wishart, D.S. (2008) Application of the random coil index to studying protein flexibility. J Biomol NMR 40, 31–48

Bers, D.M. (2002) Cardiac excitation-contraction coupling. Nature 415,198-205

Bers, D.M. (2008) Calcium cycling and signaling in cardiac myocytes. Annu. Rev. Physiol. 70, 23–49

References

Bhandari D.G, Levine B.A, Trayer I.P, Yeadon M.E. (1986) ^{1}H-NMR study of mobility and conformational constraints within the proline-rich N-terminal of the LC1 alkali light chain of skeletal myosin. Correlation with similar segments in other protein systems. Eur J Biochem. 160 349-356

Biesiadecki, B. J., T. Kobayashi, J. S. Walker, R. J. Solaro and P. P. de Tombe. (2007). The troponin C G159D mutation blunts myofilament desensitization induced by troponin I Ser23/24 phosphorylation. Circulation Research. 100, 1486-1493.

Bing, W., Fraser, I. D. C. & Marston, S. B. (1997) Troponin I And Troponin T Interact With Troponin C To Produce Different Ca^{2+}-Dependant Effects On Actin-Tropomyosin Filament Motility. Biochem. J., 327, 335-340

Blumenschein T.M.A, Stone D.B Fletterick R.J Mendelson R.A and Sykes B.D. (2006) Dynamics of the C-Terminal Region of TnI in the Troponin Complex in Solution. Biophys J 90 2436–2444

Booth H.D. (2004) Human Physiology, An integrated approach, PowerPoint Lecture Slide. Pearson Education, Inc, publishing as Benjamin Cummings

Boquet, I., Boujemaa, R. Carlier, M, F. and Preat, T. (2000) Ciboulot regulates actin assembly during Drosophila brain metamorphosis. Mol Biol Cell 102, 797-808

Bundi, A. and Wüthrich, K. (1979). ^{1}H NMR parameters of the common amino acid residues measured in aqueous solutions of the linear tetrapeptides H–Gly–Gly–X–L-Ala–OH. Biopolymers 18, 285–297

Calvert, M. J., Ward, D. G., Trayer, H. R. and Trayer, I. P. (2000) The importance of the carboxyl-terminal domain of cardiac troponin C in Ca^{2+}-sensitive muscle regulation. J Biol Chem 275, 32508-32515

References

Campbell, I. D. Dobson, C. M. Williams, R. J. P. and Wright, P. E. (1975) Pulse methods for the simplification of protein NMR spectra. FEBS Lett. 57, 96-99

Carballo, S., Robinson, P., Otway, R., Fatkin, D., Jongbloed, J. D. H., de Jonge, N., Blair, E., van Tintelen, J. P., Redwood, C. and Watkins, H. (2009) Identification and Functional Characterization of Cardiac Troponin I As a Novel Disease Gene in Autosomal Dominant Dilated Cardiomyopathy. Circ Res 105, 375-U116

Carr H.Y. and Purcell E.M. (1954) Effects of Diffusion on Free Precession in Nuclear Magnetic Resonance Experiments. Phys. Rev. 94, 630–638

Carr-Purcell two pulse sequence t , Carr H, Y. and Purcell E, M. (1954); Campbell, I. D., Dobson, C. M., Williams, R. J. P. & Wright, P. E. (1975). Diagram source - http://131.104.156.23/Lectures/CHEM_207/CHM_207_NMR.htm

Chang A.N, Parvatiyar M.S. and Potter J.D. (2008) Troponin and cardiomyopathy. Biochem. Biophys. Res. Comm. 369, 74-81

Cole H.A, Perry S.V (1975) Phosphorylation of Troponin-I from Cardiac-Muscle, Biochemical Journal. 149. 525-533

Conibear, P.B, Bagshaw, C.R, Fajer, P.G, Kovács M and Málnási-Csizmadia, A. (2003) Myosin cleft movement and its coupling to actomyosin dissociation. Nature St. Mol. Biol. 10, 831-835 http://www.nature.com/nsmb/journal/v10/n10/full/nsb986.html - a1

Cooper, J. A., Walker, S. B. and Pollard, T. D. (1983) Pyrene Actin - Documentation of the Validity of a Sensitive Assay for Actin Polymerization. J Muscle Res Cell M 4, 253-262

Cooper, J. A. (2002) Actin dynamics: Tropomyosin provides stability. Curr Biol Curr Biol 12, R523-R525

References

Cummins, B and Cummins, P. (1987) Cardiac Specific troponin-I release in canine experimental myocardial infarction: development of a sensitive enzyme-linked immunoassay. J Mol Cell Cardiol 19, 999-1010

Davis, J. P. and Tikunova, S. B. (2008) Ca^{2+} exchange with troponin C and cardiac muscle dynamics. Cardiovasc Res 77, 619-626

Deng, Y., Schmidtmann A., Kruse S., Filatov V., Heilmeyer L. M. G., Jaquet K. and Thieleczek R. (2003). Phosphorylation of human cardiac troponin I G203S and K206Q linked to familial hypertrophic cardiomyopathy affects actomyosin interaction in different ways. Journal of Molecular and Cellular Cardiology. 35, 1365-1374.

Downard K. (2004) Mass Spectrometry: A Foundation Course. The Royal Society of Chemistry, Cambridge.

Dyer, E. C., Jacques A. M., Hoskins A. C., Ward D. G., Gallon C. E., Messer A. E., Kaski J. P., Burch M., Kentish J. C. and Marston S. B. (2009). Functional Analysis of a Unique Troponin C Mutation, GLY159ASP, that Causes Familial Dilated Cardiomyopathy, Studied in Explanted Heart Muscle. Circulation-Heart Failure. 2, 456-U101.

Epstein, N.D. Cohn, G.M. Cyran, F. and Fananapazir, L. Differences in clinical expression of hypertrophic cardiomyopathy associated with two distinct mutations in the beta-myosin heavy chain gene. A. 908LeuVal mutation and a 403ArgGln mutation, Circulation 86 (1992), pp. 345–352.

EXPASY protein database http://www.expasy.ch/

Feeney, J. Batchelor, J.G. Albrand, J.P and Roberts, G.C.K. (1979) The effects of intermediate exchange processes on the estimation of equilibrium constants by NMR. J Mag Res 33.519-529

Fiaux, J., Bertelsen, E. B., Horwich, A. L. and Wuthrich, K. (2002) NMR analysis of a 900K GroEL-GroES complex. Nature 418, 207-211

Fielding L. (2003) NMR Methods for the Determination of Protein-Ligand Dissociation Constants. Curr Top Med Chem. 3, 39–53

Fielding, L. (2007) NMR methods for the determination of protein–ligand dissociation constants. Prog NMR Spectroscopy 51 219–242

Finley N, Abbott M.B, Abusamhadneh E, Gaponenko V, Dong W.J, Gasmi-Seabrook G, Howarth J.W, Rance M, Solaro R.J, Cheung H.C, Rosevear P.R (1999) NMR analysis of cardiac troponin C-troponin I complexes: effects of phosphorylation. 453, 107-112

Fischer J.J, Jardetzky O. (1965) Nuclear Magnetic Relaxation Study of Intermolecular Complexes. The Mechanism of Penicillin Binding to Serum Albumin. J Am Chem Soc. 87, 3237–3244

Foster, D. B., Noguchi, T., VanBuren, P., Murphy, A. M., and Van Eyk, J. E. (2003) C-terminal truncation of cardiac troponin I causes divergent effects on ATPase and force - Implications for the pathophysiology of myocardial stunning. Circ. Res. 93, 917-924

Galinska, A., Hatch, V., Craig, R., Murphy, A. M., Van Eyk, J. E., Wang, C. L. A., Lehman, W. and Foster, D. B. (2010) The C Terminus of Cardiac Troponin I Stabilizes the Ca^{2+}-Activated State of Tropomyosin on Actin Filaments. Circ Res 106, 705-U148

Gomes, A. V., Liang, J. S. and Potter, J. D. (2005) Mutations in human cardiac Troponin I that are associated with restrictive cardiomyopathy affect basal ATPase activity and the calcium sensitivity of force development. J Biol Chem 280, 30909-30915

References

Geeves, M.A. and Holmes, K.C. (1999) Structural mechanism of muscle contraction. Ann. Rev. Biochem. 68, 687-728

Gordon A.M, Homsher E, Regnier M. (2000) Regulation of contraction in striated muscle Physiol. Rev. 80, 853–924

Gordon A.M, Homsher E, Regnier M. (2001) Skeletal and cardiac muscle contractile activation: Tropomyosin "rocks and rolls". News Physiol. Sci. 16, 49-55

Gordon, A.M., Huxley, A.F, and Julian, F.J. (1966). The variation in isometric tension with sarcomere length in vertebrate muscle fibers. J. Physiol., 184, 170-192

Haselgrove J.C. (1972) X-ray evidence for conformational change in the actin-containing filaments of vertebrate striated muscle. Cold Spring Harbor Symp Quant Biol. 37, 341–352

Hertzog, M., van Heijenoort, C., Didry, D., Gaudier, M., Coutant, J., Gigant, B., Didelot, G., Preat, T., Knossow, M., Guittet, E. and Carlier, M. F. (2004) The beta-thymosin/WH2 domain: Structural basis for the switch from inhibition to promotion of actin assembly. Cell 117, 611-623

Hinken A.C. and Solaro J.R. (2007) A dominant role of cardiac molecular motors in the intrinsic regulation of ventricular ejection and relaxation. Physiology 22, 73-80

Holmes K,and Lehman W. (2008) Gestalt-binding of tropomyosin to actin filaments. J Mus Res Cell Motil. 29, 213–219

Holmes K.C, Schroder R.R, Sweeney H.L and Houdusse A. (2004) The structure of the rigor complex and its implications for the power stroke. Phil. Trans. R. Soc. Lond. B 359, 1819-1828

References

Holmes, K. C., Popp, D., Gebhard, W. and Kabsch, W. (1990) Atomic Model of the Actin Filament. Nature 347, 44-49

Hopkins S.C, Sabido-David C, van der Heide U.A, Ferguson R.E, Brandmeier B.D, Dale R.E, Kendrick-Jones J, Corrie J.E, Trentham D.R, Irving M and Goldman Y.E. (2002) Orientation changes of the myosin light chain domain during filament sliding in active and rigor muscle. J. Mol. Biol. 318, 1275-91

Huxley H.E. (1972) Structural changes in actin- and myosin-containing filaments during contraction. Cold Spring Harbor Symp Quant Biol. 37, 361–376

Huxley H.E. (1990) Sliding filaments and molecular motile systems. Journal of Biological Chemistry, 265, 8347-50

Jaquet, K., Thieleczek, R. and Heilmeyer, L. M. G. (1995) Pattern-Formation on Cardiac Troponin-I by Consecutive Phosphorylation and Dephosphorylation. Eur J Biochem 231, 486-490

Joel P.B, Trybus K.M, Sweeney H.L (2001) Two conserved lysines at the 50/20-kDa junction of myosin are necessary for triggering actin activation. Journal Of Biological Chemistry 276, 2998-3003

Kobayashi T and Solaro J.R. (2005) Calcium, thin filaments, and the integrative biology of cardiac contractility. Ann. Rev. Physiol. 67, 39–67

Kobayashi T, Jin L and deTombe P.P. (2008) Cardiac thin filament regulation. Pflügers Arch. - European Journal of Physiology 457. 37-46

Kobayashi, T. and Solaro, R. J. (2005) Calcium, thin filaments, and the integrative biology of cardiac contractility. Annu Rev Physiol 67, 39-67

Korn, E. D. (1982) Actin Polymerization and Its Regulation by Proteins from Non-Muscle Cells. Physiol Rev 62, 672-737

Kouyama, T. and Mihashi, K. (1981) Fluorimetry Study of "N-(1-Pyrenyl) Iodoacetamide-Labelled F-Actin - Local Structural-Change of Actin Protomer Both on Polymerization and on Binding of Heavy-Meromyosin. Eur J Biochem 114, 33-38
Lakowicz, J, R., (2006, 1999, 1983) Principles of Fluorescence Spectroscopy. Springer Science and Business Media LLC

Martin, N. H., Allen, N. W., Brown, J. D., Kmiec, D. M. and Vo, L. (2003) An NMR shielding model for protons above the plane of a carbonyl group. J Mol Graph Model 22, 127-131

Martini F.H. and Nath J.L. (2008) Fundamentals of Anatomy & Physiology (8th edition) Pearson Books (Chapter 14)

Mayer, M., and Meyer, B. (2001) Group epitope mapping by saturation transfer difference NMR to identify segments of a ligand in direct contact with a protein receptor. J. Am. Chem. Soc. 123, 6108-6117

Metzger, J. M. and Westfall, M. V. (2004) Covalent and noncovalent modification of thin filament action - The essential role of troponin in cardiac muscle regulation. Circ Res 94, 146-158

McKillop D.F. and Geeves M.A.(1993) Regulation of the interaction between actin and myosin subfragment 1: evidence for three states of the thin filament. Biophys J 65, 693–701

Mitchell, W. W. A. Levine, B. A. Ward, D. G. Perry, S. V. and Patchell, V. B. (2007) The interaction of the N-terminal of cardiac troponin I with F-actin may contribute to the modulation of calcium sensitivity by phosphorylation. J Muscle Res Cell Motil 28: 447-448

Mitchell, W. W. A. Patchell, V. B. Ward, D. G. Levine, B. A. Trayer, I. P. and Perry, S. V. (2008) Interactions of the N-terminus of cardiac troponin-I and their role in myocardial contractility. J Muscle Res Cell Motil 29: 276

Mittermaier, A.K. and Kay, L.E. (2009) Observing biological dynamics at atomic resolution using NMR. Trends Biochem Sci , 34, 601-611

Moir A.J.G, Solaro R.J, and Perry S.V. (1976) Phosphorylation of troponin I and the inotropic effect of adrenalin in the perfused rabbit heart. Nature 262, 615–617

Moir A.J.G, Solaro R.J, and Perry S.V. (1980) The Site of Phosphorylation of Troponin I in the Perfused Rabbit Heart. Biochem. J. 185, 505-513

Mornet, D., Bertrand, R., Pantel, P., Audemard, E. and Kassab, R. (1981) Structure of the Actin-Myosin Interface. Nature 292, 301-306

Moss R. L., Razumova M, and Daniel P, Fitzsimons D.P. (2004) Myosin Crossbridge Activation of Cardiac Thin Filaments: Implications for Myocardial Function in Health and Disease. Circ Res.;94, 1290-1300

Mudalige, W. A. K. A., Tao T. C. and Lehrer S. S. (2009). Ca^{2+}-Dependent Photocrosslinking of Tropomyosin Residue 146 to Residues 157-163 in the C-Terminal Domain of Troponin I in Reconstituted Skeletal Muscle Thin Filaments. Journal of Molecular Biology. 389, 575-583.

Murakami, K., Yumoto F., Ohki S., Yasunaga T., Tanokura M., and Wakabayashi T. (2005). Structural basis for Ca^{2+}-regulated muscle relaxation at interaction sites of troponin with actin and tropomyosin. J. Mol. Biol. 352:178–201.

Narolska, N. A., Piroddi, N., Belus, A., Boontje, N. M., Scellini, B., Deppermann, S., Zaremba, R., Musters, R. J., dos Remedios, C., Jaquet, K., Foster, D. B., Murphy, A. M., van Eyk, J. E., Tesi, C., Poggesi, C., van der Velden, J. and Stienen, G. J. M. (2006)

Impaired diastolic function after exchange of endogenous troponin I with C-terminal truncated troponin I in human cardiac muscle. Circ Res 99, 1012-1020

Onishi H, Mikhailenko S.V. and Morales M.F. (2006) Toward understanding actin activation of myosin ATPase: The role of myosin surface loops. Proc Natl Acad Sci U S A. 103, 6136–6141

Onishi H, and Morales M.F. (2007) A closer look at energy transduction in muscle. PNAS 104, 12714–12719

Patchell, V. B., Gallon, C. E., Hodgkin, M. A., Fattoum, A., Perry, S. V., and Levine, B. A. (2002) The inhibitory region of troponin-I alters the ability of F-actin to interact with different segments of myosin. European Journal of Biochemistry 269, 5088-5100.

Patchell, V. B., Gallon, C. E., Evans, J. S., Gao, Y., Perry, S. V., and Levine, B. A. (2005) The regulatory effects of tropomyosin and troponin-I on the interaction of myosin loop regions with F-actin. J Biol. Chem. 280, 14469-75

Pearlstone, J. R., Sykes B. D. and Smillie L. B. (1997). Interactions of structural C and regulatory N domains of troponin C with repeated sequence motifs in troponin I. Biochemistry. 36, 7601-7606.

Perry S.V. (1996) Molecular Mechanisms in Striated Muscle. Cambridge Univeristy Press.

Perry S.V. (1999) Troponin I: Inhibitor or facilitator. Mol. and Cell. Biochem. 190, 9–32

Pirani A., Vinogradova M.V, Curmi P.M, King W.A., Fletterick R.J, Craig R, Tobacman L.S., Xu C, Hatch V and Lehman W. (2006) an atomic model of the thin filament in the relaxed and Ca^{2+}-activated states. J Mol Biol, 357, 707-717

Prochniewicz, E. Zhang, Q, Howard, E.C and Thomas, D.D. (1996) Microsecond Rotational Dynamics of Actin: Spectroscopic Detection and Theoretical Simulation. J. Mol. Biol. 255, 446–457

Prochniewicz, E. and Thomas, D. D. (1999) Differences in structural dynamics of muscle and yeast actin accompany differences in functional interactions with myosin. Biochemistry 38, 14860-14867

Prochniewicz, E. and Thomas, D. D. (1999) The structure and dynamics of skeletal and yeast actin: Relationship to functional interactions with myosin. Biophys J 76, A37-A37

Quirk, P. G., Patchell V. B., Gao Y., Levine B. A. and Perry S. V. (1995). Sequential Phosphorylation of Adjacent Serine Residues on the N-Terminal Region of Cardiac Troponin-I - Structure-Activity Implications of Ordered Phosphorylation. Febs Letters. 370, 175-178.

Ray, K. P. and England, P. J. (1976) Phosphorylation of Inhibitory Subunit of Troponin and Its Effect on Calcium Dependence of Cardiac Myofibril Adenosine-Triphosphatase. Febs Lett 70, 11-16

Rayment I, Holden HM, Whittaker M, Yohn C.B, Lorenz M, Holmes K.C and Milligan R.A. (1993) Structure of the actin-myosin complex and its implications for muscle contraction. Science, 261, 58–65

Roberts G. C. K. (1993) NMR of Macromolecules- A Practical Approach. IRL Press

Robertson, S. P., Johnson, J. D., Holroyde, M. J., Kranias, E. G., Potter, J. D. and Solaro, R. J. (1982) The Effect of Troponin-I Phosphorylation on the Ca^{2+}-Binding Properties of the Ca^{2+}-Regulatory Site of Bovine Cardiac Troponin. J Biol Chem 257, 260-263

Sadayappan, S., Finley, N., Howarth, J. W., Osinska, H., Klevitsky, R., Lorenz, J. N., Rosevear, P. R. and Robbins, J. (2008) Role of the acidic N ' region of cardiac troponin I in regulating myocardial function. Faseb J 22, 1246-1257

Sakuma, A., Kimura-Sakiyama C., Onoue A., Shitaka Y., Kusakabe T. and Miki M. (2006). The second half of the fourth period of tropomyosin is a key region for Ca2+-dependent regulation of striated muscle thin filaments. Biochemistry. 45, 9550-9558.

Sarrazin M, Sari J.C, Bourdeaux-Pontier M, Briand C. (1972) NMR Study of the Interactions between Flurazepam and Human Serum Albumin. Mol Pharm. 15, 71–77

Sasaki, N., Asukagawa, H., Yasuda, R., Hiratsuka, T., and Sutoh, K. (1999) Deletion of the Myopathy Loop of Dictyostelium Myosin II and Its Impact on Motor Functions. J. Biol. Chem. 274, 37840-37844

Schimmel, P. R. and Florey, P. J. (1968) Conformational energies and configurational statistics of copolypeptides containing L-proline. J. Mol. Biol. 34,105-120

Shiels H.A. and White E. (2008) The Frank–Starling mechanism in vertebrate cardiac myocytes. J. Exp. Biol. 211, 2005-2013

Singh A, Hitchcock-DeGregori S.E. (2007) Tropomyosin's periods are quasi-equivalent for actin binding but have specific regulatory functions. Biochemistry 46: 14917–14927

Singh A, Hitchcock-DeGregori S.E. (2009) A Peek into Tropomyosin Binding and Unfolding on the Actin Filament. PLoS ONE 4, e6336

Slosarek, G., Heintz, D. and Kalbitzer, H. R. (1994) Mobile Segments in Rabbit Skeletal-Muscle F-Actin Detected by H-1 Nuclear-Magnetic-Resonance Spectroscopy. Febs Lett 351, 405-410

Solaro, R. J. Moir, A. J. G. and Perry, S. V. (1976) Phosphorylation of Troponin-I and Inotropic Effect of Adrenaline in Perfused Rabbit Heart. Nature 262, 615-617

Solaro, R.J. Rosevear, P. and Kobayashi, T. (2008) The unique functions of cardiac troponin I in the control of cardiac muscle contraction and relaxation. Biochem. Biophys. Res. Comm. 369, 82–87

Solaro, R.J. van der Velden, J. (2010) Why does troponin I have so many phosphorylation sites? Fact and fancy. Journal of Molecular and Cellular Cardiology 48, 810-816

Spudich, J. A. and Watt, S. (1971) Regulation of Rabbit Skeletal Muscle Contraction .1. Biochemical Studies of Interaction of Tropomyosin-Troponin Complex with Actin and Proteolytic Fragments of Myosin. J Biol Chem 246, 4866-4871

Steffen, W., Smith, D. and Sleep, J. (2003) The working stroke upon myosin-nucleotide complexes binding to actin. P Natl Acad Sci USA 100, 6434-6439

Sutoh, K. (1982) An Actin-Binding Site on the 20k Fragment of Myosin Subfragment-1. Biochemistry 21, 4800-4804

Sutoh, K. (1982) Identification of Myosin-Binding Sites on the Actin Sequence. Biochemistry 21, 3654-3661

Sweeney H.L and Houdusse A. (2004) The motor mechanism of myosin V: insights for muscle contraction. Phil. Trans. R. Soc. B 359, 1829–1842

Syska, H., Wilkinson, J. M., Grand, R. J. A. and Perry, S. V. (1976) Relationship between Biological-Activity and Primary Structure of Troponin-I from White Skeletal-Muscle of Rabbit. Biochem J 153, 375-387

Tachampa K, Kobayashi T, Wang H, Martin A.F, Biesiadecki B.J, Solaro R.J, de Tombe P.P. (2008) Increased Cross-bridge Cycling Kinetics after Exchange of C-terminal Truncated Troponin I in Skinned Rat Cardiac Muscle. J Biol Chem. 283, 15114–15121

Takagi Y, Shuman H and Goldman Y.E. (2004) Coupling between phosphate release and force generation in muscle actomyosin. Phil. Trans. R. Soc. Lond. B 359, 1913-1920

Takeda, S., Yamashita, A., Maeda, K. and Maeda, Y. (2003) Structure of the core domain of human cardiac troponin in the Ca^{2+}-saturated form. Nature 424, 35-41

Tang, J. X., and Janmey, P. (1996) The polyelectrolyte nature of F-actin and the mechanism of actin bundle formation. J. Biol. Chem. 271, 8556-8563

Tobacman L.S. (1996) Thin filament mediated regulation of cardiac contraction. Ann. Rev. Physiol. 58, 447–81

Tompa, P and Fuxreiter, M (2008) Fuzzy complexes: polymorphism and structural disorder in protein–protein interactions. Trends Biochem Sci , 33, 2-8

Toyoshima Y.Y, Kron S.J, McNally E.M, Niebling KR, Toyoshima C, and Spudich J.A. (1987) Myosin subfragment-1 is sufficient to move actin filaments in vitro. Nature 328, 536–539

Tripet B, Van Eyk J.E, Hodges R.S. (1997) Mapping of a second actin-tropomyosin and a second troponin C binding site within the C terminus of troponin I, and their importance in the Ca^{2+}-dependent regulation of muscle contraction. J Mol Biol. 271, 728-50.

Van Eyk J.E, Powers F, Law W, Larue C, Hodges R.S, Solaro R.J. (1998) Breakdown and release of myofilament proteins during ischemia and ischemia/reperfusion in rat

hearts: identification of degradation products and effects on the pCa-force relation. Circ Res. 82: 261–271

Vinogradova, M. V., Stone, D. B., Malanina, G. G., Karatzaferi, C., Cooke, R., Mendelson, R. A. and Fletterick, R. J. (2005) Ca^{2+}-regulated structural changes in troponin. P Natl Acad Sci USA 102, 5038-5043

Ward, D. G., Cornes M. P. and Trayer I. P. (2002). Structural consequences of cardiac troponin I phosphorylation. Journal of Biological Chemistry. 277, 41795-41801.
Ward, D. G., Brewer S. M., Comes M. P. and Trayer I. P. (2003). A cross-linking study of the N-terminal extension of human cardiac troponin I. Biochemistry. 42, 10324-10332.

Ward, D. G., Brewer S. M., Calvert M. J., Gallon C. E., Gao Y. and Trayer I. P. (2004a). Characterization of the interaction between the N-terminal extension of human cardiac troponin I and troponin C. Biochemistry. 43, 4020-4027.

Ward, D. G., Brewer S. M., Gallon C. E., Gao Y., Levine B. A. and Trayer I. P. (2004b). NMR and mutagenesis studies on the phosphorylation region of human cardiac troponin I. Biochemistry. 43, 5772-5781.

Warren, C. M., T. Kobayashi and R. J. Solaro. (2009). Sites of Intra- and Intermolecular Cross-linking of the N-terminal Extension of Troponin I in Human Cardiac Whole Troponin Complex. Journal of Biological Chemistry. 284, 14258-14266.

Watkins, H. Rosenzweig, A. Hwang, D.S. Levi, T. McKenna, W. Seidman C.E. and Seidman, J.G. Characteristics and prognostic implications of myosin missense mutations in familial hypertrophic cardiomyopathy, N. Engl. J. Med. 326 (1992), pp. 1108–1114

Weber, A. Nachmias, V, T. Pennise, C, R. Pring, M. Safer, D. (1992) Interaction of thymosin .beta.4 with muscle and platelet actin: implications for actin sequestration in resting platelets. Biochemistry, 31 (27), pp 6179–6185

Westfall M.V, Metzger J.M. (2001) Troponin I isoforms and chimeras: tuning the molecular switch of cardiac contraction. News Phyiol Sci 16, 278–281

Wilkinson, J. M. and Grand, R. J. A. (1978) Comparison of Amino-Acid Sequence of Troponin-I from Different Striated Muscles. Nature 271, 31-35

Wishart D.S, Case D.A. (2001), Use of chemical shifts in macromolecular structure determination. Methods Enzymol, 338, p3–34

Wüthrich, K. (1986) NMR of proteins and nucleic acids., John Wiley and Sons, New York

Yengo, C. M. & Sweeney, H. L. (2004) Functional role of loop 2 in myosin V. Biochemistry 43, 2605–2612

Zabrouskov, V., Ge Y., Schwartz J. and Walker J. W. (2008). Unraveling Molecular Complexity of Phosphorylated Human Cardiac Troponin I by Top Down Electron Capture Dissociation/Electron Transfer Dissociation Mass Spectrometry. Molecular & Cellular Proteomics. 7, 1838-1849.

Zhou, M. M., Harlan, J. E., Wade, W. S., Crosby, S., Ravichandran, K. S., Burakoff, S. J. and Fesik, S. W. (1995) Binding affinities of tyrosine-phosphorylated peptides to the COOH-terminal SH2 and NH2-terminal phosphotyrosine binding domains of Shc. J Biol Chem 270, 31119-31123